Ecole Doctorale EDITE

Thèse présentée pour l'obtention du diplôme de
DOCTEUR DE TELECOM & MANAGEMENT SUDPARIS

Doctorat délivré conjointement par
TELECOM & Management SudParis et l'Université Pierre et Marie Curie - Paris 6

Spécialité : Electronique et communications

Par Petros Ramantanis

Contribution à l'étude des systèmes de transmission optique utilisant le format de modulation QPSK

Soutenue le 30/09/2011 devant le jury composé de :

Président : Georges Alquié
Rapporteur : Alberto Bononi
Rapporteur : Philippe Emplit
Examinateur : Yann Frignac
Examinateur : Jean-Christophe Antona
Directeur de thèse : Badr-Eddine Benkelfat

Thèse n° 2011TELE0020

Ecole Doctorale EDITE

PhD Thesis
TELECOM & MANAGEMENT SUDPARIS

PhD jointly delivered by
TELECOM & Management SudParis and Université Pierre et Marie Curie - Paris 6

Specialty: Electronics and communications

Petros Ramantanis

Contribution to the analysis of optical transmission systems using QPSK modulation

Date of defense: 30/09/2011. Jury composition:

Head of the jury: Georges Alquié
Reviewer: Alberto Bononi
Reviewer: Philippe Emplit
Jury member : Yann Frignac
Jury member: Jean-Christophe Antona
Thesis director: Badr-Eddine Benkelfat

Thesis n° 2011TELE0020

To Elli

Acknowledgements

A simple “thanks” for the people that have contributed directly or indirectly to this manuscript is certainly not enough. Nevertheless, the few words that follow give me the chance to remember and thank them with all my heart, not only because of their help, but most importantly, for all the priceless moments that we have shared.

First and foremost, I would like to express my infinite gratitude to my thesis advisor, office colleague and dearest friend, Yann Frignac. His qualities of character, his technical expertise, as well as his endless patience and energy, have brought into our everyday office life an atmosphere of scientific stimulation and creativity, only to be (violently) interrupted by hearty laughs. A few of the strongest moments include the deliriums in front of our velleda whiteboards, the conference submissions made just a few minutes before the deadline, as well as the philosophical discussions at the end of the day, in which we were usually rebuilding the world from scratch (alias “refaire le monde”).

At this point I would also like to warmly thank my thesis director, Badr-Eddine Benkelfat. Without his kindness, his continuous encouragement and support at all levels, this work would have been impossible. When I think of Badr-Eddine I realize that I could simply not wish for a better or friendlier thesis director.

Looking back in time, I owe a great thanks to my dear friend Stelios Sygletos, who has also been my diploma thesis tutor in the National Technical University of Athens, back in 2006. Apart from sharing with me his scientific expertise, Stelios was also a constant source of inspiration and support during the years that followed. Sometimes I

feel that if it hadn't been for Stelios transferring to me all his passion for optical communications, I would never have the chance to opt for this amazing field.

Remembering the years that followed, I would also like to thank my professors François Hache, Jean-Michel Jonathan and Nathalie Westbrook, not only for their teaching skills but also for their careful advice and help during my master's year, which was also my first year in France. Furthermore, I would also like to thank Sébastien Bigo, who has kindly offered me an internship in Alcatel-Lucent back in 2007 and who was also responsible for leading me towards my PhD at Telecom SudParis. In the same context, I also owe a great thanks to Jean-Christophe Antona, my internship tutor and a member of my thesis jury, for the various inspirational discussions that we had at the time and during the years that followed, as well as for his helpful remarks on my thesis manuscript.

Concerning my actual PhD work, I would also like to thank Gabriel Charlet, not only for leading the COHDEQ40 project - the main frame of my thesis, but also for his sharp technical suggestions, as well as his constant help and support throughout these years. Moreover, I would also like to warmly thank all my other Alcatel-Lucent colleagues with which I have interacted on technical issues, Emanuel Seve, Massimiliano Salsi, Thierry Zami, Clemens Koebele and Edouard Grellier, as their suggestions and comments helped me orientate my thoughts and reinforce my technical background. Next to that, I also owe a special thanks to our two Italian colleagues from the Parma university that I have also met in Alcatel-Lucent: my dear friend (and Linux geek fellow), Paolo Serena, for our rich technical interaction, the inspiring conversations and the open source simulation program Optilux, as well as Alberto Bononi for accepting to participate in my thesis defense jury, offering at the same time his serious and well-supported feedback on my manuscript.

From the people that I have met at Telecom SudParis, I would initially like to thank Hadjira Badaoui, the first intern partly under my supervision. Apart from her important scientific contribution, I have also appreciated her character and personality, which made working with her a great pleasure. I would also like to thank my dear friend and PhD colleague Djalal Bendimerad, who has started working in Telecom SudParis nearly at the same time as me, as well as my other PhD fellows Jordi Vuong and Aida Seck with all whom I feel extremely lucky to have shared over the past years (and still share) a wonderful interaction from both a scientific and a human point view. Furthermore, I also owe a great thanks to the computer experts of Telecom SudParis Eric Doutreleau, Jehan Procaccia and Franck Gillet for bearing my continuous complaints and offering me their help in crucial moments, as well as to my friend Lazaros Inepologlou for always managing to give me well-adapted solutions to a number of programming questions. Finally, I would like to thank my foosball pals Tony, Javier, Anis and Aymen for turning our coffee breaks into special and memorable events.

Ending up, I would like to thank my parents, relatives and friends for their continuous moral support throughout all these years, while, last but not least, I would like to thank my girlfriend Elli, to whom I dedicate this manuscript, for all her caring and understanding throughout this particularly hard period of our lives.

Contents

Acronyms 1

1 Introduction 4

2 Theoretical framework 9

2.1 Concepts of Digital communications . . . 9

2.1.1 Introduction . . . 10

2.1.2 Signal representation . . . 11

2.1.3 Digital modulation . . . 12

2.1.3.1 Amplitude Shift Keying modulation . . . 13

2.1.3.2 Phase Shift Keying modulation . . . 15

2.1.3.3 Differential encoding . . . 16

2.1.3.4 Spectral characteristics of modulated signals . . . 17

2.1.4 Systems impacted by Additive White Gaussian Noise . . . 19

2.1.4.1 Additive White Gaussian Noise and Signal-to-Noise ratio . . . 20

2.1.4.2 Signal statistics and Bit Error Probability in On-Off Keying . . . 22

2.1.4.3 Signal statistics and bit error probability in Phase Shift Keying . . . 25

2.2 Lightwave communication systems . . . 48

2.2.1 Optical fibers . . . 49

2.2.1.1 Attenuation . . . 50

2.2.1.2 Chromatic dispersion . . . 52

2.2.1.3 Polarization Mode Dispersion . . . 59

2.2.1.4 Fiber Non-linearities 61
2.2.1.5 Nonlinear Schrödinger equation 64
2.2.2 Transmitters, signal modulation and modulation formats . 66
2.2.2.1 General characteristics 67
2.2.2.2 Generation of Amplitude Shift Keying modulation 68
2.2.2.3 Generation of Binary Phase Shift Keying modulation 70
2.2.2.4 Generation of Quaternary Phase Shift Keying modulation 70
2.2.3 Signal Reception 71
2.2.3.1 Photodiodes 72
2.2.3.2 Demodulation of Amplitude Shift Keying 73
2.2.3.3 Demodulation of Differential Phase Shift Keying 74
2.2.4 Amplifiers and noise 75
2.2.5 Coherent detection in lightwave communications 78
2.2.5.1 Principle of the coherent detection 80
2.2.5.2 Phase diversity homodyne receiver 82
2.2.6 Inter-channel nonlinear impairments 85
2.2.7 Intra-channel nonlinear impairments 87
2.2.8 Fundamental limitations in fiber optic channels 89
2.2.9 Impairment mitigation 92
2.2.10 Numerical simulations 94
2.2.10.1 Introduction 94
2.2.10.2 The Split Step Fourier Method 95
2.2.10.3 Resources used for our numerical simulations . . 96

3 Investigation of M-ary sequences: application on the performance evaluation of QPSK transmission systems 98
3.1 Introduction : pseudo-random sequences 98
3.2 Finite Fields : a short review 102
3.2.1 Introduction 102
3.2.2 Prime Finite Fields and polynomials 103
3.2.3 Composite Finite Fields 105

3.3 Pseudo-random sequences: generation methods and properties . . 110
3.3.1 Generation of pseudo-random sequences: a method based on shift-registers 110
3.3.2 Properties of pseudo-random sequences 114
3.3.2.1 The autocorrelation function property 115
3.3.2.2 The window property and de Bruijn sequences . . 119
3.4 Non pseudo-random sequences 123
3.5 Performance assessment of dispersion-managed links by different sequence types 127

4 Propagation influence on the statistics of QPSK modulated signals in single-channel dispersion managed systems 133
4.1 Introduction 133
4.2 Motivations 134
4.3 Simulations setup and examples 136
4.4 Statistical measures 143
4.5 Criterion of cumulative nonlinear phase 144
4.6 Dispersion Management Optimization and constellation shape . . 150
4.6.1 Optimization of dispersion management for phase and amplitude 150
4.6.2 Global phase shift 158
4.7 The constellation shape based on the data sequences carried by the signal 165
4.7.1 Pattern-dependent nonlinear degradation 165
4.7.2 Most degraded subsequences 169
4.8 Conclusion 174

5 Conclusion 176

A Differential encoding and decoding 179

References 196

Acronyms

ASE Amplified Spontaneous Emission
ASK Amplitude Shift Keying
AWGN Additive White Gaussian Noise
BEP Bit Error Probability
BER Bit Error Rate
BPSK Binary Phase Shift Keying
CMA Constant Modulus Algorithm
CPE Carrier Phase Estimation
CW Continuous Wave
DBPSK Differential Binary Phase Shift Keying
DCF Dispersion Compensating Fibers
DD Direct Detection
DGD Differential Group Delay
DM Dispersion Management
DMGD Differential Mode Group Delay
DMPSK Differential M-ary Phase Shift Keying
DPSK Differential Phase Shift Keying
DQPSK Differential Quaternary Phase Shift Keying
DSP Digital Signal Processing
EDFA Erbium-Doped Fiber Amplifier
FEC Forward-Error Correction
FFT Fast Fourier Transform
FIR Finite Impulse Response
FWM Four Wave Mixing
GVD Group Velocity Dispersion

HM Half Mirror
i-FWM Intra-channel Four Wave Mixing
IM Intensity Modulation
ISI Inter-Symbol Interference
i-SPM Intra-channel Self Phase Modulation
i-XPM Intra-channel Cross Phase Modulation
LO Local Oscillator
MAP Maximum A Posteriori
MPSK M-ary Phase Shift Keying
MZM Mach-Zehnder Modulator
NLSE Non-Linear Schrödinger Equation
NRZ Non Return to Zero
OOK On-Off Keying
OSNR Optical Signal to Noise Ratio
PBS Polarization Beam Splitter
PDF Probability Density Function
PDM Polarization-Division Multiplexing
PLL Phase Lock Loop
PMD Polarization Mode Dispersion
PR Pseudo-Random
PRBS Pseudo-Random Binary Sequence
PRQS Pseudo-Random Quaternary Sequence
PRS Pseudo-Random Sequence
PSBT Phase Shaped Binary Transmission
PSD Power Spectrum Density
PSK Phase Shift Keying
QAM Quadrature Amplitude Modulation
QPSK Quaternary Phase Shift Keying
QWP Quaternary Wave Plate
RZ Return to Zero
SNR Signal to Noise Ratio
SPM Self Phase Modulation
SSFM Split-Step Fourier Method

WDM Wavelength-Division Multiplexing
XPM Cross Phase Modulation
XPolM Cross Polarization Modulation

Chapter 1

Introduction

"...Where is the Life we have
lost in living?
Where is the wisdom we have
lost in knowledge?
Where is the knowledge we have
lost in information?..."

T. S. Eliot, The Rock (1934)

Communications and information technologies are ubiquitous in modern societies. Talking over mobile phones, exchanging photos and videos over the Internet and researching online information, is currently a commonplace for most people. To go even further, it is often said that communications and information technologies are also radically changing the idea or form of society itself[44]. It cannot be doubted that a major part of this revolution came as a result of the dramatic increase in transmitted information capacity brought by optical fibers[5].

The cornerstone for the development of fiber-optic transmission systems was doubtless the advent of single-mode, low-loss, optical fibers[64],[65],[39],[83]. This accomplishment, accompanied by other critical advances in the domains of laser technology, nonlinear optics, etc., has given birth to the emerging domain of lightwave communications, roughly since the beginning of the 80's. During the following years, further technological innovations have increased even more the dynamics of the field. A milestone in this direction has been the development

of Erbium-Doped Fiber Amplifiers (EDFAs)[33]. EDFAs made possible the simultaneous amplification of several wavelengths, practically leading to an explosion of the installed information capacity with the birth of Wavelength-Division Multiplexing (WDM) systems. Moreover, the optical amplification itself has led to the possibility of counteracting the fiber attenuation at the cost of added noise, thus offering longer propagation distances without the need of signal regeneration.

In parallel, continuous technological advances in all sub-domains of lightwave communications were continuously pushing up capacity from the order of some Gb/s during the 80's, up to tens of Tb/s in the past decade, following an almost exponential growth[46][1]. Apart from WDM, in this "quest for capacity growth", several other technological solutions contributed in a decisive manner, such as the use of Forward-Error Correction (FEC) that can considerably increase the system noise tolerance, Raman Amplification that can increase the Signal to Noise Ratio (SNR) compared to EDFAs or Dispersion Management (DM) that increases system tolerance against nonlinear effects. Nevertheless, it cannot be doubted that a radical change in the field of optical communications came along with the appearance of a modern coherent detection implementation, based on fast electronics instead of an optical Phase Lock Loop (PLL)[107]. The main advantage of coherent receivers, in general, is the possibility to use complex modulation schemes that can offer increased spectral efficiencies. Already some years before the appearance of coherent detection, the principle of modulation and direct demodulation of Quaternary Phase Shift Keying (QPSK) (which is maybe the most typical example of a spectrally efficient modulation format) has been demonstrated in optical communication systems by the authors of [55]. However, yet another advantage of the electronics-based coherent detection was the potential use of a flexible, software-based and cost-effective signal equalization at the received end, based on a programmable Digital Signal Processing (DSP) unit. This has given the opportunity to easily take advantage of Polarization-Division

[1]Nevertheless, in the last few years, several investigations have been focusing on a forthcoming "capacity crunch" (i.e. demand for installed capacity overcoming offer), as a consequence of approaching to the fundamental capacity limits of single-mode fibers[34],[36]. One of the possible solutions to continue the increase of system capacity is the use of multi-mode or multi-core fibers.

Multiplexing (PDM) techniques, exploiting both orthogonal signal polarizations of a single-mode fiber, since the separation of the two polarization was easily achieved in the electronic domain. Furthermore, many linear impairments such as chromatic dispersion or Polarization Mode Dispersion (PMD) were also shown to be compensated in a cost-effective and flexible way, in the electronic domain.

In the context of this thesis which began in 2008, we have focused on the problem of *terrestrial* long-haul or ultra-long haul communications, i.e. the problem of setting up a transmission link where the involved distances have an order of magnitude of about 200 up to 900 km (long-haul) or 1000 up to 5000 km (ultra long haul), where the propagated distance between two amplifiers is usually about 100 km[40].

Furthermore, we have adopted an axis that was primarily based on two of the aforementioned techniques, i.e. *dispersion management* and *coherent detection*, investigating the nonlinear degradation of both signal quadratures (i.e. phase and amplitude), instead of just amplitude, that was the case for most investigations concerning On-Off Keying (OOK) modulation. While linear degradation caused by chromatic dispersion can be easily compensated by a simple use of Dispersion Compensating Fiberss (DCFs), the technique of *dispersion management* consists of wisely distributing DCFs throughout the line, in order to reduce the degradation caused by nonlinear effects. However, the possibility of coherent receivers to electronically compensate dispersion together with nonlinearity issues, encouraged tin some cases he abandoning of dispersion management schemes with in-line dispersion compensation. Nevertheless, in many terrestrial networks, dispersion management comes as a legacy of existing fiber infrastructure that we wish to "upgrade", by a simple adjustment of terminal devices. Alternatively, one may consider dispersion management as a technique that may be used *in addition* or in parallel to coherent receiver algorithms, as an extra force against nonlinearities. As a result, throughout this manuscript we have adopted a vision where in all cases we consider systems with a variable dispersion management that may also benefit from a coherent receiver and a DSP unit.

More precisely, based on numerical simulations of principally single-channel 40 Gb/s QPSK transmission, we were motivated in addressing the following

questions: (1) understand the physics behind nonlinear propagation of QPSK-modulated signals in the context of a variable dispersion management, compared to OOK-modulated signals in the same context (2) understand the possible influence of adapted correction algorithms as a function of the different degradation patterns resulting from different dispersion management schemes.

In chapter §2 we present general, introductory notions, of digital communications and classical fiber optics. As the extended use of digital communications concepts into the domain of fiber-optics is relatively new (for example multi-level modulation is relatively new to fiber optic communications, since the domain was almost entirely dominated by OOK/direct detection schemes), we attempt to clarify the theoretical basis of the two domains.

In chapter §3 we address the problem of using multi-level Pseudo-Random Sequences (PRSs) in numerical simulations instead of adapted versions of Pseudo-Random Binary Sequences (PRBSs), when dealing with multi-level modulation formats. Since PRSs present a particular interest in various other areas of telecommunications, their generation process and properties have been thoroughly studied since the 1950s. However, to the best of the author's knowledge, the information concerning the generation of multi-level PRSs as well as the exact definition of their properties, is quite scattered within the existing bibliography. For reasons of clarity, we first systematically review all the underlying theory behind these special sequences, based on the theory of Finite Fields. Furthermore, since *non*-PRSs are very commonly used for numerical simulations or laboratory experiments, we also present simple numerical tools that can be used to characterize these non-PRSs with respect to their "pseudo-random characteristics". Finally, we present numerical simulation results that support the necessity of using Pseudo-Random Quaternary Sequences (PRQSs) in the context of QPSK modulation, revealing in parallel, the special system configurations for which the usage of PRQSs is most critical.

Finally, the section §4 is dedicated to the investigation of the nonlinear propagation of QPSK-modulated signals, in the context of 40 Gb/s, single-channel transmission, with a variable dispersion management. Our first goal was to verify the validity of laws, developed in the context of OOK modulated signals,

either for the optimization of the dispersion management[43], [67], or for the performance assessment of systems with an optimized dispersion management[9]. In all cases we have decoupled the transmission from the reception and our numerical results were mostly based on the complex signal statistics (of both amplitude and phase), instead of a simple Bit Error Rate (BER). Furthermore, we have thoroughly investigated the variation of these statistics for a variable dispersion management, as well as the relative variation or correlation between the degradation of the amplitude and phase quadratures, that results in constellations of very different shapes. Finally, since the degradation of signals in a single-channel transmission comes in part from Inter-Symbol Interference (ISI), we have employed a phenomenological analysis, focusing this time on the statistics of the complex samples of isolated symbols, grouped with respect to the data carried by their neighboring symbols. This approach elucidates the mechanism of ISI in the context of QPSK-modulation with dispersion management and reveals the possibilities of an adapted algorithm that can compensate for signal distortion.

Chapter 2

Theoretical framework

> Everything should be as simple
> as it is, but not simpler.
>
> Albert Einstein

In this chapter we review the fundamental theoretical background used throughout this manuscript. For reasons of clarity, the chapter is divided in two sections. In the first section, we review some fundamental mathematical concepts of digital communications that apply to all communication systems, without any reference to how these concepts are implemented in optics. Such concepts, such as complex modulation formats, have been widely used in the past in a context of wireless communications, but they have been only recently introduced in the fiber optics domain. In the second section we review the physics and the special characteristics of the optical fiber communication channel.

2.1 Concepts of Digital communications

The field of digital communications has been rapidly developing throughout the last century, principally driven by the explosion of communication networks. At the basis of all communication scenarios, lies the capacity of transmitting information between the different entities of a communication network, principally using two modes of communication: transmitting information *from one point* (i.e. node of a network, user, entity etc) *to multiple other points*, often referred to as

broadcasting, or alternatively transmitting information *from one point to another* (i.e. from one user to another or from one network node to another etc), often referred to as *point-to-point* communication. In what follows we are exclusively focusing on a *point-to-point* communication context.

2.1.1 Introduction

Point-to-point digital communication systems are often schematically represented using the structured (or layered) view of figure 2.1, with arrows representing the flow of information. The message to be transmitted, is initially converted into a *bit sequence* by the input *transducer*. Next, this sequence is further transformed into a new bit sequence by the *source encoder* that reduces the number of bits compressing the data, while the *channel encoder* increases the number of bits, adding a redundancy that allows for an error correction at the receiver side. Finally, the *modulator* maps the bit stream into waveforms and the waveforms are transmitted into the *channel*. At the receiver end, the inverse procedure is followed, with waveforms being initially mapped back into bits, and bits passing from the *channel decoder*, the *source decoder* and finally the output transducer, eventually recovering the transmitted sequence, if the passage from the channel was error free.

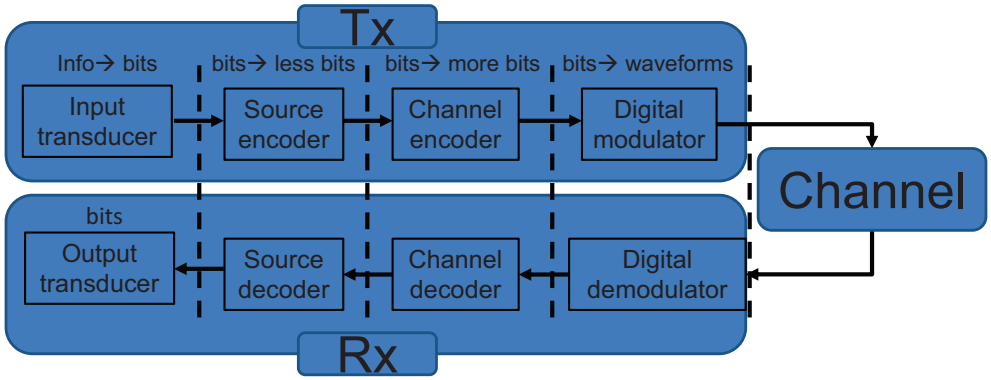

Figure 2.1: Coherent detection principle

With the structured representation we achieve the decomposition of the communication problem into independent, or semi-independent sub-problems. In this

manuscript we only refer to problems associated with the last two layers, i.e. the problem of digital modulation/demodulation and the problem of signal transmission in the channel, that is the fiber-optic channel in our case, supposing in all cases that the bit sequence $\{Ib_n\}$ enters the digital modulator layer.

Depending on the choice of the modulation format, the *bit sequence* $\{Ib_n\}$ may by alternatively represented as a *symbol sequence* $\{Is_n\}$, by considering blocks of $k = \log_2 M$ bits and substituting each block with its decimal equivalent, i.e. decimal numbers in the range $\{0, 1, ..., M-1\}$. Then, the symbol sequence $\{Is_n\}$ is transformed into the *waveform sequence* $\{I_n\}$ by mapping each symbol into one of the M possible waveforms.

As it is the case in most communication channels, the single-mode fiber-optic channel exhibits a limited bandwidth of about 0.4 μm (or 50 THz) around the telecommunication wavelength 1.55 μm (or 193 THz)[1]. As a consequence, the waveforms chosen to represent the data are in most cases band-limited, modulated signals, i.e. signals with a limited frequency extent, centered around the carrier frequency, with the carrier frequency residing inside the channel bandwidth.

2.1.2 Signal representation

Let $g(t)$ denote a bandpass signal with a central frequency f_c and a Fourier transform

$$G(f) = \int_{-\infty}^{+\infty} g(t) e^{-j2\pi ft} dt \tag{2.1}$$

or inversely

$$g(t) = \int_{-\infty}^{+\infty} G(f) e^{j2\pi ft} df \tag{2.2}$$

The signal $g(t)$ is linked to its *complex envelope*, i.e. its low-pass equivalent $\tilde{g}(t)$, by the relation

$$g(t) = \mathrm{Re}\left[\tilde{g}(t) e^{j2\pi f_c t}\right] \tag{2.3}$$

[1]This bandwidth is mainly fixed by the wavelength window where the absorption of step-index silica fibers is minimal as it will be discussed in section §2.2.1.1.

, or equivalently in the Fourier domain

$$G(f) = \frac{1}{2}\left[\tilde{G}(f - f_c) + \tilde{G}^*(-f - f_c)\right] \tag{2.4}$$

$\tilde{g}(t)$ is generally a complex function described as

$$\tilde{g}(t) = x(t) + jy(t) = a(t)\exp(j\theta(t)) \tag{2.5}$$

and $a(t), \theta(t), x(t), y(y)$ are real functions of t.

Since the modulated signal can be sufficiently described it terms of its complex envelope and the modulation frequency, in the following, we may just refer to the complex envelope $\tilde{g}(t)$ of the signal.

2.1.3 Digital modulation

Suppose that we want to transmit the symbol sequence $Is_n = \{Is_1, Is_2, ..., Is_{L_{seq}}\}$. Mapping the symbols of Is_n into digital waveforms, yields the information bearing sequence $I_n = \{I_1, I_2, ..., I_{L_{seq}}\}$. The baseband equivalent of the overall waveform entering the channel $\tilde{g}(t)$ can be expressed as a sum of partial baseband waveforms $\tilde{g}_n(t), n = 1, 2..., L_{seq}$, one for each of the L_{seq} transmitted symbols[89], often referred to as *pulses*, or mathematically

$$\tilde{g}(t) = \sum_{n=1}^{L_{seq}} \tilde{g}_n(t) \tag{2.6}$$

where $\tilde{g}_n(t)$ is the pulse corresponding to the n$^{\text{th}}$ transmitted symbol. Going further, $\tilde{g}_n(t)$ can be written as

$$\tilde{g}_n(t) = I_n p(t - nT) \tag{2.7}$$

, where $R = 1/T$ is the symbol rate and $p(t)$ is often referred to as the *shape-forming pulse*, whose choice is generally a part of the system design and optimization. Nevertheless, for reasons of simplicity, in what follows, we consider that $p(t)$ is the rectangular or gate function, i.e. $p(t) = rect(t/T)$[1], defined as

[1]Even in practice, $p(t)$ is not very different from $rect(t)$. Since $rect(t)$ is not practically realizable we are looking for a pulse shape that is practically realizable and not very different from the 'ideal" for of $rect(t)$.

$$rect(t) = \begin{cases} 1, -\frac{1}{2} \leq t \leq \frac{1}{2} \\ 0, \text{elsewhere} \end{cases} \tag{2.8}$$

Having chosen an appropriate pulse-shaping function, mapping from the sequence $\{Is_n\}$ to the sequence $\{I_n\}$ is the problem of choosing a modulation format. In the following we present the two families of modulation formats, used throughout this manuscript, i.e. Amplitude Shift Keying (ASK) and Phase Shift Keying (PSK). In both cases, the complex envelope of each transmitted symbol can be written in the form

$$\tilde{g}_n(t) = A_m \cdot p(t),\ m = 0, 1, ..., M-1 \tag{2.9}$$

, where A_m is defined in the following paragraphs.

2.1.3.1 Amplitude Shift Keying modulation

In ASK modulation, we map each transmitted symbol into a discrete *amplitude level*, i.e. in equation (2.9), each A_m corresponds to a discrete *real* number. In other words, the waveform of each symbol is a constant signal with an amplitude level defined by A_m. We also usually refer to the different A_m as the ASK *states*. The simplest way to chose A_m is to set

$$A_m = m \cdot A,\ m = 0, 1, ..., M-1 \tag{2.10}$$

,where A is a fixed difference between amplitudes with a consecutive m. Setting $M = 2$ to eq. (2.10), we get a set of two amplitude levels, $\{0, A\}$, resulting in the simplest and most widely used modulation format in optical communications, the 2-ASK or more simply On-Off Keying (OOK). In effect, with this modulation format we transmit a signal for the symbol "1" or nothing for the symbol "0", as shown in figure 2.2a.

In a different scenario, amplitude levels can be chosen so that they are symmetric with respect to zero, i.e.

$$A_m = (2m + 1 - M)\frac{A}{2},\ m = 0, 1, ..., M-1 \tag{2.11}$$

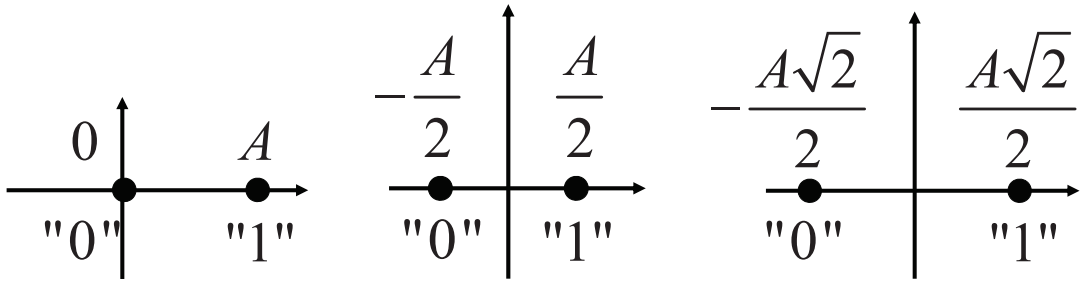

(a) Constellation for OOK modulation.

(b) Constellation for symmetric 2-ASK modulation.

(c) Constellation for symmetric 2-ASK modulation with same average power as OOK.

Figure 2.2: Comparison of different 2-ASK scenarios.

In this case, a signal with a non-zero amplitude is transmitted for all possible symbols. Setting in eq. (2.11) $M = 2$ results in a "symmetric" 2-ASK, with a constellation shown in figure 2.2b.

It is important to note that if the two symbols ("0" or "1") have an equal probability of appearance, the average signal power[1] in the first scenario is $\frac{A^2}{2}$, while in the second scenario it is $\frac{A^2}{4}$, while the distance between the two symbols is kept constant and equal to A. "Normalizing" the second scenario to the average power of the first, results in a signal with a distance of $\sqrt{2}A$ between the two levels, as shown in figure 2.2c. It is obvious that since the two symbols are separated by a greater distance between the two levels, a greater tolerance is achieved against degradation effects like noise. This tolerance is going to be quantified in a following section for the simple degradation form of additive white Gaussian noise.

We should also note that, in practice, the mapping from symbols to amplitude levels is slightly different than the one of equations (2.10) and (2.11). In fact, the mapping may chosen in such a way that neighboring symbols differ to only one bit, so that mistaking a symbol for one of its neighboring ones will only yield a single bit error. This mapping is called *Gray encoding*[89].

[1] As it is going to be discussed in following sections, the average signal power is an indicator of the penalties due to nonlinear degradations: in general, higher average signal power yields a higher penalty due to nonlinearities. Therefore, it is very common to compare modulation formats in the common basis of an equal average power[45].

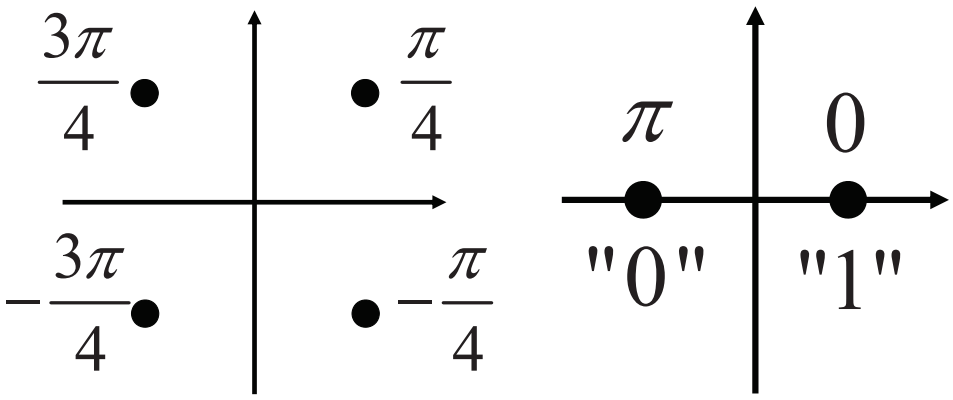

(a) Constellation for QPSK modulation.

(b) Constellation for BPSK modulation.

Figure 2.3: Constellations of PSK modulation formats.

In conclusion, amplitude modulation consists of mapping the symbol sequence $Is_n = \{Is_1, Is_2, ...\}$, where $Is_n \in \{0, 1, ..., M-1\}$, into the waveform sequence $I_n = \{I_1, I_2, ...\}$, where $I_n = A_{Is_n} p(t)$.

2.1.3.2 Phase Shift Keying modulation

In PSK modulation, we map each symbol into a discrete *phase level*, i.e. in equation (2.9), each A_m gets a discrete *imaginary* value, with one discrete phase level out of the M such possible levels, i.e.

$$A_m = e^{j \cdot \left(m \frac{2\pi}{M} + \theta_0\right)}, \; m = 0, 1, ..., M-1 \tag{2.12}$$

, where θ_0 is a fixed phase offset. PSK modulation with phase levels (or M discrete states) is also often referred to as M-ary Phase Shift Keying (MPSK).

Equivalently, the symbol sequence $I_s = \{Is_1, Is_2, ...\}$, where $Is_n \in \{0, 1, ..., M-1\}$ is mapped to the waveform sequence $I = \{I_1, I_2, ...\}$, where $I_n = A_m \cdot p(t)$.

Similar to ASK, Gray encoding is also used in PSK to ensure that adjacent phase levels are mapped from symbols that differ to only 1 bit. A constellation example for 4-PSK, (also widely known as QPSK), with Gray encoding is shown in figure 2.3a. A constellation example for 2-PSK or BPSK, is shown in figure 2.3b. As it can be noticed, 2-ASK and 2-PSK practically result in the same

format. In the context of this manuscript we will primarily focus on the QPSK modulation format.

2.1.3.3 Differential encoding

For reasons that will become clear in section §2.1.4, in many cases, instead of coding information on an absolute amplitude or phase level, information is coded in the amplitude or phase *difference* between two adjacent symbols. In this case, we refer to *differential* modulation or modulation *with memory*, since the sequence symbols are correlated. In effect, the initial information sequence is transformed into a new sequence, often referred to as *(differentially) pre-coded sequence*.

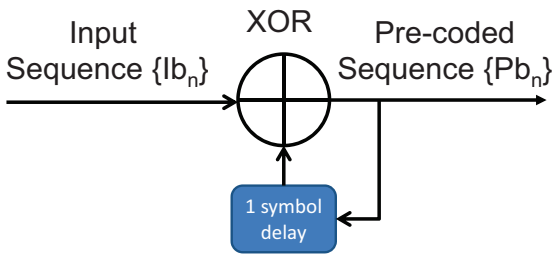

Figure 2.4: Generation of pre-coding sequence in DBPSK

In DBPSK for example, given the initial binary sequence $\{Ib_n\}$, the generation of the pre-coded sequence $\{Pb_n\}$ is achieved by the circuit shown in figure 2.4. Alternatively, the pre-coding operation may be simply described by the equation[102]

$$Pb_n = Ib_n \oplus Pb_{n-1} \tag{2.13}$$

, where the symbol $\oplus$ represents an addition modulo 2 (i.e. a port XOR). In other words, if the new symbol to be transmitted is identical to the one transmitted in the previous slot we transmit a "0", whereas if the symbol is different we transmit a "1". In Differential Quaternary Phase Shift Keying (DQPSK), precoding can be achieved in the exact same way, representing quaternary symbols as couples of bits, i.e. $\{00, 01, 10, 11\}$ and performing the modulo 2 addition bitwise. On the other hand, supposing that the sequence arriving at the receiver side is the sequence $\{Rb_n\}$, in order to recover the initially transmitted sequence (if no

errors occurred during transmission) the same XOR operator must be emulated between adjacent symbols, i.e.

$$Db_n = Rb_n \oplus Rb_{n-1} \tag{2.14}$$

In optical communications however, the pre-coding operation for DQPSK is slightly more complex[1]. The input binary sequence $\{Ib_n\}$ is first split in two sequences $\{IP_k\}$ and Q_k of half the length of $\{Ib_n\}$. For example, we may assign to $\{IP_k\}$ the odd bits of $\{Ib_n\}$, i.e. $\{IP_k\} = \{Ib_{2k-1}\}$, and to Q_k the even bits of $\{Ib_n\}$, i.e.$\{Q_k\} = \{Ib_{2k}\}$, where $k = 1, 2, ...$ Each couple (IP_k, Q_k) represents a quaternary symbol of the new quaternary sequence $\{Is_k\}$. Pre-coding consists of converting the sequence $\text{Is}_k = (IP_k, Q_k)$ into a new sequence $Ps_k = (U_k, V_k)$, where[55]

$$\begin{aligned} U_k &= \overline{(IP_k \oplus Q_k)} \cdot (IP_k \oplus U_{k-1}) + (IP_k \oplus Q_k) \cdot (Q_k \oplus V_{k-1}) \\ V_k &= \overline{(IP_k \oplus Q_k)} \cdot (IP_k \oplus V_{k-1}) + (IP_k \oplus Q_k) \cdot (Q_k \oplus U_{k-1}) \end{aligned} \tag{2.15}$$

We need to underline that since pre-coding maps the initial sequence $\{Ib_n\}$ into a new sequence $\{Pb_n\}$, it also, in general, modifies the statistics of the information sequence $\{Ib_n\}$. Furthermore, as the initial sequence is modified, the detection (demodulation) of differentially encoded signals in optical communications, involves special circuits that ensure the recovering of the initial information sequence, as it is going to be detailed in section §2.2.3.3.

2.1.3.4 Spectral characteristics of modulated signals

Since the modulated signal is transmitted in a band-pass channel, it is fundamental to study its spectral characteristics. As we can note from equation (2.7), the waveform sequence I is based on the random input symbol sequence Is and therefore the resulting modulated signal is a stochastic process.

Consider now that $g(t)$ in equation (2.3) is a sample function of the overall stochastic process. With the additional assumptions that $g(t)$ is a wide-sense sta-

[1] We describe the pre-coding operation that was introduced in optical communications by the authors of [55]. The demodulation, also performed in optics, in shown in the same paper.

tionary processes with a zero mean[1], it can be shown[89] that the autocorrelation functions of the modulated and band-pass signal are linked with the relation

$$\phi_{gg}(\tau) = \mathrm{Re}\left[\phi_{\tilde{g}\tilde{g}}(\tau)e^{j2\pi f_c\tau}\right] \tag{2.16}$$

, or equivalently, their Power Spectrum Density (PSD) with the relation

$$\Phi_{gg}(f) = \frac{1}{2}\left[\Phi_{\tilde{g}\tilde{g}}(f-f_c) + \Phi_{\tilde{g}\tilde{g}}(-f-f_c)\right] \tag{2.17}$$

As it is evident from the above, the PSD of the modulated signal can be uniquely determined by the PSD $\Phi_{\tilde{g}\tilde{g}}(f)$ of the low-pass signal $\tilde{g}(t)$. As $\tilde{g}(t)$ is a function of the information sequence I_n, in order to go further we need to make an assumption over the statistics of the information sequence Is_n and therefore, over the waveform sequence I. More precisely we suppose that the information sequence I_n is a wide-sense stationary process[2], with a mean value

$$\mu_i = E\left[I_n\right] \tag{2.18}$$

and an autocorrelation function

$$\phi_{ii}\left(m\right) = \frac{1}{2}E\left[I_n^* I_{m+n}\right] \tag{2.19}$$

The autocorrelation function of $\tilde{g}(t)$ is defined as

$$\phi_{\tilde{g}\tilde{g}}(t+\tau,t) = \frac{1}{2}E\left[\tilde{g}^*(t)\tilde{g}(t+\tau)\right] \tag{2.20}$$

and using equations (2.19), (2.6) and (2.7) it can be shown that $\tilde{g}(t)$ is a cyclostationary process with power spectral density

$$\bar{\Phi}_{\tilde{g}\tilde{g}}\left(f\right) = \frac{1}{T}\Phi_{ii}\left(f\right)\left|P(f)\right|^2 \tag{2.21}$$

, where the PSD Φ_{ii} of the information sequence $\{I_n\}$ is defined as

[1] A wide-sense stationary stochastic process $X(t)$ has a fixed mean value (independent of t) and an autocorrelation function $E\left[X(t_1), X(t_2)\right] = \varphi\left(t_1, t_2\right) = \varphi\left(t_1 - t_2\right) = \varphi\left(\tau\right)$.

[2] i.e. the mean value is time-independent and for the autocorrelation function holds $\varphi(t_1, t_2) = \varphi(t_1 - t_2) = \varphi(\tau)$[56]. A detailed discussion and a demonstration in the context of pseudo-random is going to be shown in chapter §3.

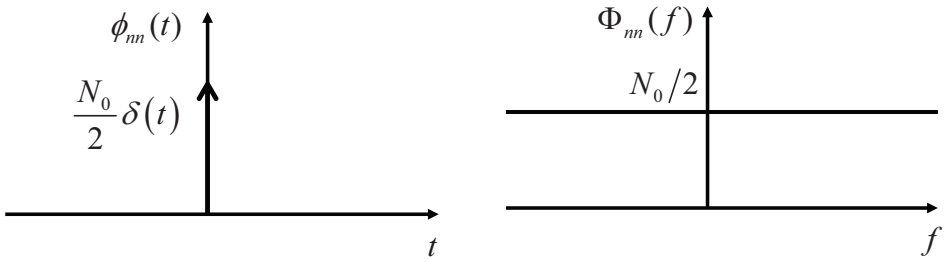

(a) [Autocorrelation function of white noise.

(b) PSD.

Figure 2.5: Characteristics of AWGN.

$$\Phi_{ii}(f) = \sum_{k=-\infty}^{+\infty} \varphi_{ii}(k) \cdot e^{-2\pi f k T} \tag{2.22}$$

and $P(f)$ is the Fourier transform of the pulse-shaping function $p(t)$.

As it can be easily seen from equation(2.21) that $\bar{\Phi}_{\tilde{g}\tilde{g}}(f)$ depends on both the pulse-shaping function $p(t)$ and the correlation characteristics of the information sequence, expressed via the term Φ_{ii}.

2.1.4 Systems impacted by Additive White Gaussian Noise

The term "noise" is used to designate spontaneous fluctuations of the quantity used to transfer the information in our transmission system. As it is going to be discussed in §2.2, the two major sources of signal distortion in optical communication systems are *noise* and *fiber nonlinearities*. The combined result of these distortions is often referred to in the literature as "non-linear phase noise"[1].

Focusing on noise, however, it may be shown that the dominant source of noise is spontaneous emission noise, added by amplifiers (discussed with more details in §2.2.4), a noise source that can be adequately described by the notion of AWGN as shown in [50].

[1]Linear effects like chromatic dispersion also introduce a signal distortion, but when they act alone they are easily compensated. By nonlinearities we refer to the interplay between linear and nonlinear effects.

In the following sections, we describe the properties of AWGN and we focus on the degradation purely coming from an AWGN. Being primarily interested in the two modulation formats reviewed in section §2.1.3 (i.e. ASK and PSK), in the following sections we derive the statistics of the signal cylindrical quadratures (i.e. amplitude and phase) in the presence of AWGN. More precisely, we derive their corresponding Probability Density Functions (PDFs), we calculate their first moments and we, finally, derive the bit error probabilities for ASK or PSK modulation.

2.1.4.1 Additive White Gaussian Noise and Signal-to-Noise ratio

Denoting by $n(t)$ the stochastic AWGN process with a zero mean, $n(t)$ is defined via its autocorrelation function (figure 2.5a)

$$\varphi_{nn}(\tau) = \frac{\mathrm{N}_0}{2}\delta(\tau) \tag{2.23}$$

, or equivalently by it power spectral density (figure 2.5b)

$$\Phi_{nn}(f) = \frac{\mathrm{N}_0}{2} \tag{2.24}$$

, where N_0 is given in W/Hz. We note that AWGN has a flat spectrum density for all frequencies and an autocorrelation function corresponding to a Dirac function. These characteristics are linked to completely random processes. In chapter §3 we will see that pseudo-random sequences have properties that are very similar to the properties of AWGN, even though they are sequences created in a deterministic way.

Considering that an AWGN is applied to an ideal low pass filter of bandwidth W, the resulting stochastic process $N(t)$ will be characterized by a new couple of PSD and autocorrelation, given by

$$\Phi_{NN}(f) = \begin{cases} \frac{N_0}{2}, -W < f < W \\ 0, otherwise \end{cases} \tag{2.25}$$

$$\varphi_{NN}(\tau) = N_0 W \sin c(2W\tau) \tag{2.26}$$

The variance σ_N^2 of the noise samples, being equal to the expected value of the noise power (since the process mean is zero) is given by the relation

$$\sigma_{\mathrm{N}}^2 = E\left[N^2\right] = \varphi_{NN}(0) = N_0 W \tag{2.27}$$

When a (low-pass) signal $\tilde{g}(t)$ is impacted by an AWGN $n(t)$, the resulting signal $\tilde{r}(t)$ may be written as

$$r(t) = \tilde{g}(t) + n(t) \tag{2.28}$$

, where $n(t) = x(t) + j \cdot y(t)$ is the complex sample function of the AWGN process with its two components $x(t)$ and $y(t)$, i.e. the in-phase and the quadrature noise component correspondingly, are jointly Gaussian real random variables AWGN processes with the characteristics of each being described by the equations (2.23), (2.24).

In such a case, denoting with $P = A^2$ the signal average power, the Signal to Noise Ratio (SNR), (denoted as ρ in what follows), is defined as

$$\rho = \frac{A^2}{2\sigma^2} = \frac{P}{2\sigma^2} = \frac{P}{WN_0} \tag{2.29}$$

Let X and Y be the identically distributed random variables of the sample functions $x(t)$ and $y(t)$. More precisely,

$$p_X(x) = \frac{1}{\sqrt{2\pi}\sigma} e^{-\frac{x^2}{2\sigma^2}} \tag{2.30}$$

Setting $A = X^2$ the PDF of A reads:

$$p_A(a) = \frac{1}{\sqrt{2\pi a}\sigma} e^{-\frac{a}{2\sigma^2}} \tag{2.31}$$

The characteristic function of A is given by:

$$\psi_A(iu) = E\left[e^{iuA}\right] = f\left\{p_A(a)\right\} = \frac{1}{\sqrt{1 - i2u\sigma^2}} \tag{2.32}$$

Defining a new random variable that describes the optical power of the signal S with $S = R^2 = X^2 + Y^2$ and as X and Y are identically distributed, we get

$$\psi_S(iu) = \frac{1}{1 - i2u\sigma^2} \tag{2.33}$$

and

$$p_S(s) = \frac{e^{-\frac{s}{2\sigma^2}}}{2\sigma^2} \tag{2.34}$$

The distribution of the equation (2.34) is also known as *chi-square* distribution with two degrees of freedom. This distribution is very useful in optical communications, since the photocurrent is directly proportional to the optical power (see section §2.2.3.1). Therefore, the received photo-current after a cascade of additive white Gaussian noise sources, is going to follow a chi-square distribution.

Finally, defining the complex modulus $R = \sqrt{S}$ and using (2.34) we get the pdf of R:

$$p_R(r) = r \cdot \frac{e^{-\frac{r^2}{2\sigma^2}}}{\sigma^2} \tag{2.35}$$

On the other hand, by defining $\Theta = tan^{-1}\left(\frac{Y}{X}\right)$ and noting that X and Y are identically distributed, we get that Θ is uniformly distributed in $[0, 2\pi]$, or

$$p_\Theta(\theta) = \frac{1}{2\pi} \tag{2.36}$$

An alternative way of calculating the PDFs of R and Θ is to consider the joint distribution of X and Y, i.e. $p_{X,Y}(x,y) = \frac{1}{2\pi\sigma}e^{-\frac{x^2+y^2}{2\sigma^2}}$, if we perform a variable change with $R = \sqrt{X^2+Y^2}$ and $\Theta = tan^{-1}\left(\frac{Y}{X}\right)$ we finally get that $p_{R,\Theta}(r,\theta) = \frac{r}{2\pi\sigma^2}e^{-\frac{r^2}{2\sigma^2}}$ and consequently we get the equations (2.35) and (2.36).

2.1.4.2 Signal statistics and Bit Error Probability in On-Off Keying

In OOK modulation, as presented in §2.1.3.1, the possible symbols are mapped into two distinct amplitude levels, named x_0 and x_1. The bit error probability in this case is given by

$$BEP = p(0) \cdot P(1/0) + p(1) \cdot P(0/1) \tag{2.37}$$

, where $p(0)$, $p(1)$ are the probabilities of initially transmitting a "0" or a "1" and $P(1/0)$, $P(0/1)$ are the probabilities of falsely detecting a "1" and falsely detecting a "0" correspondingly. If "0"s and "1"s are transmitted with the same probability, equation (2.37) becomes

$$BEP = \frac{1}{2}\left(P(1/0) + P(0/1)\right) \tag{2.38}$$

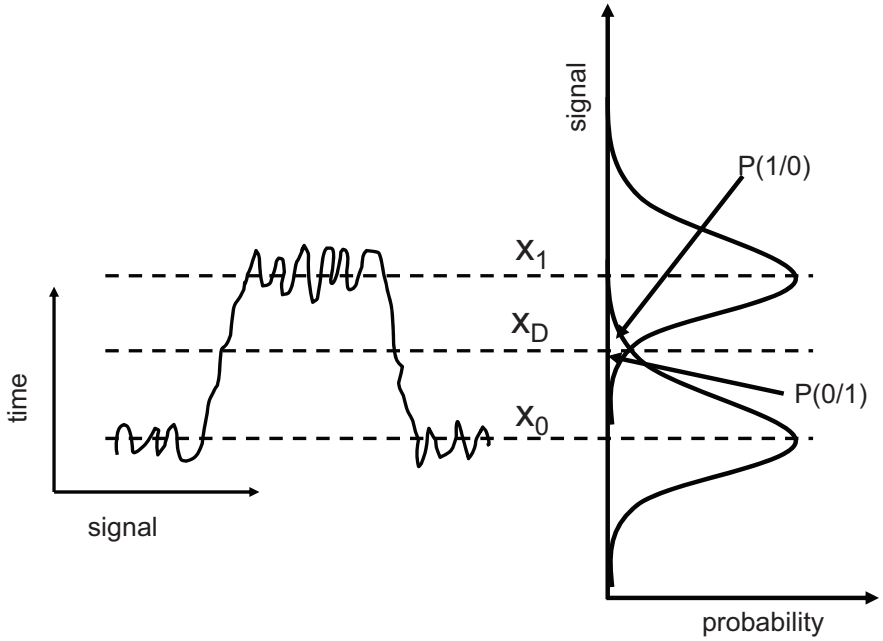

Figure 2.6: Q factor

Assuming an AWGN, the PDF of level "1" can be described by the relation

$$p_1(x) = \frac{1}{\sqrt{2\pi}\sigma_1} e^{-\frac{(x-x_1)^2}{2\sigma_1^2}} \tag{2.39}$$

, while the PDF of level "0" is described by the relation

$$p_0(x) = \frac{1}{\sqrt{2\pi}\sigma_0} e^{-\frac{(x-x_0)^2}{2\sigma_0^2}} \tag{2.40}$$

, where σ_0 and σ_1 are the standard deviations of level "0" and level "1" correspondingly.

Supposing that the decision threshold is set to x_D as shown in figure 2.6 and using equations (2.39) and (2.40), the error probabilities $P(1/0)$ and $P(0/1)$ are calculated as

$$P(1/0) = \int_{x_D}^{+\infty} p_0(x)dx = \frac{1}{2} erfc\left(\frac{x_D - x_0}{\sqrt{2}\sigma_0}\right) \tag{2.41}$$

and

$$P(0/1) = \int_{-\infty}^{x_D} p_1(x)dx = \frac{1}{2} erfc\left(\frac{x_1 - x_D}{\sqrt{2}\sigma_1}\right) \tag{2.42}$$

Finally, combining the equations (2.38), (2.41) and (2.42), the bit error probability reads

$$BEP(x_D) = \frac{1}{4}\left(erfc\left(\frac{x_1 - x_D}{\sqrt{2}\sigma_1}\right) + erfc\left(\frac{x_D - x_0}{\sqrt{2}\sigma_0}\right)\right) \tag{2.43}$$

As it is evident from the equation (2.43), the Bit Error Probability (BEP) depends on the threshold x_D and it is minimized when $BEP'(x_D) = 0$. Solving the equation $BEP'(x_D) = 0$ for the optimal threshold x_D and supposing that $\ln \frac{\sigma_1}{\sigma_0} \approx 0$ we get

$$x_D = \frac{\sigma_0 x_1 + \sigma_1 \mathrm{x}_0}{\sigma_0 + \sigma_1} \tag{2.44}$$

Defining the Q *factor* as

$$\frac{(x_D - x_0)}{\sigma_0} = \frac{(x_1 - x_D)}{\sigma_1} \triangleq Q \tag{2.45}$$

and substituting (2.44) into (2.45) we finally get

$$Q = \frac{x_1 - x_0}{\sigma_0 + \sigma_1} \tag{2.46}$$

Q is directly proportional to the separation of the levels averages $x_1 - x_0$, while it is inversely proportional to the sum of their noise standard deviations σ_0 and σ_1. At the same time, we intuitively expect that the bit error rate will be high when the levels are close to each other, or/and when the noise variance in each level increases.

In effect, by setting the threshold to its optimal value of eq. (2.44), or equivalently replacing (2.45) into (2.43), we get an expression linking bijectively the Q factor to the bit error probability[1]

$$BEP = \frac{1}{2} erfc\left(\frac{Q}{\sqrt{2}}\right) \tag{2.47}$$

In conclusion, with the above procedure, we can analytically link the BEP of an OOK transmission system corrupted by AWGN to the Q factor. We have to underline that the above analysis is accurate *only* in the context of OOK modulation and when the system is impacted *only* by AWGN. In optical communications, as it will be briefly discussed in §2.2.3.1, photo-current noise may be assumed to have Gaussian statistics and therefore, this analysis is quite accurate for back-to-back measurements, employing OOK modulation. However, when a transmission line is present, the amplified spontaneous emission noise generated by the amplifiers overwhelms the shot or thermal noise and, as noted before, the optical power and therefore the photocurrent, follow a chi-square distribution.

Nevertheless, since the Q factor is linked to the BEP bijectively, for comparison reasons, in many cases we convert measured bit error probabilities for arbitrary modulation formats, into a "fake" Q factor by taking the inverse function of (2.47), i.e.

$$Q = \sqrt{2} \cdot erfc^{-1}\left(2 \cdot BEP\right) \tag{2.48}$$

In the rest of this manuscript, when we refer to a Q factor we implicitly mean the "fake" Q factor defined by the equation (2.48).

2.1.4.3 Signal statistics and bit error probability in Phase Shift Keying

Without loss of generality we may consider that the equivalent low pass signal corresponding to one state of a PSK signal, in a system impacted by AWGN is

[1] A distinction has to be made between the *Q function*, commonly used in the digital communications literature, and the *Q factor*. The Q function, is defined as $Q(x) = \frac{1}{2} erfc(\frac{x}{\sqrt{2}})$ and it may be used to simplify the expressions of bit error rates. It may also be used to link the BEP to the Q factor but this is not done here for reasons of clarity. As a consequence, in this manuscript we are always using the letter "Q" to refer to the Q factor.

described by the relation[1]

$$S = A + N \tag{2.49}$$

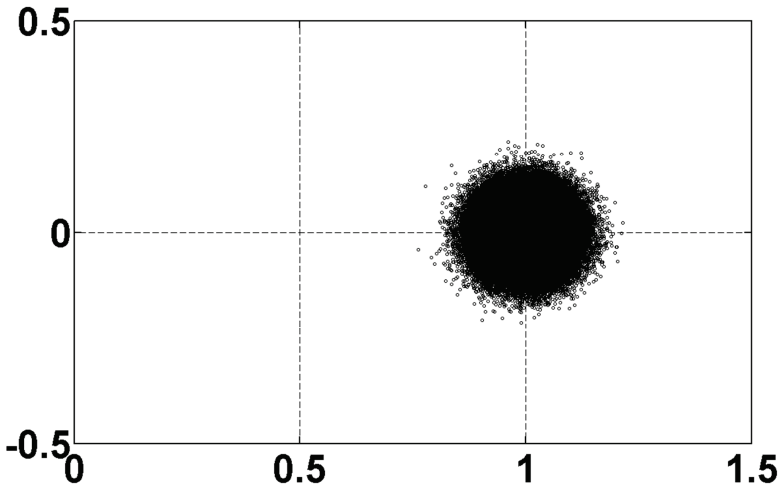

Figure 2.7: CW + noise

, where A is a real fixed number and N represents the AWGN along the two signal quadratures with $N = N_1 + j \cdot N_2$, N_1 and N_2 being identically distributed, Gaussian Random variables with zero mean and standard deviation σ (figure 2.7). The received signal vector may then be represented by a new complex random variable: $S = A + N_1 + jN_2 = X + jY$, with PDFs of the real and imaginary part given by

$$p_X(x) = \frac{1}{\sqrt{2\pi}\sigma} e^{-\frac{(x-A)^2}{2\sigma^2}} \tag{2.50}$$

$$p_Y(y) = \frac{1}{\sqrt{2\pi}\sigma} e^{-\frac{y^2}{2\sigma^2}} \tag{2.51}$$

, and a joint PDF of X and Y given by:

$$p_{X,Y}(x,y) = \frac{1}{2\pi\sigma^2} e^{-\frac{(x-A)^2+y^2}{2\sigma^2}} \tag{2.52}$$

[1] In the following we follow the procedure and present results appearing in [19] and [58]

Passing to polar coordinates by defining

$$R = \sqrt{X^2 + Y^2} \tag{2.53}$$

and

$$\Theta = \tan^{-1}\frac{Y}{X} \tag{2.54}$$

the joint pdf is now given by

$$p_{R,\Theta}(r,\theta) = \frac{r}{2\pi\sigma^2} e^{-\frac{r^2+A^2-2Ar\cos\theta}{2\sigma^2}} \tag{2.55}$$

Integrating (2.55) we can get the PDFs of R and Θ, i.e.

$$p_R(r) = \frac{r}{\sigma^2} e^{-\frac{r^2+A^2}{2\sigma^2}} \mathrm{I}_o\left(\frac{\mathrm{A}r}{\sigma^2}\right), r \geq 0 \tag{2.56}$$

, where I_0 is the modified Bessel function of the first kind, and

$$p_\Theta(\theta) = \frac{e^{-\rho}}{2\pi} + \frac{\sqrt{\rho}\cdot e^{-\rho\cdot\sin^2\theta}}{\sqrt{4\pi}} \cos(\theta)\, erfc(-\sqrt{\rho}\cdot\cos\theta) \tag{2.57}$$

, where the term ρ appearing in (2.57) is the SNR, defined in (2.29) with $P = A^2$. For high SNRs, equation (2.57) reads

$$p_\Theta(\theta) \approx \sqrt{\frac{\rho}{\pi}} e^{-\rho\cdot\sin^2\theta} \cos(\theta) \tag{2.58}$$

Moreover, it can be easily noted from eq. (2.57) that $p_\Theta(\theta)$ is a function of $cos(\theta)$ it is periodic and as a periodic function it can be expanded in a Taylor series. Following this expansion eq. (2.57) can be re-written as[18]

$$p_\Theta(\theta) = \frac{1}{2\pi} + \frac{e^{-\frac{\rho}{2}}}{2}\frac{\sqrt{\rho}}{\sqrt{\pi}} \sum_{m=1}^{\infty} \frac{(-1)^m}{m^2} \left[I_{\frac{m-1}{2}}\left(\frac{\rho}{2}\right) + I_{\frac{m+1}{2}}\left(\frac{\rho}{2}\right)\right] \cos(m\theta) \tag{2.59}$$

The last expression is very useful for the calculation of the error rates, as it will be discussed later in the chapter.

Finally, as mentioned before, since the photocurrent is directly proportional to the optical power of the signal, it is interesting to investigate the statistics of

the optical power. Setting $S = R^2$ with S being the random variable describing the optical power, the pdf of S reads

$$p_S(s) = \frac{e^{-\frac{s+A^2}{2\sigma^2}} \mathrm{I}_0(\frac{\mathrm{A}\sqrt{s}}{\sigma^2})}{2\sigma^2} \tag{2.60}$$

with a characteristic function

$$\psi_S(ju) = E[e^{juS}] = \frac{e^{\frac{juA^2}{1-j2u\sigma^2}}}{1 - j2u\sigma^2} \tag{2.61}$$

As shown from equation (2.57), $p_\Theta(\theta)$ can be effectively expressed as a function of only θ and ρ. In figure 2.8 we plot $p_\Theta(\theta)$ for various values of ρ.

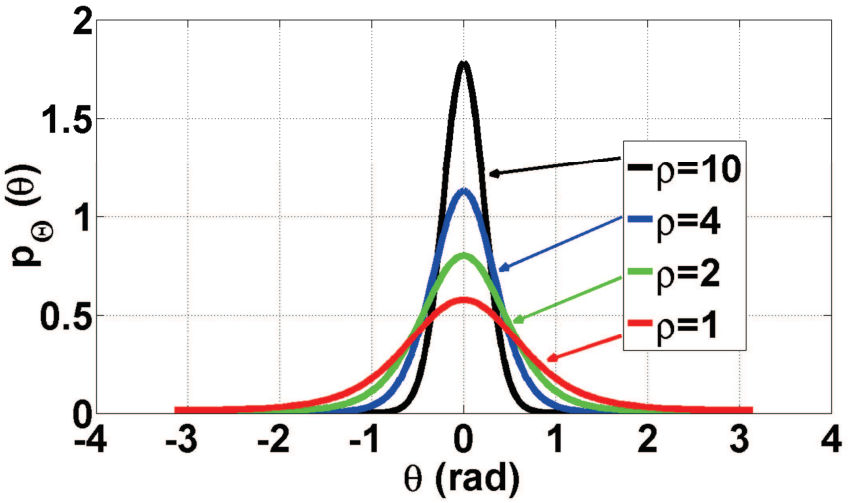

Figure 2.8: $p_\Theta(\theta)$ for various values of ρ.

2.1.4.3.1 Calculation of the first moments

Having the exact expression for the PDF $p_X(x)$ of the random variable X, one may calculate the m-order moments of X using the formula

$$E[X^m] = \int_{-\infty}^{+\infty} x^m p_X(x) dx \tag{2.62}$$

and the m-order *central* moments of X using the formula

$$E[(X-\mu_X)^m] = \int_{-\infty}^{+\infty} (x-\mu_X)^m p_X(x)dx \tag{2.63}$$

, where μ_X is the average value of the random variable X with μ_X= E[X].

The 2nd order central moment, or *variance*, noted as σ_X^2, is of particular interest as it provides a rough measure of the random variable "spread". However, we are usually based on the variance square root, or *standard deviation*. Developing (2.63) for $m = 2$, we get

$$\sigma_X = \sqrt{E\left[X^2\right] - \mu_X^2} \tag{2.64}$$

Having the exact expressions for the PDFs of R and Θ we can use the equations (2.62) and (2.64) in order to calculate the standard deviations σ_R and σ_Θ. Beginning with the variable R, we get its average

$$E[R] = \mu_R = \sigma\sqrt{\frac{\pi}{2}} e^{-\frac{\rho}{2}} \left[(1+\rho)\cdot \mathrm{I}_0\left(\frac{\rho}{2}\right) + \rho \cdot \mathrm{I}_1\left(\frac{\rho}{2}\right)\right] \tag{2.65}$$

, the 2^{nd} order moment

$$E[R^2] = \mathrm{A}^2 + 2\sigma^2 = 2\sigma^2\left(1+\rho\right) \tag{2.66}$$

and the standard deviation

$$\sigma_R = \sigma\sqrt{2\left(1+\rho\right) - \frac{\pi}{2} e^{-\rho}\left[(1+\rho)\cdot \mathrm{I}_0\left(\frac{\rho}{2}\right) + \rho \cdot \mathrm{I}_1\left(\frac{\rho}{2}\right)\right]^2} \tag{2.67}$$

In order ot get more intuition on equation (2.67), in figure 2.9a we plot the quantity $\frac{\sigma_R}{\sigma}$ against ρ (in linear scale). We note that the function σ_R/σ has a lower bound $\frac{\sigma_R}{\sigma}\Big|_{\rho=0} = \sqrt{2-\frac{\pi}{2}} \approx 0.6551$, while $\frac{\sigma_R}{\sigma} < 1$ with $\lim_{\rho\to\infty} \frac{\sigma_R}{\sigma} = 1$. In a realistic optical-communication systems, SNRs typically[1] take values around $\rho = 10$, for which σ_R is slightly lower but very close to σ.

[1]In optical communications, instead of SNR, it is common to use the Optical Signal to Noise Ratio (OSNR) in a reference bandwidth of 12.5 GHz or 0.1 nm around 1.55 μm (OSNR will be properly defined in section §2.2.4). For reasons of comparison we just note that for a noise bandwidth of 50 GHz (for example, almost entirely containing a 20 $Gbaud$ signal) $\rho = 10$ corresponds to $OSNR_{0.1\ nm} = 13\ dB$.

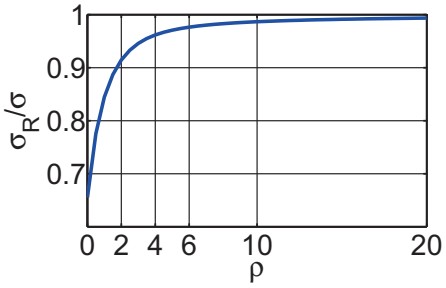

(a) σ_R/σ as a function of the signal-to-noise ratio in a system impacted by AWGN.

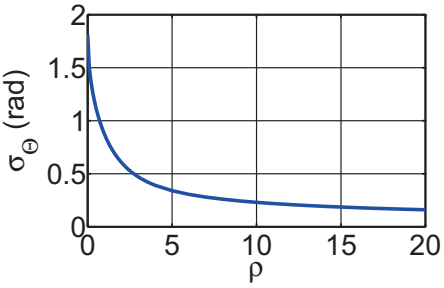

(b) σ_Θ as a function of the signal-to-noise ratio in a system impacted by AWGN.

Figure 2.9: σ_Θ and σ_R/σ as a function of ρ.

On the other hand, for the variable Θ we get its average value

$$E[\Theta] = 0 \tag{2.68}$$

, its variance (using eq. (2.59))

$$E[\Theta^2] = \frac{\pi^2}{3} + 2e^{-\frac{\rho}{2}}\sqrt{\pi\rho}\sum_{m=1}^{+\infty}\frac{(-1)^m}{m^2}\left[\mathrm{I}_{\frac{m-1}{2}}\left(\frac{\rho}{2}\right) + \mathrm{I}_{\frac{m+1}{2}}\left(\frac{\rho}{2}\right)\right] \tag{2.69}$$

and its standard deviation[19]

$$\sigma_\Theta = \sqrt{\frac{\pi^2}{3} + 2e^{-\frac{\rho}{2}}\sqrt{\pi\rho}\sum_{m=1}^{+\infty}\frac{(-1)^m}{m^2}\left[\mathrm{I}_{\frac{m-1}{2}}\left(\frac{\rho}{2}\right) + \mathrm{I}_{\frac{m+1}{2}}\left(\frac{\rho}{2}\right)\right]} \tag{2.70}$$

Moreover, a simplified relation can be obtained for high SNR ($\rho \geq 10$) by using the PDF of the equation (2.58), or

$$\sigma_\Theta \approx \sqrt{\frac{1}{2\rho}} \tag{2.71}$$

In figure 2.9b, we plot σ_Θ as a function of ρ. Considering the limits of σ_Θ we can easily see that $\sigma_\theta(0) = \sqrt{\frac{\pi^2}{3}} \approx 1.8138$ and $\lim_{\rho\to\infty}\sigma_\Theta = 0$.

Fusing on the approximate expression (2.71), we see that σ_Θ is bijectively linked to ρ As standard deviations provide an estimation for the spread of a random variable, it serves as a simple indicator of the signal degradation, in cases

where we are not interested in performing a strict calculation of the symbol error probability or run a brute-force Monte-Carlo Bit Error Rate (BER) estimation. In coherently detected PSK modulation, as the decision is based on the phase of the signal, σ_Θ provides the appropriate quantity that captures the phase degradation and therefore, the phase standard deviation may provide a rough estimation of the PSK signal degradation. However, it should be underlined that the detection method plays an important role and it may drastically change the statistics of the detected signal quadratures[1].

A careful observation of the equations (2.70) and (2.67) reveals that σ_Θ is a function of just ρ, while σ_R is a function of both the noise standard deviation σ and ρ. Suppose now that un unknown noise source corrupts our signal. Since we have no precise information about this source, it is very useful, at a preliminary stage, to measure its resemblance to AWGN, by means of simple measurements of the complex mean A_{est}, the standard deviations σ_Θ, σ_R and an estimation of the "noise" standard deviation σ_{est}. For this, we introduce at this point the parameter

$$Bn \triangleq \frac{\sigma_{\Theta,est}\sigma_{est}}{\sigma_{R,est}h\left(\frac{|\mathrm{A}_{est}|^2}{2\sigma_{est}^2}\right)} \tag{2.72}$$

, where the function $h(\rho)$ is analytically calculated using the equations (2.70) and (2.67), defined as

$$h(\rho) = \frac{\sqrt{\frac{\pi^2}{3} + 2e^{-\frac{\rho}{2}}\sqrt{\pi\rho}\sum_{m=1}^{+\infty}\frac{(-1)^m}{m^2}\left[\mathrm{I}_{\frac{m-1}{2}}\left(\frac{\rho}{2}\right) + \mathrm{I}_{\frac{m+1}{2}}\left(\frac{\rho}{2}\right)\right]}}{\sqrt{2\left(1+\rho\right) - \frac{\pi}{2}e^{-\rho}\left[(1+\rho)\cdot\mathrm{I}_0\left(\frac{\rho}{2}\right) + \rho\cdot\mathrm{I}_1\left(\frac{\rho}{2}\right)\right]^2}} \tag{2.73}$$

From the above definition, it is obvious that when the signal deformation is caused by AWGN, the distortion is symmetric, yielding $Bn = 1$. On the other hand, when $Bn > 1$, the phase quadrature has a larger variance compared to the variance of the amplitude quadrature, while when $Bn < 1$, the amplitude quadrature has a larger variance compared to the phase quadrature variance.

[1]For example, in contrast to coherently detected systems, differentially systems do not yield the same statistics, as it will be discussed later.

The parameter Bn is going to be used in chapter §4 in order to be characterize the shape of the constellations resulting from the interaction between chromatic dispersion and fiber nonlinearities. In those cases we will see that the constellation shape is generally not symmetric over the two Cartesian quadratures.

In practice, in order to calculate the quantity Bn for a given signal, we first extract the signal samples corresponding to one particular symbol (for example, for QPSK signals, we initially extract one of the four possible QPSK states), we calculate Bn over the samples of this state and finally, we take the average of Bn over all states. For the calculation of Bn over each state, the quantities $\sigma_{\Theta,est}$ and $\sigma_{R,est}$ are found in a straight-forward manner over the complex samples of the state, while A_{est} may also be directly found as the state complex average. Finally, σ_{est} may be calculated as the average of the standard deviations of the Cartesian coordinates σ_{Re} and σ_{Im}, i.e. $\sigma_{est} = \frac{\sigma_{\mathrm{Re}}+\sigma_{\mathrm{Im}}}{2}$. However, we should underline that there exist different ways to calculate A_{est} and σ_{est}. For example, A_{est} may be alternatively calculated as the complex argument that maximizes the resulting PDF, while σ_{est} may be estimated by the standard deviations following the axes of a rotated coordinate system, for example, with one of its axes passing from the state complex average. It is obvious that when the signal is degraded by AWGN, all the above variants converge into the same result. Nevertheless, we need to note that different choices of A_{est} and σ_{est} will generally result into slightly different estimations of the quantity Bn.

2.1.4.3.2 Calculation of the bit error probability for coherently detected PSK

The probability of the *M-ary symbol* being detected *correctly* (noted as $SCDP_M$) is equal to the probability of the detected phase lying inside the phase interval $\left[-\frac{\pi}{M}, \frac{\pi}{M}\right]$. Noting by

$$p_m = P\left(\frac{2m-1}{\mathrm{M}}\pi < \Theta < \frac{2m+1}{\mathrm{M}}\pi\right) = \int_{\frac{2m-1}{\mathrm{M}}\pi}^{\frac{2m+1}{\mathrm{M}}} p_\Theta(\theta)d\theta \tag{2.74}$$

the symbol error probability is simply given by:

$$\mathrm{SCDP}_M = p_0 \tag{2.75}$$

Equivalently, the probability of the M-ary symbol being mistaken for another one, or the *symbol error probability* (noted as SEP_M), is given by

$$SEP_M = 1 - \mathrm{SCDP}_M = 1 - p_0 \tag{2.76}$$

Combining (2.57) and (2.76) we get

$$SEP_M = 1 - \frac{e^{-\rho}}{\mathrm{M}} - \int_0^{\frac{\pi}{M}} \left(\frac{\sqrt{\rho} \cdot e^{-\rho \cdot \sin^2\theta}}{\sqrt{\pi}} \cos(\theta)\, erfc(-\sqrt{\rho} \cdot \cos\theta) \right) d\theta \tag{2.77}$$

The last integral of the equation (2.77) cannot be expressed in terms of existing functions for all arbitrary values of M and it generally has to be calculated numerically. However, for $M = 2$ an analytical solution exists and in that case the equation (2.77) reads

$$SEP_2 = \frac{1}{2} erfc(\sqrt{\rho}) \tag{2.78}$$

It is important to note that the equation (2.78) has the same form as the equation (2.47) and we may therefore conclude that the bit error probability is *exactly the same* for binary ASK and BPSK. This conclusion may also be reached with the simple observation made in section §2.1.3.2 that these two modulation formats have the exact same representation in the complex plane.

An analytical expression may also be provided for $M = 4$ by noting that the QPSK modulation is made-up from two independent BPSK signals in phase quadrature. Since there is no interference between the two quadrature phase carriers and the noise on these carriers is statistically independent, the probability of a quaternary symbol being detected correctly is equal to the probability of both BPSK symbols being correctly detected independently, or

$$SEP_4 = erfc(\sqrt{\frac{\rho}{2}}) \cdot \left[1 - \frac{1}{4} ercf\left(\sqrt{\frac{\rho}{2}}\right) \right] \tag{2.79}$$

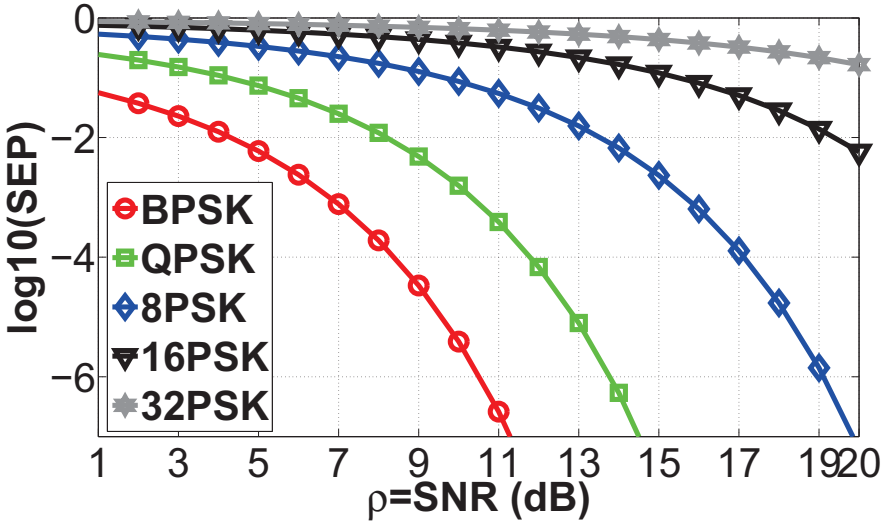

Figure 2.10: Symbol Error Probability as a function of SNR.

For the symbol error probabilities when $M > 4$ we use the formula (2.77), calculating the integral numerically.

Furthermore, in some cases, it is very useful to express symbol error probabilities as a function of the standard deviations of the polar coordinates, as, for example, in PSK modulation, the information is coded in the phase of the optical signal. More specifically, as it will be discussed in more detail in chapter §4, we often use the standard deviation of the phase coordinate σ_Θ as a rough estimation of the signal degradation and in this case, it is very useful to express the symbol error rates introduces above for PSK modulation, as a function of σ_Θ. While this is quite complicated in the general case, when $\rho \geq 10$ we may combine the equations (2.71) and (2.78), to get an approximation of the symbol error rates in the case of BPSK

$$SEP_2 = \frac{1}{2} erfc(\frac{1}{\sigma_\Theta \sqrt{2}}) \tag{2.80}$$

and QPSK

$$SEP_4 = erfc(\frac{1}{2\sigma_\Theta}) \cdot \left[1 - \frac{1}{4} ercf\left(\frac{1}{2\sigma_\Theta}\right)\right] \tag{2.81}$$

, while these relations can be generalized to higher-level modulation formats.

Coming back to equations (2.78)-(2.77), in figure 2.10 we plot the resulting symbol error probability as a function of ρ for different values of M. As expected, higher level modulation requires higher levels of SNR to achieve the same symbol error rate. However, this figure does not provide enough information on the "efficiency" of each modulation format. In other words, it doesn't answer the ultimate question: "Which is the best modulation format for a transmission system limited by AWGN?".

In order to answer this question we need to define what we mean by "efficient". The useful and measurable qualities for a system are the bit error probability BEP, the bit rate B, the bandwidth utilization W, the complexity, the cost, the throughput etc. Here we are going to neglect economical and implementation complexities and we are going to focus principally on the first three efficiency criteria.

At first, we need to convert the symbol error rate, for the curves of figure 2.10, to an equivalent bit error rate for all modulation formats. For this, we need the information of how the different bits are mapped into symbols, since a wrong decision over a symbol may not necessarily imply a wrong decision over all $\log_2 M$ bits of the symbol. In practice, it is more probable that, due to noise, a symbol error will most possibly signify mistaking the symbol for one of its closest neighbors on the complex plane. This information can be exploited by designing the mapping in such a way that symbols with an adjacent phase (in the case of PSK signals) represent tuples that differ to only 1 bit. It can be shown that this is the optimum mapping, also known as *Gray encoding*[89]. An accurate evaluation of the BEP in the case of Gray coded MPSK was presented in [70]. However, a fairly accurate simple approximation may be considered by noting that in the case of Gray encoding, a symbol error will yield in most times a single bit error. In this case, the bit error probability is given as a function of the symbol error probability by the formula

$$BEP_M = \frac{SEP_M}{\log_2 M} \tag{2.82}$$

Secondly, we need to note that different modulation formats (and therefore the different curves of figure 2.10) naturally provide a different bit rate B for the

same amount of bandwidth W, as each symbol carries a tuple of $log_2 M$ bits. The symbol rate R is linked to the bit rate B_M (the index M signifies the symbol rate for M-ary PSK) by the formula

$$B = R_M \cdot \log_2 M \tag{2.83}$$

Furthermore, for the purposes of this analysis we admit that this bandwidth occupied by the signal is equal to the symbol rate R[1], i.e.

$$\mathrm{W}_M = \mathrm{R}_M = \frac{B}{\log_2 M} = \frac{W_2}{\log_2 M} \tag{2.84}$$

and modulation of order $M > 2$ occupies $log_2 M$ less bandwidth than modulation with $M = 2$.

From the above it is obvious that a simple criterion like the "SNR required to deliver a certain bit error probability" is not sufficient to describe the quality of a signal. For this we need to introduce a new quantity that takes the SNR requirement down to the level of one bit. The SNR/bit is defined by replacing W in the equation (2.29) by the bitrate B as defined in the equation (2.83)

$$\rho_b = \frac{P}{N_0 B} \tag{2.85}$$

or combining the equations (2.85) and (2.84)

$$\rho_b = \frac{\rho}{\log_2 M} \tag{2.86}$$

In figure 2.11 we plot the BEP versus ρ_b. An interesting remark concerning this figure is that BPSK and QPSK have the *exact* same performance in terms of BEP as a function of ρ_b. However, the notable difference between the solutions BPSK and QPSK is that QPSK naturally uses half the bandwidth than BPSK.

[1] There exist several definitions for the notion of bandwidth (see [102]). In optical communications, the definition mostly used is the *null-to-null* bandwidth, i.e. if the symbol shaping pulse used has the form of $rect\left(\frac{t}{T}\right)$ with $T = R^{-}1$ being the symbol period, then its Fourier transform is $T \cdot \mathrm{sinc}\,(T \cdot t)$ a function with its central lobe-and most of the spectrum contained into $\frac{2}{T} = 2R$. In practice, when tight optical filtering is applied at the reception or for channel extraction, its bandwidth is about $2R$, or a little less. The difference with the assumption of this analysis is just a factor of 2.

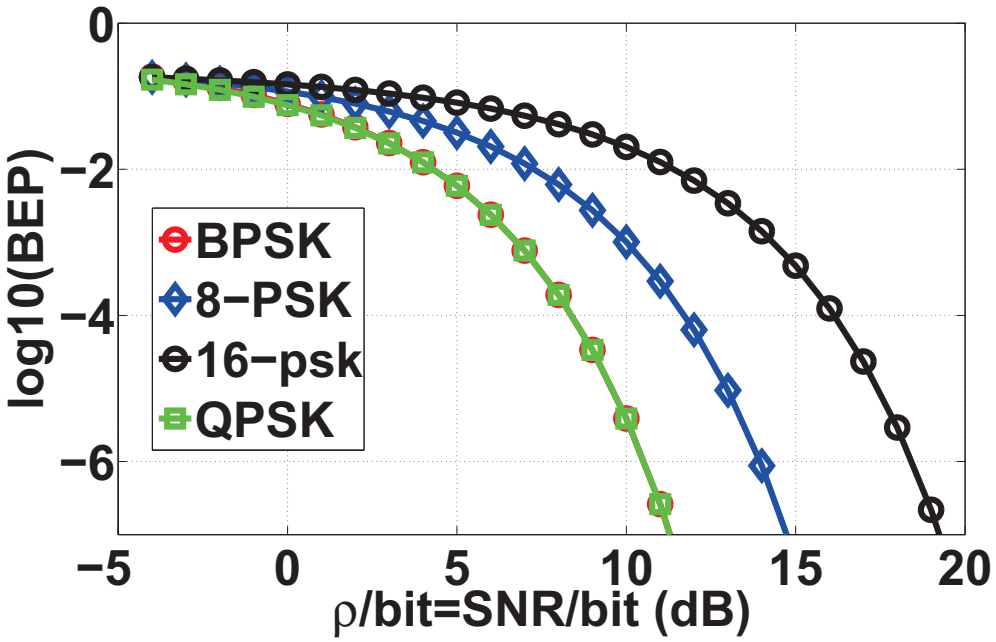

Figure 2.11: BEP Vs SNR/bit.

Therefore QPSK and BPSK have the same performance in terms of BEP, but somewhat, QPSK uses more efficiently the given spectrum. In order to distinguish BPSK and QPSK with respect to this last "quality", we usually refer to the quantity "spectral efficiency"[1] defined as

$$\eta \triangleq \frac{B}{W} \tag{2.87}$$

In order to take η into account in the comparison of different modulation formats, we need to normalize the amount of bandwidth used by each modulation format, or equivalently, compare the different solutions by fixing the amount of bandwidth used. To simplify the analysis, without loss of generality, we may consider that for all values of M the signal power is fixed and the noise spectral density is also fixed. Consequently, SNR depends only on the bandwidth W_M occupied by an MPSK signal.

[1] In the context of dense Wavelength-Division Multiplexing (WDM) optical communication systems (which is the case for this work) spectral efficiency of a given modulation format is of extreme importance.

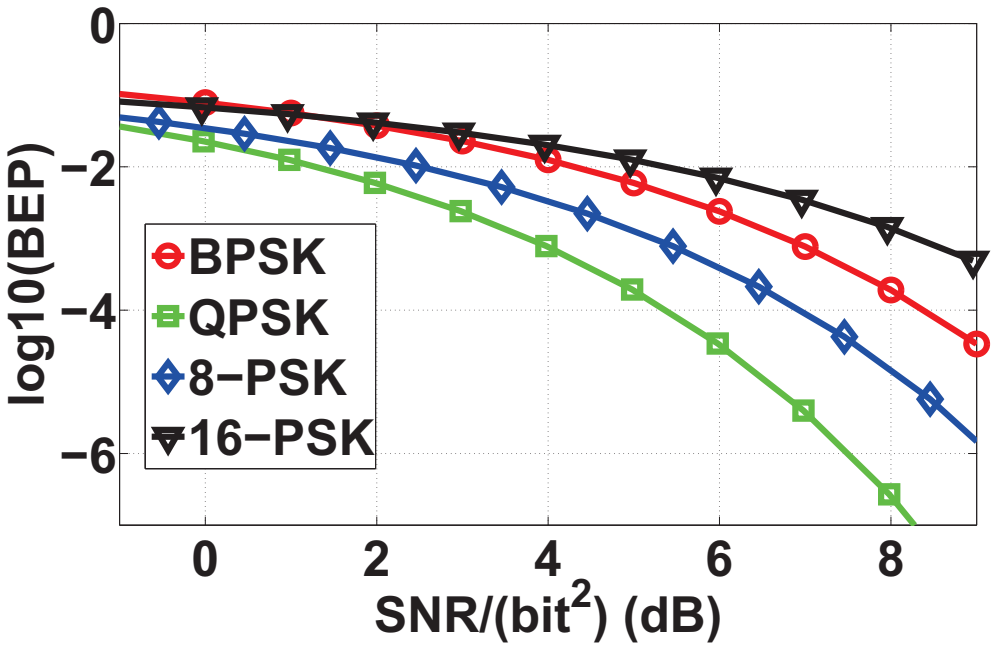

Figure 2.12: BEP Vs SNR/bit^2.

Normalizing the formats to the same bandwidth utilization (or the same spectral efficiency), we define the quantity SNR/bit^2 as

$$\rho_{b2} = \frac{\rho}{(\log_2 M)^2} \tag{2.88}$$

In figure 2.12 we plot the BEP as a function of ρ_{b2}. It is evident that QPSK provides the best solution with respect to this combined criterion of required SNR/bit and spectral efficiency, whereas 8-PSK, BPSK and 16-PSK follow.

Optical telecommunications were dominated for a long time by classical OOK modulated signals. As we have seen in section §2.1.4.2, the BEP of OOK-modulated signals impacted by AWGN can be expressed in terms of a quantity that called the Q factor by a "1-1" relation (eq. (2.47)). Nevertheless, in optical communications, even when it comes to non-OOK modulation, the measured BERs is very often converted into a "fake Q factor" by inverting eq. (2.47). Apart from reasons of comparison and "backward compatibility", this conversion also offers the advantage that when it comes to binary modulated signals impacted by AWGN, Q^2 is a linear function of the SNR and the signal quality for any SNR

may be simply predicted by BER measurement for just a few values of SNR.

In effect, for BPSK modulation, combining the equations (2.48) and (2.78), we can verify in a straight-forward manner that this property holds, i.e.

$$Q^2 = 2\rho \tag{2.89}$$

However, for QPSK modulation, combining the equations (2.48) and (2.79), we get

$$Q^2 = 2\left(erfc^{-1}\left(2 \cdot erfc(\sqrt{\frac{\rho}{2}})\left(1 - \frac{1}{4}erfc(\sqrt{\frac{\rho}{2}})\right)\right)\right)^2 \tag{2.90}$$

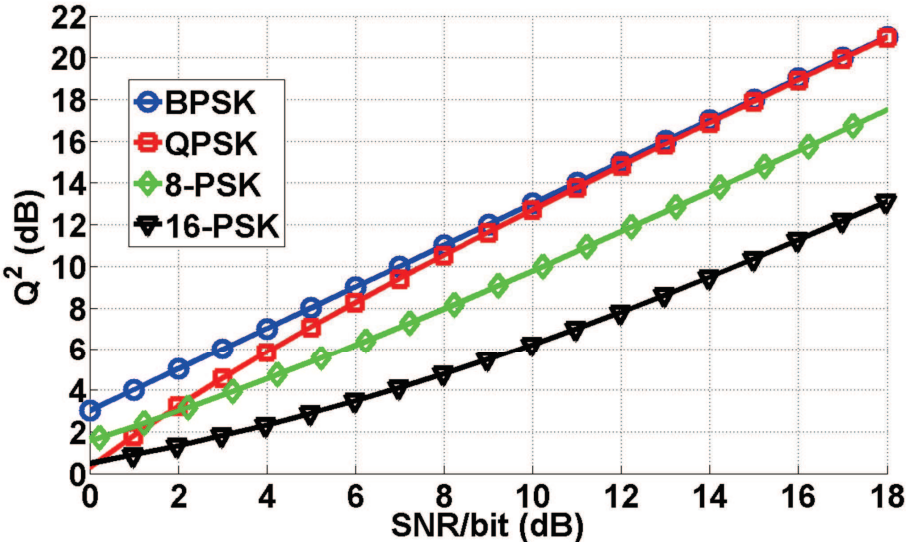

Figure 2.13: $Q^2(dB)$ Vs SNR/bit

In figure 2.13 we plot the Q^2 factor against the SNR/bit for $M = 2$ up to 16. We see that the fake conversion to Q factor should be used with caution, since Q^2 does not remain a linear function of the SNR/bit for an MPSK modulation with $M > 2$.

2.1.4.3.2.1 Performance comparison with respect to spectral efficiency - Shannon's formula An alternative way of comparing modulation

formats with respect to their spectral efficiency is to compare them to the ultimate spectral efficiency limit, derived by Shannon in [100]. In Shannon's work, by means of information-theoretic calculations, a limit is derived providing the highest achievable information rate allowing for reliable communication, in an AWGN channel of bandwidth W, given by

$$B = W\log_2\left(1 + \frac{P_{av}}{N_0 W}\right) \tag{2.91}$$

, where B is the bit-rate in $bits/sec$, W is the bandwidth in Hz, P_{av} is the average power in Watts and N_0 is the PSD of the AWGN. Equation (2.91) may be also re-written in terms of the spectral efficiency η and ρ_b as[89]

$$\eta = \log_2\left(1 + \eta \cdot \rho_b\right) \tag{2.92}$$

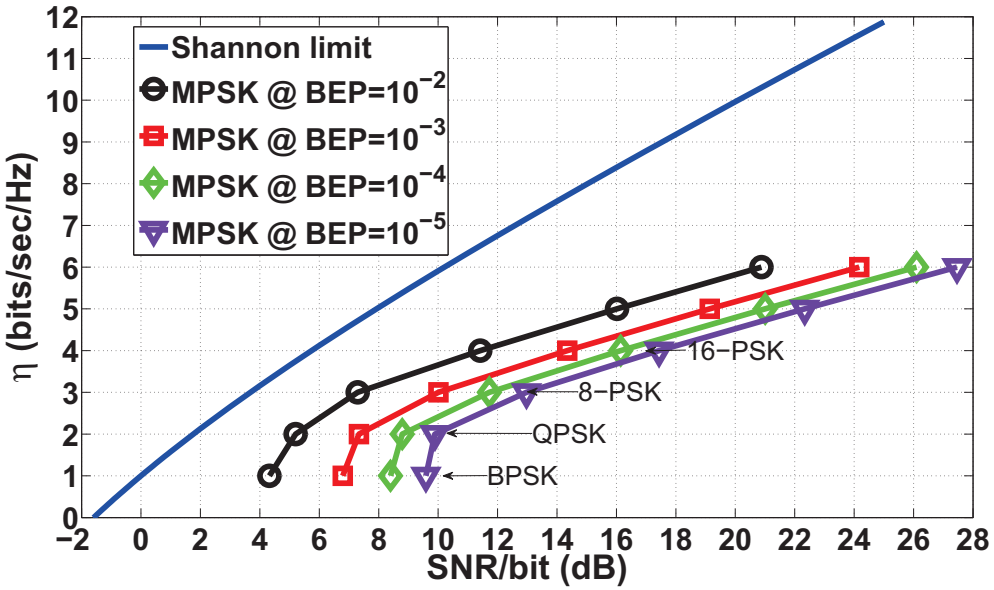

Figure 2.14: Spectral efficiency $\eta(bits/sec/Hz)$ as a function of ρ_b for various modulation formats at various bit error probabilities.

In figure 2.14, the solid blue line represents the theoretical spectral efficiency limit of the equation (2.92), for several PSK modulation formats (and thus different levels of spectral efficiency), for a range of different fixed BEPs. If we focus,

for example, in a BEP of 10^{-3} (which is usually the BER requested in practical optical communication system before the use of Forward-Error Correction (FEC)), we may note that, for a given SNR/bit, QPSK modulation offers the lowest difference in terms of spectral efficiency among M-ary PSK formats, with respect to the ultimate spectral efficiency limit given by Shannon. In this way, it may be alternatively verified that QPSK modulation presents the best choice of a system designer when it comes to transmission systems, limited by AWGN[1]. However, in chapter §4, we thoroughly analyze an optical transmission channel and we show that the equivalent "noise" added by the optical channel onto the signal is not necessarily an AWGN and it strongly depends on the chosen system parameters.

2.1.4.3.3 Calculation of the bit error probability for differentially encoded, coherently detected PSK

Let the waveform $\tilde{g}_k$ corresponding to the k^{th} transmitted symbol be expressed in the form

$$\tilde{g}_k = A_k e^{j(\omega t+\phi_k+\psi_k+\theta)} \tag{2.93}$$

, where ω is the carrier frequency, ϕ_k is the phase level corresponding to the k^{th} transmitted symbol, ψ_k is the term of phase noise or distortion and θ is the carrier phase at the receiver side. In the previous paragraph we have silently supposed that the *coherent detection* is ideal in the sense that the receiver has a perfect knowledge of the carrier phase. That means that the receiver has a perfect knowledge of the parameter θ appearing in eq. (2.93).

While θ is supposed to be a deterministic quantity, its a priori knowledge supposes a perfect control (and knowledge) of the channel and a perfect knowledge of all the system parameters and possible variables. In practice, however, several reasons result in the fact that the parameter θ is unknown (or extremely hard to calculate) including imperfections of the fiber construction, random twists, temperature variations, imperfect control of the laser central frequency, imperfect synchronization of the laser frequency at the receiver side etc. The result is, therefore, a random, time-variable parameter that is most commonly modeled by

[1]Extensive work on this matter may be also found in [6].

a uniformly distributed random variable in the range $[0, 2\pi]$ and it usually has to be estimated a posteriori.

In order to see the effect of the parameter θ, consider, for example, the initially transmitted QPSK symbols $\{0, 2, 3, 1\}$ that acquire, accordingly, one of the four phase levels $\left\{\frac{\pi}{4}, \frac{3\pi}{4}, \frac{5\pi}{4}, \frac{7\pi}{4}\right\}$. In the absence of noise or any other source of degradation (i.e. $\psi_k = 0, \forall k$ in eq. (2.93)), the phase levels detected by the receiver, would be shifted by θ, i.e. $\left\{\theta + \frac{\pi}{4}, \theta + \frac{3\pi}{4}, \theta + \frac{5\pi}{4}, \theta + \frac{7\pi}{4}\right\}$.

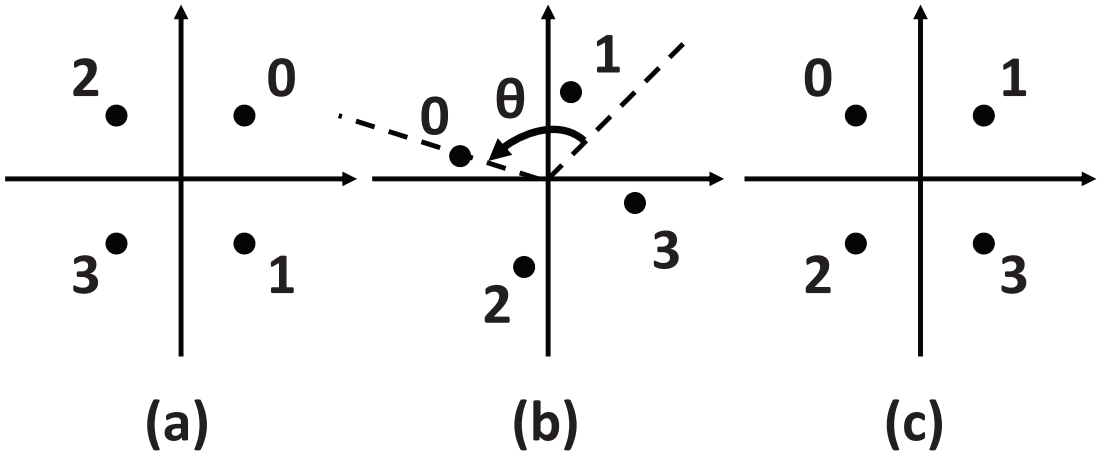

Figure 2.15: (a) Initial QPSK constellation (b) Constellation including a random carrier phase θ (c) Constellation with a de-rotation of $\theta - \frac{\pi}{2}$ resulting in an error to all transmitted symbols

At first glance, this problem does not seem complicated, since the receiver needs to perform a simple de-rotation of the received constellation by $-\theta$ in order to recuperate the initial phase levels $\left\{\frac{\pi}{4}, \frac{3\pi}{4}, \frac{5\pi}{4}, \frac{7\pi}{4}\right\}$. However, this cannot be achieved by a simple observation of the received constellation, since, if the symbols have almost the same probability of occurrence, a seemingly identical constellation is produced for any de-rotation phase shift $\theta + m\frac{\pi}{2}, m \in \mathbb{Z}$, introducing an error to all detected symbols, unless this de-rotation is (by pure luck) successful (see figure 2.15). This problem is generally referred to as the problem of *phase ambiguity* and $m\frac{\pi}{2}$, (or $m\frac{2\pi}{M}$ for the general M-PSK case) is usually referred to as *phase ambiguity factor*. The same sort of phase ambiguity is introduced when one tries to extract the parameter θ from the signal by means of the Viterbi & Viterbi process[110]. Neglecting the noise term, in this process we first

raise $\tilde{g}_k$ to the power of M(i.e. $M = 2$ for BPSK, $M = 4$ for QPSK etc.) thus obtaining

$$\tilde{g}_k^M = A_k^M e^{j(M\omega t + M\phi_k + M\theta)} \tag{2.94}$$

, while we afterwards apply a lowpass filter. The filter will remove the rapidly varying $M\omega t$ frequency component, while the term $M \cdot \phi_k$ will also disappear since ϕ_k takes one of the values $\left\{0, \frac{2\pi}{\mathrm{M}}, ..., \frac{2\pi}{\mathrm{M}}(\mathrm{M}-1)\right\}$ and $M \cdot \phi_k$ will be always equal to $2 \cdot m \cdot \pi, m \in \mathbb{Z}$. However, taking the M^{th} root of $\tilde{g}_k^M$ in order to recover the phase θ, we get

$$\tilde{g}_{k,est} = A_k e^{j(\theta + \frac{2m\pi}{M})}, m \in \mathbb{Z} \tag{2.95}$$

, where $\frac{2m\pi}{M}$ is the phase ambiguity factor.

One solution to the problem of the phase ambiguity is the use of a *preamble* or *training sequence*. In this case, a fixed symbol sequence, known to the receiver, is sent at the beginning of the transmission or whenever we estimate that our system needs to be re-synchronized[15]. This small bandwidth sacrifice allows the receiver to always know exactly the de-rotation phase shift $-\theta$ that needs to be applied, given that it may be calculated as the phase shift that minimizes the bit error rate over the training sequence. However, in practice, θ is time-variable[1] and the training sequence has to be relaunched quite frequently.

The technique that is mainly used to overcome phase ambiguity in modern optical coherent transmission systems consists of coding the information on *phase differences*, rather than absolute phase levels. In this case, the first step of the detection process incorporates a coherent detection and a simple decision for the symbols $\tilde{g}_{k-1}$ and $\tilde{g}_k$, neglecting the possible impact of phase ambiguity. For example, in figure 2.15b, all symbols "0" would be falsely detected as "2", all symbols "1" would be falsely detected as "0" etc. Nevertheless, the second step, incorporates a simple phase comparator between the symbols $\tilde{g}_{k-1}$ and $\tilde{g}_k$, finally yielding the phase difference between these two successive symbols that is kept constant, disregarding the phase ambiguity. This scheme is often referred

[1] In optical communications θ generally depends on random stress applied on fibers, temperature, aging of the fiber etc.

to as *differentially encoded, coherently detected* PSK, while for simplicity, in this manuscript we refer to it as *differentially-coherent* PSK. A more elaborate formalism regarding differential encoding and decoding may be found in appendix §A.

Transmitted symbols	0	1	1	3	1	0	2	2	1	2	0	3	3	2	3	0
Transmitted absolute phases	$\frac{\pi}{4}$	$-\frac{\pi}{4}$	$-\frac{\pi}{4}$	$-\frac{3\pi}{4}$	$-\frac{\pi}{4}$	$\frac{\pi}{4}$	$\frac{3\pi}{4}$	$\frac{3\pi}{4}$	$-\frac{\pi}{4}$	$\frac{3\pi}{4}$	$\frac{\pi}{4}$	$-\frac{3\pi}{4}$	$-\frac{3\pi}{4}$	$\frac{3\pi}{4}$	$-\frac{3\pi}{4}$	$\frac{\pi}{4}$
Received phases with ambiguity $\frac{\pi}{4}$	$\frac{3\pi}{4}$	$\frac{\pi}{4}$	$\frac{\pi}{4}$	$-\frac{\pi}{4}$	$\frac{\pi}{4}$	$\frac{3\pi}{4}$	$-\frac{3\pi}{4}$	$-\frac{3\pi}{4}$	$\frac{\pi}{4}$	$-\frac{3\pi}{4}$	$\frac{3\pi}{4}$	$-\frac{\pi}{4}$	$-\frac{\pi}{4}$	$-\frac{3\pi}{4}$	$-\frac{\pi}{4}$	$\frac{3\pi}{4}$
Phase differences $\Phi_k - \Phi_{k-1}$	0	$-\frac{\pi}{2}$	0	$-\frac{\pi}{2}$	$\frac{\pi}{2}$	$\frac{\pi}{2}$	$-\frac{\pi}{2}$	0	π	π	$-\frac{\pi}{2}$	π	0	$-\frac{\pi}{2}$	$\frac{\pi}{2}$	π

Figure 2.16: Phase ambiguity

In figure 2.16 we show a simple example of a transmitted symbol sequence, with each quaternary symbol being coded by a phase level. The signal is transmitted thought a noiseless channel that introduces a phase shift and the receiver fails to restore the phase of the initially transmitted symbols, resulting in a phase ambiguity of $pi/4$. However, one may easily notice that the *phase difference* between two consecutive symbols $\phi_k - \phi_{k-1}$ is the same for the transmitted and the received phase sequence, despite the phase ambiguity.

In order to calculate the BEP in the case of this particular detection scheme[1], we first note by Φ_{k-1}, Φ_k the random variables describing the received phases of two consecutive symbols. Exploiting the symmetry of PSK constellations we may suppose without loss of generality that the two consecutive symbols were initially carrying the same information and therefore had the same phase level. A correct decision is made when the phases of both symbols Φ_{k-1}, Φ_k lie in the same $\frac{2\pi}{M}$ range, happening when one of the following *mutually exclusive* events occurs

$$c_m \triangleq \left\{ \frac{2m-1}{M}\pi \leqslant \Phi_{k-1} \leqslant \frac{2m+1}{M}\pi, \frac{2m-1}{M}\pi \leqslant \Phi_k \leqslant \frac{2m+1}{M}\pi \right\} \tag{2.96}$$

, where $m = 0, 1, ..., M-1$. For $m = 0$, a correct detection is made when the noise (or distortion) component of both symbols is not so strong as to lead the

[1] We have followed the procedure detailed in [15]

phase of one of the two symbols into an "erroneous" detection, were it not for the phase ambiguity θ. However, there also appear the less probable events ($m = 1, ..., M-1$) of both symbols phases being drifted into *the same direction*, leading into the *same* "erroneous" detection. Such a case will not lead into an error since two "errors" occurred, both in the same sense so as to be mutually annulled. The overall error probability $DESCDP_M$ is then a sum of the probabilities of the mutually exclusive events c_m for all m, or

$$DESCDP_M = \sum_{m=0}^{M-1} P(c_m) \tag{2.97}$$

In the context of AWGN, taking into consideration that Φ_k and Φ_{k-1} are independent and identically distributed, we may not note that

$$\begin{array}{l} P\left(\frac{2m-1}{\mathrm{M}}\pi < \Phi_k < \frac{2m+1}{\mathrm{M}}, \frac{2m-1}{\mathrm{M}}\pi < \Phi_{k-1} < \frac{2m+1}{\mathrm{M}}\right) = \\ P\left(\frac{2m-1}{\mathrm{M}}\pi < \Phi_k < \frac{2m+1}{\mathrm{M}}\right) P\left(\frac{2m-1}{\mathrm{M}}\pi < \Phi_{k-1} < \frac{2m+1}{\mathrm{M}}\right) = \\ P\left(\frac{2m-1}{\mathrm{M}}\pi < \Phi_k < \frac{2m+1}{\mathrm{M}}\right)^2 = p_m^2 \end{array} \tag{2.98}$$

In this case, the probability of a symbol error in the case of a differentially encoded, coherently detected PSK system reads

$$SEP_M = 1 - DESCDP_M = 1 - \sum_{m=0}^{M-1} p_m^2 \tag{2.99}$$

, where the values p_m are given by the equation (2.74).

Using the equation (2.99), in figure 2.17 we plot the symbol error probability for differentially-encoded coherent PSK as a function of the signal-to-noise ratio ρ (equation (2.99)). We also plot for reasons of comparison the equivalent symbol error probabilities for normal PSK (equation (2.76)). It should be noted that for almost all values of ρ and M, the difference between the two symbol error probabilities is a factor of 2. This can be roughly interpreted by the fact that, putting aside the global phase shift (i.e. the receiver has a perfect knowledge of this phase shift), if the k^{th} detected absolute phase ϕ_k is detected erroneously, this influences *two* phase differences: $\phi_k - \phi_{k-1}$ and $\phi_{k+1} - \phi_k$. Thus, one erroneous absolute phase will yield two symbol errors.

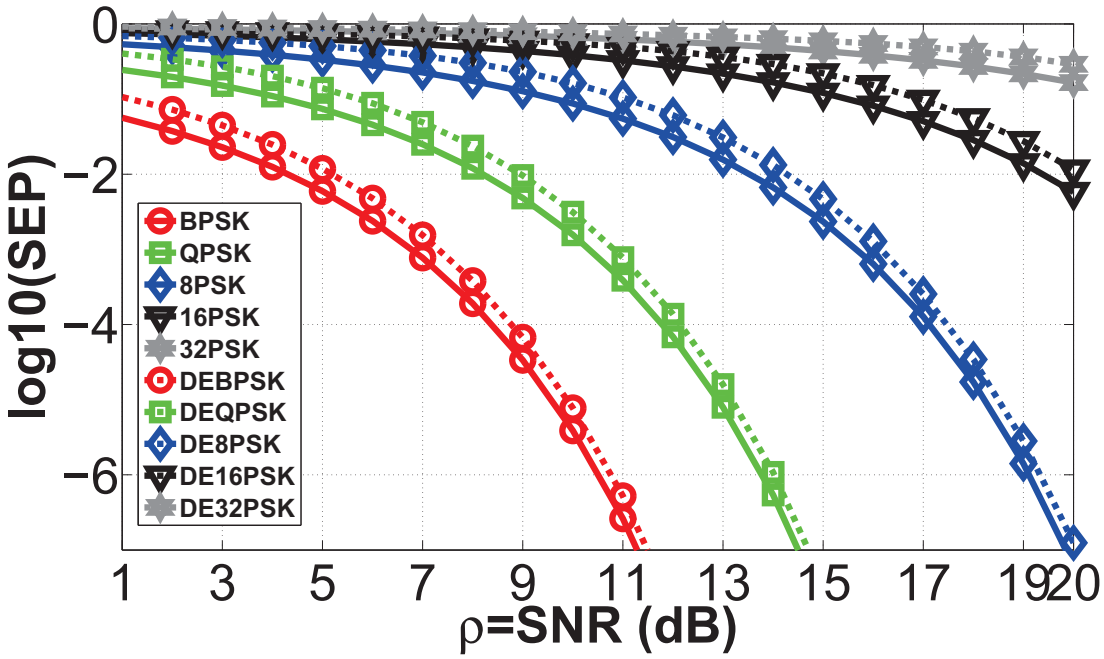

Figure 2.17: Comparison between coherent PSK and differentially encoded, coherently detected PSK

2.1.4.3.4 Bit error probability for differential phase shift keying

So fat we have admitted that the demodulation is performed with the use of a local oscillator at the receiver, leading to a coherent detection of the modulated signal. Very often, however, a coherent detection is not available, most commonly because of complexity/cost issues. Another technique commonly used is to consider as a reference for the demodulation of a symbol, the previous in time symbol. In this case, information is usually coded, as well, in the phase difference between two successive symbols. This modulation is commonly referred to as Differential Phase Shift Keying (DPSK).

In order to calculate the bit error probability for a DPSK system in the presence of additive white Gaussian noise, we note that at the receiver side, after some form of perfect down-conversion of the signal, at the k^{th} signaling interval, the demodulator output is given by

$$r_k = Ae^{j(\varphi_k - \theta)} + n_k \tag{2.100}$$

where ϕ_k is the information bearing phase level, θ is the unknown carrier phase and n_k is a realization of the two-dimensional AWGN corrupting the channel. Similarly, for the $(k-1)^{\text{th}}$ signaling interval, the output is

$$r_{k-1} = Ae^{j(\varphi_{k-1}-\theta)} + n_{k-1} \tag{2.101}$$

As in the case of coherently detected differentially encoded PSK, the decision variable is, in the absence of noise, the absolute phase difference between two consecutive symbols. Closely observing the equations (2.100) and (2.101), we notice that this phase difference may be formed by the projection of r_k over r_{k-1} and the decision can be based on the quantity

$$\Delta\beta = \arg(r_k r_{k-1}^*) \tag{2.102}$$

, where $r_k r_{k-1}^*$ may be developed into the relation

$$r_k r_{k-1}^* = A^2 e^{j(\varphi_k-\varphi k-1)} + n_k A e^{-j(\varphi k-1-\theta)} + A n_{k-1}^* e^{j(\varphi_k-\theta)} + n_k n_{k-1}^* \tag{2.103}$$

From the equation (2.103) we note that, in the absence of noise, the first term captures the absolute phase difference between two consecutive symbols, remaining uninfluenced by the global phase shift θ. The last equation may be simplified more by assuming without loss of generality that $\varphi_k - \varphi_{k-1} = 0$, while the terms $e^{-j(\varphi_{k-1}-\theta)}$ and $e^{j(\varphi_k-\theta)}$ can be absorbed into the noise terms n_k and n_{k-1}^*. Nevertheless, the analytical derivation of the BEP in the case of DPSK is quite complicated, mostly because of the presence of the term $n_k n_{k-1}^*$.

In order to see the relative impact of this last term, in figure 2.18 we plot the approximate PDF of the quantity $\left|\frac{n_k n_{k-1}^*}{A\left(n_k+n_{k-1}^*\right)}\right|$ for four different values of SNR and 1000000 noise samples for each received signal sample. As it is obvious from figure 2.18, the term $n_k n_{k-1}^*$ is around 0.1 for SNR levels around 10 and it further decreases for higher SNRs.

Using all the previous assumptions and neglecting the term $n_k n_{k-1}^*$, (2.103) can be simplified into

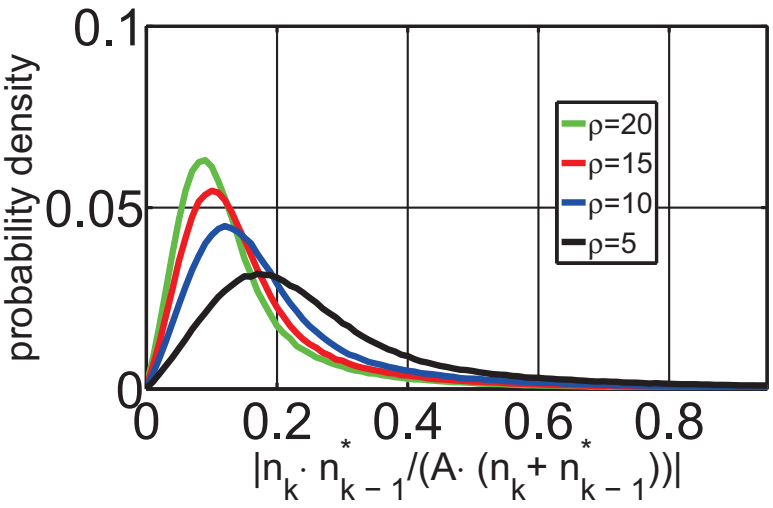

Figure 2.18: Approximate PDF of the quantity $\left|\frac{n_k n_{k-1}^*}{A\left(n_k+n_{k-1}^*\right)}\right|$ for 10^6 noise samples.

$$r_k r_{k-1}^* = A^2 + A\left(n_k + n_{k-1}^*\right) = A\left(A + \underbrace{n_k + n_{k-1}^*}_{n_D}\right) \tag{2.104}$$

The above formula is fairly accurate for $M \geq 4$, but it is pessimistic for $M = 2$[89],[15]. From the equation (2.104) we may note that neglecting the multiplicative term A, the problem of estimating the bit error probability under a channel corrupted by additive white Gaussian noise for DPSK can be approximately converted into the problem of a coherently detected PSK, as it was described by the equation (2.49), with twice as much noise since in the DPSK case $n_D = n_k + n_{k-1}^*$.

As a result, all the relations of the previous sections are approximately correct for DPSK by replacing σ by 2σ, or equivalently, ρ by $\frac{\rho}{2}$. In other words, in the case of DPSK we need twice as much SNR (or equivalently 3 dB) as in the case of coherent PSK in order to achieve the same bit error probability.

2.2 Lightwave communication systems

The possibility of transmitting information using light was based on a series of inventions that assured the fundamental functions needed in a point-to-point

communication system, i.e. a transmitter, a channel and a receiver. It cannot be doubted that the major motivation behind fiber-optic communications lied with the possibility of exploiting the vast channel bandwidth (and relatively low cost) provided by optical fiber waveguides. In parallel, the development of semiconductor lasers that could operate in room temperatures assured the transmitter function, while the receiver could be assured by photo-diodes, converting the optical power into electrical current. In the latter we may add several other important milestones such as the advent of large bandwidth amplifiers allowing a propagation of several kilometers before signal regeneration, or quite recently, the re-birth of coherent detection, allowing the use of advanced modulation formats and a more efficient utilization of available bandwidth[4].

In what follows we review the most important aspects of modern light-wave systems, starting with the physics of optical fibers, discussing how modulation formats, mathematically presented in section §2.1.3, are realized in optics, optical amplifiers and noise issues, while we also review the fundamental concepts around the modern practical implementation of coherent detection.

2.2.1 Optical fibers

The simplest kind of optical fiber is the step-index fiber, a cylindrical silica tube with two distinct concentric regions (see figure 2.19). The inner region, called core, is extended at a radius a, with a refractive index n_1, while the outer region, called cladding, is comprised between a radius a and b with a refractive index n_2 respectively. Propagation of the optical wave is achieved as a consequence of the total reflection, provoked by a slight difference between the refractive indexes n_1 and n_2.

Step-index fibers are characterized by two important quantities, the relative refractive index difference between core and cladding

$$\Delta = \frac{n_2 - n_1}{n_1} \tag{2.105}$$

and the V parameter

$$V = \frac{2\pi}{\lambda} a \sqrt{n_1^2 - n_2^2} \tag{2.106}$$

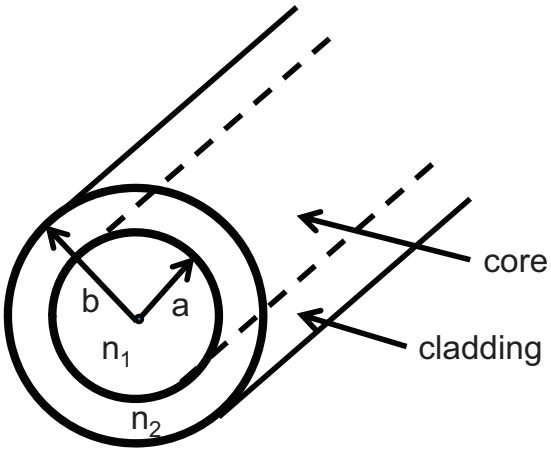

Figure 2.19: Representation of step index fiber.

, where a is the core radius and λ is the wavelength of light. The value of V, which has been seen to be directly proportional to the core radius, determines the number of modes that will propagate in the fiber[3]. More precisely, the number of modes increases with an increasing V, while with $V < 2.405$ we can limit the transmission to just one mode. In most cases, single-mode propagation is preferable, since multi-mode propagation and a higher core radius are usually linked with high bending losses and enhanced degradation due to Differential Mode Group Delay (DMGD). On the other hand, the core radius is inversely proportional to the strength of nonlinear Kerr effects, that have a particularly negative impact on signal quality, as it will become clear in section §2.2.1.4. Thus, there exists an important trade-off between the number of modes and the strength of nonlinear Kerr effects. In the context of this manuscript we focus on single-mode step-index fibers. In the following, we discuss the most important characteristics of optical fibers, i.e. the attenuation of the optical field, the effect of chromatic dispersion and the fiber nonlinearities.

2.2.1.1 Attenuation

Light that propagates in optical fibers is inevitably attenuated as its energy is absorbed or scattered by the material itself, lost in bendings or scattered at the core-cladding interface. While fiber attenuation was initially quite important,

the revolution of fiber optics was mainly a consequence of the ability to construct fibers with a relatively low loss[1], became possible after a series of important contributions in fiber fabrication[64],[65],[39],[83]. As shown in figure 2.20, the lowest attenuation is usually achieved for a wavelength around $1.55\mu m$, being finally stabilized to about $0.2dB/km$. In addition, recent advances have pushed even lower the loss of optical fibers[28] (about 0.148 dB/km) by approaching even more the fundamental intrinsic loss limit caused by Rayleigh scattering and silica absorption[3] (shown by the dashed line in figure 2.20). Nevertheless, attenuation remains the primary limiting effect in fiber-optics transmission as fiber losses determines the distance at which a pulse can travel before it has to be amplified or regenerated.

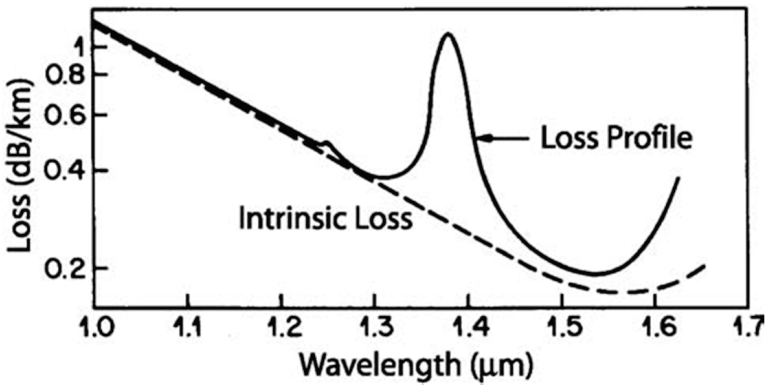

Figure 2.20: Fiber attenuation coefficient for different wavelengths.

If P_0 is the launch power at the fiber input, after a propagation length z the optical power is given by

$$P(z) = P_0 \exp(\alpha z) \tag{2.107}$$

, where α (in km^{-1}) is the attenuation coefficient, or equivalently, $\alpha_{dB} = 10\log_{10}(e) \cdot \alpha$, where α_{dB} is given the attenuation coefficient given in $dB \cdot km^{-1}$.

[1] i.e. passing from $1000dB/km$ to $20dB/km$ until the end of 70s

2.2.1.2 Chromatic dispersion

Light propagating in a medium is being slowed down by a factor of n, where n is the medium refractive index. In a fundamental level, chromatic dispersion is a result of the light interaction with the material bound electrons. As bound electrons can oscillate at different resonance frequencies, this interaction is frequency- (or wavelength-) dependent and therefore, $n = n(\omega) = n(\lambda)$. The *frequency dependence* of the medium refractive index is exactly what is referred to as chromatic dispersion[78].

The fiber refractive index as a function of the wavelength λ can be adequately described, for bulk-fused silica far from the medium resonances by the Sellmeier equation[78],[76],[3],[29]

$$n(\lambda) = \sqrt{1 + \frac{0.6961663\lambda^2}{\lambda^2 - 0.0684043^2} + \frac{0.4079426\lambda^2}{\lambda^2 - 0.1162414^2} + \frac{0.8974794\lambda^2}{\lambda^2 - 9.896161^2}} \tag{2.108}$$

As a direct consequence of the refractive index frequency dependence, since the phase velocity is a function of the refractive index ($\upsilon = \frac{c}{n}$), for dispersive media we will also have $\upsilon = \upsilon(\omega)$[117]. A modulated field may be described as an infinite sum of different frequency components (i.e. a Fourier transform). For such a field, the effect of a dispersive medium will result in different frequency components traveling at different velocities.

Suppose now that such a modulated pulse is described by the electric field $\mathrm{E}(t) = \mathrm{E}(z = 0, t)$ at the entrance of a material. With the help of the Fourier transform, $\mathrm{E}(t)$ can be written as

$$\mathrm{E}(t) = \int_{-\infty}^{+\infty} \widetilde{\mathrm{E}}(\omega) e^{j\omega t} \frac{d\omega}{2\pi} \tag{2.109}$$

, where $\widetilde{\mathrm{E}}(\omega) = \widetilde{\mathrm{E}}(z = 0, \omega)$ is the Fourier transform of $\mathrm{E}(t)$, spread around a central frequency ω_0. Neglecting all other effects (like loss, nonlinearities etc), propagating a distance z can be described by a multiplication of $\mathrm{E}(t)$ by the term $\mathrm{e}^{-j\beta(\omega)z}$. With the help of equation (2.109) the evolution of the field as a function of t and z may be given by

$$\mathrm{E}\left(z,t\right)=\mathrm{E}\left(t\right)\cdot\mathrm{e}^{-j\beta(\omega)z}=\int_{-\infty}^{+\infty}\widetilde{\mathrm{E}}(\omega)e^{j[\omega t-\beta(\omega)z]}\frac{d\omega}{2\pi} \tag{2.110}$$

, where the propagation constant β is a function of ω, as mentioned before, given by the relation

$$\beta(\omega)=n(\omega)\frac{\omega}{c} \tag{2.111}$$

Furthermore, expanding $\beta(\omega)$ around the central frequency ω_0 we get:

$$\beta(\omega)=\beta_0+\beta_1\left(\omega-\omega_0\right)+\frac{1}{2}\beta_2(\omega-\omega_0)^2+\frac{1}{6}\beta_3(\omega-\omega_0)^3+\cdots \tag{2.112}$$

, where

$$\beta_k=\left.\frac{d^k\beta}{d\omega^k}\right|_{\omega=\omega_0}\quad k=0,1,2,... \tag{2.113}$$

The parameters β_k may be calculated using the equations (2.111), (2.112) and (2.113). Calculating the coefficients for and order up to 3 we get

$$\beta_1=\frac{d\beta}{d\omega}=\frac{1}{c}\left(\frac{dn}{d\omega}\omega+n\right)=\frac{1}{c}\left(-\frac{dn}{d\lambda}\lambda+n\right) \tag{2.114}$$

$$\beta_2=\frac{d^2\beta}{d\omega^2}=\frac{1}{c}\left(2\frac{dn}{d\omega}+\omega\frac{d^2n}{d\omega^2}\right)=\frac{\lambda^3}{2\pi c^2}\frac{d^2n}{d\lambda^2} \tag{2.115}$$

$$\beta_3=\frac{d^3\beta}{d\omega^3}=\frac{1}{c}\left(3\frac{d^2n}{d\omega^2}+\omega\frac{d^3n}{d\omega^3}\right)=-\left(\frac{\lambda^5}{4\pi^2c^3}\frac{d^3n}{d\lambda^3}+\frac{3\lambda^4}{4\pi^2c^3}\frac{d^2n}{d\lambda^2}\right) \tag{2.116}$$

Starting from β_1, one may notice by the definition of the equation (2.114) that $\beta_1=\frac{1}{v_g}$, where v_g is the group velocity of the pulse, i.e. the velocity at which the pulse travels. In effect, if we neglect the terms superior to order 1 and we substitute (2.112) into (2.110), we get

$$\mathrm{E}\left(z,t\right)=e^{-j(\beta_0-\beta_1\omega_0)z}\mathrm{E}\left(t-\frac{z}{v_g}\right) \tag{2.117}$$

It becomes then obvious that, in this case, apart from a global phase factor, the optical field remains undistorted while it travels with a velocity v_g. The analysis can be further simplified by neglecting the global phase factor $e^{-j\beta_0 \cdot z}$, by considering a baseband transmission ($\omega_0 = 0\ rad$) and by placing ourselves in a frame of reference moving at the velocity v_g observing the pulse as it travels (or equivalently setting $T = t - \frac{z}{v_g}$) and focusing on $E(T)$. With the previous simplifications it is evident that only the dispersion terms of an order greater than 2 are meaningful for an analysis of the signal distortion.

The term β_2 (given in ps^2/km) is referred to as Group Velocity Dispersion (GVD) parameter and it is responsible for temporal pulse broadening and Inter-Symbol Interference (ISI). However, in most cases we use the *dispersion parameter* D (in $ps/(nm \cdot km)$) defined as

$$D = \frac{d\beta_1}{d\lambda} = -\frac{\lambda}{c}\frac{d^2 n}{d\lambda^2} = -\frac{2\pi c}{\lambda^2}\beta_2 \tag{2.118}$$

Combining the equations (2.108), (2.115) and (2.118) we plot in figure 2.21 the parameters β_2 and D as a function of the wavelength λ.

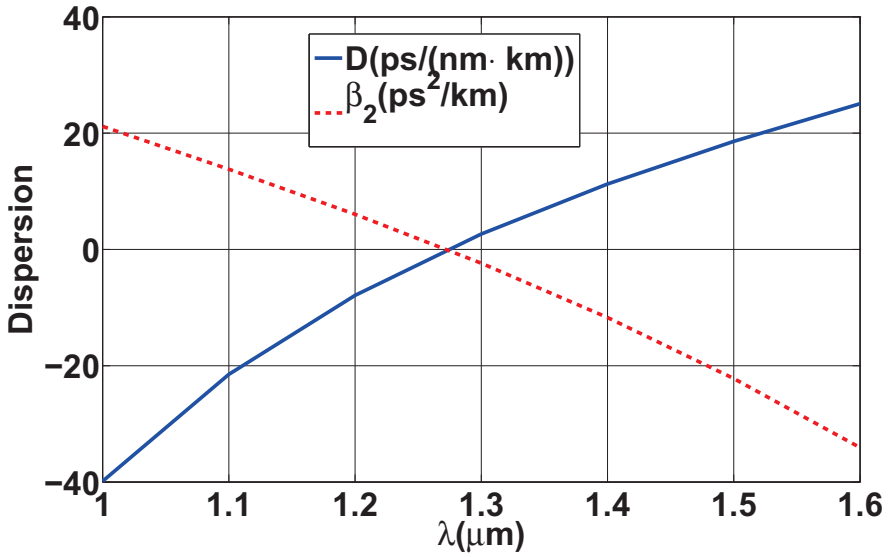

Figure 2.21: Dispersion parameters D and β_2 versus wavelength λ.

From figure 2.21 we see that D is not very far from being linear with respect to λ. This means that in most cases it is sufficient to consider in equation (2.112)

terms of order up to 2. From figure 2.21 we can also see that β_2 and D vanish for $\lambda = \lambda_D \approx 1.27nm$. In the case where λ approaches λ_D we need to take into account β_3 as well. Given that in our numerical simulations we have considered just single channel transmission with a central wavelength of 1.55 μm, in this manuscript we always consider terms up to β_2. Finally, from figure 2.21 we may also notice that there are two regions for $\lambda < \lambda_D$ and $\lambda > \lambda_D$. When $\lambda < \lambda_D$, i.e. β_2 is positive and D is negative the fiber is said to exhibit *normal dispersion* and when $\lambda > \lambda_D$ the fiber is said to exhibit *anomalous dispersion*.

As mentioned above, using (2.112) and (2.110) including just the term relative to β_2 we get

$$\mathrm{E}\left(z,t\right) = \mathrm{E}\left(t\right) \cdot \mathrm{e}^{-j\beta(\omega)z} = \int_{-\infty}^{+\infty} \widetilde{\mathrm{E}}(\omega) e^{-j\frac{1}{2}\beta_2\omega^2 z} e^{j\omega t} \frac{d\omega}{2\pi} \tag{2.119}$$

, where we may replace

$$\widetilde{\mathrm{E}}(z,\omega) = \widetilde{\mathrm{E}}(\omega) e^{-j\frac{1}{2}\beta_2\omega^2 z} = \int_{-\infty}^{+\infty} \mathrm{E}\left(z,t\right) e^{-j\omega t} dt \tag{2.120}$$

, where

$$H_f\left(\omega\right) = e^{-j\frac{1}{2}\beta_2\omega^2 z} \tag{2.121}$$

can be seen as the fiber transfer function when just dispersion is present.

From equation (2.120) we see that chromatic dispersion adds a parabolic phase on the signal spectrum, while the spectrum modulus remains intact. This results in a flattening of the pulse modulus with respect to time.

As an example we consider at the input of a dispersive fiber a Gaussian pulse with a flat phase

$$E\left(t\right) = e^{-\frac{t^2}{2T_0^2}} \tag{2.122}$$

Applying (2.121) on (2.122) we get

$$E\left(z,t\right) = \frac{\mathrm{T}_0}{\sqrt{\mathrm{T}_0^2 + j\beta_2 z}} \exp\left(-\frac{t^2}{2\left(\mathrm{T}_0^2 + j\beta_2 z\right)}\right) \tag{2.123}$$

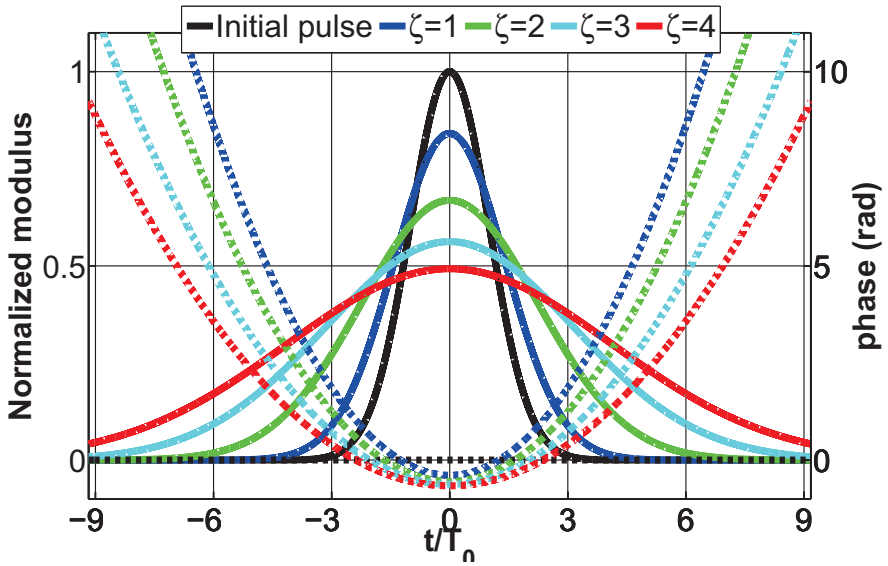

Figure 2.22: Dispersion effect on Gaussian pulse. The time is normalized to T_0 and the dispersion is given as a function of parameter $\zeta = \{1, 2, 3, 4\}$. Solid lines represent the signal modulus, while dashed lines represent signal phase.

or written in a modulus/phase style

$$\frac{\exp\left[-\frac{t^2}{2T_0^2(1+\zeta^2)}\right]}{(1+\zeta^2)^{\frac{1}{4}}} \exp\left[j\left(\frac{t^2\zeta}{2T_0^2\left(1+\zeta^2\right)} - \frac{\tan^{-1}(\zeta)}{2}\right)\right] \tag{2.124}$$

, where the normalized distance ζ is defined as

$$\zeta = \frac{z}{L_D} \tag{2.125}$$

with the *dispersion length* L_D defined[79] as

$$L_D = \frac{T_0^2}{\beta_2} \tag{2.126}$$

We note that for anomalous dispersion fibers, L_D is negative, whereas for normal dispersion fibers L_D is positive. We will see later that the absolute value of the dispersion length, expresses the relative effect of chromatic dispersion.

In figure 2.22 we show the example of an isolated Gaussian pulse (equation (2.122) with $T_0 = 100\ ps$) affected by chromatic dispersion using the parameter

ζ. Commenting on figure 2.22 we see that chromatic dispersion in time domain has an effect on both modulus and phase of the initial pulse. The modulus stays Gaussian but it is significantly flattened, while the phase of the pulse follows a quadratic-like time evolution. From the previous we can also conclude that the pulse edges acquire a higher phase shift in comparison to the center of the pulse ($t/T_0 = 0$). Furthermore we may notice that for $t/T_0 = 0$, higher values of ζ result in lower peak modulus and also a slightly lower phase level. This phase level may be easily calculated by setting $t = 0$ in equation (2.123) and taking the phase of the signal

$$\varphi_0 = -\frac{\tan^{-1}(\zeta)}{2} \tag{2.127}$$

, where we may also easily notice that $\varphi_0 \to -\frac{\pi}{4}$ as $\zeta \to +\infty$.

In the context of optical transmission systems, several pulses are transmitted with a possibly variable phase from one pulse to the other. In this case chromatic dispersion introduces *memory*[98] in the system and neighboring pulses are set to interfere. For classical OOK systems, ISI can be often understood by the fact that the pulse energy penetrates its neighboring slots. If the neighboring symbols are "1"s intensity addition can result in amplitude fluctuations, while if the neighboring symbol was a "0" energy could fill with energy a slot that was initially empty.

If PSK modulation is used, information is coded in the phase of the optical signal and in this case we are mostly interested in the degradation of *phase levels* by chromatic dispersion. We should keep in mind though that as the absolute phase level of the signal cannot be easily recovered at the receiver, the demodulation scheme may be based on the phase difference between adjacent pulses. Furthermore, in other demodulation schemes, (for example a differential scheme), as each pulse interferes with its previous-in-time neighbor, signal modulus may also be important. Finally, we should also keep in mind that a receiver will finally sample the signal, ideally around the center of the pulse and, as a consequence, our interest usually focuses on the central portion of the pulses with respect to time.

In order to get an idea of what may be the effect of chromatic dispersion on PSK modulation systems, in figures 2.23a, 2.23b, 2.23c and 2.23d we investigate

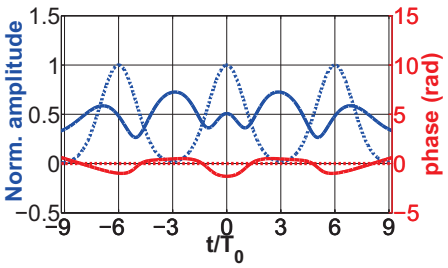

(a) Phase levels 0, 0 and 0 rads

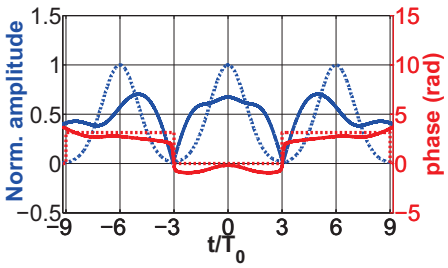

(b) Phase levels π, 0 and π rads

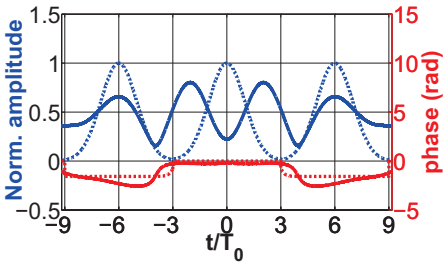

(c) Phase levels $-\pi/2$, 0 and $-\pi/2$ rads

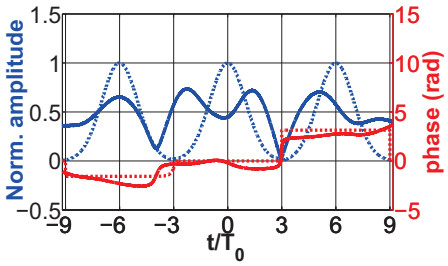

(d) Phase levels $-\pi/2$, 0 and π) rads

Figure 2.23: Effect of chromatic dispersion on three pulses with different phase levels. Dashed lines correspond to the initial pulses and solid lines correspond to pulses after a cumulative chromatic dispersion $D_{cum} = 30000\ ps/nm$. Time slots are equal to $6T_0$ and thus, symbols are centered to $-6T_0$, 0 and $6T_0$, while $T_0 = 100\ ps$.

a simplified case of three adjacent Gaussian pulses with different phase levels, interfering under the effect of chromatic dispersion. We use the phase levels of QPSK, i.e. $\{-\pi/2, 0, \pi/2, \pi\}$, thus approximately emulating three pulses in the context of Return to Zero (RZ)-QPSK transmission.

More precisely, in figure 2.23a the three Gaussian pulses initially have the same phase level (0), in figure 2.23b $\{\pi,\ 0,\ \pi\}$ (symmetric antipodal neighbors around the central symbol), $\{-\pi/2,\ 0,\ \pi\}$, in figure 2.23d and $\{-\pi/2,\ 0,\ -\pi/2\ rad\}$ in figure 2.23c. In all cases, chromatic dispersion results in oscillations of the signal modulus that differ slightly as interferences between symbols may be constructive or destructive. Phase, on the other hand, oscillates as well, with relatively different interference patterns being formed in each case. More precisely, focusing on the phase differences at the center of each pulse and comparing adjacent

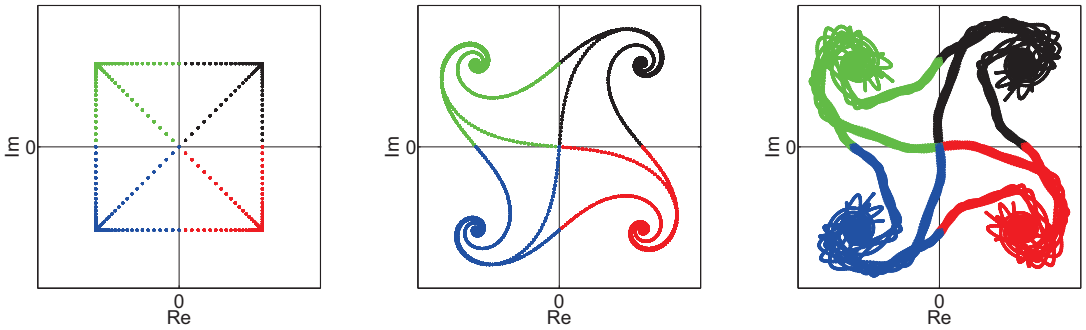

(a) $D_{cum} = 0\ ps/nm$ (b) $D_{cum} = 15\ ps/nm$ (c) $D_{cum} = 40\ ps/nm$

Figure 2.24: Effect of cumulative chromatic dispersion over an NRZ-QPSK signal

pulses, we should note that in the case of 2.23a and 2.23b this difference is minimal, whereas in figure 2.23d it becomes maximal. Of course, a different level of cumulative dispersion could yield completely different results.

Finally, we show some examples of signal constellations under the effect of chromatic dispersion on a NRZ-QPSK signal. In figure 2.24a we observe the initial constellation, while in figures 2.24b and 2.24c, the constellations resulting from the effect of a cumulative dispersion of $D_{cum} = 15\ ps/nm$ and $D_{cum} = 40\ ps/nm$. Commenting on figure 2.24b for such a low value of D_{cum}, the constellation has a characteristic "spiral" shape. More precisely, the samples located near the origin $(Re, Im) = (0, 0)$ i.e. the state transitions, as they normally correspond to high frequencies, they acquire a high positive phase shift. On the other hand, samples located at the center of the pulse, as they correspond to low frequencies, they acquire a very low negative phase shift given by eq. (2.127). In figure 2.24c on the other hand, in addition to the frequency-dependent phase shift due to the isolated-pulse chromatic dispersion effect, we also visualize the effect of ISI. Indeed, since D_{cum} is relatively higher, the overall field is the coherent sum of the fields of all interfering symbols and therefore, the constellation shape is no more a pure spiral.

2.2.1.3 Polarization Mode Dispersion

Chromatic dispersion is not the only effect that results in different components experiencing a different refractive index and therefore a different velocity. In the

context of single mode fibers, the two degenerate polarization components may experience a slightly different refractive index, as well. Although silica fibers are generally isotropic and cylindrically symmetric, small random variations in their shape, changes in temperature, random stresses applied after its installation etc., may result in a minor refractive index difference (also known as *birefringence magnitude*) B_m between the two polarization components[62], where

$$B_m = |n_x - n_y| \tag{2.128}$$

The result will be that one polarization component will propagate faster than the other and it will also induce a periodic coupling between the two components with a period

$$L_B = \frac{\lambda}{\mathrm{B}_m} \tag{2.129}$$

, where B_m was defined in (2.128) and λ is the signal wavelength. Supposing that an input OOK pulse excites both polarization components of a fiber, the difference in their propagation speed will result in the two pulses being detected at a slightly different time. Since photo-diodes (described later in section §2.2.3.1) are indifferent to polarization changes, the photo-current will contain a "superposition" of the two pulses giving the impression of a pulse broadening, changing randomly since in practice B_m changes randomly. This phenomenon is known as Polarization Mode Dispersion (PMD). The extent of pulse broadening may be estimated from the delay between the two polarization components during a propagation of a distance L in the fiber, known as Differential Group Delay (DGD) and defined as

$$\Delta\mathrm{T} = L\left|\frac{1}{v_{g,x}} - \frac{1}{v_{g,y}}\right| = L\,|\beta_{1,x} - \beta_{1,y}| \tag{2.130}$$

, where $\beta_{1,x}$, $\beta_{1,y}$ refer to the term β_1 of the eq. (2.112) expansion, of the polarization x or y correspondingly. PMD is actually characterized by the variance of the ΔT quantity, defined in eq. (2.130). In the context of this manuscript we consider propagation in only one polarization and thus, we neglect all effects relative to PMD.

2.2.1.4 Fiber Non-linearities

The electric displacement vector in a dielectric medium is given by

$$\overrightarrow{D} = \varepsilon_0 \overrightarrow{\mathrm{E}} + \overrightarrow{P} \tag{2.131}$$

, where ϵ_0 is the vacuum permittivity and $\overrightarrow{P}$ is the material *polarization density vector*. Far from material resonances, polarization can be generally described by the phenomenological relation[101]

$$\overrightarrow{P} = \varepsilon_0 \left(\chi^{(1)} \cdot \overrightarrow{\mathrm{E}} + \chi^{(2)} : \overrightarrow{\mathrm{E}}\,\overrightarrow{\mathrm{E}} + \chi^{(3)} \vdots \overrightarrow{\mathrm{E}} + \cdots \right) = \overrightarrow{P_L} + \overrightarrow{P_{NL}} \tag{2.132}$$

, where χ^j is the j^{th} order susceptibility tensor, $\overrightarrow{P_L}$ corresponds to just the inclusion of 1^{rst} order term (linear term) $\varepsilon_0 \chi^{(1)} \cdot \overrightarrow{\mathrm{E}}$ and all the higher order terms (nonlinear terms) are included in $\overrightarrow{P_{NL}}$. It is obvious that higher order nonlinear terms are significant only for relatively high optical power levels. Moreover, for a silica fiber the 2^{nd} order term vanishes as silica molecules present an inversion symmetry[3]. Therefore, the lower order nonlinear effects appearing in fibers, stems from the third order susceptibility tensor $\chi^{(3)}$.

Nonlinear effects in fibers can be classified to two categories: *nonlinear refraction* (also referred to as Kerr effect) and inelastic scattering involving *Stimulated Raman Scattering* and *Stimulated Brillouin Scattering*. In the context of this thesis, all numerical simulations take into consideration the most significant nonlinear effect, i.e. the Kerr effect.

Kerr nonlinearity manifests itself as an almost instantaneous[1] modification of the medium refractive index linearly with the optical field intensity, i.e.

$$\tilde{n}\left(\omega, |E|^2\right) = n\left(\omega\right) + n_2 |E|^2 = n_L + n_{NL} \tag{2.133}$$

, where the medium refractive index contains two contributions, a linear one ($n_L = n\left(\omega\right)$) and a nonlinear one ($n_{NL} = n_2 |E|^2$), where n_2 is the *nonlinear-index coefficient* and $|E|^2$ is the optical field intensity. In other words, high

[1] In order for the Kerr effect to be considered instantaneous, the transmitted pulses should not be shorter than approximately 1 ps.[3]

optical intensity results in a higher refractive index and a higher refractive index results in a slower propagation in the medium. The optical intensity of modulated pulses presents variations with respect to time and therefore, each "part" of the pulse is experiencing a different refractive index and is accumulating a different phase. Since E is measured in V/m, the units for n_2 should normally be m^2/V^2. However, it is more convenient[2] to write $n_{NL} = n_2^I I$ and use the coefficient $n_2^I I$, where the intensity of the optical field I is linked to the electric field by the relation

$$I = \frac{1}{2}\varepsilon_0 cn\,|E|^2 \tag{2.134}$$

,where ε_0 is the vacuum permittivity ($\varepsilon_0 = 8.85421 \cdot 10^{12}\ F/m$), c is the velocity of light ($c = 2.998 \cdot 10^8\ m/s$) and n is the linear part of the refractive index $n \approx 1.45$. In this case the parameter $n_2^I I$ has units m^2/W and is related to n_2 by the relation

$$n_2^I = \frac{2n_2}{\varepsilon_0 cn} \tag{2.135}$$

Introducing a time frame moving with the complex envelope of A of the field, absorbing fiber attenuation and normalizing A by introducing the quantity U, defined via the relation $A = \sqrt{P_0}\exp\left(-\frac{\alpha z}{2}\right)U$, it can be shown[3] that if Kerr nonlinearities act alone, the evolution of $U(z,T)$ may be given by

$$U\,(z,T) = U\,(0,T)\exp\left(-j\phi_{NL}(T)\right) \tag{2.136}$$

, where $T = t - \beta_1 \cdot z$ and we also introduce the quantities *effective length* L_{eff}

$$L_{eff} = \frac{1-\exp\left(-\alpha z\right)}{\alpha} \tag{2.137}$$

, *nonlinear length* L_{NL}

$$L_{NL} = \frac{1}{\gamma P_0} \tag{2.138}$$

, *max nonlinear phase* $\varphi_{\max}$

$$\varphi_{\max} = \frac{L_{eff}}{L_{NL}} \tag{2.139}$$

and finally the *nonlinear phase* $\varphi_{NL}(t)$

$$\varphi_{NL}(t) = |U(0,t)|^2 \frac{L_{eff}}{L_{NL}} \tag{2.140}$$

We should also note that often the definition of $\varphi_{\max}$ is extended to include multi-span systems with flat gain repeaters, i.e.

$$\varphi_{\max} = N_s \cdot \frac{L_{eff}}{L_{NL}} \tag{2.141}$$

, where N_s is the number of spans.

From equations (2.136) and (2.139) it is obvious that when Kerr nonlinearities act alone (i.e. when dispersion is neglected), only the phase of the complex envelope is modified, whereas the modulus remains intact. Moreover, the added phase $\varphi_{NL}(t)$ depends on two critical parameters: $\varphi_{\max}$ which quantifies the strength of nonlinear effects and the initial pulse shape $U(0,t)$. Since the phase of the field is modified following its own intensity shape, this phenomenon is called *self-phase modulation*, or Self Phase Modulation (SPM).

In OOK communications information is coded on signal modulus and the detection is performed by photo-detectors that are sensible to optical power. Therefore, if SPM is acting alone distorting the signal phase (i.e. chromatic dispersion is neglected), since the phase is discarded, there is no impact on the signal quality. In PSK modulation, on the other hand, nonlinear effects change the absolute phase level of the signal and, at first glance, this may seem detrimental for the signal quality. However, considering that all PSK states have initially the same power profile, based on equation (2.140) we can see that even with absolute phase changing, phase differences between states are maintained. Thus, focusing for example on the central part of each pulse (where information is usually coded) and considering a differentially coherent detection (or an ideal phase-lock loop), we equivalently deduce that nonlinearities have no impact on measured bit error rate.

As an example we consider the initial signal constellation of figure 2.24a being subject to Kerr nonlinearities only. In figures 2.25a, 2.25b and 2.25c we show the

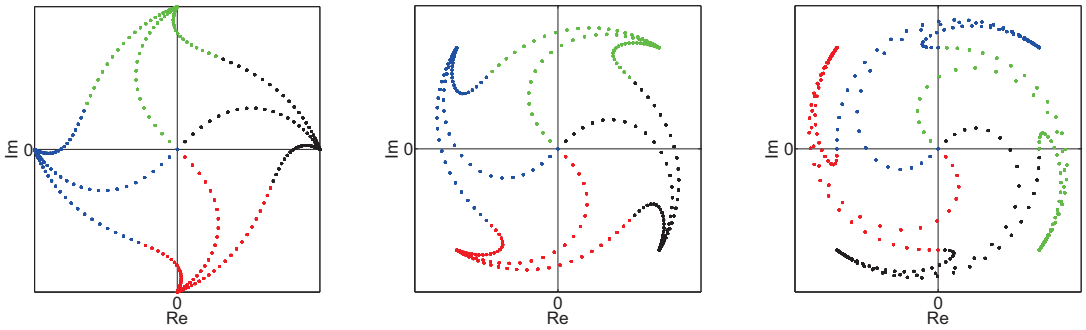

(a) $\varphi_{max} = \pi/4\ rad$ or a propagation of about 13 spans

(b) $\varphi_{max} = \pi/2\ rad$ or a propagation of about 26 spans

(c) $\varphi_{max} = \pi\ rad$ or a propagation of about 52 spans

Figure 2.25: Effect of Kerr nonlinearities if they act alone. Examples of QPSK constellations are shown, where in all cases φ_{max} is given as well as an approximate equivalent number of spans for a propagation over a fiber with $D = 0\ ps/(nm{\cdot}km)$ and all the rest of the characteristics (i.e. n_2, A_{eff} and attenuation) the same as in SMF, for a central wavelength of $1.55\mu m$ and an injection power per span $P_{in} = 3\ dBm$.

resulting constellations for characteristic levels of $\varphi_{\max}$ equal to $\pi/4$, π and $3\pi/4$. For example, in figure 2.25a where we consider $\varphi_{max} = \pi/4\ rad$, we see that all four QPSK states are de-phased by exactly $-\pi/4$, while it is evident that this is the part that corresponds exactly to the symbols center. On the other hand, transitions are de-phased in a different way, since higher power parts acquire a higher phase shift, lower power parts acquire a lower phase shift, while parts that are close to the edges of the symbol slot are not de-phased at all. Finally, we can see that sampling the signal at the center of each symbol slot and removing the global phase shift results in a perfect recovery of the initial signal.

2.2.1.5 Nonlinear Schrödinger equation

In a simplified scenario

In a simplified scenario (explained in detail below) the propagation of the slowly varying complex envelope of the optical field $A(t)$ is governed by the Non-Linear Schrödinger Equation (NLSE)[3]:

$$\frac{\partial A}{\partial z} = j\frac{\beta_2}{2}\frac{\partial^2 A}{\partial T^2} - j\gamma\left|A\right|^2 A - \frac{\alpha(z)}{2}A \tag{2.142}$$

, where z is the propagation distance, $T = t - z/v_g = t - \beta_1 \cdot z$ is a transformed time adjusted to the propagating pulse, α is the attenuation coefficient, β_2 the group velocity dispersion parameter, $\gamma = \frac{2\pi}{\lambda}\frac{n_2}{A_{eff}}$ the nonlinear parameter, λ the signal wavelength, n_2 the nonlinear-index coefficient and A_{eff} the effective mode area of the fiber.

Furthermore, we use the normalized distance defined in eq. (2.125), the normalized time τ defined as

$$\tau = \frac{t - z/v_g}{T_0} = \frac{T}{T_0} \tag{2.143}$$

, where T_0 is the pulse duration and, finally, the normalized pulse $U(\zeta, \tau)$ defined by the relation

$$A = \sqrt{P_0}e^{-\frac{\alpha z}{2}}U \tag{2.144}$$

, where $P_0 = |A|^2$ is the pulse power.

Combining the equations (2.125),(2.143),(2.144) it can be shown that eq. (2.142) can be written as

$$\frac{\partial U}{\partial \zeta} = j\frac{1}{2}\frac{\partial^2 U}{\partial \tau^2} - jN^2 e^{-\alpha z}\left|U\right|^2 U \tag{2.145}$$

, where the parameter N is defined as

$$N^2 = \frac{L_D}{L_{NL}} = \frac{\gamma P_0 T_0^2}{\beta_2} \tag{2.146}$$

, with the characteristic length L_D and L_{NL} defined by the equations (2.126) and (2.138).

Equation (2.142) is derived after having silently made three important assumptions: 1) the term $\overrightarrow{P_{NL}}$ in equation (2.132) is negligible in front of the term $\overrightarrow{P_L}$, (2) the optical field is assumed to maintain its polarization along propagation and (3) the optical field is quasi-monochromatic, where the slowly varying complex envelope approximation is applicable. The first assumption is generally true

since nonlinear changes in the refractive index are $< 10^{-}6$. The second assumption holds for polarization maintaining fibers only but it also works quite well in practice. For the purposes of this manuscript we will consider that this assumption is also fulfilled. The third assumption is equivalent to considering that the spectral width Δf of our field is very small compared to the central frequency f_0, or $\frac{\Delta f}{f_0} << 1$. In our case, $f_0 \approx 200THz$ and this condition is still approximately fulfilled for modulated signal with its main lobe occupying a spectral width of about $\Delta f \approx 20THz$ (or a pulse width of about 0.1ps[3]). For the purposes of this manuscript we consider that this assumption is fulfilled, as well.

2.2.2 Transmitters, signal modulation and modulation formats

Fiber-optic systems were dominated for many years by transmission/reception schemes based on simple OOK modulation formats, i.e. optical power in the form of NRZ or RZ pulses representing "1"s and no power representing "0"s (see §2.1.3.1). The reasons behind this choice were technological, economical and historical. Indeed, a flexible choice of modulation format supposes a coherent receiver, as previously achieved in the domain of wireless communications. In optics, despite the early efforts in this direction[84] and the relative advantages of coherent detection against direct detection (see section §2.2.5), research on coherent receivers was stalled as optical Phase Lock Loops (PLLs) remained complex and the advent of Erbium-Doped Fiber Amplifiers (EDFAs) has completely reoriented research to rapidly take advantage of the possibilities of an immediate increase of system capacity.

Nevertheless, in 2002, generation and differential, non-coherent de-multiplexing of QPSK was demonstrated in optics[55], re-vitalizing the research in modulation formats. Moreover, with the re-birth of coherent detection in mid 2000s, research on different modulation formats has been revitalized with the objective to reveal their advantages/disadvantages in different contexts.

In the following we describe the generation process of three modulation formats, used in this manuscript, i.e. OOK, (D)BPSK and (D)QPSK, with NRZ-

or RZ-shaped pulses. For each of these formats we also describe a non-coherent demodulation method, principally used before the advent of coherent detection.

2.2.2.1 General characteristics

In most cases where external modulation is used, the light from a laser that is set to a Continuous Wave (CW) mode, is modulated by a Mach-Zehnder Modulator (MZM)[31] (see figure 2.26).

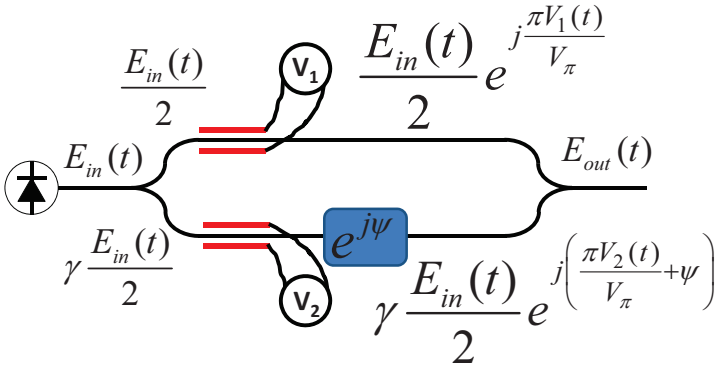

Figure 2.26: Mach-Zehnder Modulator

The MZM[31] is made up by a $3-dB$ coupler that splits the incoming signal $E_{in}(t)$ in two parts, $E_1(t)$ and $\gamma \cdot E_2(t)$, two electro-optic cells that according to the applied tensions $V_1(t)$, $V_2(t)$ induce on the signal a phase shift $\varphi_1(t)$ or $\varphi_2(t)$ correspondingly, and finally another $3-dB$ coupler to sum up the contributions over the two arms. Optionally, we may also include a component in the second arm that provokes a fixed phase shift ψ, referred to as the modulator bias[115].

The parameter γ is defined as

$$\gamma = \frac{\sqrt{\delta}-1}{\sqrt{\delta}+1} \tag{2.147}$$

with δ being the dc extinction ratio of the modulator. In the context of our numerical simulations we have always considered an ideal MZM, i.e. $\delta \to +\infty$ or $\gamma \to 1$.

The output field $E_{out}(t)$ is then given by

$$E_{out}(t) = \frac{E_{in}(t)}{2}\left(e^{j\varphi_1(t)} + e^{j\varphi_2(t)}\right) = \frac{E_{in}(t)}{2}\left(e^{j\frac{\pi V_1(t)}{V_\pi}} + e^{j\frac{\pi V_2(t)}{V_\pi}}\right) \tag{2.148}$$

, where V_π is the modulator extinction voltage, a fixed value that characterizes the electro-optic material. Following equation (2.148), the output electric field can be written as

$$E_{out}(t) = E_{in}(t)e^{j\left[\frac{\pi}{2V_\pi}(V_1(t)+V_2(t))+\frac{\psi}{2}\right]}\cos\left[\frac{\pi}{2V_\pi}\left(V_1(t) - V_2(t)\right) - \frac{\psi}{2}\right] \tag{2.149}$$

As it appears, at the output of the modulator, the electric field E_{out} is equal to the input field E_{in} multiplied by two terms: one representing a phase modulation and one representing an amplitude modulation. The phase modulation (chirp) is often unwanted and it can be eliminated by choosing $V_1(t) + V_2(t) = V_b = cst$, where V_b is a constant tension, referred to as *bias tension*. This condition is noted as *balanced driving* or push-pull operation of the MZM. In the case of balanced driving when we also set $\psi = 0$, the optical field transfer function of the Mach-Zehnder is given by

$$\mathrm{T}_E(\mathrm{V}_1(\mathrm{t})) = e^{j\left(\frac{\pi}{2V_\pi}V_b\right)}\cos\left[\frac{\pi}{2V_\pi}\left(2V_1(t) - V_b\right)\right] \tag{2.150}$$

Mach-Zehnder modulators appear in the generation process of all types of modulation formats, as it will be shown in the following sections.

2.2.2.2 Generation of Amplitude Shift Keying modulation

In amplitude modulation, information is coded in two logical modulus (or intensity) levels, while phase is disregarded[1]. These levels are normally represented in the electric field by a high tension (logical "1") or a zero tension (logical "0").

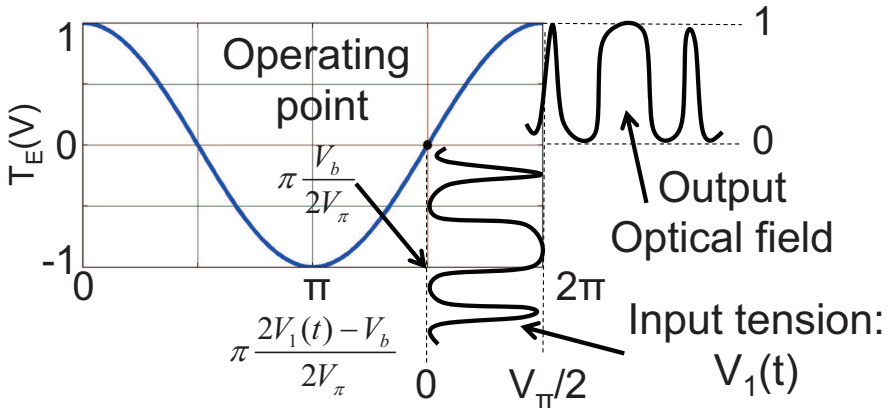

Figure 2.27: MZM function: generating OOK-NRZ modulation.

2.2.2.2.1 Generation of Amplitude Modulation

In order to "transfer" this signal into the optical domain we would ideally need an element with a transfer function being a straight line with a slope equal to 1, for varying values of V_1 between 0 and 1. In the case of the MZM we can emulate this function by setting $\frac{\pi V_b}{2V_\pi} = \frac{\pi}{2} \Rightarrow V_b = V_\pi$ in equation (2.150). By neglecting the global phase term, in this case we get the optical transfer function of the NRZ modulator:

$$T_E\left[V_e(t)\right] = \sin\left[\frac{\pi V_1(t)}{V_\pi}\right] \tag{2.151}$$

We can easily verify that when the electric signal $V_1(t)$ varies in the range $\left\{0, \frac{V_\pi}{2}\right\}$, the modulator function is monotonically increasing in the range $\{0, 1\}$ with the NRZ electric signal being "transfered" to the optical domain. We can also note that since the Mach-Zehnder transfer function is not a linear function of $V_1(t)$, the created optical signal will be slightly "filtered" by the $sin(\cdot)$ function.

[1] In certain OOK modulation formats like duobinary or Phase Shaped Binary Transmission (PSBT)[86], certain phase conditions we used between adjacent pulses, in order to increase the pulse tolerance against chromatic dispersion. Nevertheless, even in this case, the pulse phase was eventually discarded by photodiodes.

2.2.2.3 Generation of Binary Phase Shift Keying modulation

A (normalized) BPSK signal is characterized by an almost fixed modulus and a phase of 0 or π radians or equivalently, a modulus varying in the range $\{-1, 1\}$. In order to generate an optical BPSK signal, we need to use a portion of the modulator transfer function that similarly varies in the range $\{-1, 1\}$ with a slope as close as possible to $+1$. In this case we may set $V_b = V_\pi$ in equation (2.150), but noting that this time, $V_1(t)$ varies in the range $\left\{-\frac{V_\pi}{2}, \frac{V_\pi}{2}\right\}$ (figure 2.28).

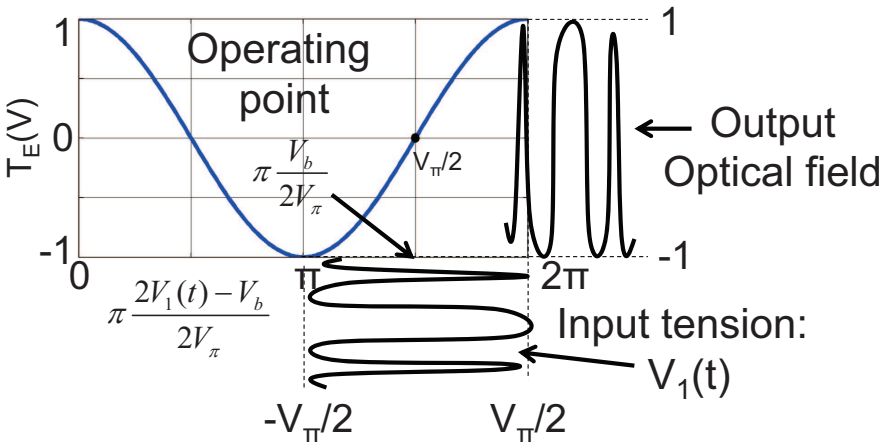

Figure 2.28: Generation of BPSK modulation.

2.2.2.4 Generation of Quaternary Phase Shift Keying modulation

As demonstrated in [55], QPSK modulation can be achieved by using a Cartesian modulator, based on nested Mach-Zehnder configuration. The idea is to modulate the two independent complex signal quadratures independently and then sum up the two contributions. The configuration is shown in figure 2.29.

The laser source is split up with the use of a 3-dB coupler into two arms, where a MZM set in push-pull operation is found. The driving signals of the MZM are two independent BPSK signals, namely U and V, that after modulation result in two BPSK optical signals (shown with constellations in figure 2.29), as described in section §2.2.2.3.

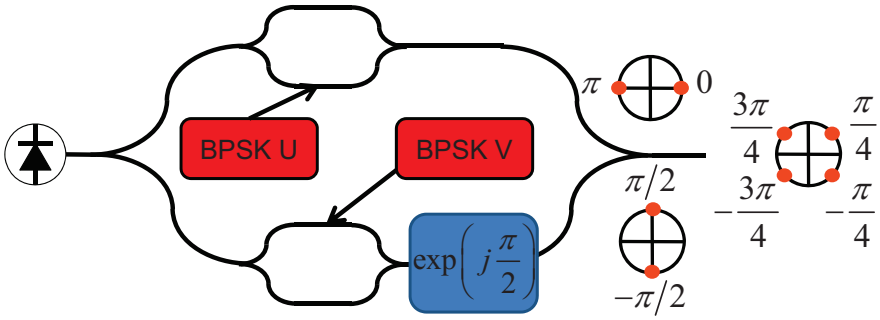

Figure 2.29: Generation of QPSK modulation.

By the above process it is evident that U will give birth to an optical BPSK field with the same characteristics of U. On the other hand, the optical field created after the signal V is additionally de-phased by $\frac{\pi}{2}$. Finally, the two fields are summed up by another 3-dB coupler. In the resulting field, each quaternary symbol will be the result of the (coherent) sum of the two contributions (i.e. either $\{0, \pi\}$ or $\{-\pi/2, \pi/2\}$), resulting in an overall QPSK signal.

Finally, in order to generate a RZ-QPSK waveform with a Gaussian-like shape (instead of NRZ-QPSK where intensity is almost constant) a *pulse carver* needs to be added after the last MZM. A pulse carver is actually another modulator (MZM for instance), driven by a sinusoidal waveform with a frequency equal to the data rate (for 50%-RZ)[115].

2.2.3 Signal Reception

The key element found in signal reception of any modulation format is the *photo-diode*. As it will be detailed below, the output of a photodiode is a current that is proportional to the incident optical power. Using a photodiode, the detection of OOK modulated signals is straight-forward since a high current intensity corresponds to a high optical power intensity and therefore a possibly transmitted "1", whereas a low current intensity corresponds to a low optical power and a possibly transmitted "0". Nevertheless, even PSK modulated signals are demodulated using photo-diodes. In all cases, detection is achieved by, either an interference of each symbol with the previous symbol, or by a local oscillator reference signal, while at the end, a photo-current is usually detected. In the following we review

the most important aspects of photodiodes and very briefly describe the detection of ASK signals, eventually focusing on the detection of PSK signals, that are our main interest in this manuscript.

2.2.3.1 Photodiodes

Photodetectors (photoreceivers or photodiodes) ideally convert incident optical power into an electric current, often called *photocurrent*. The conversion is generally linear, i.e.

$$I = R_d P_{in} \tag{2.152}$$

where R_d is the *responsivity* of the diode with

$$R_d = \frac{\eta q}{h\nu} \tag{2.153}$$

with η being the quantum efficiency of the photodiode, q being the electron charge and $h \cdot \nu$ being the photon energy.

However, unfortunately, the resulting photocurrent, apart from the contribution that is proportional to the signal power, it also contains noise added by the photodetector. This noise comes from two independent sources, (1) the fact that the photocurrent is a stream of electrons generated at random times[1], referred to as *shot noise*, and (2) to the thermal motion of electrons inside a resistor[2] that, even in the absence of external voltage, results in a current fluctuation, referred to as *thermal noise*. Furthermore, it can be shown[5] that these two processes have approximately Gaussian statistics with zero average and standard deviations σ_s and σ_t correspondingly. Thus, the overall process can be equivalently described by a Gaussian random variable with zero average and standard deviation $\sigma_s t$, given by the equation

$$\sigma_{st}^2 = \sigma_s^2 + \sigma_t^2 = N_{st}\Delta f = \left(2q\left(\bar{I} + I_d\right) + \frac{4k_B T}{R_L}F_n\right)\Delta f \tag{2.154}$$

[1]Shot noise is related to vacuum fluctuations and it is the inevitable consequence of the quantum nature of light, rather than a receiver imperfection.

[2]The load resistor at the front end of a photodetector can cause such fluctuations.

where F_n is the amplifier noise figure, $k_B \cdot T$ is the energy associated with electrons at a finite temperature, R_L is the load resistance, q is the electron charge, $\bar{I}$ is the average current, I_d is the dark current and finally δf is the effective noise bandwidth. We should underline that the contribution of the shot-noise (σ_s) depends on the average current, while the thermal noise contribution does not.

In optical transmission systems where the predominant noise contribution is the amplified spontaneous emission noise of in-line amplifiers, all other types of noise, as thermal noise or shot noise are neglected.

2.2.3.2 Demodulation of Amplitude Shift Keying

As mentioned before, the demodulation of ASK with the use of photodiodes is quite straightforward. Since each amplitude level is mapped into a discrete power level, after detection it eventually leads to a discrete photocurrent level. Superposing all symbols at the same time frame results in what is often referred to as an *eye diagram*. In figure 2.30 we show a typical eye digram for OOK modulation where signal degradation is not so important.

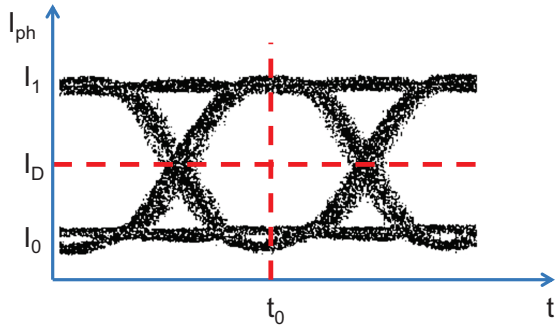

Figure 2.30: Eye digram for OOK modulation.

Setting the threshold current level I_D, or choosing the time instant t_0 (clock) are often subject to an optimization process, as a function of the system characteristics. A current integration at the instant t_0 and a decision circuit based on I_D are finally used, in order to count the number symbols that are transmitted erroneously and build up the system BER.

2.2.3.3 Demodulation of Differential Phase Shift Keying

The demodulation principle of DBPSK is shown in figure 2.31a. The incoming signal is set to interfere with its delayed version by one symbol period and the resulting signal is passing in the photodiode. We then map a zero photocurrent into the symbol "0" and a non-zero photocurrent into the symbol "1".

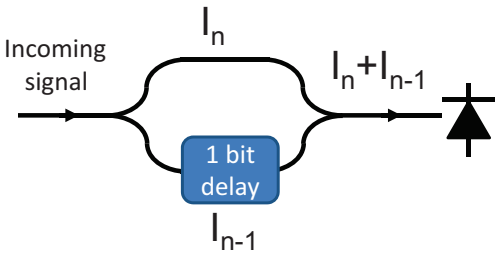

(a) Experimental set-up achieving DBPSK demodulation.

{Ib$_n$}	0	0	1	1	0	1	0	0	1	0	1
{Pb$_n$}	0	0	1	0	0	1	1	1	0	0	1
{I$_n$}	-1	-1	1	-1	-1	1	1	1	-1	-1	1
{Ip$_n$}	1	1	0	0	1	0	1	1	0	1	0
{Id$_n$}	0	0	1	1	0	1	0	0	1	0	1

(b) Example of a sequence pre-coding and decoding.

Figure 2.31: Principle of demodulation in DBPSK.

When the two interfering symbols are different (i.e. one with a phase 0 rad and one with a phase π rad), the interference is destructive and the overall field vanishes, eventually yielding a null photocurrent. On the contrary, when the two symbols are identical, the interference is constructive and the photocurrent is non zero. In table 2.31b we show an example of a sequence pre-coding and decoding. The initial bit sequence $\{Ib_n\}$ is pre-coded resulting into the sequence $\{Pb_n\}$ and the sequence $\{Pb_n\}$ is transmitted mapping "0" to the phase level π and "1" to the phase level 0. The detected (decoded) sequence $\{Id_n\}$ is then the inverse of the sequence resulting from the photo-current $\{Ip_n\}$ and if no errors have occurred during transmission $\{Id_n\} = \{Ib_n\} = \{\overline{Ip_n}\}$. We need to note that in practice, for the demodulation of DBPSK a balanced photodiode is used, with a better performance than the simple photodiode, as discussed in [45].

The demodulation of DQPSK is performed in a similar way as in the DBPSK case, although it is slightly more complicated. The demodulator principle is shown in figure 2.31. The incoming signal, based on the precoded binary sequences U_k and V_k as described in section §2.1.3.3, after propagation is split up in two branches. At each branch, a phase shifted and a symbol-period delayed

version of the signal interfere in a destructive and in a constructive way, finally ending up in two balanced photo-detectors with photocurrents I_{IP} and I_Q.

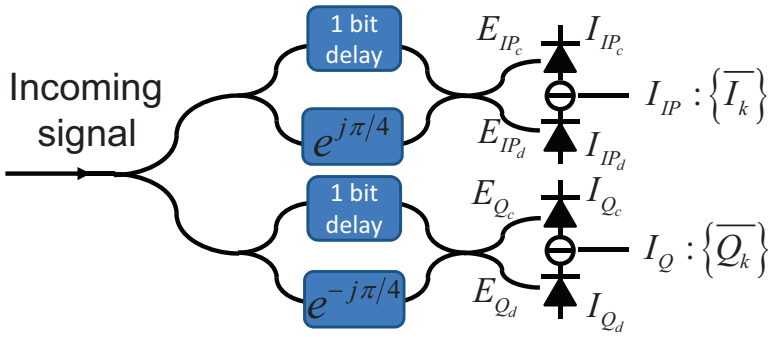

Figure 2.32: Principle of demodulation in Differential Binary Shift Keying.

In effect, supposing that the current symbol has a phase ϕ and its previous one has a phase ϕ_T, it can be shown that the photocurrents are described by the equations

$$\begin{aligned} I_{IP} &= \mathrm{I}_{IP_c} - \mathrm{I}_{IP_d} \sim 4\cos\left(\varphi - \varphi_T + \tfrac{\pi}{4}\right) \\ I_Q &= \mathrm{I}_{Q_c} - \mathrm{I}_{Q_d} \sim 4\cos\left(\varphi - \varphi_T - \tfrac{\pi}{4}\right) \end{aligned} \tag{2.155}$$

A positive photo-current is interpreted as "1" and a negative photo-current is interpreted as "0". If no error occurs during transmission, the sequences $\{\overline{IP_k}\}$ and $\{\overline{Q_k}\}$ are successfully detected.

2.2.4 Amplifiers and noise

As we have seen in section §2.2.1, despite the constant technological progress, the primary limiting physical effect in fibers still remains the attenuation of the optical field, especially in cases where one is interested in transmitting information over high distances. In order to overcome this obstacle, optical amplifiers are used, especially when it comes to long-haul systems where light travels over several hundreds of kilometers before finally reaching the receiver. Nevertheless, the amplification comes at the cost of adding noise to the transmitted signal.

There are two possible amplification schemes: distributed amplification or lumped amplification. In the case of distributed amplification, the signal is amplified during its propagation throughout the transmission fiber that becomes the

amplification medium in this case. When talking about distributed amplification, the most common case crossing one's mind is the Raman amplification[57]. On the other hand, in lumped amplification, in order to compensate for fiber losses, an amplifier is placed at the end of every fiber section. A typical case of lumped amplifiers are the EDFAs. In this manuscript we only consider lumped amplification, at the end of every span.

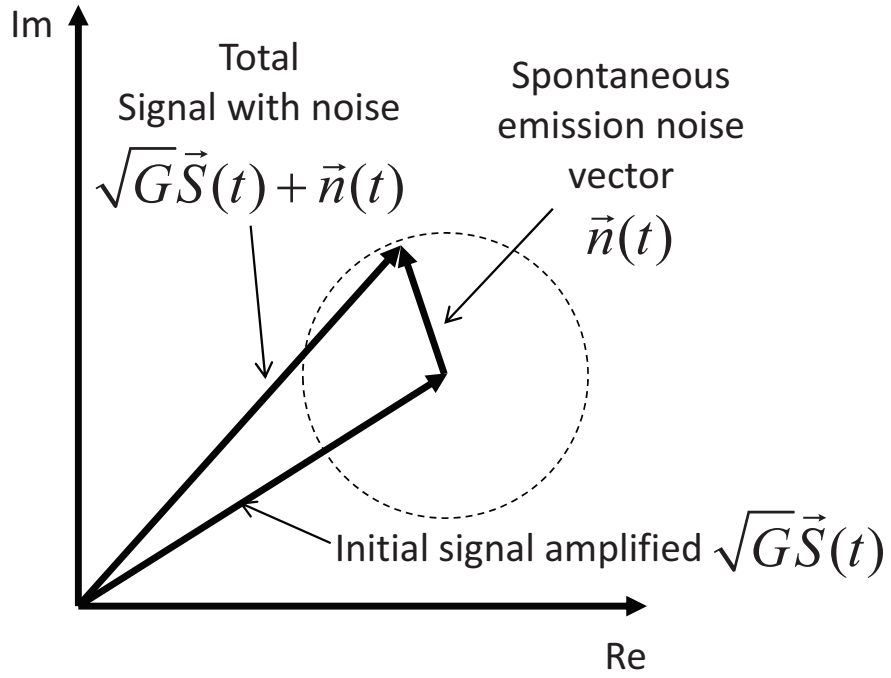

Figure 2.33: Spontaneous emission

In a medium with gain, optical amplification is achieved through *stimulated photon emission* from the excited states of the medium ions (for example, erbium ions when it comes to EDFAs[13]). More precisely, if P_{in} is the power of a CW at the input of an amplifier and P_{out} is the power at the output, then

$$G = \frac{P_{out}}{P_{in}} \tag{2.156}$$

, where G is the *amplifier gain*.

However, from time to time, a photon is spontaneously emitted from the excited state with a random phase and polarization, occasionally perturbing the

signal, as shown in figure 2.33. This process is known as *amplified spontaneous emission*. In a fundamental level, amplified spontaneous emission has its origins at vacuum fluctuations and therefore at the quantum-mechanical nature of light. Using either a semi-classical or a quantum mechanical treatment of the amplification process, it has been demonstrated in the literature that the Amplified Spontaneous Emission (ASE) noise can be considered as an AWGN with and autocorrelation function

$$\varphi_{nn,ASE}(\tau) = n_{sp} h\upsilon (G-1)\,\delta(\tau) \tag{2.157}$$

, or alternatively a power spectral density

$$N_{ASE} = n_{sp} h\nu (G-1) \tag{2.158}$$

, where G is the amplifier gain, h is the constant of Planck, ν is the wavelength of the signal and n_{sp} is the inversion factor, linked to population of the fundamental state N_1 and the population of the excited state N_2 by the relation

$$n_{sp} = \frac{N_2}{N_2 - N_1} \tag{2.159}$$

Considering an ideal optical filter of bandwidth W just after the amplifier to reduce the amount of added noise, the power of ASE noise becomes

$$P_{ASE} = 2N_{ASE}W \tag{2.160}$$

, where the factor 2 is due to the fact that noise is added in both signal polarizations. However, we need to note that only one noise quadrature has an influence on the signal.

In optical communication system with lumped amplification, we very commonly use the OSNR, of a signal with an input power $P_{s,in}$, after a cascade of N_A amplifiers with a gain G and a power spectral density N_{ASE} as defined by eq. (2.158), where amplifiers perfectly compensate for the span losses ($a_i = G_i$ as shown in figure 2.34). In this case, OSNR is defined as

$$OSNR = \frac{G \cdot P_{s,in}}{2N_{ASE}N_A W_{ref}} \tag{2.161}$$

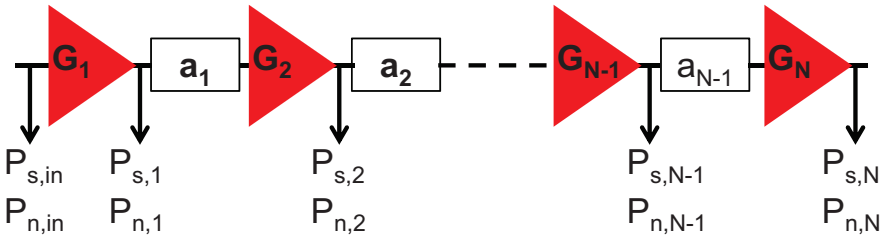

Figure 2.34: Cascade of amplifiers and fiber spans. We usually consider that amplifiers perfectly compensate for the span losses.

, where once more, the factor 2 corresponds to the fact that we count the contributions of both signal polarizations, while W_{ref} is a reference bandwidth. W_{ref} is very commonly chosen to be 12.5 GHz and since 12.5 GHz corresponds to approximately 0.1 nm around the wavelength 1.55μm, we refer to $OSNR_{0.1}$ (an OSNR in 0.1 nm). Replacing eq. (2.158) in (2.161) and taking a reference bandwidth of $W_{ref} = 12.5\ GHz$, eq. (2.161) may be written in dB scale as

$$OSNR_{0.1}\,(dB) = P_{out,amp}\,(dBm) - NF\,(dB) - N_A\,(dB) + 58\,(dBm) \quad (2.162)$$

, where the noise factor NF is defined as

$$NF = 2n_{sp}\frac{G-1}{G} \quad (2.163)$$

and the number 58 comes from the dB conversion of the product $h \cdot v \cdot B_{ref}$ and the conversion of power from Watts into dBm. The previous formula is very useful when it comes to determining the input power in an amplifier of a given NF, in order to achieve a specific $OSNR$. In what follows we always refer to an OSNR at the reference bandwidth of 0.1 nm.

2.2.5 Coherent detection in lightwave communications

In the first operational fiber optic systems, information was coded on the *intensity* of the optical signal. In this case, at the transmitter side, the binary information is "printed" on an electric bit stream (for example with non-zero intensity for each "1" and zero intensity for each "0") that most often linearly

modulates the intensity of an optical carrier, while at the same time the receiver is directly converting the optical power into a current with the use of a photo-diode, thus detecting a "1" (non-zero intensity of the photo-current) or a "0" (zero intensity of the photo-current). The main advantage of this scheme, usually referred to as Intensity Modulation (IM)/Direct Detection (DD), is its undeniable simplicity. Nevertheless, it remains "primitive" in the sense that reception uses just one signal quadrature (modulus), while the information contained in the phase of the signal carrier is discarded during demodulation, essentially remaining unexploited[84].

It has been known for a fact that in the context of wireless communications, with advanced modulation formats and exploitation of both signal quadratures, there comes the potential of a better utilization of the medium bandwidth and thus an increase of spectral efficiency. Such schemes involve a receiver that is sensible to both phase and modulus of the transmitted signal, known as *coherent receiver*. Moreover, a bonus coming with optical coherent receivers is an increased signal gain coming from the local oscillator, leading to an increased receiver sensitivity that is being "pushed" towards the shot noise limit[4],[63] of photo-diodes. For repeater-less systems, the benefit of increased receiver sensitivity could be directly converted into achieving greater distances, as constraints over the fiber span loss may be relaxed[96].

Motivated by the above benefits, research efforts quickly focused on coherent receivers during the eighties. However, technological obstacles and problems linked to the receiver complexity (such as, the complexity of optical PLLs), prevented an immediate practical implementation of coherent systems. In parallel, over the same period, the invention of EDFAs[33] made less significant the receiver sensitivity benefit promised by coherent receivers, since spontaneous emission noise is dominant over shot noise, while they offered at the same time the possibility to dramatically increase capacity by a simultaneous transmission of a wide range wavelengths. The overall result was that, in the forthcoming years, research over coherent systems was temporarily stalled, while the vast majority of installed systems were based on an OOK modulation coupled with a DD.

Similarly, the comeback of coherent detection around mid 2000s, is undoubtedly a combined result of technical, historical, and economical circumstances[96].

At first, discussion over different modulation formats was re-opened by Griffin and Carter, proposing in [55] a scheme for the modulation of both the in-phase and quadrature of an optical signal, while they have also proposed a direct differential detection scheme for QPSK. A little later, Kahn and Ho, indicated in [61] the need for more spectrally efficient modulation formats, while, finally, Taylor suggested in [107] a method of coherent demodulation and a carrier phase estimation based on high-speed electronics, thus bypassing the need for a phase-locked loop. This method was experimentally tested by Tsukamoto et al in [109] and various other teams, confirming the re-birth of coherent detection in the optical communications field. At the same time, as coherent receiver was coming with the potential of digital signal processing, the use of algorithms for the compensation of physical effects, such as chromatic or polarization mode dispersion, were thoroughly investigated[108],[24],[12].

In this section we review the most important concepts around coherent detection, including its modern, efficient implementation method.

2.2.5.1 Principle of the coherent detection

In optical communications, with the term *coherent systems* we refer to systems that involve a local oscillator at the reception, (i.e. a laser) which is the key element in this case. More specifically, the signal that is about to be detected, before passing into a photo-diode it is added to (or mixed with) the local oscillator signal. A simplified scheme of a coherent detection is shown in figure 2.35.

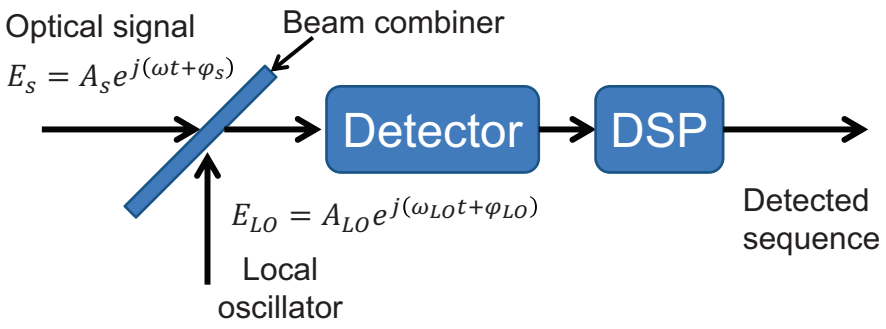

Figure 2.35: Coherent detection principle

Supposing that both signals are identically polarized, the initial signal is given by

$$E_s = A_s e^{j(\omega t + \varphi_s)} \tag{2.164}$$

, where A_s is the signal amplitude, ω is the carrier frequency and φ_s is the signal phase (possibly including some kind of phase modulation) and the local oscillator signal is given by

$$E_{LO} = A_{LO} e^{j(\omega_{LO} t + \varphi_{LO})} \tag{2.165}$$

, where A_{LO} is the amplitude of the local oscillator signal, ω_{LO} is the frequency of the local oscillator (that differs from ω) and φ_{LO} is the local oscillator phase.

The detector is sensitive to the overall power of the optical field $P_{tot}(t)$, generating (in the absence of noise) a photo-current $I_{ph}(t) = R \cdot P_{tot}(t)$, i.e.

$$I_{ph}(t) = R \cdot P_{tot}(t) = R \cdot \left(P_s + P_{LO} + 2\sqrt{P_s}\sqrt{P_{LO}} \cos\left(\omega_{IF} t + \varphi_s - \varphi_{LO}\right) \right) \tag{2.166}$$

, where $P_s = A_s^2$, $P_{LO} = A_{LO}^2$ and $\omega_{IF} = \omega - \omega_{LO}$ is known as *intermediate frequency*. We focus on the second term since it is the term containing the modulation[1].

When $\omega_{IF} = 0$ we refer to a *homodyne detection*, while if $\omega_{IF} \neq 0$ the detection is called *heterodyne*[4]. Homodyne and heterodyne detection have advantages and disadvantages. For example, homodyne systems have a superior receiver sensitivity of 3 dB with respect to heterodyne systems but there is a need of an optical PLL, an implementation of which is very complex[4] and therefore, heterodyne systems were preferred in comparison to homodyne systems. However, the author of [107] has shown that using ultrafast electronics could provide a "software" alternative for the optical PLL and therefore release the major complexity problem of homodyne receivers.

[1] In reality this term is isolated by passing from a 3 dB coupler and a balanced photo-diode, or alternatively, from a 90 deg optical hybrid in the case of a polarization diversity detector. In general, the resulting current is the outcome of a subtraction of the two photo-currents[66].

2.2.5.2 Phase diversity homodyne receiver

In practice, the coherent mixer is implemented using a number of free space components as shown in figure 2.36, a Local Oscillator (LO), a Quaternary Wave Plate (QWP), a Half Mirror (HM), two Polarization Beam Splitters (PBSs) and collimators (Coll) at the input and output ports.

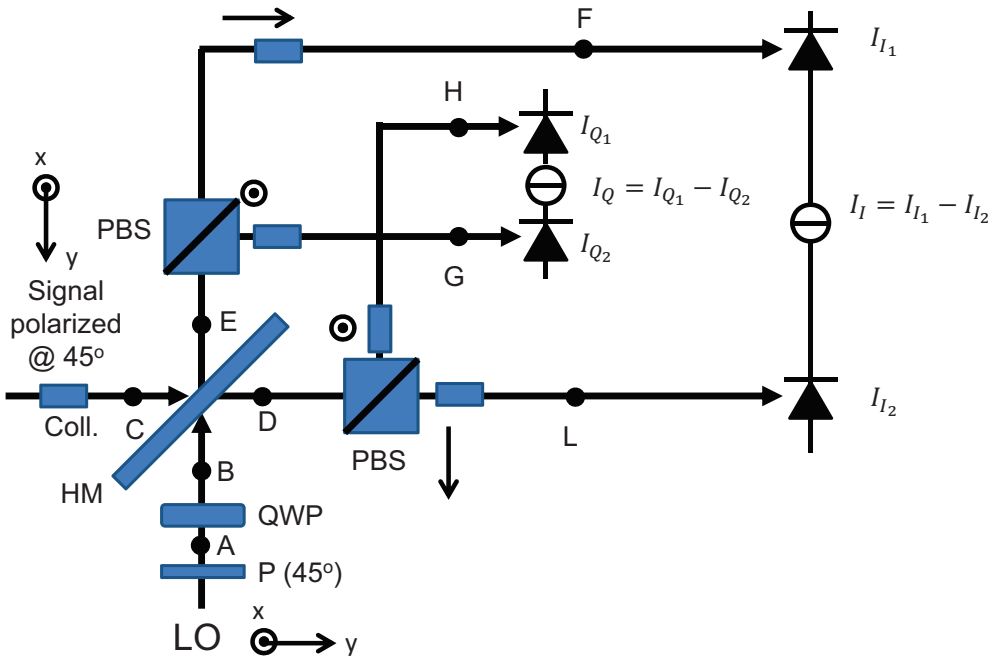

Figure 2.36: Coherent detection with phase diversity

Supposing that the incoming optical signal is polarized at 45 deg with respect to the x and y axes and that the local oscillator signal immediately passes from a 45 deg polarizer, the optical field vector at the points A, B and C are given by $\overrightarrow{E_A(t)} = \frac{1}{\sqrt{2}} \begin{bmatrix} 1 \\ 1 \end{bmatrix} A_{LO} e^{j(\omega_{LO}t+\varphi_{LO})}$, $\overrightarrow{E_B(t)} = \frac{1}{\sqrt{2}} \begin{bmatrix} 1 \\ e^{j\frac{\pi}{2}} \end{bmatrix} A_{LO} e^{j(\omega_{LO}t+\varphi_{LO})}$ and $\overrightarrow{E_C(t)} = \frac{1}{\sqrt{2}} \begin{bmatrix} 1 \\ 1 \end{bmatrix} A_s e^{j(\omega t+\varphi_s)}$.

Getting past HM the new field vectors become

$$\overrightarrow{E_D(t)} = \frac{1}{2} \left(\begin{bmatrix} 1 \\ e^{j\frac{\pi}{2}} \end{bmatrix} A_{LO} e^{j(\omega_{LO}t+\varphi_{LO}+\frac{\pi}{2})} + \begin{bmatrix} 1 \\ 1 \end{bmatrix} A_s e^{j(\omega t+\varphi_s)} \right) \tag{2.167}$$

and

$$\overrightarrow{E_E(t)} = \frac{1}{2}\left(\begin{bmatrix} 1 \\ e^{j\frac{\pi}{2}} \end{bmatrix} A_{LO}e^{j(\omega_{LO}t+\varphi_{LO})} + \begin{bmatrix} 1 \\ 1 \end{bmatrix} A_s e^{j(\omega t+\varphi_s+\frac{\pi}{2})}\right) \tag{2.168}$$

The optical fields and consequently the incident optical power at the level of each photo-diode are given by

$$\overrightarrow{E_F(t)} = \hat{y}\frac{1}{2}\left(A_{LO}e^{j(\omega_{LO}t+\varphi_{LO}+\frac{\pi}{2})} + A_s e^{j(\omega t+\varphi_s+\frac{\pi}{2})}\right) \tag{2.169}$$

$$\overrightarrow{E_G(t)} = \hat{x}\frac{1}{2}\left(A_{LO}e^{j(\omega_{LO}t+\varphi_{LO})} + jA_s e^{j(\omega t+\varphi_s)}\right) \tag{2.170}$$

$$\overrightarrow{E_H(t)} = \hat{x}\frac{1}{2}\left(A_{LO}e^{j(\omega_{LO}t+\varphi_{LO}+\frac{\pi}{2})} + A_s e^{j(\omega t+\varphi_s)}\right) \tag{2.171}$$

$$\overrightarrow{E_L(t)} = \hat{y}\frac{1}{2}\left(-A_{LO}e^{j(\omega_{LO}t+\varphi_{LO})} + A_s e^{j(\omega t+\varphi_s)}\right) \tag{2.172}$$

and finally,using the equations (2.169), (2.170), (2.171), (2.172), the photo-currents are given by

$$\mathrm{I_I}(t) = RA_sA_{LO}\cos\left(\left(\omega-\omega_{LO}\right)t+\varphi_s-\varphi_{LO}\right) \tag{2.173}$$

$$\mathrm{I_Q}(t) = RA_sA_{LO}\sin\left(\left(\omega-\omega_{LO}\right)t+\varphi_s-\varphi_{LO}\right) \tag{2.174}$$

or

$$I_c(t) = RA_sA_{LO}\exp\left[j\left(\left(\omega-\omega_{LO}\right)t+\phi_s-\phi_{LO}\right)\right] \tag{2.175}$$

From equation (2.175) we see that we can recuperate both signal quadratures. If our signal contains two orthogonal polarizations we use PBSs at the input of both E_s and E_{LO} in order to isolate each polarization component. Then, each polarization component is recovered separately by a configuration similar to the one of figure 2.36, called polarization diversity coherent mixer.

In order to recover the actual information, sampling and digitizing the signal of the equation (2.175) will result in the discrete signal $I_c(k\cdot T)$, where T is the symbol period (we finally keep one sample per symbol). Then, usually a maximal

ratio combiner is used[66] in order to recover the transmitted information. For the purposes of this manuscript, the recovery of the signal polarization components and complex quadratures is supposed ideal and if not indicated otherwise, simulations are done for single polarization systems.

In practical modern coherent detection systems, we focus on a homodyne detection where the two signal quadratures are extracted with the help of electronics. More precisely, the local oscillator frequency is considered to be sufficiently close to the signal frequency (near to homodyne detection), without necessarily being exactly the same[1]. Thus, in the equation (2.175), we consider that ω_{IF} is very small but not zero and $f_{IF} = \frac{\omega_{IF}}{2\pi}$ is in any case lower than the symbol modulation rate.

For MPSK, equation (2.175) may be written as

$$\begin{aligned} I_c(t) &= RA_sA_{LO}\exp\left[j\left(\left(\omega-\omega_{LO}\right)t+\phi_M+\phi_{s,n}-\phi_{LO}\right)\right]= \\ &= RA_sA_{LO}\exp\left[j\left(\left(j\omega-\omega_{LO}\right)t+\phi_M+\phi_n\right)\right]=RA_sA_{LO}\exp\left(j\theta\right) \end{aligned} \tag{2.176}$$

, where φ_M is the modulation term (for example, in MPSK $\phi_M \in \left\{0, \frac{2\pi}{\mathrm{M}}, 2\frac{2\pi}{\mathrm{M}}, ..., (\mathrm{M}-1)\,\frac{2\pi}{\mathrm{M}}\right\}$), where $\phi_{s,n}$ is the noise term associated with the signal, φ_{LO} is the local oscillator phase, φ_n is the total phase noise and finally, we note with θ the overall phase of the detected signal.

From (2.176) we see that the phase of the detected signal, apart from the modulation term ϕ_M, it also contains the terms $\omega_{IF}\cdot t$ and ϕ_n. The evaluation of ϕ_M is most often done by following the algorithm described in [110]: We first rise the complex samples $I_C(k\cdot t)$ at the M^{th} power and then we divide by M. By this procedure we remove the modulation as it may be easily observed that $M\cdot\phi_M = 2k\pi, k\in\mathbb{Z}$. Furthermore, in order to overcome the redundant noise ϕ_n, we emulate a low pass filter by taking the average over a *block* of $2n+1$ symbols with the block size being a function of the noise term[74],[47]. Equivalently, the estimation is given by

$$\theta_e(kT) = \frac{\arg\left(\sum_{l=-n}^{n} I_C[(k+l)\,T]^M\right)}{M} \tag{2.177}$$

[1]In any case the transmitter and local oscillator linewidths may vary up to about 10 MHz.

Thus, the estimated phase of the symbol k is given by

$$\widehat{\phi_M(kT)} = \theta(kT) - \theta_e(kT) \tag{2.178}$$

We note that the phase detection method used above, is a variant of a differentially encoded, coherently detected PSK, as the one described in section §2.1.4.3.3.

In practical transmission systems, coherent receivers incorporate polarization and phase diversity. In this case, a "chain" of adapted algorithms[95] may be used to electronically compensate for the residual chromatic dispersion, the PMD or separate the two polarization components with the use of an adapted algorithm (Constant Modulus Algorithm (CMA) for example). Since our main interest is to study the transmission effects we are not going to get into the details of the aforementioned algorithms.

2.2.6 Inter-channel nonlinear impairments

As we have seen above, EDFAs have provided the potential of signal amplification over a wide range of frequencies (or wavelengths), allowing for a dense WDM. This practically means that several signals modulated at different frequencies (or wavelengths) can propagate in the fiber at the same time. In this case, the overall propagating field $A(z,T)$ may be written as

$$A = \sum_{k=1}^{L_{ch}} A_k e^{j2\pi F_k t} \tag{2.179}$$

, where $F_k = f_k - f_0$, f_k is the carrier frequency of the k^{th} channel and f_0 is the reference carrier frequency that has been used to derived eq. (2.142). Supposing that eq. (2.142) is still valid for the new field A made up of all channels and replacing eq. (2.179) into (2.142) we get the expression

$$\begin{aligned} &\sum_{k=1}^{L_{ch}} \left(\frac{\partial A_k}{\partial z} + 2\pi F_k \beta_2 \frac{\partial A_k}{\partial T} - j\frac{\beta_2}{2}\frac{\partial^2 A_k}{\partial T^2} + \frac{\alpha(z)}{2} A_k + j\frac{\beta_2}{2} 2\pi F_k^2 A_k \right) = \\ &= -j\gamma \sum_{k=1}^{L_{ch}} A_k \sum_{l=1}^{L_{ch}} A_l^* e^{-j2\pi F_l t} \sum_{m=1}^{L_{ch}} A_m e^{j2\pi F_m t} \end{aligned} \tag{2.180}$$

It is obvious that eq. (2.180) is equivalent to a set of L_{ch} coupled equations, with each equation describing the evolution of the complex envelope A_k of the k^{th} channel

$$\begin{aligned}&\frac{\partial A_k}{\partial z}+\left(2\pi F_k\right)\beta_2\frac{\partial A_k}{\partial T}-j\frac{\beta_2}{2}\frac{\partial^2 A_k}{\partial T^2}+\frac{\alpha(z)}{2}A_k+j\frac{\beta_2}{2}\left(2\pi F_k\right)^2 A_k=\\&=-j\gamma A_k\sum_{l=1}^{L_{ch}}A_l^* e^{-j2\pi F_l t}\sum_{m=1}^{L_{ch}}A_m e^{j2\pi F_m t}\end{aligned} \tag{2.181}$$

, while there are L_{seq} equations like (2.181), for $k=1,2,...,L_{ch}$.

We note that the left part of eq. (2.181) represents the linear operator of NLSE, while the right part is the nonlinear operator, appearing in the form of a double summation. Developing and re-arranging the nonlinear term, it may be alternatively written in the form

$$\begin{aligned}&-j\gamma A_k\sum_{l=1}^{L_{ch}}A_l^* e^{-j2\pi F_l t}\sum_{m=1}^{L_{ch}}A_m e^{j2\pi F_m t}=\\&-j\gamma\left(\underbrace{A_k\left|A_k\right|^2}_{SPM}+\underbrace{2A_k\sum_{\substack{l=1,\\l\neq k}}^{L_{ch}}\left|A_l\right|^2}_{XPM}+\underbrace{A_k\sum_{\substack{l=1,\\l\neq k}}^{L_{ch}}e^{-j2\pi F_l t}A_l^*\sum_{\substack{m=1,\\m\neq l}}^{L_{ch}}e^{j2\pi F_m t}A_m}_{FWM}\right)\end{aligned} \tag{2.182}$$

At the right part of eq. (2.182) we see three terms appearing, denoted as SPM, Cross Phase Modulation (XPM) and Four Wave Mixing (FWM). The term SPM is the same as the nonlinear term appearing in eq. (2.142). It represents the contribution of pure SPM impacting the waveform of the k^{th} channel, or otherwise, the term that is responsible for *intra-channel nonlinearities*. In section §2.2.7 we will get into more details, subdividing intra-channel nonlinearities into different kinds. On the other hand, the terms XPM and FWM represent nonlinearities that are induced to the k^{th} channel by the other channels. These nonlinearities are referred to as *inter-channel nonlinearities*. The XPM term quantifies the phase modulation for which power from other channels is responsible, instead of the power of the k^{th} channel itself. Finally, the FWM term, is responsible for high-peaked oscillations of the optical field, resulting from a mechanism of summing

three frequency components to create a components at a frequency that is the sum of the other three. It is evident that FWM can be particularly detrimental for the channel waveform.

In the context of this manuscript, as all simulation results refer to single channel propagation, we are not going to discuss inter-channel nonlinearities. However, similar mechanisms as XPM and FWM exist in single channel propagation, as it will be shown in the what follows.

2.2.7 Intra-channel nonlinear impairments

The optical fiber is a dispersive and nonlinear medium. Under the effect of chromatic dispersion, the energy of each pulse "penetrates" neighboring symbol slots and interferes with them. Since chromatic dispersion is a linear effect, such an interference would be easily recoverable with dispersion compensating fibers. However, the Kerr effect provokes a nonlinear interaction between symbols turning inter-symbol interference nonlinear. The overall result is that, even if at the receiver, chromatic dispersion is fully compensated, inevitably, each symbol contains a "residual" degradation that each symbol has collected during nonlinear interaction with its n neighboring symbols. In this case we often say that the channel has a *memory*[98] of n symbols.

An intuitive way to understand inter-symbol interference under the effect of fiber nonlinearities is to follow the same procedure as in section §2.2.6 describing inter-channel effects. More precisely, we decompose eq. (2.142) into a set of (coupled) equations, where the field of each symbol (or pulse) is considered separately[72],[5].

Rewriting eq. (2.6) here for convenience, the overall field A is given as a sum of all partial fields A_k, where A_k is the field of the k^{th} symbol, i.e.

$$A = \sum_{k=1}^{L_{seq}} A_k \tag{2.183}$$

Replacing eq. (2.183) into (2.142), we get the expression

$$\left(\frac{\partial}{\partial z} - j\frac{\beta_2}{2}\frac{\partial^2}{\partial T^2} + \frac{\alpha(z)}{2}\right)\left(\sum_{k=1}^{L_{seq}} A_k\right) = -j\gamma \sum_{k=1}^{N} A_k \sum_{l=1}^{N} A_l^* \sum_{m=1}^{N} A_m \tag{2.184}$$

We note that the left part of eq. (2.184) represents the linear operator of NLSE, while the right part is the nonlinear operator, appearing in the form of a triple sum. Developing and re-arranging the terms of the triple sum, it may be alternatively written in the form

$$\begin{aligned}&\sum_{k=1}^{N} A_k \sum_{l=1}^{N} A_l^* \sum_{m=1}^{N} A_m = \\ &\sum_{k=1}^{L_{seq}} |A_k|^2 A_k + 2\sum_{k=1}^{L_{seq}} A_k \sum_{\substack{l=1,\\ l\neq k}}^{L_{seq}} |A_l|^2 + \sum_{k=1}^{L_{seq}} A_k \sum_{\substack{l=1,\\ l\neq k}}^{L_{seq}} A_l^* \sum_{\substack{m=1,\\ m\neq l}}^{L_{seq}} A_m\end{aligned} \tag{2.185}$$

, or finally, re-writing eq. (2.185) as a set of L_{seq} coupled equations describing the evolution of each partial field A_k for $k = 1, 2, ..., L_{seq}$

$$\begin{aligned}&\left(\tfrac{\partial}{\partial z} - j\tfrac{\beta_2}{2}\tfrac{\partial^2}{\partial T^2} + \tfrac{\alpha(z)}{2}\right) A_k = \\ &= -j\gamma\left(\underbrace{A_k |A_k|^2}_{i-SPM} + \underbrace{2A_k \sum_{\substack{l=1,\\ l\neq k}}^{L_{seq}} |A_l|^2}_{i-XPM} + \underbrace{A_k \sum_{\substack{l=1,\\ l\neq k}}^{L_{seq}} A_l^* \sum_{\substack{m=1,\\ m\neq l}}^{L_{seq}} A_m}_{i-FWM}\right)\end{aligned} \tag{2.186}$$

At the right part of eq. (2.186) we see three terms appearing: Intra-channel Self Phase Modulation (i-SPM), Intra-channel Cross Phase Modulation (i-XPM) and Intra-channel Four Wave Mixing (i-FWM). Similarly as in the case of inter-channel nonlinearities, the term i-SPM (*intra-channel self-phase modulation*) depends on the pulse power itself and it corresponds to the SPM that the isolated pulse induces to itself. The term i-XPM (*intra-channel cross-phase modulation*) includes the power "contributions" of all other pulses but the one of interest.

It quantifies the portion of SPM that is provoked by neighboring pulses to the pulse of interest and it is obvious that for such an interaction to take place, chromatic dispersion needs to have introduced a considerable pulse overlap. Finally, the term i-FWM (*intra-channel four-wave mixing*), includes the contributions of various symbols on the phase modulation of the pulse of interest. We need to note that a mechanism including an exact phase-matching is needed for this nonlinearity to be "efficient".

Intra-channel nonlinearities have been widely studied in the past, with a focus on OOK modulation systems. Typical examples of work towards this direction may be found in [99], [35], [77], [80], [1] and [113]. The investigation of intra-channel nonlinearities is also the main objective of this thesis[1].

2.2.8 Fundamental limitations in fiber optic channels

As it becomes clear, there are two degradation sources that *fundamentally* limit an optical transmission system performance[2]: (1) spontaneous emission noise added by fiber amplifiers and (2) fiber non-linearities. In order to qualitatively understand the impact of these sources we briefly review the fundamental limits present in optical transmission.

In long- or ultra-long haul systems where signal amplification is needed, the first fundamental limitation comes from ASE noise added by an amplifier. Moreover, since noise in this case is linked to the quantum-mechanical nature of light, it cannot be avoided or reduced below a certain level (see section §2.2.4), yielding a first fundamental limitation of fiber-optic systems. With a fixed noise quantity, SNR is uniquely influenced by the level of signal power and since performance in terms of BEP is bijectively linked to SNR, the system BEP is bijectively linked to signal power.

[1] When this thesis began in 2008, detailed investigations of intra-channel nonlinearities for PSK modulated systems we rare. However, as our work was in progress, such investigations appeared, for example the work in [71], [116] or [81].

[2] When we talk about system performance we basically refer to the maximum bit-rate that can support reliable communications for a given distance or equivalently, the system spectral density if we also fix the system bandwidth.

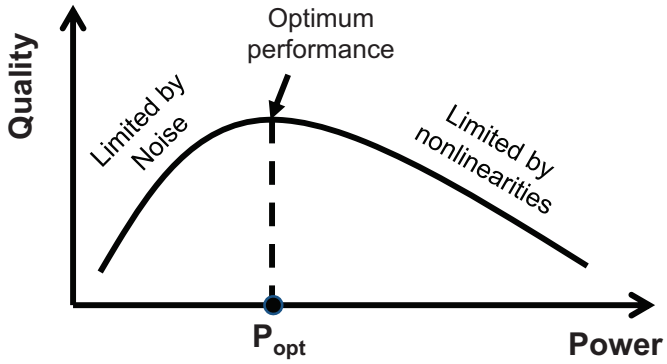

Figure 2.37: Qualitative curve of system quality (or equivalently system reach) in optical telecommunication systems as a function of the injected power per span.

For a low signal power, fiber nonlinearities are negligible and the system is practically linear. In this case the system is dominated by additive white Gaussian noise and as discussed in section §2.1.4, another fundamental limitation comes from the fact that reliable communications induce an upper limit on information spectral density, given by Shannon's formula (equation (2.92)). In this formula, information spectral density η is a monotonically increasing, logarithmic function of the signal-to-noise ratio per bit SNR/bit and since noise power has a fundamental lower limit, SNR/bit (and η) may be increased by increasing the signal power.

At first glance, a power increase seems safe since a fiber optic channel is not a fundamentally power-limited channel[1]. Therefore, it would seem reasonable to infinitely increase information spectral density by increasing the signal injected power. Nevertheless, increasing signal power, lets another fundamental limitation of optical fibers comes into play and that is fiber nonlinearities. The authors of [82] have built a model for which the nonlinear fiber-optic system is qualitatively described by an equivalent linear system with *multiplicative noise*. Multiplicative noise can be understood as the result of XPM, since it represents a form of interference of neighboring channels that contain generally unknown information. It is also argued that, even in single-channel transmission, multiplicative noise is

[1]Such as, for example a satellite channel where the increase of power in a wavelength would directly imply an interference to another.

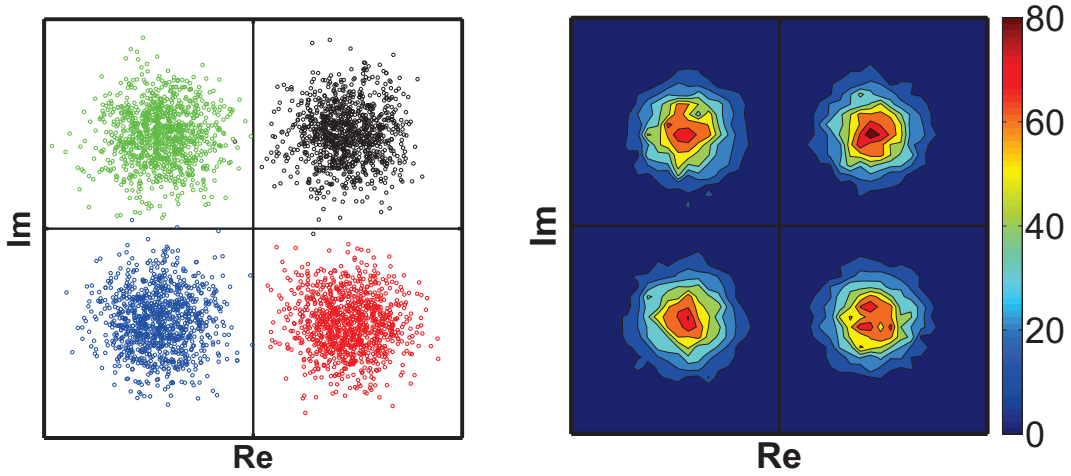

(a) Signal constellation (b) Signal PDF

Figure 2.38: Example of degraded signal degraded just by AWGN with an $OSNR_{0.1} = 11\ dB$ and a Gaussian filter.

generated through the cubic nonlinear term of eq. (2.142), by the stochastic (noise) part of the signal.

In figure 2.37 we plot a qualitative "bell-shaped" curve summarizing the above fundamental limits. Signal quality, usually expressed in terms of Q^2 factor converted from BER, is plotted as a function of the injected power per span, for a fixed distance. When the injection power is low, nonlinearities are negligible and the system is linear, impacted by noise. Linear effects can be almost perfectly compensated and in this case the system is usually referred to as *noise-limited*. The left part of the curve should, therefore, be identical to one of the curves of figure 2.13, for PSK modulation and an ideal coherent detection. A constellation and PDF example of a configuration impacted just by additive white Gaussian noise is shown in figures 2.38a, 2.38b. On the other hand, at the right end of the graph, signal power (and SNR) is high. However, multiplicative noise coming from nonlinearities is deteriorating the system performance and this regime is usually referred to as *nonlinearity-limited*. Finally, the exact evolution of the signal quality, as a function of the injected power, depends on the system parameters and/or the correction algorithms applied by the coherent receiver.

2.2.9 Impairment mitigation

As discussed in section §2.2.1, propagation in optical fibers is subject to several physical effects that eventually degrade the input signal and increase the system performance in terms of bit error probability. However, for each degrading factor there exist technological solutions or techniques aiming to compensate for the degradation and restore the signal to its original shape.

The principal degradation factor in fiber propagation is the *attenuation* of the optical field. Nevertheless, fiber attenuation was efficiently tackled, while ultra long-haul transmissions were made easily possible after the invention of EDFAs (see section §2.2.4), at the price of the added noise to the optical signal and the deterioration of the signal-to-noise ratio.

Another historically important "problem" in optical communications is *chromatic dispersion*, that when acting alone provokes a pulse broadening, resulting into an ISI. Even though chromatic dispersion is a linear effect when acting alone, it may be very efficiently compensated with the use of *dispersion compensating fibers* compensating for the cumulative chromatic dispersion at the end of every span or adapted Finite Impulse Response (FIR) filters that compensate for the total cumulative chromatic dispersion electronically, in systems equipped with a coherent receiver.

Nevertheless, the specificity of the fiber-optic channel that eventually limits the transmission distance is the degradation due to the interplay between linear effects and *fiber nonlinearities*. The technique mainly employed in the past to mitigate the impact of nonlinearities was *dispersion management*. The basic idea behind this technique is a system design employing a wise distribution of the dispersion compensating fiber modules along the line, so that the impact of nonlinearities is minimal. In addition, since the re-appearance of coherent detection, several research efforts have been also focusing on correction algorithms, suitable for the correction of nonlinear effects. In the following we present the basic concepts behind dispersion management.

Dispersion managed systems involve an arrangement of fibers with alternate GVD parameter signs, for example $D_1, D_2, D_3, ...$ where $D_k > 0$, when $k = even$ and $D_k < 0$, when $k = odd$. Furthermore, the cumulative dispersions

$D_{cum,1}, D_{cum,2}, ...$ are usually chosen in a wise manner (for example following a specific law) so that the impact of nonlinear effects is minimized. The ensemble of the values $Dcum, k$ are usually referred to as *dispersion map*.

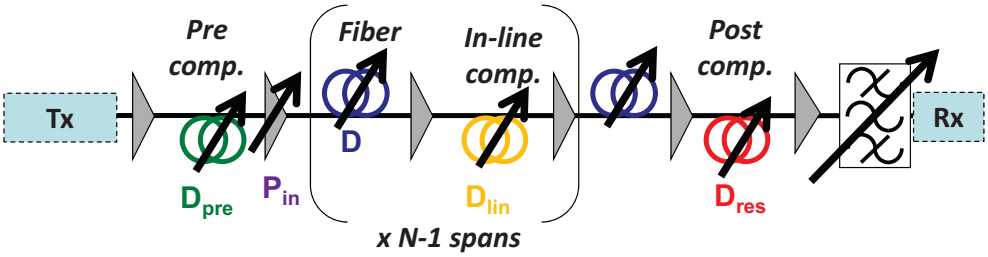

Figure 2.39: Dispersion managed transmission system

An example of such an N-span system is graphically represented in figure 2.39. As it is shown in figure 2.39, a dispersion compensating module is usually placed before the line fiber, pre-distorting the signal entering the system, referred to as *pre-compensation*. The signal is then amplified, enters the line fiber and propagates for a span length of usually around $80 - 100$ km. Based on a typical value for the fiber attenuation of about 0.2 dB/km, the signal power at this point has fallen down to $\frac{1}{100}^{\text{th}}$ of its initial value and the signal needs to be re-amplified. This amplification is usually done by two consecutive amplifiers with a dispersion compensating module between them (i.e. a two stage amplification scheme), achieving an *in-line dispersion compensation*. This step is repeated $N_s - 1$ times, while at the end of the transmission another dispersion compensating fiber is used to achieve a *post-compensation*.

In figure 2.40 we plot the evolution of the cumulative dispersion D_{cum} of the system, as a function of the system distance z, for a system with $N_s = 8$ spans. In the following we note the cumulative pre-compensation as D_{pre}, the fiber GVD parameter as D, the in-line cumulative dispersion as D_{lin} and the residual cumulative dispersion as D_{res}. The dispersion map used in this example, where the in-line cumulative dispersion has a fixed value is usually referred to as *simple period* as opposed to other more advanced dispersion map schemes existing in the literature[10]. In this thesis we are only focusing on single-period dispersion maps.

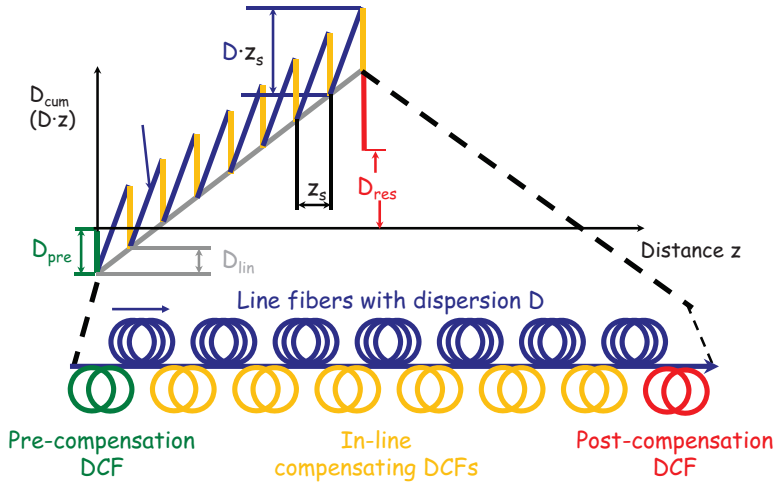

Figure 2.40: Cumulative dispersion as a function of the distance for a dispersion managed system (single-period dispersion map).

2.2.10 Numerical simulations

2.2.10.1 Introduction

Given that our most important task concerns the evaluation of the system performance, it is very common to refer to a number of different, generic techniques that may help to accomplish this task: formula-based calculations (computer-aided or not), numerical waveform-level simulations and laboratory measurements[60].

The first technique, consists of employing analytical rules or models, that are usually simplifying a more complicated system, by usually isolating usually a particular subset of the involved physical phenomena. These models are of extreme importance as they may provide rapid ways of exploring a system design, or they may also provide invaluable physical insights and deeper understanding. However, most of these models cannot be easily applied in real-life systems, as their exactness compared to physical reality is often very limited.

At the other extreme, there is no doubt that laboratory measurements are the most reliable and closest to reality technique that one could use. Nevertheless, it is also quite often the most expensive and time-consuming method of evaluating a system performance. Furthermore, it is the least flexible technique, and this lack of flexibility limits our understanding to the conducted experiment.

Technique	Accuracy w.r.t. reality	Speed/flexibility
Analytical models	Low	High
Numerical simulations	Medium	Medium
Laboratory experiments	High	Low

Figure 2.41: Comparison of different techniques

Finally, numerical simulations stand somewhere in between the two previous ones, both concerning time-consumption and distance from reality (see figure 2.41). In effect, numerical simulation results are a lot less intuitive than analytic models. However, provided that our numerical model is close to the physical reality, we can achieve relatively good accuracy and gain a lot more insight than laboratory measurements, especially when it comes to comparing different configuration possibilities or revealing the predominant physical effects. Moreover, numerical simulations are usually more flexible and less time consuming than laboratory measurements.

2.2.10.2 The Split Step Fourier Method

The propagation of the optical field in fibers, in the absence of polarization effects is described by the NLSE (2.142). However, since it is a nonlinear partial differential equation, generic analytical solutions do not exist, except from very special cases (such as solitons). Therefore, apart from laboratory measurements, performance assessment can only be conducted numerically. In this thesis, performance assessment was exclusively achieved through numerical simulations.

The method used in numerical simulations is the Split-Step Fourier Method (SSFM)[38]. This method consists of re-writing eq. (2.142) as

$$\frac{\partial A}{\partial z} = \left(\hat{D} + \hat{N}\right) A \tag{2.187}$$

, where linear effects (attenuation and chromatic dispersion) are grouped into the operator $\hat{D}$ and nonlinearities are grouped into the operator $\hat{N}$. For example, neglecting higher order dispersion effects (i.e. involving terms β_3, β_4 etc)

and higher order nonlinear effects (i.e. involving Stimulated Raman Scattering, Stimulated Brillouin Scattering, self-steepening etc), the operators are given by

$$\hat{D} = j\frac{\beta_2}{2}\frac{\partial^2}{\partial T^2} - \frac{\alpha(z)}{2} \tag{2.188}$$

$$\hat{N} = -j\gamma\left|A\right|^2 \tag{2.189}$$

In reality, dispersion and nonlinearities are acting simultaneously along fiber length. However, the main assumption of the SSFM is that for small propagation distances, dispersion and nonlinearities are assumed to act independently, where at a first step the effect of dispersion alone is taken into account and at a second step nonlinearities alone are taken into account. As we have seen above, the nonlinearities step is straightforward in the time domain where it involves the addition of a phase depending on the time-shape of the pulse power profile, whereas the chromatic dispersion step is straightforward in the frequency domain, where it is equivalent to the addition of a parabolic phase. For the passage from one domain to the other, the Fast Fourier Transform (FFT) is used and thus the overall complexity of the method is the complexity of FFT. In practice a small variation is used called symmetrized SSFM, where the nonlinearity step is applied in the middle of two dispersion steps of half the cumulative dispersion. The symmetrized SSFM was the method used in our numerical simulations.

2.2.10.3 Resources used for our numerical simulations

In the context of this work, for our numerical simulations we have used a combination of different software and hardware resources.

For the emulation of the fiber nonlinear propagation based on the SSFM process, we have used the proprietary software OCEAN®, provided by the company Alcatel-Lucent in the context of a national French government project for coherent detection in $40Gbp/s$ optical transmission systems. The inputs of the simulator were the optical signal entering the system (i.e. the optical field after the modulator) and the different parameter values used by the simulator for the optical field propagation (i.e. the number of spans, the injection power, the

fiber GVD etc). The output optical field was then saved into a hard disk and a separate routine was used for the signal reception.

For all the other tasks involving the generation of optical formats, the generation of the data sequences upon which the optical formats were based, the signal reception involving a quality estimation by either the use of a Monte-Carlo error counting or a calculation of the signal quadrature statistic, Matlab® programming was employed. In addition, we have used a combination of Matlab® and Linux programming to create an interface between the previous routines written in Matlab® and the OCEAN® simulator that is programmed in C.

Finally, since a vast number of time-consuming simulations with variable parameters had to be performed in the context of this work (for example an exploration of many possible dispersion management, different noise seeds etc.), a special interface has been developed, allowing for a parallel processing of both the transmission and the reception of the optical signals. The previous tool gave us the opportunity to benefit from a great number of hardware resources, including 9 dual core computers used in a permanent basis, 104 shared dual core computers, a shared octo-core server and a shared cluster of 16 quad-core nodes.

Chapter 3

Investigation of M-ary sequences: application on the performance evaluation of QPSK transmission systems

> God may not play dice with the universe, but something strange is going on with the prime numbers.
>
> Paul Erdos

3.1 Introduction : pseudo-random sequences

The first step towards the design of a communications system is the performance assessment of an existing link with given characteristics. This may be achieved through various ways such as direct formula-based calculations, numerical simulations based on transmission models or laboratory measurements (see section §2.2.10). Especially in the last two cases, since the link under design should eventually be installed to work in an actual communications network, performance

assessment is necessarily subject to *assumptions* concerning the emulation of the data traffic, carried by the link.

In the previous section we have seen the equation (2.21), indicating that the modulated signal $\tilde{g}(t)$, expressed via its power spectral density, depends on the spectrum of the deterministic shape-forming pulse $p(t)$ and on the power spectrum density Φ_{ii} of the stochastic information sequence $\{I_n\}$. An unbiased (or fair) assumption about the information sequence would imply that there is no correlation between the different transmitted symbols. This is equivalent to considering that Φ_{ii} is flat for all frequencies (for example, $\Phi_{ii} = 1$), or equivalently, their autocorrelation function is a Dirac function, thus approaching to the autocorrelation function of white noise (eq. (2.24)). In other words, the most unbiased version of information sequence is a "white sequence", where the data symbols sent by users are completely random and there is no correlation between them.

Even if this hypothesis about the random data generation is sufficiently close to reality of actual communication networks, in practice, the information sequence does not necessarily have the aforementioned characteristics. For example, even if the user-generated data is initially random with no correlation between symbols, the use of FEC results in adding redundancy to the data sequence and therefore introducing a correlation. Another example concerns headers added by upper network layers, since the addition of fixed headers in a series of random symbols may influence the overall balance of different patterns in the transmitted sequence. Nevertheless, an information sequence having properties close to the properties of white noise is (by definition), the most objective choice for a given sequence length and, in all cases, it provides an *unbiased reference*.

Summing up the previous statements, the desired properties of the data sequence that should be used in performance assessment test should be as much close to the following:

1. *Infinite length* if we consider that data is permanently circulating in the link.

2. Randomness in the sense that data symbols generated by users should be *uncorrelated*.

3. Randomness in the sense that *all possible symbol patterns* should equally appear in this sequence in a balanced way.

Even though the last two properties may appear to be similar, we should underline that they are only expected to converge into the (one) property infinite sequence lengths, while for finite sequence lengths they are distinct. However, completely random sequences with an infinite length cannot be generated in practice and for this, we are obliged to settle for *finite length* sequences, that nevertheless, possess nearly-ideal properties, close to the ones mentioned above. A group of well-known and widely used sequences satisfying the above properties are the so-called Pseudo-Random Sequences (PRSs).

PRSs are deterministically generated sequences of a finite length with properties that converge to the desired properties mentioned above, for an increasing sequence length. More precisely, q-ary PRSs of a length $L_{seq} = q^n - 1$, have a periodic autocorrelation function with just two levels, whereas, within their sequence length we can find all possible patterns of n symbols, exactly once. When it comes to numerical simulations, emulating system traffic with PRSs is very time-efficient, since for a given sequence length (and therefore a limited duration of this simulation), we assess the system performance with a sequence that "seems to be" completely random, whereas at the same time we are sure to be exploring all possible symbol patterns that could appear for a given sequence length exactly once.

The need for a balanced exploration of all possible patterns within a sequence length practically stems from the fact that the fiber-optic channel is dispersive and nonlinear, a combination of effects that induces ISI or memory[98], [22]. As it will be discussed in section §4, ISI generally leads to a degradation that is *pattern-dependent*. This practically means that there are some specific symbol combinations for which inter-symbol interference will be particularly degrading and those patterns will eventually yield errors, while some other patterns will be correctly transmitted through the channel[1]. It is obvious that using a sequence where all possible patterns of a given length appear exactly once, implies an

[1]It will be shown in chapter §4, that the receiver implementation plays an important role in determining the most degraded subsequences

objective performance assessment, where the bit error probability of the system is neither over- nor under-estimated with respect to the unbiased case.

Furthermore, increasing the sequence length guarantees that the BEP of the system can only *monotonically increase*, since new, eventually degrading, patterns can only be *added* into the sequence, while for very high sequence length BEP should finally converge into a stable value. The lowest sequence length yielding a sufficiently accurate BEP prediction may be safely used in performance assessment, since it combines accurate and time efficiency.

Pseudo-Random Binary Sequences (PRBSs) were primarily used for the performance assessment of optical transmission systems based on binary modulation formats, such as OOK (see section §2.1.3.1). With the arrival, however, of multi-level modulation and coherent detection, the problem of choosing the most suitable sequences for the performance assessment was re-opened[105]. At the same time, alternative methods for the assessment of a system performance have also been recently proposed[53], [54].

Focusing on multi-level sequences, the main objective was, therefore, to investigate their properties and the influence that they may have into the performance assessment of systems based on multi-level modulation. Since, to the best of the author's knowledge, there exist no bibliographical references that describe in a self-consistent way the properties and the generation process of multi-level pseudo-random sequences (the information is rather scattered in various bibliographical references), an effort has been made to systematically present the basic theory behind multi-level PRSs, before proceeding to numerical simulation results.

The generation of PRSs is based on the theory of finite (or Galois) fields. In section§3.2 we review the most important characteristics of finite fields, referred to later on in this chapter[1]. In section§3.3 we review the most important properties of pseudo-random sequences, we present the generation method as well as

[1]Throughout this review process we present the basic notions and theorems, while we also propose elementary examples that help the reader understand and reproduce, if needed, the basics of finite fields. For reasons of completeness, in many cases we also remind elementary notions, well-known in other fields of mathematics. The reader that is already familiar with finite fields may omit this section.

some practical numerical tools that allow for a direct comparison between sequences, not necessarily pseudo-random, with respect to their pseudo-random characteristics. In section §3.4 we present the results of comparison between non pseudo-random sequences and finally, in section §3.5 we present simulation results in the context of dispersion-managed QPSK transmission systems, commenting on the performance yielded by different sequence types and their relative differences.

3.2 Finite Fields : a short review

3.2.1 Introduction

A **field** is a group of elements, together with the notions of the binary operations "addition", "subtraction", "multiplication" and "division". For a field F and the elements $a, b, c \in F$, the **axioms** satisfied are the following[73]:

1. Closure under addition and multiplication, or $a + b \in F$ and $a \cdot b \in F$.
2. Associativity of addition and multiplication, or $a + (b + c) = (a + b) + c$ and $a \cdot (b \cdot c) = (a \cdot b) \cdot c$.
3. Commutativity of addition and multiplication, or $a+b = b+a$ and $a \cdot b = b \cdot a$.
4. Additive and multiplicative identity, or there exists an element of F denoted as 0, such that $a + 0 = a$ and respectively there exists an element of F denoted as 1, such that for $a \neq 0, a \cdot 1 = a$.
5. Additive and multiplicative inverses, or $\exists \ -a \in F : a + (-a) = 0$ and $\exists\, a^{-1} \in F : a \cdot a^{-1} = 1$.
6. Distributivity of multiplication over addition, or $a \cdot (b + c) = a \cdot b + a \cdot c$.

It can be verified that all the above axioms hold for the most typical example of a field, i.e. the field of real numbers $\mathbb{R}$. The field $\mathbb{R}$, however, has infinitely many elements, since the real numbers are *infinite*. Fields that have only a finite number of elements are called **finite Fields** or **Galois fields**, in memory of the French mathematician Evariste Galois who first studied their properties.

For a number of elements of the field equal to q, the finite field is denoted $\mathbb{F}_q$ or $GF(q)$. We should note from this point that finite fields with q elements are the key for the generation of $q-$ary sequences. For example, we may define the simplest field $GF(2)$ with only two elements $\{0,1\}$ and the operations of addition and multiplication being defined similar to the logical operators "XOR" and "AND" respectively. It may be easily verified that for this field, all the axioms defined before hold.

However, we should underline that not every positive integer has the ability to yield a finite field. Indeed, for certain integers r it is impossible to define operators that the field-defining axioms hold and therefore it is impossible to construct a finite field with r elements. Consequently, if $GF(r)$ does not exist, it is also impossible to create r-ary PRSs[1].

3.2.2 Prime Finite Fields and polynomials

The most simple type of finite field rises when the number of elements is a prime number. In this case we refer to this field as a *prime finite field*, denoted as $GF(p)$[2]. It is usually convenient to map the elements of prime finite field into the integers $\{0,1,2,...,p-1\}$ (we may also note $GF(p)=\{0,1,2,...,p-1\}$) and all the operations like addition, multiplication etc are performed the usual way, modulo p. For example, $GF(5)=\{0,1,2,3,4\}$, $2+4=1$ (as $6\ (mod\ 5)=1$), $1-4=2$ and $3\cdot 4=2$. Once more, it can be easily verified that all the axioms of section §3.2.1 are satisfied for $GF(5)$. In section §3.2.3 we will see that finite fields may be also created if the number of elements is equal to a positive power of a prime number. In this case we refer to an *extension* of the prime finite field $GF(p)$, or to the *composite finite field* $GF(p^m)$, with m being a positive integer. We may already note that, in order to generate pseudo-random sequences suitable for QPSK modulation (quaternary sequences), we will need to refer to the composite finite field $GF(4)=GF(2^2)$.

[1] For example, we cannot construct a finite field with 6 elements[88] and therefore it is also impossible to construct a 6-ary PRS

[2] In the following, if not specifically clarified, when we refer to the field $GF(p)$ we implicitly suppose that p is a prime number, whereas when we refer to the finite field $GF(q)$ we suppose that q may be a prime or a power of a prime.

A *polynomial* $h(x)$ of *degree* n, over a finite field $GF(q)$ is a polynomial where all the multiplicative coefficients of the powers of x are elements of $GF(q)$, i.e.:

$$h(x) = h_n x^n + h_{n-1}x^{n-1} + \cdots + h_1 x + h_0, h_i \in GF(q) \tag{3.1}$$

, while we denote $h(x) \in GF[q, x]$. Furthermore, if in formula (3.1) $h_n = 1$ the polynomial is called *monic*. For example, the polynomial $h(x) = x^4 + x + 1$ is a monic polynomial in $GF[2, x]$. Since the information of such a polynomial lies in the coefficients that multiply each power of x, the *polynomial representation* is equivalent to a *tuple*, *vector* or *sequence* representation with coefficients over a finite field. For example, the polynomial $h(x) = x^4+x+1$ can also be represented by the tuple (or sequence) [1 0 0 1 1].

Operations over polynomials in $GF(q)$ are held in the exact same way as for usual polynomials, with operations over their coefficients held in the $GF(q)$ way. For example, if $h_1(x) = x + 1, h_2(x) = x^2 + x + 1 \in GF[2, x]$, we get $h(x) = h_1(x)\cdot h_2(x) = (x+1)\cdot(x^2+x+1) = x^3+ \underbrace{x^2 + x^2}_{(1+1)\cdot x^2 = 0\cdot x^2} + \underbrace{x + x}_{(1+1)\cdot x = 0\cdot x} +1 = x^3+1$. Similar to regular polynomials, we also say that $x = -1 = 1$ is a *root* of the polynomial $x^3 + 1$ and that $x^2 + x + 1$ *divides* $x^3 + 1$.

Furthermore, slightly changing the above example and considering the division of $f_1(x) = x^3$ by $f_2(x) = x^2+x+1$, we may also see that $x^3 = (x+1)\cdot(x^2+x+1)+1$, where the *quotient* is equal to $q(x) = x + 1$ and the *remainder*, $r(x) = 1$.

For a polynomial $f(x)$ over $GF[q, x]$ of degree n and $f(0) \neq 0$, the least possible integer e for which $f(x)$ divides $x^e - 1$, is called *order* of the polynomial. A monic polynomial $h(x)$ of degree n with $h(0) \neq 0$ and order $e = q^n - 1$ is called *primitive polynomial* of degree n over $GF(q)$. It can also be proved that for a given degree n we can *always* find a primitive polynomial over $GF(q)$ and that primitive polynomials are automatically *irreducible*. This last property means that a primitive polynomial cannot be factorized into multiple terms with none of them being a constant.

As an example, we may try to calculate the order or the polynomial $h(x) = x^2 + x + 1 \in GF[2, x]$. From the above example we see that $x^3 - 1$ divides $h(x)$ since $x^3 - 1 = x^3 + 1 = (x + 1)(x^2 + x + 1)$ and therefore $e = 3$. We can also note that the degree of $h(x)$ is 2, that $h(x)$ is monic, $h(0) = 1 \neq 0$ and

$e = 3 = 2^2 - 1$. Therefore, the conditions mentioned before and met and $h(x)$ is a primitive polynomial of degree 2 over $GF(2)$.

Primitive polynomials play a central role in the theory of finite fields and they have been studied extensively in the literature. As it will be shown in section §3.3.1, primitive polynomials over $GF(q)$, are the key ingredient for the generation of q-ary PRSs, whereas primitive polynomials over $GF(p)$, with p being a prime number, are the "gateway" to composite finite fields, discussed in section §3.2.3.

There exist several copious algorithmic methods that allow the determination of *all* possible primitive polynomials of a certain degree over a finite field $GF(q)$. A recent survey over such methods may be found in [30] and tables of primitive polynomials for small orders and fields can be found in [75], [7], [73], [106], [52][1]. In the following, we consider that primitive polynomials of any order are available from tables or programs, for, at least, all prime finite fields.

3.2.3 Composite Finite Fields

Since 2 is a prime number, the notion of prime finite fields is sufficient to describe the properties and the construction of pseudo-random binary sequences. However, in order to generate PRSs with a number of levels being a power of 2, like quaternary sequences for instance, we need to introduce another type of finite field with p^m elements, where m is a positive integer. This kind of field is called an *extension* of $GF(p)$ and $GF(p)$ in this context is called the *base field*. Moreover, it can be shown[73] that any given finite field must necessarily have p^m elements, where p is prime and $m \in \mathbb{N}$. This last theorem implies that there exists no finite field with a number of elements not being either a prime or a power of a prime.

An extension field over $GF(p^m)$ can be seen as a *vector space* of dimension m over the prime field $GF(p)$. In other words, if $\{\alpha_1, ..., \alpha_m\}$ is a basis of $GF(p^m)$ over $GF(p)$, then each element $\alpha \in GF(p^m)$ can be uniquely represented in the form $\alpha = c_1 \cdot \alpha_1 + \cdots + c_m \cdot \alpha_m, c_j \in GF(p), 1 \leq j \leq m$. Having in mind the equivalence between polynomials over finite fields and vectors, it is obvious that an

[1] All primitive polynomials of degree m over $GF(2)$ can also be easily obtained in Matlab®by the command primpoly(m,'all')

element over the composite field $GF(p^m)$ may be also represented by a polynomial of order $(m-1)$ over $GF(p)$, where in this case $\{\alpha_1, ..., \alpha_m\} = \{1, x, ..., x^{m-1}\}$. For example, any element of the extended finite field $GF(2^3) = GF(8)$ over GF(2), can be represented by a 3-component vector, with each component being an element of $GF(2)$. The 8 elements of $GF(8)$ can be then represented by the binary vectors [0 0 0], [0 0 1], [0 1 0]..., [1 1 1], their decimal form $\{0, 1, ..., 7\}$ or finally the polynomials $(0), (1), (x), ..., (x^2 + x + 1)$.

The "passage" from a prime finite field $GF(p)$ to the extension $GF(p^m)$ is achieved through a primitive polynomial $h(x)$ of degree m. As explained above, since $h(x)$ is also irreducible, it admits no roots in $GF(p)$. However, in the extension field $GF(p^m)$, $h(x)$ has exactly m distinct roots, namely $\{\omega, \omega^p, \omega^{p^2}, ..., \omega^{p^{m-1}}\}$, or

$$h(\omega) = h(\omega^p) = h(\omega^{p^2}) = \cdots = h(\omega^{p^{m-1}}) = 0 \tag{3.2}$$

, where ω is referred to as *a primitive element* of $GF(p^m)$[1].

In the field $GF(p^m)$ each element can be expressed in two ways: the traditional one where the element is expressed as a polynomial of ω with coefficients from $GF(p)$ and a degree less or equal to $m-1$, or as a polynomial with a single power of ω, possibly greater than $m-1$. As it is going to be explained with examples later, the two representation forms are mathematically equal modulo $h(x)$. However, in practice, the two forms of representation may also be easily obtained by a procedure involving a type of a *shift register*[2]. The general form of such a shift register is given in figure 3.1.

A shift register is, in the general case, a cascade of m memory units, where each unit is capable of storing an element of $GF(p)$, as for example, standard flip-flops can store elements of $GF(2)$. As a consequence, the whole register can store an element of $GF(p^m)$ or alternatively the coefficients of the polynomial representing

[1] An analogy can be made between the extended finite fields and complex numbers. In the field of real numbers, the equation $h(x) = x^2 + 1 = 0$ does not have a solution but it has exactly two solutions in the field of complex numbers. The element $j = sqrt(-1)$ may be considered as a primitive element of the complex numbers field, since $h(j) = 0$.

[2] We will discuss in section §3.3.1 a slightly different type of shift register, upon which we will base the construction of pseudo-random sequences.

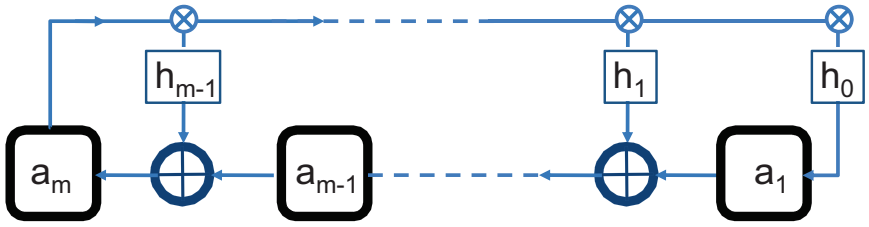

Figure 3.1: Shift register giving elements of $GF(p^m)$, when the passage from $GF(p)$ into $GF(p^m)$ is done via the primitive polynomial $h(x) = x^m + h_{m-1}x^{m-1} + \cdots + h_1 x + h_0$.

the element of $GF(p^m)$. Shift registers are equipped with a *clock* that triggers the change of the register state, and a *feedback loop* from the last unit towards each one of the other units, "weighted" by the coefficients $h_m, h_{m-1}, ..., h_0$ of the primitive polynomial $h(x) \in GF[p, x]$. We note that since the polynomial $h(x)$ is primitive, it is also monic ($h_m = 1$) and thus, the feedback line corresponding to h_m is always represented by a simple line.

If register is initialized to the state $[a_m, a_{m-1}, ..., a_1]$ (or, as discussed before, to the $GF(p^m)$ element $a_m\omega^{m-1} + \cdots + a_1\omega + a_0$), in each "clock tick" $k = 1, 2, ...$ (supposing that $k = 0$ corresponds to the initial state), the new register state $[a_1^{(k+1)}, a_2^{(k+1)}, ..., a_m^{(k+1)}]$ is given as a function of the older state $[a_1^{(k)}, a_2^{(k)}, ..., a_m^{(k)}]$ by the relations

$$\begin{aligned} a_1^{(k)} &= a_m^{(k-1)} \cdot h_0 \\ a_i^{(k)} &= a_m^{(k-1)} \cdot h_{i-1} + a_{i-1}^{(k-1)}, 2 \leq i \leq m \end{aligned} \tag{3.3}$$

, where all the operations are held in the basis field $GF(p)$.

If the register is initialized to the state $[0, 0, ..., 1] = \omega^0$, the 1^{rst} clock tick will change the contents of the register to $[0, ..., 1, 0]$ that is also equal to $\omega^1 = \omega$ etc. At the clock tick k, the register state contains the polynomial representation of the element in $GF(p^m)$, whereas the power representation state is ω^k. The fact that the polynomial $h(x)$ is primitive, guarantees that the initial state of the register is going be re-appearing periodically after $p^m - 1$ clock ticks. The choice of the initial state may be random with the only forbidden choice being the state $[\underbrace{0, 0, ..., 0}_{m \text{ times}}]$, since in that case, the state of the register will never change. The

polynomials produced by the $p^m - 1$ different register states together with the zero element $\underbrace{[0, 0, ..., 0]}_{m \text{ times}}$, form the composite finite field $GF(p^m)$.

In order to define the operations of addition and multiplication over two elements a and b over the composite field $GF(p^m)$, we first represent these elements as polynomials of a maximum degree $m-1$ over $GF(p)$. Then the *sum* $a+b$ is obtained by the polynomial sum of a and b, as defined in section §3.2.2, and the *product* $a \cdot b$ is equal to the polynomial product of a and b, modulo $h(x)$.

More precisely, since the addition is done element-wise, the resulting polynomial will always be of a maximum degree $m-1$. However, the multiplication may result in a polynomial of a degree greater than $m-1$ (i.e. not an element of $GF(p^m)$). In this case we consider the *equivalent* form of the polynomial, modulo $h(x)$. A direct consequence of the above is that the choice of the primitive polynomial is critical for the definition of the composite finite field and the results of addition and multiplication may vary as a function of this polynomial.

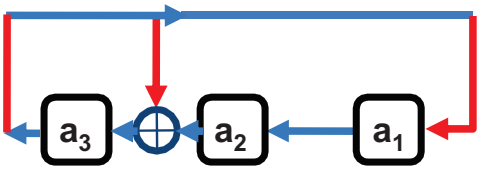

$h(x) = 1 \cdot x^3 + 1 \cdot x^2 + 0 \cdot x + 1$

State	a_3	a_2	a_1	Polynomial	Power
1	0	0	1	1	ω^0
2	0	1	0	ω	ω^1
3	1	0	0	ω^2	ω^2
4	1	0	1	$\omega^2 + 1$	ω^3
5	1	1	1	$\omega^2 + \omega + 1$	ω^4
6	0	1	1	$\omega+1$	ω^5
7	1	1	0	$\omega^2 + \omega$	ω^6
1	0	0	1	1	ω^7
2	0	1	0	ω	ω^8

Figure 3.2: Shift register giving elements of $GF(8)$ for the primitive polynomial $h(x) = x^3 + x + 1$.

As an example, for the passage to $GF(8) = GF(2^3)$, we need a primitive

polynomial of degree 3 over $GF(2)$. From tables we find that there are two primitive polynomials of degree 3 over $GF(2)$, $h_1(x) = x^3 + x + 1$ and $h_2(x) = x^3 + x^2 + 1$. We randomly chose the polynomial $h(x) = h_1(x) = x^3 + x + 1$ and based on that we construct the shift register of figure 3.2, yielding the elements of $GF(8)$ with their polynomial and power representation. First, we verify that eq. (3.2) holds for the three roots of $h(x)$. Secondly, the laws of addition and multiplication defined above, hold in all possible ways. Considering, for example, the elements of $GF(8)$, $a = \omega^5 = \omega^2 + \omega + 1$ and $b = \omega^3 = \omega + 1$, the sum of a and b yields $a + b = (\omega^2 + \omega + 1) + (\omega + 1) = \omega^2$ and the product $a \cdot b = \omega^3 + 1 = (\omega^3 + \omega + 1) + \omega = \omega$. It should be noted that an alternative, easier way to obtain the product of a and b is to consider the power representation of a and b yielding, $a \cdot b = \omega^5 \cdot \omega^3 = \omega^8 = \omega^{7+1} = \omega$. Therefore, the polynomial representation is more suitable when it comes to additions and the power representation is more suitable when it comes to multiplications.

The notion of polynomials (including the notion of *primitive polynomials*) exists in the same way for composite finite fields as it exists for prime finite fields: the only difference is that their coefficients are elements over $GF(p^m)$ instead of $GF(p)$. For example, the polynomial $h(x) = x^2 + x + \omega^2$, is a primitive polynomial over $GF(4)$. Consequently, $h(x)$ can be alternatively represented in the form of a tuple (or sequence) in the form $[1\ 1\ \omega^2]$, or furthermore, as soon as the elements of $GF(4)$ may be expressed as vectors over $GF(2)$ the polynomial may also be written as a row of column vectors (also called a *vector sequence*), where each column vector represents an element of $GF(4)$: $\begin{bmatrix} 0 & 0 & 1 \\ 1 & 1 & 1 \end{bmatrix}$

As mentioned before, primitive polynomials over $GF(q)$ are particularly important since they are the key ingredient for the generation of q-ary pseudo-random sequences, with $q = p^m$. However, we need to underline that tables of primitive polynomials can be easily found in the literature either only for small values of m, or just for prime finite fields. On the other hand, producing all the possible primitive polynomials for any degree over all possible extension fields is an extremely complicated and time consuming task. In section §3.3.1 we are going to review a method for the generation of PRSs over composite finite fields

$GF(p^m)$, without the need of primitive polynomials over the extended finite field, but based on a PRS over the corresponding prime field $GF(p)$.

After establishing the basic properties of prime and composite finite fields, we may now proceed to the generation process and definition of the properties of PRSs.

3.3 Pseudo-random sequences: generation methods and properties

Pseudo-random sequences, also known as *Pseudo-Noise*, *Maximum Length Register Shift* or *m-Sequences*, are deterministically constructed sequences of elements over a prime or extended finite field $GF(q)$, of a length $q^n - 1$, where $n \in \mathbb{N}$. In what follows we are first going to present a practical method of generating pseudo-random sequences over any type of prime or composite finite field, for any degree n. Then we are going to present the properties of pseudo-random sequences (directly resulting from their generation method), as well as tools that allow the quantification of these properties.

3.3.1 Generation of pseudo-random sequences: a method based on shift-registers

The generation of pseudo-random sequences over $GF(q)$, where $q = p^m$ with p prime and $m \in \mathbb{N}$, is based once more on a shift-register type, similar to the one used in section §3.2.3 for the generation of a composite finite field. The general form of such a register is shown in figure 3.3.

Initializing the feedback branches following the coefficients $h_k, k = 0, 1, ..., m$ of a degree m primitive polynomial $h(x) = x^m + h_{n-1}x^{m-1} + \cdots + h_1 x + h_0 \in GF[q, x]$ and initializing the register to *any* state except from $\underbrace{[0, 0, ..., 0]}_{n\text{times}}$, at each clock tick k, the element stored in the unit a_1 exits the system generating the k^{th} element of the pseudo-random sequence, $Seq_{out}(k)$. The fact that the polynomial $h(x)$ is primitive guarantees that the register will periodically return to the same

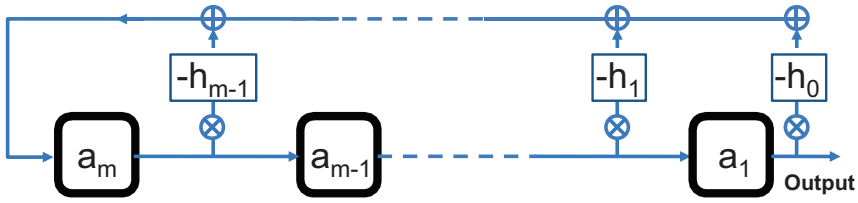

Figure 3.3: Shift register generating a sequence with elements from $GF(q)$ using a primitive polynomial $h(x) = x^m + h_{n-1}x^{m-1} + \cdots + h_1 x + h_0 \ \in GF[q, x]$.

state with a period of $k = q^n - 1$ ticks, thus leading to the creation of a pseudo-random sequence with length $L_{seq} = q^n - 1$.

Addition				
+	0	1	ω	ω^2
0	0	1	ω	ω^2
1	1	0	ω^2	ω
ω	ω	ω^2	0	1
ω^2	ω^2	ω	1	0

(a) Addition rules over $GF(4)$.

Multiplication				
×	0	1	ω	ω^2
0	0	0	0	0
1	0	1	ω	ω^2
ω	0	ω	ω^2	1
ω^2	0	ω^2	1	ω

(b) Multiplication rules over $GF(4)$.

Figure 3.4: Mathematical operations in $GF(4)$, based on the primitive polynomial $h_1(x) = x^2 + x + 1, \in GF[2, x]$.

As an example, we consider the generation of a pseudo-random sequence over $GF(4)$, of a length $4^2 - 1 = 15$. First, we need to generate the finite field $GF(4)$ and for this we need a primitive polynomial of degree 2 over $GF(2)$. From tables we find that the only primitive polynomial of degree 2 over $GF(2)$ is the polynomial $h_1(x) = x^2 + x + 1$. Based on $h_1(x)$, and following the shift-register procedure described in section §3.2.3, we can generate the composite finite field $GF(4) = \{0, \omega^0, \omega^1, \omega^2\} = \{0, 1, \omega, \omega + 1\}$. Furthermore, for convenience we also construct the addition and multiplication tables shown in figures 3.4a and 3.4b respectively.

Next, for the generation of the pseudo-random sequence of length $4^2 - 1 = 15$ we need a primitive polynomial of degree 2 over $GF(4)$. From tables, we find such a primitive polynomial $h_2(x) = x^2 + x + \omega^2$ and we construct the corresponding shift-register, shown in figure 3.5a. The generated sequence Seq_{out} is shown in table of figure 3.5b.

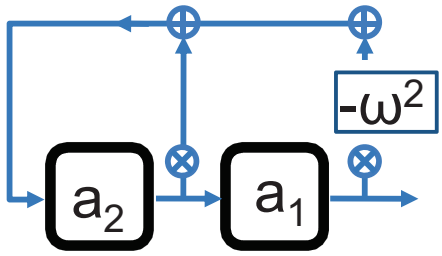

(a) Shift register for the generation of a 15-long sequence over $GF(4)$.

State	0	1	2	3	4	5	6	7	8	9	10	11	12	13	14	15	16
a_2	0	ω^2	ω^2	1	ω^2	0	ω	ω	ω^2	ω	0	1	1	ω	1	0	ω^2
a_1	1	0	ω^2	ω^2	1	ω^2	0	ω	ω	ω^2	ω	0	1	1	ω	1	0
Seq_{out}	-	**1**	**0**	**ω^2**	**ω^2**	**1**	**ω^2**	**0**	**ω**	**ω**	**ω^2**	**ω**	**0**	**1**	**1**	**ω**	**1**

(b) Successive states of the shift register.

Figure 3.5: Generation of a quaternary sequence of a length $L_{seq} = 15$.

The method described above provides a way of generating a $q-$ary PRS of a length $q^n - 1$ given a primitive polynomial over $GF(q)$ of degree n, where in the general case $q = p^m$ with p a prime number and $m \in \mathbb{N}$. However, such a primitive polynomial is not be always available from tables, especially when m and n are high[1]. In the following we review the method proposed in [68] for the generation of pseudo-random sequences of a length $q^n - 1$ over a composite field $GF(q = p^m)$ for *any* positive value of m or n, provided that we already have a primitive polynomial of degree n over only the prime field $GF(p)$. This is particularly useful in our case since we usually need to generate pseudo-random

[1]For example, the generation method used in http://theory.cs.uvic.ca/gen/poly.html regroups several tables of the literature but it only provides primitive polynomials for a composite field of up to $GF(8)$ ($m \leq 3$), while $n \leq 64$.

sequences with 2^m levels, for modulation formats like QPSK, 8-PSK, 16-QAM, 64-QAM etc and primitive polynomials over $GF(2)$, as $GF(2)$ has been extensively studied in the past, they are generally available even for up to very high orders.

In the proposed method, in order to generate a PRS of a length $q^n - 1$ over the composite finite field $GF(q) = GF(p^m)$, we first generate a pseudo-random sequence of a length $p^{m \cdot n} - 1$ over the prime finite field $GF(p)$, using a primitive polynomial of degree $(m \cdot n)$ over $GF(p)$ and the method described in section §3.3.1. Then, the pseudo-random sequence d over $GF(p^m)$ can be represented as a *vector sequence* by interleaving m shifted versions of the initial sequence over $GF(p)$.

More precisely, given a primitive polynomial $h(x)$ of degree $(m \cdot n)$ over $GF(p)$, and its associated pseudo-random sequence c of a length $p^{m \cdot n} - 1$ over $GF(p)$, it can be show that the pseudo-random sequence d of a length $p^{m \cdot n} - 1$ over $GF(p^m)$ can be expressed in the polynomial form:

$$d = \sum_{j=0}^{m-1} \gamma^j T^{z \cdot k_j} c \tag{3.4}$$

where γ is a primitive element of $GF(p^m)$, $T^i c$ indicates a left shift of c by i elements, z is a decimal number defined as

$$z = \frac{p^{m \cdot n} - 1}{p^m - 1} \tag{3.5}$$

and $k_i, 1 \leq i \leq m - 1$ are multiplicative shift factors, calculated from the following two equations:

$$\gamma^{k_{m-i}} = b_m \left[\sum_{j=1}^{i} h_{m-i+j} \gamma^j \right], i = 1, 2, ..., m - 1 \tag{3.6}$$

$$b_m = \begin{cases} \gamma^{\frac{(q-2)(q^m-1)}{q-1}}, & q \text{ and } m \text{ odd or } q \text{ even} \\ \gamma^{\frac{(q-3)(q^m-1)}{2(q-1)}}, & q \text{ odd and } m \text{ even} \end{cases}. \tag{3.7}$$

As an example, we calculate the shift factors needed for the generation of an 8-ary sequence with a length $8^2 - 1 = 2^{3 \cdot 2} - 1 = 63$, thus $p = 2$, $m = 3$ and $n = 2$. First, we need to generate the field $GF(8)$ by using a primitive polynomial of degree 3 over $GF(2)$. Finding from tables the primitive $h_1(x) = x^3 + x^2 + 1$ we

generate the extension field $GF(8)$ that is the same as the one shown in figure 3.2. Secondly, we need to generate a binary pseudo-random sequence of length $2^{2\cdot3} - 1 = 2^6 - 1 = 63$. For this we chose a primitive polynomial of degree 6, say $h_2(x) = x^6 + x + 1$ and following the procedure described in section §3.3.1 we generate the sequence

$$c = [100000100001100010100111101000111001001011011101100110101011111]$$

Next we calculate z from equation (3.5), $z = \frac{2^6-1}{2^3-1} = \frac{63}{7} = 9$ and, finally, we calculate the shift factors k_i for $i = 1, 2$. Using equation (3.7) we get $b_3 = \gamma^0 = 1$ and substituting b_3 in equation (3.6) we get $\gamma^{k_2} = h_3\gamma = \gamma \Rightarrow k_2 = 1$, $\gamma^{k_2} = h_2\gamma + h_3\gamma^2 = \gamma + \gamma^2 = \gamma^6 \Rightarrow k_1 = 6$. Consequently, from equation (3.4) we get $d = c + \gamma T^{54}c + \gamma^2 T^9 c$, or equivalently

$$d = \begin{bmatrix} 100000100001100010100111101000111001001011011101100110101011111 \\ 101011111100000100001100010100111101000111001001011011101100110 \\ 001100010100111101000111001001011011101100110101011111100000100 \end{bmatrix}$$

or furthermore, by replacing the binary columns with their decimal equivalent we get the 8-ary PRS

$$d = [603122632304511341402755425201677217105366156507433573706244764]$$

Summing up, we have presented a global method for the generation of pseudo-random sequences over any finite field, as well as a method for the generation of PRSs over composite finite fields, with the prerequisite generation of a PRS over the prime finite field. In the next section we are going to review the most important properties that manifest the importance of pseudo-random sequences..

3.3.2 Properties of pseudo-random sequences

As mentioned in the introduction, PRSs have been extensively studied primarily because of their two interesting properties: the two-level, almost ideal[1], autocor-

[1] As discussed in section §2.1.4.1, AWGN is defined to have an autocorrelation function proportional to $\delta(t)$, revealing the fact that successive noise samples are, by default, not correlated to each other. A similar property would be desirable for data sequences as we have no particular reason to suppose there exists a correlation between time-shifted version of the sequence.

relation function (referred to as the *autocorrelation property*) and the fact that all possible sub-sequences (or tuples) of m elements (except from one) can be "seen" within their length (referred to as the *window property*). PRSs have various other properties listed in [118], [75], [49] but based on the main conjecture of [48], the two properties of autocorrelation and window are the necessary and sufficient conditions that a sequence should satisfy to be pseudo-random.

3.3.2.1 The autocorrelation function property

The autocorrelation function R of all pseudo-random sequences should satisfy in all cases the general condition noted by [75]:

$$R(\tau) = \begin{cases} 1 & , \tau = 0 \ (\textbf{mod } L_{seq}) \\ -\frac{1}{L_{seq}} & , otherwise \end{cases} \tag{3.8}$$

where $\tau \in \mathbb{N}$ is the discrete time variable and L_{seq} is the sequence length.

We can easily notice that $\lim_{L_{seq}\to\infty} \left(-\frac{1}{L_{seq}}\right) = 0 \Rightarrow R(\tau) \to \delta(\tau)$. This last property means that as the sequence length increases the autocorrelation function of the sequence ideally approaches the autocorrelation function of white noise.

So far we have been talking about elements over finite fields and sequences of such elements, usually mapping elements into decimal numbers. However, we should underline the fact that this mapping was just a mathematical convenience and the properties of PRSs should remain invariant, even if we chose to represent finite field elements with colors, letters etc.

Whereas the definition of an autocorrelation function for complex signal is trivial, the autocorrelation function of an abstract sequence of "objects" is a quite complicated task. In general, the autocorrelation function captures the *similarity* between a signal (or sequence) and a cyclically time-shifted version of itself. When the similarity is perfect, when for instance, the shift between the two versions of the signal is zero, the autocorrelation function is equal to 1. Otherwise, the more the two versions are *different* the closer the autocorrelation to zero. If we wanted to define the autocorrelation for an abstract sequence of non-numeric elements $c = c_1c_2...c_n$, it would look like:

$$R(\tau) = \frac{1}{n}\sum_{k=1}^{n} f_R(c_k, c_{1+(k+\tau-1) \bmod n}) \tag{3.9}$$

where f_R is a function quantifying the *similarity* between two elements of c and the division by n is done for normalization purposes. We should note that the definition of the function f_R should normally depend on the mapping used for the elements of the finite field.

There exist numerous definitions in the literature for the function f_R over the sequence c together with mappings of the elements over a finite field towards real or complex values or vectors. In all cases, for the equation (3.8) to hold, f_R is required to be equal to 1 when the two elements are the same and a negative value when the elements are different. Given a finite field $GF(q = p^m)$ with elements $e_1e_2...e_q$, some very common examples of mappings M of the elements $e_i, 1 \leq i \leq q$ are:

- *Mapping to integers.*

$$M_I(e_k) = k - 1, 1 \leq k \leq q \tag{3.10}$$

  The result is the mapping of elements $e_1e_2...e_q$ over $GF(q)$ into the integers $\{0, 1, ...q-1\}$. This is the mapping used so far.

- *Mapping to m-vectors over $GF(p)$.*

$$M_V(e_k) = \begin{pmatrix} e_{k1} \\ \vdots \\ e_{km} \end{pmatrix}, 1 \leq k \leq q \tag{3.11}$$

  where $e_{ki}, 1 \leq i \leq m$, with $0 \leq e_{ki} \leq p$ are the coefficients from the polynomial representation of e_k over $GF(p)$. We note that if q is a prime number the vectors degenerate to scalars and this mapping is equivalent to the mapping to integers.

- *Mapping to complex roots of unity.*

$$M_C(e_k) = \exp\left[j\frac{2\pi}{q}(k-1)\right], 1 \leq k \leq q \tag{3.12}$$

Thus, the elements $e_1 e_2 ... e_q$ are mapped towards the q^{th} complex roots of unity $\{\exp(j\frac{2\pi}{q} \cdot 0), \exp(j\frac{2\pi}{q} \cdot 1), ... \exp(j\frac{2\pi}{q} \cdot (q-1))\}$.

The simplest and most intuitive choice is the mapping M_I together with a definition of f_R as a simple multiplication, i.e:

$$f_{R,I}(e_i, e_j) = M_I(e_i) \cdot M_I(e_j) \tag{3.13}$$

In order to test those definitions on a sample sequence, we consider the ternary sequence with elements over $GF(3)$, $c_1 = [01220211]$. Combining the equations (3.9), (3.10) and (3.13), after a normalization for $\tau = 0$, we get the autocorrelation function of figure 3.6a. As we can easily notice, with the mapping M_I, equation (3.8) is not satisfied as, the autocorrelation presents a peak and moreover, the low level is not equal to $-1/8$, but it is rather situated about 0.6.

On the other hand, the mapping M_C appears a very promising choice as the distance of each element from 0 is the same. Furthermore, it appears as a very natural choice in the context of q-ary PSK modulated signals. In this case we can define the function f_R as:

$$f_{R,C}(e_i, e_j) = M_C(e_i) \cdot M_C(e_j)^* \tag{3.14}$$

where $*$ denotes the complex conjugate. We can already notice that this definition f_R succeeds in returning 1 when the elements are the same, without any normalization, as $\exp(j\frac{2\pi}{q}k) \cdot \exp(-j\frac{2\pi}{q}k) = 1$. Combining eqs. (3.9), (3.12) and (3.14), we plot the resulting autocorrelation function for the sequence c_1 in figure 3.6b and, apparently, equation (3.8) is satisfied.

In order to further test the mapping (3.14), we consider the quaternary sequence $c_2 = [1033130223201121]$. Applying (3.9), (3.12) and (3.14) for the sequence c_2, we get an autocorrelation function with a real part following (3.8) (figure 3.6c), but also with an additional imaginary part that presents two discrete peaks (figure 3.6d). Therefore, it seems that the last combination of mapping and definition of autocorrelation function yields the desired result for the ternary sequence but not for the quaternary sequence.

It can be shown[75], [97] that a mapping to the complex roots of unity satisfies the condition (3.8) only for sequences over *prime* finite fields. On the other hand,

this mapping fails to satisfy (3.8) for sequences over composite finite fields as it is $q = 2^2$, as also discussed in [11] and [23]. Therefore, we conclude that M_C fails, as well, to preserve (3.8) for all kinds of PRSs.

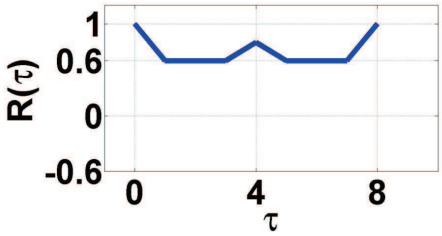

(a) $R(\tau)$ for c_1 using the mapping M_I.

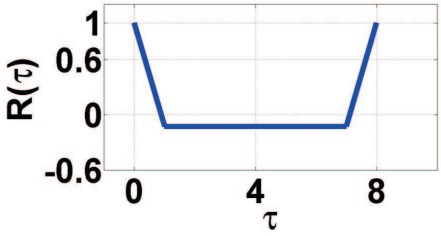

(b) $R(\tau)$ for c_1 using the mapping M_C.

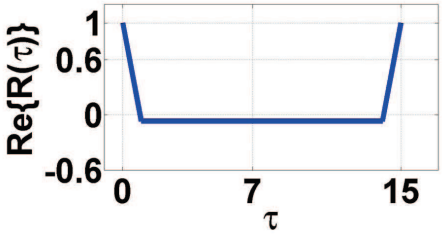

(c) $|R(\tau)|$ for c_2 using the mapping M_C.

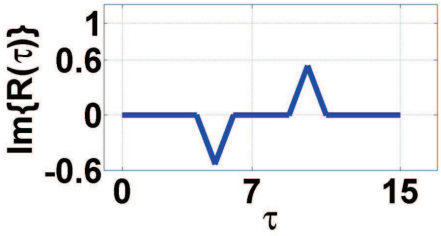

(d) $Im\{R(\tau)\}$ for c_2 using the mapping M_C.

Figure 3.6: Autocorrelation function for different mappings.

A mapping found to preserve the property (3.8) for all types of finite fields (composite or prime) was proposed in [85]. This mapping uses the m-vector mapping following (3.11) to generalize the complex root mapping following (3.12). More precisely, it is defined for the elements over the composite (or prime) finite field $GF(q) = GF(p^m)$ that have already been mapped following eq. (3.11) as follows:

$$M_{CV}(e_k) = \left(\exp\left[j\tfrac{2\pi}{p}(e_{k1} - 1)\right] \quad \cdots \quad \exp\left[j\tfrac{2\pi}{p}(e_{km} - 1)\right] \right) \tag{3.15}$$

We can note that when q is a prime, this mapping is identical to the complex-root mapping of eq. (3.12), whereas for composite finite fields $GF(p^m)$, the q

elements are first mapped into complex vectors with m components, then each component is re-mapped into a p^{th} complex root of unity following (3.12).

For this mapping, the function f_R is defined as:

$$f_{CV}(e_i, e_j) = \frac{1}{m} M_{CV}(e_i) \cdot \{M_{CV}(e_j)^*\}^T \tag{3.16}$$

where $*$ denotes a complex conjugate and T denotes a matrix transposition.

It can be verified that for this definition of the autocorrelation function, equation (3.8) is satisfied for both prime and composite finite fields. In the following, when we refer to the calculation of the autocorrelation function we will implicitly refer to the mapping and f_R definitions of equations (3.15) and (3.16).

3.3.2.2 The window property and de Bruijn sequences

Considering a pseudo-random sequence over $GF(q)$ of q^n-1 elements, the window property (also called the "span n" property) refers to the fact that, regarding the sequence as cyclical, within its length there can be observed *all* the possible tuples (or sub-sequences) of n elements (i.e. all n-*tuples*) exactly once, *except from one*, which is usually the tuple $\underbrace{00...0}_{n \text{ times}}$. In figure 3.7 we show an example of a binary sequence of 15 symbols, where the above property can be easily confirmed.

A sequence of length q^n over which all the possible n-tuples may be observed once (including the tuple $\underbrace{00...0}_{n \text{ times}}$) is called a *de Bruijn* sequence. Given a PRS c, we may generate its *De Bruijn associate* $deBr(c)$, where the operator $deBr$ is defined following the prescription: "Find the longest subsequence of zeros in c and add another zero in it". It is obvious that the operator $deBr$ may be also defined for any sequence over the same finite field, not a necessarily pseudo-random one.

The inclusion of all possible m-tuples is fundamental for the accurate assessment of system performance. In order to quantify this property for non pseudo-random sequences that, as we are going to see in section §3.4, are commonly used in system performance assessment, we define the parameter κ for an arbitrary sequence c as follows:

$$\kappa = \frac{|\text{number of m} - \text{tuples seen in a } deBr(c)|}{|\text{number of m} - \text{tuples in a de Bruijnsequencewith same lengthasc}|} \tag{3.17}$$

tuple	1	2	3	4	5	6	7	8	9	10	11	12	13	14	15
1	0	0	0	1	1	1	1	0	1	0	1	1	0	0	1
2	0	0	0	1	1	1	1	0	1	0	1	1	0	0	1
3	0	0	0	1	1	1	1	0	1	0	1	1	0	0	1
...	...	...	...	...	...	...	...	...	...	...	...	...	...	...	...
14	0	0	0	1	1	1	1	0	1	0	1	1	0	0	1
15	0	0	0	1	1	1	1	0	1	0	1	1	0	0	1

Figure 3.7: Window property over a binary pseudo-random sequence of $2^4-1 = 15$ elements.

.

From the above definition and the fact that PRSs have, by default, the window property, for PRSs we have:

$$\kappa = 1 \tag{3.18}$$

The problem of constructing a de Bruijn sequence is mathematically equivalent to following an Euler path[1] through the nodes of de Bruijn graph. It can be shown that for an alphabet of q elements we may have N_{dBS} possible *distinct* de Bruijn sequences, with N_{dBS} given by the relation

$$N_{dBS} = \frac{(q!)^{q^{n-1}}}{q^n} \tag{3.19}$$

In figure 3.8 we show an example of generation of a binary 16-element de Bruijn sequence. In order to visit all the edges, one possible path is to start from the node 000 and follow the path: [000] → [000] → [001] → [011] → [111] → [111] → [110] → [101] → [011] → [110] → [100] → [001] → [010] → [101] → [010] → [100] → [000]. Passing from all the edges guarantees that all the possible 4-tuples are going to appear exactly once The De Bruijn sequence is then formed by the label of each edge, up until reaching the initial node 000, i.e.: $c_{db} = [0111101100101000]$.

As a pseudo-random sequence contains by default all the possible m-tuples except from the tuple $\underbrace{00...0}_{m \text{ times}}$, a 0 can be manually added in the longest subsequence

[1] A path that visits all edges exactly once.

of 0s in order to transform the pseudo-random sequence into its De Bruijn associate. Such a transformation is particularly common in the context of numerical simulations using SSFM not only because we include the missing pattern $\underbrace{00...0}_{m \text{ times}}$ in the sequence (thus creating a signal that contains all the possible degradation patterns with respect to the physical effects of the fiber), but also because a De Bruijn sequence has 2^k elements and an FFT can be applied to speed up the process. However, we should stress that the De Bruijn associate of a pseudo-random sequence is no more pseudo-random, as the autocorrelation function does not generally satisfy the equation (3.8).

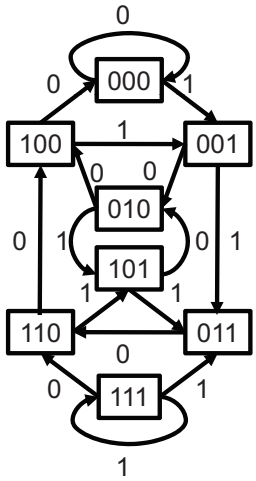

Figure 3.8: De Bruijn graph generating a de Bruijn sequence

The inverse process is also possible. Given a de Bruijn sequence, we can remove a 0 from the longest subsequence of 0s, so that the resulting sequence will have the same length as a pseudo-random sequence (*the pseudo-random associate* of a de Bruijn sequence).In a similar way, however, we should underline that, the resulting sequence is not necessarily a pseudo-random sequence, i.e. the autocorrelation property is not always satisfied. More precisely, the de Bruijn associates of PRSs, generally form a small subgroup within the group of all possible de Bruijn sequences for a given length.

In figure 3.9 we show examples of autocorrelation functions for a PRBS sequence of length 15 (figure 3.9a), its de Bruijn associate (figure 3.9b) and the pseudo-random associate of the de Bruijn sequence (figure 3.9c) generated in figure 3.8. Applying eq. (3.19) for $q = 2$ and $n = 4$, we find that there exist 16 possible de Bruijn sequences. At the same time, for a PRBS of a length $2^4 - 1$ there exist only two distinct primitive polynomials, which means that there are only two de Bruijn sequences out of 16,

for which, their pseudo-random associates also have the autocorrelation property. $c_{db} = [0111101100101000]$ is one of those sequences, since the autocorrelation function of its pseudo-random associate does not satisfy the condition (3.8).

For reasons of completeness, we note that there exist sequences having the property (3.8) but not the property (3.18). One example of such a case comes up when constructing the *sequence of transitions* of a PRS. The sequence of transitions c_{tr} of a sequence c over $GF(q)$ with L_{seq} elements is a new sequence over $GF(q^2)$ of L_{seq} elements as well, with elements being the 2-tuples of each couples of consecutive elements of the sequence c.

Consider for example the de Bruijn associate of a PRS $c_b = 0011110101100100$. There are 4 possible types of transitions in this sequence as the sequence is binary and there are 4 distinct tuples of two symbols, i.e. $[00], [01], [10], [11]$ or $0, 1, 2, 3$ in decimal format. Taking the bits of the sequence in consecutive couples (also considering the cyclic couple between the last and first bit) we construct the sequence of the transitions $c_{b,tr} = 0133321213201200$. It is easy to notice that this sequence is not a de Bruijn sequence as half of all possible tuples of two symbols are missing, whereas other tuples appear twice. However, the pseudo-random associate of this sequence, rather surprisingly, has an ideal, two level autocorrelation function, satisfying (3.8), like the autocorrelation of figure 3.9a.

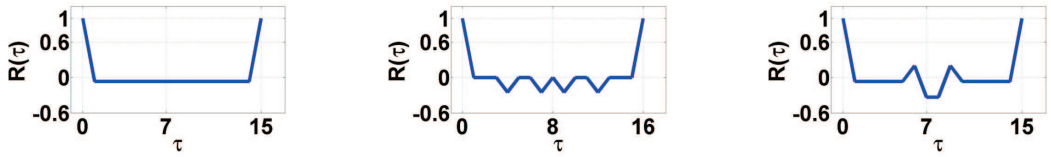

(a) A PRBS sequence of length $2^4 - 1 = 15$.

(b) The de Bruijn associate of the PRBS sequence.

(c) The pseudo-random associate of the de Bruijn sequence c_{db}.

Figure 3.9: Autocorrelation function for different sequences.

Summarizing this section, the two properties of *autocorrelation function* and *window* are necessary for a sequence to be characterized as pseudo-random. As we will see in section §3.4, for commonly used non pseudo-random sequences, κ takes values lower than 1 as such sequences generally contain a smaller number of

different patterns than the maximum possible. Furthermore, non pseudo-random sequences are going to be generally studied with respect to their "quality" of being close to a pseudo-random sequence, i.e. with respect to the "flatness" of their autocorrelation function as well.

3.4 Non pseudo-random sequences

While PRBSs were commonly used for OOK modulation formats, it was not until recently that the appearance of multi-level modulation has re-opened the discussion over the used data sequences.

Especially during the first steps of the passage from OOK to multi-level modulation, multi-level sequences were constructed by interleaving binary sequences with a random delay between them. As we have already seen in the past sections, the resulting sequence is not necessarily pseudo-random if the shift between the two PRBSs is not carefully chosen, i.e. the resulting sequence will not have the properties of equations (3.8) and (3.18).

Seq.	1	2	3	4	5	6	7	8	9	10	11	12	13	14	15
c_1	0	0	1	1	1	1	0	1	0	1	1	0	0	1	0
c_2	0	0	1	0	0	1	1	0	1	0	1	1	1	1	0
c_3	0	0	3	2	2	3	1	2	1	2	3	2	2	3	0

(a) Interleaving c_1 and c_2 to get c_3.

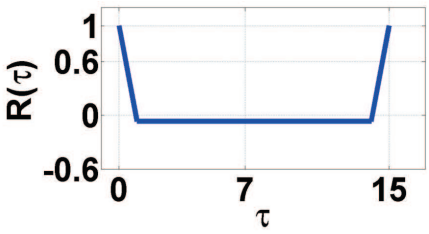

(b) Autocorrelation function.

κ	0.75
Prob{0}	0.25
Prob{1}	0.25
Prob{2}	0.25
Prob{3}	0.25

(c) κ and symbol probabilities.

Figure 3.10: Characteristics of quaternary sequence c_3, resulting from the multiplexing of two pseudo-random binary sequences c_1 and c_2.

The authors of [105] studied the performance of a given link for variable sequence lengths using, either a quaternary sequence generated by interleaving two independent PRBSs, either an actual Pseudo-Random Quaternary Sequence (PRQS) sequence. Numerical evidence is used in the paper to support the statement that non pseudo-random sequences yield "abnormalities" in the BEP assessment. One of these abnormalities is that increasing the sequence length does not monotonically increase BEP, with BEP consequently not converging for increasing sequence lengths. Equivalently, we could say that, whereas with PRSs we can approach the "truly correct" assessment by increasing the sequence length, if our sequence is not pseudo-random, increasing the sequence length does not necessarily lead to more accurate estimations of the BEP. The reason is that increasing the sequence length of a non pseudo-random sequence does not necessarily add more degrading patterns in a balanced way. It is also stated in the paper that the difference between the two estimations is reported to rise up to 10 orders of magnitude in terms of BER.

Seq.	1	2	3	4	5	6	7	8	9	10	11	12	13	14	15
c_1	0	1	1	1	1	1	0	0	1	1	0	1	0	0	1
c_2	0	0	0	1	0	1	0	1	1	1	0	1	1	0	0
c_3	0	2	2	3	2	3	0	1	3	3	0	3	1	0	2

(a) Interleaving c_1 and c_2 to get c_3.

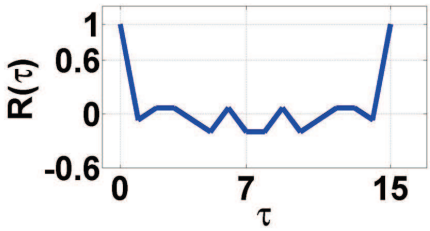

(b) Autocorrelation function.

κ	0.75
Prob{0}	0.3125
Prob{1}	0.1250
Prob{2}	0.2500
Prob{3}	0.3125

(c) κ and symbol probabilities.

Figure 3.11: Characteristics of quaternary sequence c_3, resulting from the multiplexing of two pseudo-random binary sequences c_1 and c_2.

To illustrate the above, in figure 3.10a we show an example of two PRBSss (c_1 and c_2) being multiplexed (with a random shift between them) to generate a

quaternary sequence (c_3). Even though the autocorrelation function of c_3 satisfies (3.8) and also, in the de Bruijn associate of the function all symbols have the same probability of occurrence (marked by $Prob(k), k = 0, 1, 2, 3$), as shown in figures 3.10b and 3.10c, one can easily verify that not all possible tuples of two symbols are present in the sequence, leading to $\kappa = 0.75$.

An alternative option to construct a quaternary sequence of a length $q^n - 1$ would be to interleave the two sequences resulting from the even and odd bits of a PRBS of a length $q^{n+1} - 1 = 2q^n - 1$ [1]. In figure 3.11 we show the properties of this sequence. It may be easily confirmed that c_3 is not pseudo-random, something that is indicated by both the non-ideal autocorrelation function and the κ parameter. Additionally, in this case, the probabilities of occurrence for each symbol are not identical, which means that some symbols are more likely to be found in the sequence than others.

Sequence Type	1	2	3	4	5	6	7	8	9	10	11	12	13	14	15
C_{PRQS}	0	1	1	2	1	0	3	3	1	3	0	2	2	3	0
$C_{PRQSPrec}$	**0**	**2**	**3**	**2**	**3**	**3**	**0**	**3**	**1**	**2**	**2**	**0**	**1**	**2**	**0**
C_{2PRBS}	0	0	3	2	2	3	1	2	1	2	3	1	1	3	0
$C_{2PRBSPrec}$	**0**	**0**	**3**	**2**	**0**	**3**	**1**	**3**	**1**	**3**	**0**	**2**	**3**	**0**	**0**
C_{PRBS2X}	0	2	2	3	2	3	0	1	3	3	0	3	1	0	2
$C_{PRBS2XPrec}$	**0**	**1**	**3**	**0**	**1**	**2**	**2**	**3**	**0**	**3**	**3**	**0**	**2**	**2**	**0**

Figure 3.12: Quaternary sequence table with a pseudo-random quaternary sequence (C_{PRQS}), a quaternary sequence from two interleaved pseudo-random binary sequences (C_{2PRBS}), a quaternary sequence from one pseudo-random binary sequence interleaving odd and even bits (C_{PRBS2X}) and their corresponding precoded versions $C_{PRQSPrec}$, $C_{QS2PRBSPrec}$ and $C_{QSPRBS2XPrec}$.

Finally, it is also common, especially for modulation formats incorporating either directly a differential detection or a differentially detected coherent detection, to use precoded sequences (see section §2.1.3.3) in order to assess the system performance. It can be easily verified that a precoding over a PRS following the

[1] To be precise, in order to make a quaternary sequence of $q^n - 1$ symbols we just need the $2q^n - 2$ bits of the pseudo-random sequence, so we drop off a "0" from the biggest subsequence of zeros.

equation (2.13) (or the procedure of figure 2.4) results into a shifted version of the same PRS and therefore, it does not degrade the pseudo-random characteristics of the sequence. However, especially for DQPSK modulation in optical communications, a different type of precoding is commonly used (also presented in section §2.1.3.3) that degrades the pseudo-random characteristics of the PRS.

In figure 3.12 we show some precoded versions for all the sequence types presented so far, including a PRQS (C_{PRQS}), a sequence made up of interleaved PRBS (C_{2PRBS}) and a sequence made up of interleaved odd and even bits of a PRBS sequence (C_{PRBS2X}). The autocorrelation, the values of the κ parameter and the symbol probabilities are shown in 3.13, where we can see neither of the equations (3.8) or (3.18) are satisfied. However, the autocorrelation function seems to be closer to (3.8) in the case of $C_{PRQSPrec}$ while $C_{PRBS2XPrec}$ seems to have the most "degraded" autocorrelation. Concerning the κ parameters, the worse case is presented for $C_{2PRBSPrec}$ where almost half the patterns are missing from the sequence, while for the same sequence even the symbol probabilities are severely unbalanced with the symbol "0" appearing with a probability of about 43%.

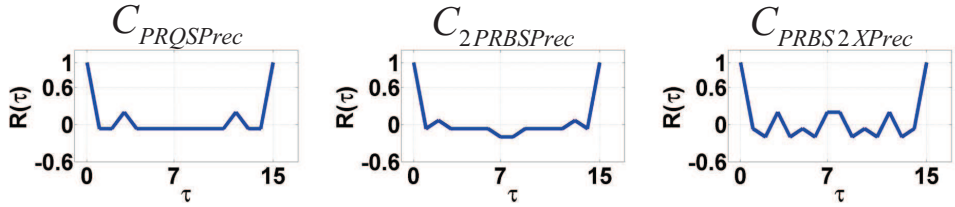

κ	0.75
Prob{0}	0.3125
Prob{1}	0.1250
Prob{2}	0.3125
Prob{3}	0.2500

(a)

κ	0.5625
Prob{0}	0.4375
Prob{1}	0.1250
Prob{2}	0.1250
Prob{3}	0.3125

(b)

κ	0.6875
Prob{0}	0.3750
Prob{1}	0.1250
Prob{2}	0.2500
Prob{3}	0.2500

(c)

Figure 3.13: Autocorrelation, κ and occurrence probability of: (a) Precoded PRQS ($C_{PRQSPrec}$) (b) precoded C_{2PRBS} ($C_{2PRBSPrec}$) (c) precoded C_{PRBS2X} ($C_{PRBS2XPrec}$).

Summarizing this section, we have tried to quantify the pseudo-random properties of commonly used quaternary sequences and we have shown that in all

cases, these sequences are not pseudo-random, i.e. the properties (3.8) and (3.18) are not simultaneously satisfied (one of them can be satisfied though). We have also shown that the operation of pre-coding *systematically degrades* the pseudo-random properties of these sequences, in terms of both autocorrelation function and resemblance to a De Bruijn sequence. Finally, in most cases the probabilities of symbols are not equal, i.e. some symbols appear a lot more often than others.

However, up to this point, it is not clear how these "degraded" pseudo-random properties influence the accuracy on the system performance estimation. In section §3.5 we present numerical simulation results quantifying the difference between performance assessed via pseudo-random or non pseudo-random sequences.

3.5 Performance assessment of dispersion-managed links by different sequence types

The system used in our numerical simulations is shown in figure 2.39. The transmitted QPSK single-channel signal is modulated at $R = 21.51$ Gsymbols/s (or $R_B = 43$ Gbits/s), entering a system with variable Dispersion Management (DM), variable injection power per span P_{in} and a variable number of spans N_s (the complete variation of parameters are indicated in figure 3.14). For reasons of simplicity, in-line ASE noise was neglected and the BER was calculated at the receiver with $OSNR = 13\ dB$ using the noise loading technique[1].

Apart from the variation of the aforementioned parameters, the propagation was simulated for five different sequence lengths L_{seq}, 256, 1024, 4096 and 16384 symbols as well as four different sequence types including, the de Bruijn associate of a pseudo-random quaternary sequence (noted as $c_{PRQSDebr}$), the precoded version of $c_{PRQSDebr}$ (noted as $c_{PRQSDebrPrec}$), the de Bruijn associate of a quaternary sequence created by interleaving two distinct pseudo-random binary sequences

[1]Dispersion-managed systems at this symbol rate and chromatic dispersion are known to be impacted by nonlinear signal-noise interaction[21]. Nevertheless, in this investigation we are only interested in the performance difference of fixed configurations, estimated by different sequence types. In this context, we believe that the reached conclusions qualitatively hold in the case of a realistic system with in-line ASE noise.

(noted as $c_{2PRBSDebr}$) and finally, the precoded version of $c_{2PRBSDebr}$ (noted as $c_{2PRBSDebrPrec}$).

Parameter	Range
R	21.51 Gbaud
D	17 ps·nm^{-1}·km^{-1}
n_2	2.7·10^{-20} m^2·W^{-1}
A_{eff}	80 μm^2
α	0.2 dB/km
P_{in}	[-3, -1, 1, 3, 5, 7, 9] dBm
N_{spans}	[5, 10, 15, 20]
D_{res}	0 ps·nm^{-1}
RDPS	[0, 100, 1700] ps·nm^{-1}
D_{pre}	-(D/α) - RDPS · (N_{spans} -1)/2

Figure 3.14: Parameter value ranges for the simulated system

Following the analysis of section §3.4, we already noted that the performance assessment of the system will be different following the different sequence types and the most balanced estimation will be yielded by the PRQS. In order to quantify this difference between the performance yielded by the pseudo-random sequence and the other non pseudo-random sequence types, we examine in the following this Q^2 difference as a function of ϕ_{NL}, for varying sequence lengths. If we denote ${Q^2}_{PRQSDebr}$ the quality in terms of Q^2 yielded by $c_{PRQSDebr}$, ${Q^2}_{PRQSDebrPrec}$ the quality yielded by $c_{PRQSDebrPrec}$, ${Q^2}_{2PRBSDebr}$ the quality yielded by $c_{2PRBSDebr}$ and ${Q^2}_{2PRBSDebrPrec}$ the quality yielded by $c_{2PRBSDebrPrec}$, we represent only the differences $\delta{Q^2}_{PRQSPrec} = {Q^2}_{PRQSDebrPrec} - {Q^2}_{PRQSDebr}$, $\delta{Q^2}_{2PRBS} = {Q^2}_{2PRBSDebr} - {Q^2}_{PRQSDebr}$ and finally, $\delta{Q^2}_{2PRBSPrec} = {Q^2}_{2PRBSDebrPrec} - {Q^2}_{PRQSDebr}$.

In figure 3.15 we represent these differences for the configuration of $D_{lin} = 0\ ps \cdot nm^{-1} \cdot km^{-1}$ and varying sequence length. We first note that for almost all sequence lengths and low levels of ϕ_{NL}, the differences between pseudo-random and non pseudo-random sequences are not important. Indeed, for relatively low levels of ϕ_{NL}, the signal is not particularly deformed and thus, as there are very few errors, all sequences yield, more or less, the same performance. On the other hand, for high levels of ϕ_{NL} important differences are observed. These differences may reach up to 2 dBs for low sequence lengths[1]. However, even for high sequence

[1]The memory of the system is not very important for a system with full dispersion compensation after every span as shown in [114], [98]. However, we should note that a sequence length of 256 symbols may be insufficient for a correct assessment of the system performance, even in this case

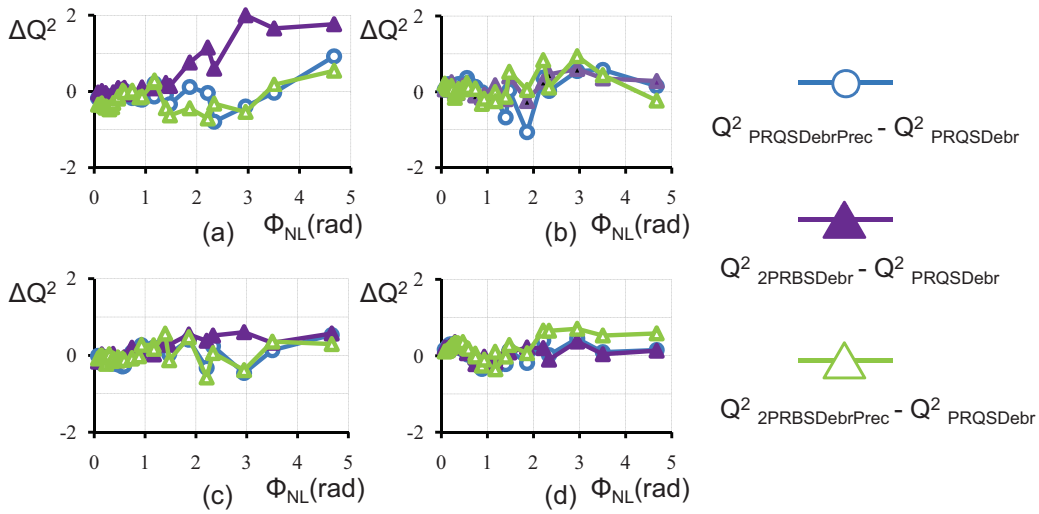

Figure 3.15: Configuration with $D_{lin} = 0\ ps \cdot nm^{-1} \cdot km^{-1}$ (a) $L_{seq} = 256$, (b) $L_{seq} = 1024$, (c) $L_{seq} = 4096$, (d) $L_{seq} = 16384$

lengths[1], we still note differences that may approach almost 1 dB.

The observed difference is probably due to the fact that intra-channel effects, significantly exaggerated for $D_{lin} = 0\ ps \cdot nm^{-1} \cdot km^{-1}$ (full in-line dispersion compensation), are very sensitive to data patterns. This practically means that increasing the sequence length has no impact on the insertion of important patterns that determine the system quality. Finally, we also note that there are oscillations of these differences between different kinds of sequences, meaning, for instance, that one sequence type is not systematically more "optimistic" or more "pessimistic" with respect to the other sequence types. The "period" of these oscillations seems to be lower for low sequence lengths.

In figures 3.16 and 3.17 we plot the same differences for two other common DM configurations of $RDPS = 100\ ps \cdot nm^{-1} \cdot km^{-1}$ (partial in-line dispersion compensation) and $RDPS = 1700\ ps \cdot nm^{-1} \cdot km^{-1}$ (no in-line dispersions compensation). Commenting on figure 3.16 we note that the differences are even more important than the previous case of full dispersion compensation, especially for low sequence lengths, remaining important even for the highest sequence length. On the other hand, for the configuration of no in-line dispersion compensation

[1] A sequence length of 16384 symbols is definitely sufficient in this case

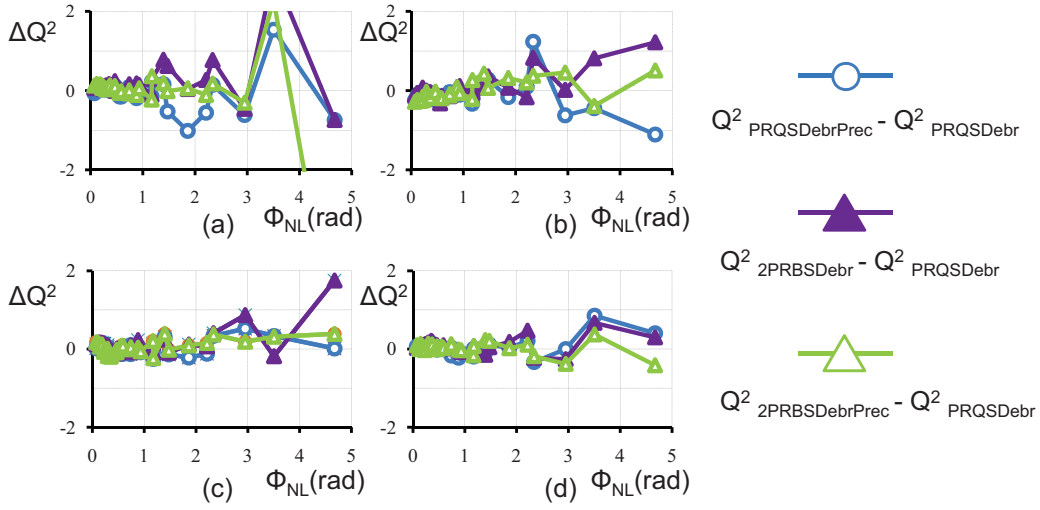

Figure 3.16: Configuration with $D_{lin} = 100\ ps \cdot nm^{-1} \cdot km^{-1}$ (a) $L_{seq} = 256$, (b) $L_{seq} = 1024$, (c) $L_{seq} = 4096$, (d) $L_{seq} = 16384$

(figure 3.16), we observe that for the highest sequence length, all sequences seem to converge, yielding more or less the same estimation. This may be explained from the fact that in a system like this where the energy of each symbol is scattered over all the other sequence symbols, the notion of data-pattern becomes a lot less important and using a true PRS is not crucial for the performance assessment. All the observations made above are synthetically summarized in figure 3.18

Commenting on figure 3.18, we note once again that in all our simulation results, a visual threshold of ϕ_{NL} at about 1 rad in observed. Below this threshold, for all configurations, sequence types and sequence lengths, the performance has a maximum variation of about 0.5 dB, in terms of Q^2. This may be intuitively understood from the fact that for low ϕ_{NL}, inter-symbol interference is not highly nonlinear and signal degradation due to intra-channel effects is certainly not excessive. In this case, all symbols are equally well preserved and since nonlinear interaction between them is minimal, the symbol pattern is not so significant for the performance assessment. At the extent where we can tolerate this maximum "error" of about 0.5 dB, we could claim that, in this regime, PRSs are not indispensable.

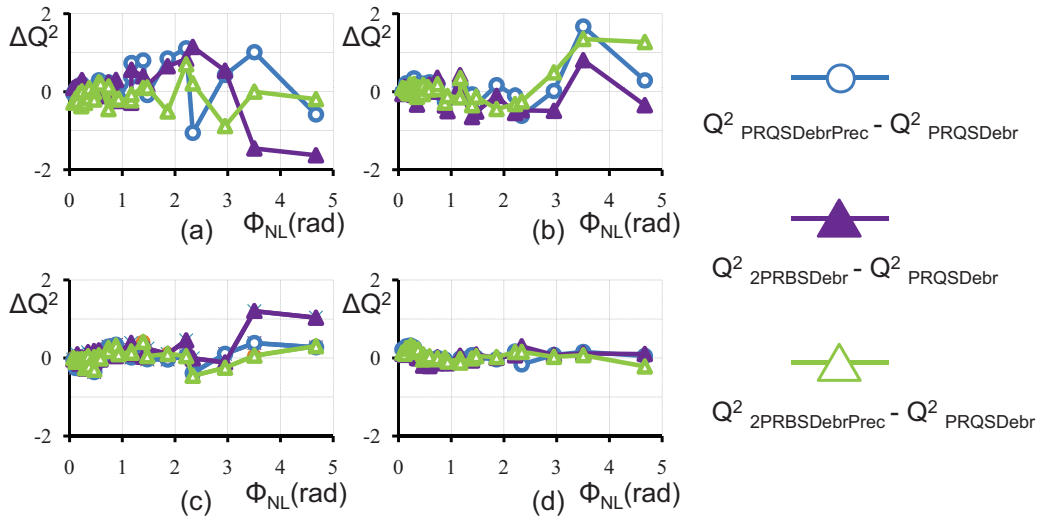

Figure 3.17: Configuration with $D_{lin} = 1700\ ps \cdot nm^{-1} \cdot km^{-1}$ (a) $L_{seq} = 256$, (b) $L_{seq} = 1024$, (c) $L_{seq} = 4096$, (d) $L_{seq} = 16384$

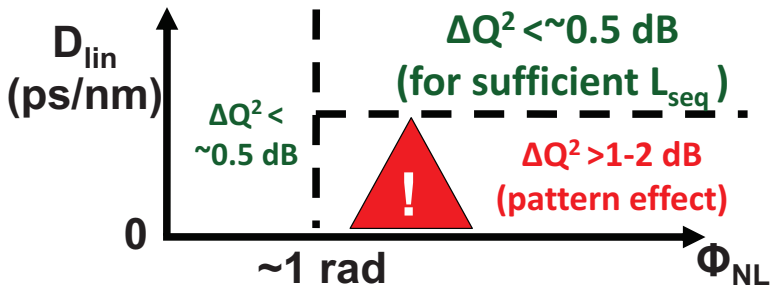

Figure 3.18: General conclusions for the use of pseudo-random sequences.

At the other extreme, when the cumulative dispersion per span is high, the notion of data-pattern is lost since there is a nonlinear interaction of each symbol with a great number of other symbols and almost all sequence types yield more or less the same performance. We should underline however that, in this latter case, only simulations with high sequence lengths may be considered relevant.

Finally, there exists a region, that of high ϕ_{NL} levels and almost full dispersion compensation, where intra-channel nonlinearities are strong and different sequence types yield different evaluations of the system performance, even for very high sequence lengths. This may be equally understood by the fact that, in this regime, few symbols strongly interact in a nonlinear way and therefore, the pattern in this case is critical. This intuition is confirmed by the important differences of $1-2\ dBs$ in terms of Q^2 observed for the performance assessed by non pseudo-random sequences in comparison to the PRQS case.

In conclusion, we see that, out of the four regimes examined, in three of them, performance differences due to the pattern are not so important and may be eventually tolerated. Nevertheless, there is one regime where different sequences yield a radically different performance, even for high sequence lengths. Therefore, it is generally preferable to use PRSs for any kind of configuration since, in any case, they are proved to be the most balanced choice in terms of the included patterns.

Chapter 4

Propagation influence on the statistics of QPSK modulated signals in single-channel dispersion managed systems

> People take the longest possible paths, digress to numerous dead ends, and make all kinds of mistakes. Then historians come along and write summaries of this messy, nonlinear process and make it appear like a simple, straight line.
>
> Dean Kamen

4.1 Introduction

In the previous chapter we have discussed in detail the generation method and the most important properties of multi-level pseudo-random sequences. Furthermore, we have provided theoretical insights and numerical evidence supporting the necessity of using pseudo-random sequences for an unbiased assessment of

the signal distortion. In this chapter, based on quaternary pseudo-random sequences, we numerically investigate transmission degradations in the context of QPSK-modulated signals. Since all our simulations were held in a single-channel configuration, we explicitly focus on *intra-channel nonlinearities*, considering systems with *variable dispersion management*. In all cases it is our objective to de-couple as much as possible the "transmission problem" from the "reception problem", therefore adopting the structured view of figure 2.1[1]. However one may ask: "why *only* intra-channel nonlinearities" and "why dispersion management"?

4.2 Motivations

Understanding intra-channel nonlinearity in systems with dispersion management, is the first step in the process of understanding transmission issues in more complicated systems with phase modulation. In practice, one of the most popular configurations used in record experiments is QPSK modulation, with wavelength and polarization division multiplexing[94]. In such a system, apart from intra-channel nonlinearities (SPM), other sources of nonlinearities also fundamentally limit the system performance such as XPM, FWM and Cross Polarization Modulation (XPolM). Nevertheless, as discussed in [82], not all nonlinearities act in the same way.

In a WDM scenario, based on the fact that we do not have access to the data of neighboring channels, XPM may be modeled as a *multiplicative noise* and FWM may be modeled as an *additive noise*, therefore fundamentally limiting system performance. To fight against inter-channel nonlinearities, several techniques have been proposed, such as reducing or removing in-line dispersion

[1] When On-Off Keying and direct detection dominated optical communications, the receiver was rather fixed and performance improvement could uniquely come from either pure technological advances or from changes in the link design. However, with the appearance of coherent detection and the potential of signal-processing, could also come from algorithms applied at the received side. Therefore, separately understanding the two possible "sources of benefit" is necessary. Furthermore, the coherent receiver itself was, for a period, a source of continuous development as well, involving, for example, an optimization of the choice of the number of taps needed in the Carrier Phase Estimation (CPE) unit, that could also vary as a function of the system parameters.

compensation[103],[8] or temporally de-correlating channels after every span[104], while interleaving RZ-QPSK pulses and increasing PMD has been shown to increase tolerance against XPolM[16], [17]. In all above cases, performance improvement is achieved by limiting the "interference" from foreign signal sources and thus, returning in a scenario where the major source of degradation is intra-channel nonlinearity. On the other hand, SPM degradation is not considered as an irreversible effect since we may (at least theoretically) achieve a channel inversion, for example by using a reverse split-step algorithm[59].

The beginning of this work roughly coincided with the re-birth of coherent detection, the exploration of multi-level modulation and the potential of a Digital Signal Processing (DSP) at the receiver, mitigating signal distortions. While intra-channel nonlinearities in OOK systems with variable dispersion management has been extensively studied in the past (see section §2.2.7), similar investigations in the context of PSK modulation and coherent detection were rather rare.

Furthermore, the barrier between phase "noise" resulting from deterministic degradations and phase noise coming from stochastic sources was not fully clarified. More precisely, in system equipped with a coherent receiver, phase fluctuations may be due to a frequency mismatch with the local oscillator, pure AWGN noise coming from the last amplifier, phase fluctuations coming from the interaction between AWGN and fiber nonlinearities[51],[20], pure deterministic degradation due to fiber nonlinearities coming from neighboring channels (noted as inter-channel nonlinearities and discussed in section §2.2.6), or finally, deterministic fluctuations coming from the interaction of linear effects such as chromatic dispersion and Kerr nonlinearities, known as intra-channel nonlinearities as discussed in section §2.2.7.

In this chapter, we focus on the last case, i.e. intra-channel nonlinearities. More specifically, we present numerical simulation results, motivated by an attempt to elucidate the following issues:

1. What is the "form" of the deterministic distortion, caused by intra-channel nonlinearities? In other words, what is the form and the constellation shape

resulting from single-channel transmission, for variable dispersion management parameters?

2. In OOK modulation there existed criteria such as the cumulative nonlinear phase[9], for the performance assessment of OOK systems with *optimal dispersion management*. Is this criterion valid for phase-modulated systems? What does optimizing the dispersion management involve?

3. In OOK modulation, since information was coded only on signal amplitude, the statistics of the signal phase were neglected. In coherent communications however, both amplitude and phase are recovered. Are there any qualitative differences on the statistics of the two signal quadratures when varying the dispersion management?

4. In OOK modulation there existed analytical laws[43],[67] providing "rules of thumb" for the optimization of the dispersion map in 10 or 40 Gb/s. Are these rules accurate for PSK modulation, and more particularly, can they also accurately describe the behavior of the phase (instead of the amplitude) of a signal?

5. What is the influence of parameters such as the clock recovery on system performance? How should the clock recovery be done to maximize the probability of a correct symbol detection?

6. What is the influence of dispersion management on the potential of specific correction algorithms? In other words, knowing that a specific algorithm is going to be used at the receiver, what it is the optimal dispersion management scheme?

4.3 Simulations setup and examples

For all numerical simulation we are based on the generic system of figure 2.39, reproduced here for convenience. In all cases we investigate the statistical properties of a QPSK signal after transmission of a single channel ($\lambda = 1.55\ \mu m$),

modulated at a symbol rate of $R = 21.51$ *Gbaud*, for a variable dispersion management. The numerical signal was based on the De Bruijn associate of a PRQS with a length of either $4^6 = 4096$ or $4^7 = 16384$ symbols (see section §3.3.2.2 for the generation process)[1], always considering 64 samples per symbol.

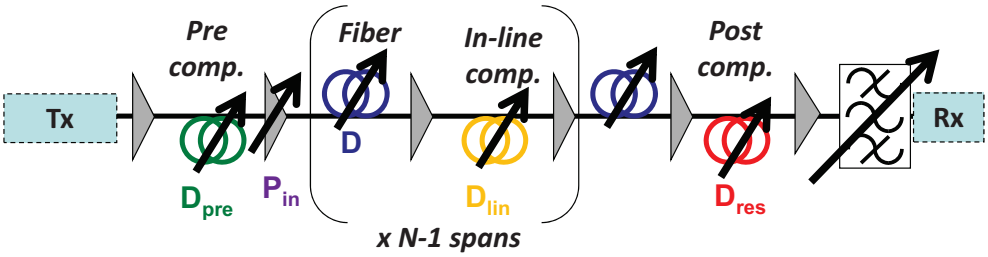

Figure 4.1: Dispersion managed transmission system

Concerning the dispersion management, we are based on a single-period dispersion map (explained in figure 2.40), varying the pre-compensation D_{pre}, the residual in-line cumulative dispersion D_{lin} (the span length is fixed at $z_s = 100\ km$), the residual dispersion D_{res}, the fiber GVD parameter D, the injection power at the beginning of every span P_{in} and the number of spans N_s. The variation range of these parameters is shown in figure 4.2 corresponding to about 10000 numerical simulations.

Parameter	Range of values
D	**[4 : 4 : 24] ps·nm^{-1}·km^{-1} (6 values)**
P_{in}	**[-5 : 2 : 9] dBm (8 values)**
D_{pre}	**[-900 : 300] ps·nm^{-1} (13 values)**
D_{lin}	**[0 : 125] % of compensation (15 values)**
N_s	**[2 : 2 : 22] (11 values)**
D_{res}	**[-120: 120] ps·nm^{-1} (13 values)**

Figure 4.2: Parameter ranges for numerical simulations.

[1] In one case we have also used a non-Pseudo-Random (PR) sequence as it will be explicitly indicated.

Furthermore, in order to focus on the interplay between chromatic dispersion and nonlinearities, we consider a scalar propagation (and thus we neglect all polarization effects including PMD and XPolM), amplifiers are considered flat-gain repeaters (except from one special case), while we also consider no nonlinearities or losses in the Dispersion Compensating Fiberss (DCFs).

Finally, in order to decouple the transmission from the reception problem, for all numerical simulations results presented here, the reception is emulated by an artificial extraction of the numerical samples. More precisely, suppose that each symbol is numerically represented by the discrete complex signal $s[n]$, with $n = 1, ..., M$, with M being the number of complex samples per symbol (see figure 4.3). To emulate an idealized detection of this symbol we simply keep the complex average of its l *middle* samples. For example, for $l = 4$ the "detected sample" s_d is given by: $s_d = \frac{s[M/2-1]+s[M/2]+s[M/2+1]+s[M/2+2]}{4}$[1]. Performing the reception in such a way we also implicitly consider a sampling at the center of the symbol slot[2]. In other words, having in mind the coherent detection described in section §2.2.5.2, we consider that the received signal is described by the equation (2.175) with $\omega_{LO} = \omega_{LO}$ and $\phi_{LO} = 0$, without the need to pass from a Viterbi-Viterbi algorithm.

Furthermore, in general, transmission results in an additional phase shift of all signal states, thus rotating the initial signal constellation. This phase shift contains the stochastic component θ discussed in section §2.1.4.3.3 which is present in systems impacted only by AWGN, corresponding to the fact that the transmitter phase reference is generally unknown to the receiver due to random (or very hard to control) medium fluctuations (stemming from PMD, for example, changing with temperature or tension). To this last we should also add any additional phase shift coming from the local oscillator phase ϕ_{LO}, an initial signal

[1] With such a numerical reception, we are implicitly emulating a filter with a bandwidth $B_{samp} = \frac{N_{sps}}{l} R$, where N_{sps} is the number of samples per symbols and R is the symbol rate. For the example of our numerical simulations, using $N_{sps} = 64$, $R = 21.51\ Gbaud$ and $l = 4$ yields $B_{samp} = 344.16\ GHz$. Although this receiver bandwidth is totally unrealistic even for modern electronics, it allows for an unbiased view of transmission effects, eliminating any possible signal distortions due to receiver filtering.

[2] Small variations, sampling at times different than the center of the pulses, will also be considered, later in this chapter.

phase ϕ_0 (that may be known or controlled at the transmitter side) or the additional phase shift coming from the signal propagation of a distance L, that can be calculated to be equal to $\beta_1 \cdot L$. Finally, as it will be discussed in more detail in this chapter, there also appears another average phase shift component, resulting from the interplay between chromatic dispersion and nonlinear effects, referred to in the following as θ_{rot}. In other words, θ_{rot} is the average additional global phase shift of a signal, for which we have numerically simulated a nonlinear propagation using SSFM and received with a coherent detection as described above. In the rest of this chapter, when we refer to a global phase shift we refer only to θ_{rot}, neglecting all the other aforementioned sources of phase shift.

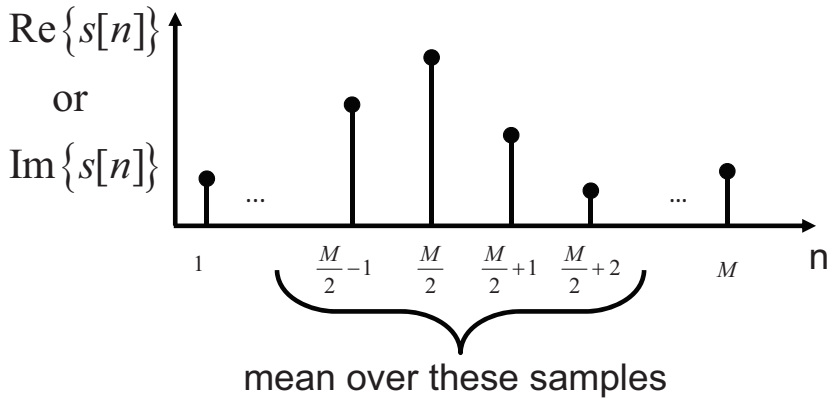

Figure 4.3: Idealized coherent detection, taking the average of the real and imaginary part of the complex signal $s[n]$ of each symbol.

Having knowledge of the phase shift is equivalent to considering that the receiver has a perfect knowledge of the carrier phase, or that the receiver manages to perform a flawless CPE, similar to the detection process of section §2.1.4.3. Although this process is quite complicated and in practice it is often linked to a sacrifice of bandwidth (for example with the use of a PLL and a training sequence), for the purposes of this manuscript we simplify the analysis by calculating the parameter θ_{rot} a posteriori over all symbols of our simulated signal, using the knowledge of the initially transmitted data sequence. In other words, the decision may be then performed after a rotation of the coordinate system by $-\theta_{rot}$. In the following we will refer to this scheme as *ideal coherent receiver* and to the reception as *ideal coherent reception*.

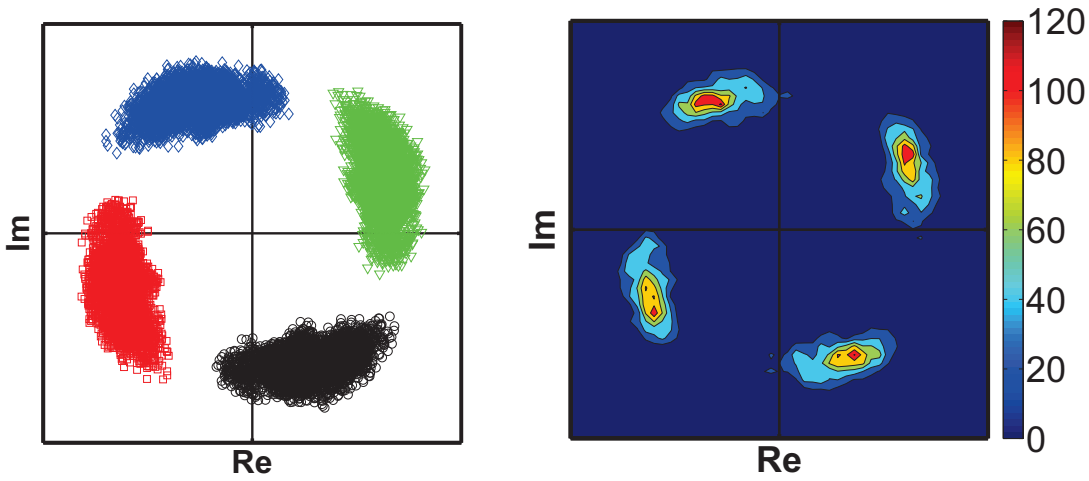

(a) Signal constellation (b) Signal PDF

Figure 4.4: Example of degraded signal after a transmission with $D = 16\ ps/(nm \cdot km)$, $P_{in} = 9\ dBm$, $N_s = 6$, $D_{pre} = 0\ ps/nm$, $D_{line} = 0\ ps/nm$, $D_{res} = 0\ ps/nm$.

However, since a knowledge of the absolute phase is in most practical cases very hard to achieve, differential schemes are used, coding information in the *phase difference* between successive symbols instead of phase levels as described in section §2.1.4.3.4. In order to emulate this alternative receiver scheme, based on the initially recovered numerical signal described before, we use the relation (2.102) to construct a new signal. We note that the statistics of the new complex signal are most possibly going to be influenced by this detection process, involving both amplitude and phase of the initial signal. We refer to this scheme as *ideal differentially-coherent receiver* and to the reception as an *ideal differentially-coherent reception*. In what follows, when no special reference is made we implicitly suppose that reception was emulated by an ideal coherent receiver. Nevertheless, we show some few typical examples for an ideal differentially-coherent receiver, in order to illustrate the possible differences between these schemes.

In figure 4.4b we plot the received constellation and an estimation of the corresponding signal PDF in figure 4.4b, for a configuration with system parameters $D = 16\ ps/(nm \cdot km)$, $P_{in} = 9\ dBm$, $N_s = 6$, $D_{pre} = 0\ ps/nm$, $D_{lin} = 0\ ps/nm$, $D_{res} = 0\ ps/nm$. The initial constellation before the transmission, is shown in figure 2.24a, while the PDF is obtained by dividing the complex plane in small

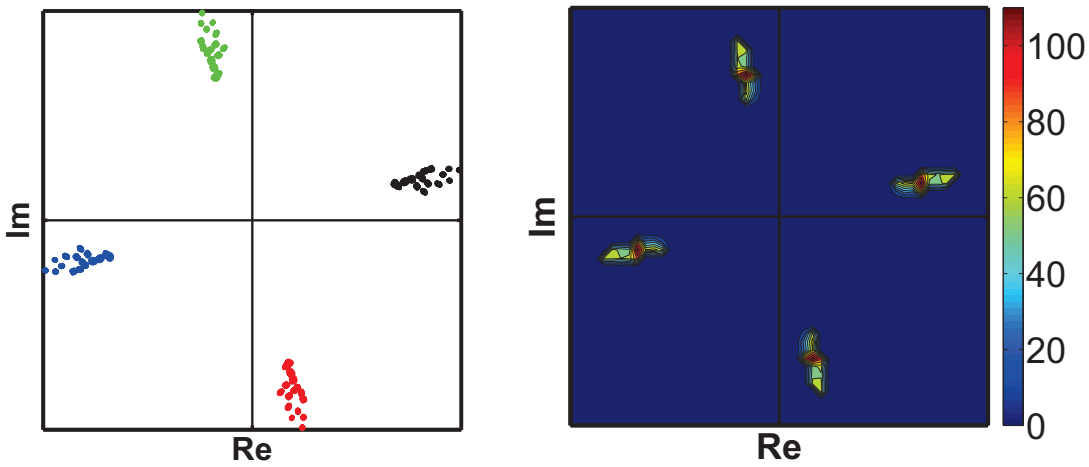

(a) Signal constellation (b) Signal PDF

Figure 4.5: Example of degraded signal after a transmission with $D = 4\ ps \cdot nm^{-1} \cdot km^{-1}$, $P_{in} = 5\ dBm$, $N_s = 6$, $D_{pre} = -100\ ps \cdot nm^{-1}$, $D_{lin} = 8\ ps \cdot nm^{-1}$, $D_{res} = -40\ ps \cdot nm^{-1}$.

boxes and counting the number of samples that fall in each box (the colorbar at the right of the figure indicates the number of samples that fall in each box). Furthermore, having knowledge of the initially transmitted data, in the constellation of figure 4.4b, we paint with a different marker and color samples corresponding to a different initial QPSK state, or a different initially transmitted quaternary symbol. For example, in the De Bruijn associate of a PRQS with a length of 4096 symbols, we find 1024 symbols of each kind, i.e. 0,1,2 or 3, being eventually mapped into 1024 complex samples for each state.

Carefully inspecting figure 4.4b, we note that the four QPSK states have acquired a (global) phase shift $\theta \simeq -\frac{\pi}{2}$. We also note that the constellation has a rather special, "bean-like" shape, extended more in terms of phase, than in amplitude. In the literature, this constellation shape is very often attributed to the interplay of fiber nonlinearities and amplifier noise[51]. However, it is obvious that here, such a shape may also directly stem from the interplay between chromatic dispersion and nonlinearities.

In figures 4.5a and 4.5b we show another constellation and PDF example for a configuration with parameters $D = 4\ ps/(nm \cdot km)$, $P_{in} = 5\ dBm$, $N_s = 6$,

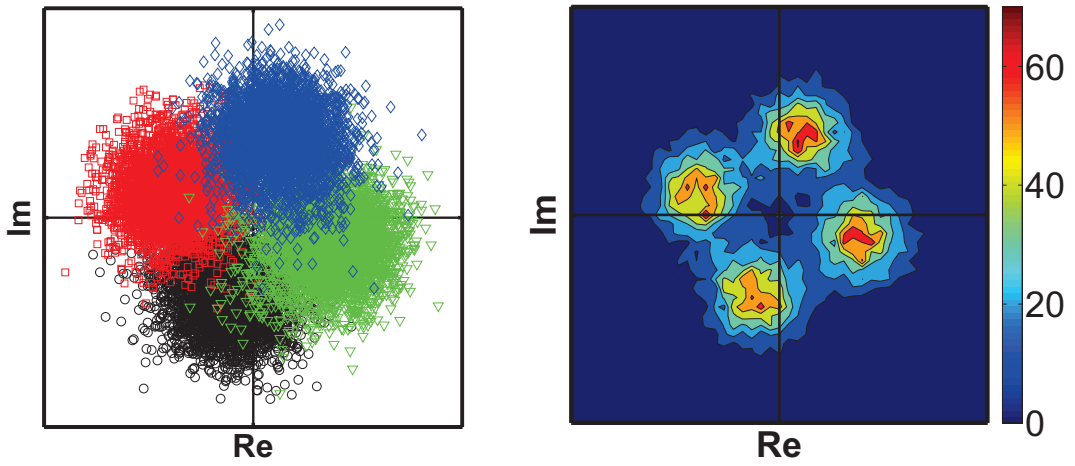

(a) Signal constellation

(b) Signal PDF

Figure 4.6: Example of degraded signal after a transmission with $D = 16\ ps \cdot nm^{-1} \cdot km^{-1}$, $P_{in} = 9\ dBm$, $N_s = 6$, $D_{pre} = 0\ ps \cdot nm^{-1}$, $D_{lin} = 1600\ ps \cdot nm^{-1}$, $D_{res} = 0\ ps \cdot nm^{-1}$.

$D_{pre} = -100\ ps/nm$, $D_{lin} = 8\ ps/nm$, $D_{res} = -40\ ps/nm$. The constellation shape is quite similar to the one of figure 4.4b, except that, in this case, the amplitude quadrature is more spread that the phase quadrature.

Finally, one last configuration example is given in figures 4.6a and 4.6b for a configuration with parameters $D = 16\ ps \cdot nm^{-1} \cdot km^{-1}$, $P_{in} = 9\ dBm$, $N_s = 6$, $D_{pre} = 0\ ps \cdot nm^{-1}$, $D_{lin} = 1600\ ps \cdot nm^{-1}$, $D_{res} = 0\ ps \cdot nm^{-1}$. This corresponds to a configuration where all in-line DCFs were removed. Commenting on figure 4.6a, in this case the constellation is similar to the Gaussian constellation of figure 2.38a, appearing like a white Gaussian noise.

Summarizing the above observations, it is evident that dispersion management severely influences the constellation shape and PDF. Furthermore the two signal quadratures do not appear to have the same statistics as dispersion management varies. Even if in PSK modulation, information is coded in phase, amplitude may also be of an importance, for example in a differential scheme where information is recovered through an interference of two adjacent symbols.

4.4 Statistical measures

We have seen that different dispersion maps generally result in different constellation shapes. While even a simple visual observation of a constellation may be quite informative, in order to generalize and quantify our observations for a wide range of parameters, we perform a statistical analysis by calculation of a series of standard deviations over quantities that may be of interest[1].

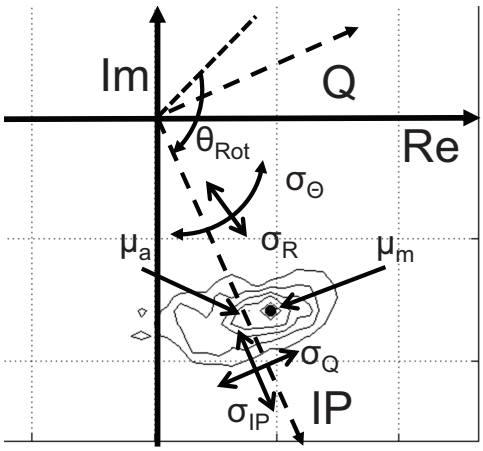

Figure 4.7: Zoom in the PDF of one state.

In figure 4.7 we zoom in just one state of the PDF previously shown in figure 4.4b. As the signal is phase-modulated, the standard deviation of the phase calculated on the state samples, σ_Θ, provides a rough estimation of the transmission performance. At the same time, the standard deviation of the signal amplitude, σ_R provides a measurement of the degradation of the in-phase component of the signal. In figure 4.7 we also indicate the position of the state complex average, θ_{rot} which is the phase shift of the complex average with respect to its initial

[1] As the complex signal is a two dimensional quantity (real-imaginary part, amplitude-phase etc), "degradation" may be captured by several different parameters.

position ($\frac{\pi}{4}$) and the PDF maximum. We note here that the complex average and the PDF maximum are close but generally not superposed.

Furthermore, using the complex average vector we plot two new axes, the in-phase (IP) and the quadrature axis (Q), over which we decompose the complex signal and calculate the corresponding standard deviations σ_{IP} and σ_Q. As discussed in section §2.1.4.3.1, in the case of an AWGN (or AWGN-like) signal degradation with a standard deviation $\sigma = \sigma_{IP} = \sigma_Q$, the quantities σ_Θ and σ_R can be analytically linked to σ. For example, we have seen in the AWGN case that σ_R is always smaller than σ approaching σ for high SNR levels, while σ_Θ is inversely proportional to the square root of σ. However, when the degradation is not AWGN-like, for example when $\sigma_Q > \sigma_{IP}$, σ_R is usually greater than σ_{IP}, while in cases where $\sigma_Q < sigma_{IP}$, as in the AWGN case, σ_R remains smaller than (but very close, though, to) σ_{IP}[1].

Finally, noting by N_{ss} the number of the complex samples s_k of the state, we estimate the spread of the state by *the complex standard deviation* σ_C, given by the formula

$$\sigma_C = \sqrt{\frac{\sum_{k=1}^{N_{ss}} |s_k - \mu_a|^2}{N_{ss}}} \tag{4.1}$$

In the following we are based on the system of 2.39, varying the system parameters as defined in the table of figure 4.2. At the end of the transmission, an ideal coherent detection is performed, as mentioned in section §4.1, and the quality is quantified by a calculation of the five statistical quantities described before: σ_R, σ_Θ, σ_{IP}, σ_Q and σ_C.

4.5 Criterion of cumulative nonlinear phase

Since the main particularity of the optical channel is nonlinearity, many research efforts have been traditionally focused on assessing the system performance in the nonlinear regime, or the right part of figure 2.37. The usual representation in this case involves, plotting the system performance (for example, in terms of Q

[1]Such useful conclusions may be drawn by studying bivariate Gaussian degradation where

factor) as a function of the injection power per span P_{in}, while all other system parameters are fixed. Furthermore, it can be easily shown in this context that, for a different number of spans N_s, we generally result in a different, distinct curve of the system quality as a function of the injection power per span.

Nevertheless, the authors of [9] have shown in the context of OOK modulation, that the system quality can be drawn as a function of a combined parameter including P_{in} and N_s, called "cumulative nonlinear phase" or Φ_{NL}, under the condition of an "optimal dispersion management". Since the system quality can be represented as a function of Φ_{NL} (i.e. a bijective curve of quality VS Φ_{NL}), this parameter may be used as a criterion to assess a system performance. Φ_{NL} is defined in [9] in the same way as in the equation (2.139), with the only difference that the average power P_{av} is used in the place of the peak power P_0, with the quantity Φ_{NL} being, therefore, proportional to the product $P_{av} \cdot N_s$. The motivation for this section is to verify the validity of this observation in the context of single channel QPSK systems. Since systems with no in-line dispersion compensation are becoming increasingly interesting lately, we are also separately investigating the system performance for that particular case.

In figure 4.8a we plot the parameter σ_Θ as a function of Φ_{NL} after an optimization of the dispersion management parameters, i.e. D_{pre}, D_{lin} and D_{res}. The system degradation (expressed in terms of σ_Θ in our case) is initially zero while it increases monotonically as a function of Φ_{NL}, as similarly verified for OOK systems. Furthermore, quality is generally better for low dispersion fibers since the combined effect of chromatic dispersion and nonlinearities increases for an increasing fiber GVD parameter. In effect, the best performance (lowest σ_Θ) is achieved by the fiber with $D = 4\ ps \cdot nm^{-1} \cdot km^{-1}$ and the worst performance is achieved for the fiber with $D = 24\ ps \cdot nm^{-1} \cdot km^{-1}$, noting, however, that the difference in performance is slowly saturating for high dispersion fibers.

In figure 4.8b on the other hand, we plot σ_Θ as a function of Φ_{NL} as before, with the only difference that only systems with no in-line dispersion compensation were considered, or equivalently, $D_{lin} = D \cdot L_s$, where D is the dispersion parameter of the fiber and L_s is the span length. The difference between the two figures is that the above tendency is completely reversed, i.e. low dispersion parameter fibers tend to yield the worst performance, while high dispersion fibers

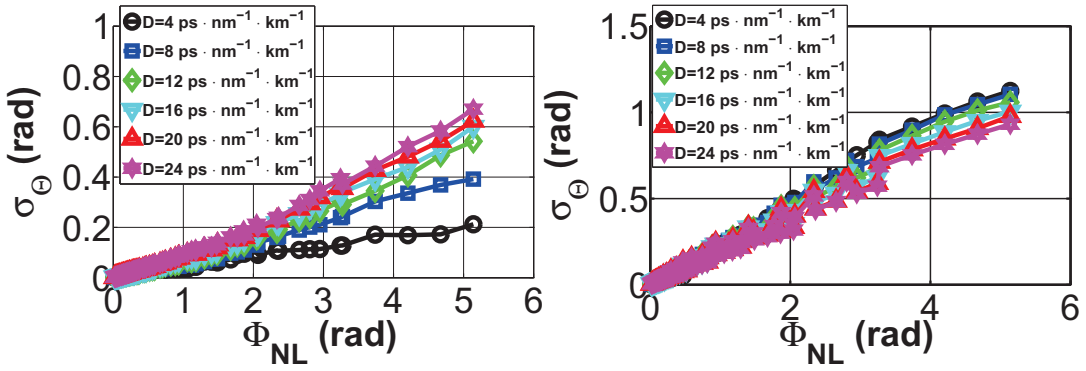

(a) DM with an optimal in-line dispersion compensation

(b) DM with no in-line dispersion compensation

Figure 4.8: Curves of σ_Θ as a function of the system cumulative Φ_{NL} for an optimal dispersion management without optical filtering. The system parameters were varied following the table of figure 4.2. After fixing a value for the chromatic dispersion D, the optimization was separately achieved for each couple of values (P_{in}, N_{spans}), choosing the lowest σ_Θ for the variable parameters D_{lin} (for figure (a)), D_{pre} and D_{res}.

tend to yield the best performance. Nevertheless, we should note that the system of figure 4.8a generally yields a higher performance compared to the case with no in-line dispersion compensation.

In figure 4.9a, the same curves are plotted with the only difference that this time, a 2^{nd} order Gaussian filter with $0.31nm$ bandwidth is used before the ideal coherent reception. We note that in this filtered case, similarly to OOK systems, the degradation is non zero for $\Phi_{NL} \approx 0\ rad$ (i.e. back-to-back), in contradiction to the filter-less case. This is a result of the fact that optical filtering, in back-to-back configuration, slightly degrades the system performance. Then, as Φ_{NL} increases σ_Θ slightly decreases, before increasing again for high values of Φ_{NL}. Similar conclusions as before may be also reached in the case of no in-line dispersion compensation shown in figure 4.9b. The only remarkable difference between figures 4.9b and 4.8b is a slightly worse performance in the filtered case for high values of Φ_{NL}.

The data of the curves 4.8a and 4.9a, can also be plotted in a slightly different

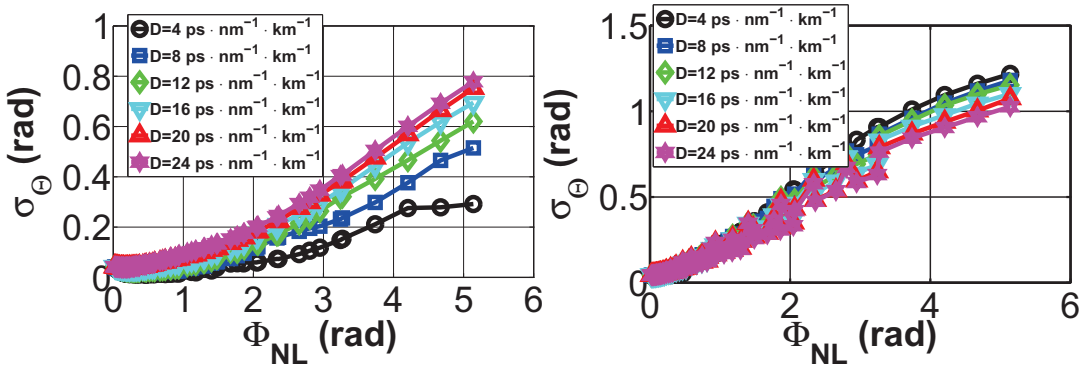

(a) DM with an optimal in-line dispersion compensation.

(b) DM with no in-line dispersion compensation.

Figure 4.9: Curves of σ_Θ as a function of the system cumulative Φ_{NL} for an optimal dispersion management and a 2^{nd} order Gaussian filter with $0.31nm$ bandwidth at the receiver end. The system parameters were varied following the table of figure 4.2. After fixing a value for the chromatic dispersion D, the optimization was separately achieved for each couple of values (P_{in}, N_s), choosing the lowest σ_Θ for the variable parameters D_{lin} (figure (a)), D_{pre} and D_{res}.

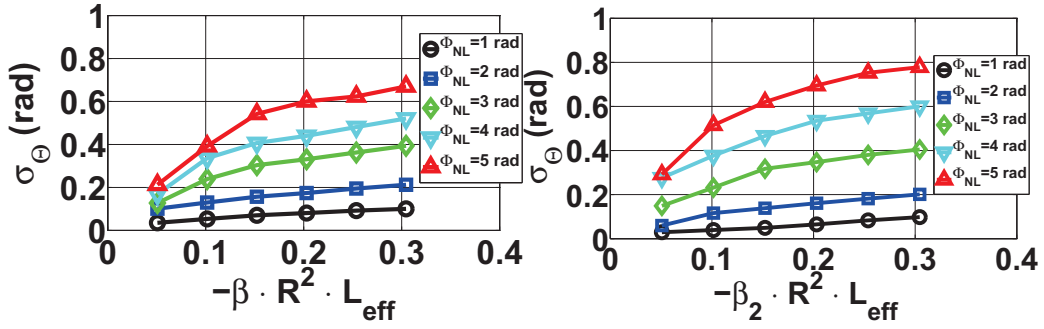

(a) Without optical filtering

(b) With optical filtering

Figure 4.10: Curves of σ_Θ as a function of p_s, fixing the nonlinear phase at $\Phi_{NL} = 2\ rad$, with/without optical filtering. In the second case we have used a 2^{nd} order Gaussian filter with $0.31\ nm$ bandwidth. In all cases, the system parameters vary following the table of figure 4.2.

way, by fixing a value of Φ_{NL} and presenting σ_Θ as a function of a parameter that approximately quantifies the pulse spread, also used in [69], [27], [37] and [21]:

$$p_s = -\beta_2 \cdot R^2 \cdot L_{eff} \tag{4.2}$$

In order to compare our results with the existing literature results, in figure 4.10a and 4.10b we plot σ_Θ as a function of p_s, with and without an optical filter. However, in the context of our numerical investigation where the symbol rate was fixed at 21.51 *Gbaud* and the GVD parameters where roughly following the GVD values of commercial fibers, the range of p_s was insufficient to cover p_s the levels presented in [37]. Nevertheless, for the explored values of p_s we observe a similar behavior.

Another parameter that could possibly have an influence on system performance is the sampling instant. In order to explore this parameter we repeat all previous simulations but, instead of recovering the central samples, we also recover the samples centered at a distance of $[-20, 10, 10, 20]\%(symbol\ period)$ with respect to the center of the symbol center.

In figure 4.11, we re-plot some of the curves of figure 4.8a using the same markers, for four different values of chromatic dispersion, i.e. $[4, 8, 16, 24]ps/(nm \cdot km)$. We limit our view only to relatively low values of Φ_{NL}. Solid curves correspond to a sampling instant at the center of the symbol period (thus reproducing the results of figure 4.8a), while dashed curves correspond to the quality subject to an optimization of the sampling instant as well. We can note a minor difference between the two sets of curves and we can generally admit that, for the range of Φ_{NL} values presented, the differences seem higher for relatively high values of Φ_{NL} and low values of D. For example, we see that for $D = 8ps/(nm \cdot km)$ a mediocre gain of about 0.02 *rad* may be claimed by optimizing the sampling instant, for a Φ_{NL} value around 1.5 rad[1]. This gain seems even less significant as we increase the fiber dispersion, as for high dispersion values the two sets of curves are practically superposed.

[1]We may get an approximate order of magnitude the impact that a $\sigma_\Theta = 0.2\ rad$ may have on a system performance by using the equations (2.81) and (2.82). Doing so, we see that while initially $\sigma_\Theta = 0$ and $BEP = 0$ ($Q^2(dB) = \infty$), for $\sigma_\Theta = 0.2\ rad$ we calculate $BEP = 4 \cdot 10^-4$ ($Q^2(dB) = 10.496$).

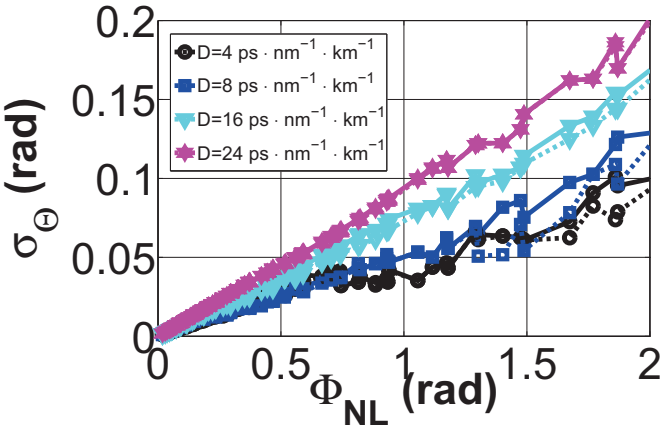

Figure 4.11: Influence of the sampling instant on system performance. System parameters were varied following the table of figure 4.2, while the sampling instant vary in the time interval $[-20, 10, 10, 20]\%(symbol\ period)$ with respect to the center of each symbol.

Summing up this section, we conclude that there are no obvious qualitative differences between OOK and QPSK systems with respect to the law concerning Φ_{NL} for optimized dispersion managed systems. Furthermore, optimizing the sampling instant does not seem to provide a considerable benefit, even for strongly dispersion managed systems with a non zero optimal residual dispersion, as it was the case for OOK modulation[1]. Similar results, supporting the verification that the law concerning Φ_{NL} is valid for QPSK modulation, has also been reported in [54].

However, as it is also mentioned in [54], this law is not expected to provide a meaningful criterion for the performance assessment of highly dispersive systems (i.e. for example, when no in-line dispersion compensation is used) and in this case, other criterions have to be applied. In such cases, the performance may be easily estimated, even analytically by the use of simple models[87],[26].

[1]Nevertheless, a different reception scheme (for example differential or coherent with a correction algorithm) could lead to different conclusions.

4.6 Dispersion Management Optimization and constellation shape

4.6.1 Optimization of dispersion management for phase and amplitude

A number studies have dealt with the problem of the *dispersion management optimization*, or equivalently, the problem of finding the set of parameters D_{pre}, D_{lin} and D_{res} that optimize the system performance. Papers like [67], [43] dealt with this problem in the context of OOK modulation, providing analytic rules for the direct calculation of the optimal pre-compensation as a function of the residual in-line cumulative dispersion. More precisely, the law of [67] proposed the use of a pre-compensation equal to

$$D_{pre,1} = -\frac{D}{\alpha} \cdot \ln\left(\frac{2}{1+e^{-\alpha \cdot L}}\right) - \frac{N_s}{2} D_{lin} \tag{4.3}$$

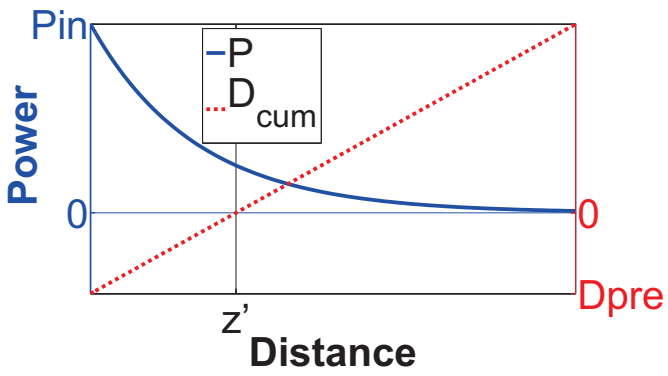

Figure 4.12: Signal power/cumulative dispersion as a function of the distance, for a propagation of one span.

The idea behind this law (see figure 4.12) was the empirical observation that after the propagation of one span in a fiber with chromatic dispersion parameter D, the degradation cause by intra-channel nonlinearities, i.e. i-XPM and i-FWM was minimized when the pre-compensation was set at $D_{pre} = -D \cdot z'$, where z' is the power barycenter, satisfying the equation

$$\int_{0}^{z'} P_{in} e^{-\alpha \cdot z} dz = \int_{z'}^{L_s} P_{in} e^{-\alpha \cdot z} dz \tag{4.4}$$

, with P_{in} being the span injection power, α the fiber attenuation and L_s is the span length.

On the other hand, the law of [41] proposed the use of a pre-compensation equal to

$$D_{pre,2} = -\frac{D}{\alpha} - \frac{N_s - 1}{2} D_{lin} \tag{4.5}$$

In this latter case, the idea behind the law was the minimization of the power fluctuations, induced by the conversion of *phase to intensity*. More specifically, the small-signal conversion matrix of [112] was used, concentrating on the term corresponding to the phase-to-intensity conversion. Then, using the integration method of [14], the intensity fluctuations were linearly "summed up" up until the end of the transmission.

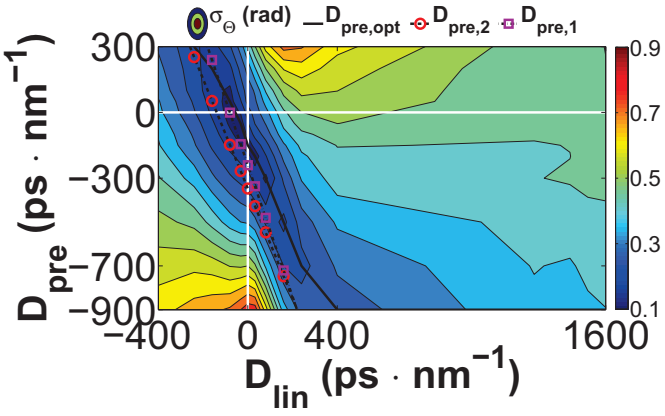

Figure 4.13: σ_Θ as a function of D_{lin} and D_{pre}. System parameters: $D = 16\ ps \cdot nm^{-1} \cdot km^{-1}$, $P_{in} = 9\ dBm$, $N_s = 6$, $D_{res} = 0\ ps \cdot nm^{-1}$, D_{pre} varying from -900 to $300\ ps \cdot nm^{-1}$ and D_{lin} varying from -400 up to $1600\ ps \cdot nm^{-1}$. With a solid line the true minimum σ_Θ, with round markers the law of [43] and with square markers the law of [67]. No optical filtering was performed.

Passing from OOK to PSK, as the information is coded in the phase of the optical signal, it is interesting to investigate the validity of the former rules. In

this section we initially investigate the validity of the above rules, against an optimization of the measured σ_Θ. In figure 4.13 we illustrate an example of σ_Θ evolution as a function of D_{lin} and D_{pre} for system parameters: $D = 16\ ps{\cdot}nm^{-1}{\cdot}km^{-1}$, $P_{in} = 9\ dBm$, $N_s = 6$ and $D_{pre} = -100\ ps \cdot nm^{-1}$, $D_{line} = 8\ ps \cdot nm^{-1}$, $D_{res} = 0\ ps \cdot nm^{-1}$. As we can see, similarly to OOK, the optimum (minimum) σ_Θ appear for a D_{pre} that can be well approximated as a function of D_{lin} by the laws of [67] (noted as $D_{pre,1}$ in the figure) and [43] (noted as $D_{pre,2}$ in the figure). To be more precise we should note while for OOK transmission eq. (4.5) seemed to be better adapted, in our case (i.e. PSK transmission) it is eq. (4.3) that seems to be better adapted.

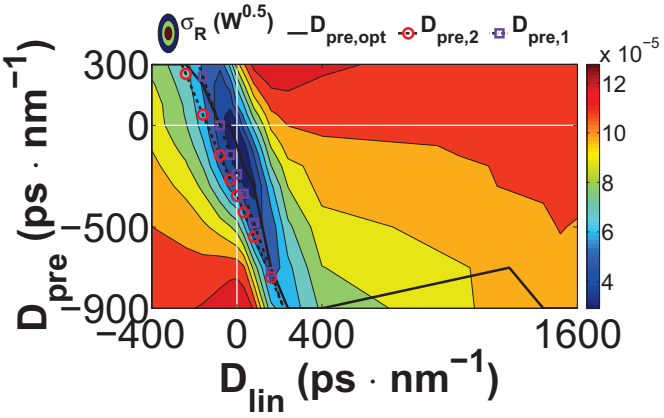

Figure 4.14: σ_R as a function of D_{lin} and D_{pre}. System parameters: $D = 16\ ps \cdot nm^{-1} \cdot km^{-1}$, $P_{in} = 9\ dBm$, $N_s = 6$, $D_{res} = 0\ ps \cdot nm^{-1}$, D_{pre} varying from -900 to $300\ ps \cdot nm^{-1}$ and D_{lin} varying from -400 up to $1600\ ps \cdot nm^{-1}$. With a solid line the true minimum σ_R, with round markers the law of [43] and with square markers the law of [67]. No optical filtering was performed.

The deformation of the amplitude is not supposed to be playing an immediate role in the detection process when it comes for an ideal coherent detection of a PSK signal. Nevertheless, for reasons of comparison we also show the evolution of σ_R as a function of D_{lin} and D_{pre} in figure 4.14. We note that, similarly as before, σ_R appears to be minimized for a value of D_{pre} that can be given as a function of D_{lin} approximately following the laws of [67] and [43], while, once more, the law of [67] seems to be slightly closer to the actual minimum. Furthermore, there do

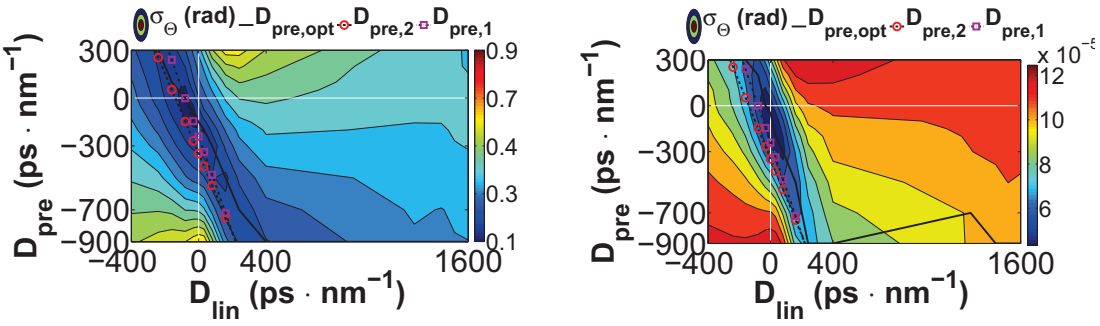

(a) σ_Θ as a function of D_{lin} and D_{pre}.

(b) σ_R as a function of D_{lin} and D_{pre}.

Figure 4.15: σ_Θ and σ_R plotted as a function of D_{lin} and D_{pre}. System parameters: $D = 16\ ps \cdot nm^{-1} \cdot km^{-1}$, $P_{in} = 9\ dBm$, $N_s = 6$, $D_{res} = 0\ ps \cdot nm^{-1}$, D_{pre} varying from -900 to $300\ ps \cdot nm^{-1}$ and D_{lin} varying from -400 up to $1600\ ps \cdot nm^{-1}$. With a solid line the true minimum σ_R, with round markers the law of [43] and with square markers the law of [67]. Optical 2^{nd} order Gaussian filtering was performed before the receiver.

not appear to be any important qualitative differences between the evolution of σ_Θ or σ_R as a function of D_{lin} and D_{pre}.

Including an optical filtering before the receiver does not qualitatively change the conclusions reached above. Indeed, in figures 4.15a and 4.15b we plot σ_Θ and σ_R exactly as before but, considering this time the presence of a realistic optical filter before the receiver. It can be easily noted that one more, the optimum values of σ_Θ and σ_R are reached for regions of D_{pre} and D_{lin} that are sufficiently close to the values indicated by the laws of [43] and [67], while the law of [67] always seems to be slightly closer to the actual minimum. Finally, in both cases of σ_Θ or σ_R, qualitatively similar conclusions can be reached for other dispersion values, combinations of N_s and P_{in} and D_{res}.

Nevertheless, it would be also interesting to see if there is an influence of the receiver type on the optimization of the dispersion management. In the following, we slightly modify the reception scheme from an ideal coherent detection to an ideal differential detection, as described above.

In figure 4.16 we plot σ_Θ for the same configuration parameters as before, when the reception type used is an ideal differential detection. Comparing figure

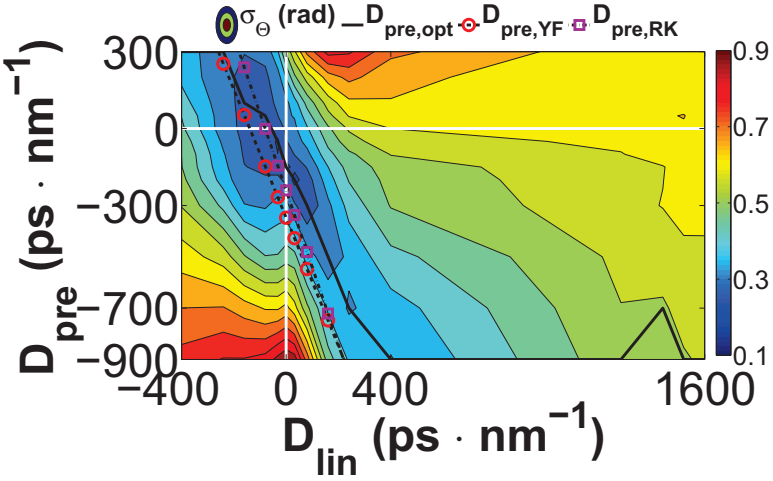

Figure 4.16: σ_Θ for an ideal differentially coherent detection as a function of D_{lin} and D_{pre}. System parameters: $D = 16\ ps \cdot nm^{-1} \cdot km^{-1}$, $P_{in} = 9\ dBm$, $N_s = 6$, $D_{res} = 0\ ps \cdot nm^{-1}$, D_{pre} varying from -900 to $300\ ps \cdot nm^{-1}$ and D_{lin} varying from -400 up to $1600\ ps \cdot nm^{-1}$. With a solid line the true minimum σ_Θ, with round markers the law of [43] and with square markers the law of [67]. No optical filtering was performed.

4.16 against figure 4.13 we can distinguish two basic differences that may be interpreted in the basis of eq. (2.102). First, as expected, the global quality is higher in the case of an ideal coherent detection compared to the case of an ideal differential detection. This may be intuitively understood by the fact that, in the second case, the phase reference upon which we are based to detect the new symbol, already contains some form of "deterministic noise" because of the interplay GVD/nonlinearities and the new "symbol" calculated from eq. (2.102) will be based on the contributions of two noisy samples instead of one. Secondly, although the global form of the two figures is very similar, we can distinguish a small difference for parameter regions with D_{pre} close to 0 ps/nm and D_{lin} close to 0 ps/nm. More precisely, for the aforementioned parameter region we observe a slightly higher tolerance to D_{lin} in the differentially-coherent case compared to the coherent case, near the region of D_{lin} that minimizes σ_Θ. In order to illustrate this effect, in figure 4.17 we isolate just a projection of figures 4.16 and 4.13 for $D_{pre} = -150\ ps/nm$. We can indeed note that in the region around

$D_{lin} = 0\ ps/nm$, the difference in terms of σ_Θ between the two detection types becomes slightly higher than for other values of D_{lin}.

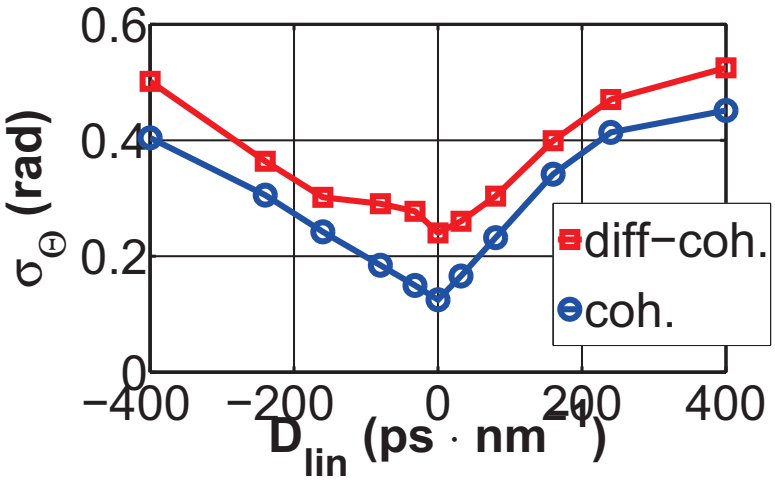

Figure 4.17: σ_Θ for an ideal coherent detection (round and blue markers) and an ideal differentially-coherent detection (square and red markers) as a function of D_{lin} for $D_{pre} = -150\ ps/nm$. System parameters: $D = 16\ ps \cdot nm^{-1} \cdot km^{-1}$, $P_{in} = 9\ dBm$, $N_s = 6$, $D_{res} = 0\ ps \cdot nm^{-1}$ and D_{lin} varying from -400 up to $400\ ps \cdot nm^{-1}$.

An intuitive explanation of the above result, is based on the fact that for a low value of D_{lin} the signal memory is low. In this case, the deterministic noise of successive symbols may be *correlated* in some way and this may lead to a reduced phase difference between two successive symbols. Similar hints about the fact that differential detection schemes appear to outperform in some cases the classic coherent schemes can be found in [32] and [79].

For reasons of completeness, in figure 4.18 we plot σ_R as a function of D_{pre} and D_{lin} for the same configuration as before, after an ideal differential detection. Although the absolute scale of σ_R values in figures 4.18 and 4.14 cannot be directly compared to each other, we may conclude that, once more, the two cases do not present qualitatively important changes.

The relative differences between the (independent) optimization of the signal amplitude and phase for a variable dispersion management motivates us to investigate more on this subject. More precisely, it is interesting to verify if

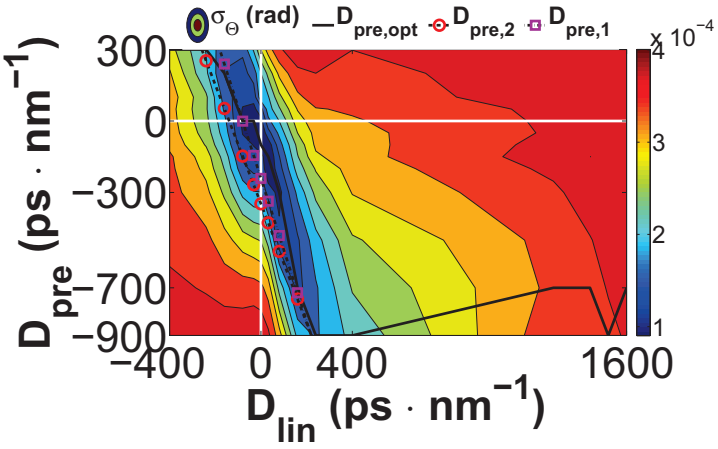

Figure 4.18: σ_R for an ideal differentially coherent detection as a function of D_{lin} and D_{pre}. System parameters: $D = 16\ ps \cdot nm^{-1} \cdot km^{-1}$, $P_{in} = 9\ dBm$, $N_s = 6$, $D_{res} = 0\ ps \cdot nm^{-1}$, D_{pre} varying from -900 to $300\ ps \cdot nm^{-1}$ and D_{lin} varying from -400 up to $1600\ ps \cdot nm^{-1}$. With a solid line the true minimum σ_R, with round markers the law of [43] and with square markers the law of [67]. No optical filtering was performed.

the amplitude and phase vary in the *exact* same way as a function of the DM parameters.

Coming back to an ideal coherent detection scheme, in order to get a better vision on this matter, in figures 4.19a and 4.19b we plot σ_Θ and σ_R against Φ_{NL}, focusing on a configuration with chromatic dispersion $D = 16\ ps/(nm \cdot km)$. In both cases, for each value of Φ_{NL} we retain the dispersion management parameters that optimize either σ_Θ or σ_R. More precisely, in figure 4.19a we plot σ_Θ versus Φ_{NL} optimizing σ_Θ (denoted $\sigma_\Theta(opt\ \sigma_\Theta)$), or optimizing σ_R (denoted $\sigma_\Theta(opt\ \sigma_R)$), while in figure 4.19b, we plot σ_R versus Φ_{NL} optimizing σ_R (denoted $\sigma_R(opt\ \sigma_R)$), or optimizing σ_Θ (denoted $\sigma_R(opt\ \sigma_\Theta)$). Comparing $\sigma_\Theta(opt\ \sigma_\Theta)$ to $\sigma_R(opt\ \sigma_\Theta)$, we see that the dispersion management schemes that optimize σ_Θ do not necessarily optimize σ_R, something that is clearly illustrated by the peaks of $\sigma_R(opt\ \sigma_\Theta)$ in figure 4.19b. Similar intuitions can be reached comparing $\sigma_R(opt\ \sigma_R)$ and $\sigma_\Theta(opt\ \sigma_R)$, certifying that the optimization of the dispersion management is not exactly equivalent for both amplitude and phase.

We have already seen specific examples where constellations could have a com-

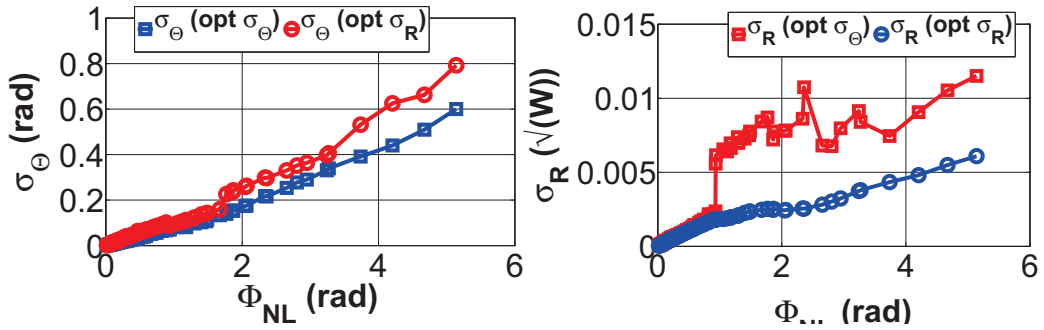

(a) σ_Θ Vs Φ_{NL} for optimized σ_Θ (square(b) σ_R Vs Φ_{NL} for optimized σ_R (round markers), σ_Θ Vs Φ_{NL} for optimized $\sigma_R$markers), σ_R Vs Φ_{NL} for optimized σ_Θ (round markers). (square markers).

Figure 4.19: σ_Θ and σ_R Vs Φ_{NL} for $D = 16\ ps/(nm \cdot km)$ and an optimized dispersion management in terms of D_{pre}, D_{lin} and D_{res}.

pletely different form, following different configurations of dispersion management or fiber type (see figures 4.4b and 4.5a). To get an better insight on the shape of the constellation states we use the quantity Bn, defined in equation (2.72). Bn quantifies the relative spread of the phase quadrature with respect to the spread of the amplitude quadrature and we remind that $Bn = 1$ corresponds exactly to a deformation coming from AWGN that is, therefore, symmetric for the two Cartesian coordinates. However, when $Bn > 1$ the angular spread is higher than the amplitude spread, whereas when $Bn < 1$ the amplitude spread is higher than the angular spread. The parameter A_{est} appearing in eq. (2.72) is calculated as the complex average over the samples of each state, while σ_{est} is calculated as $\sigma_{est} = \frac{\sigma_{IP}+\sigma_Q}{2}$, where the calculation of σ_{IP} and σ_Q is explained in figure 4.7.

In figure 4.20a we plot Bn as a function of D_{lin} and D_{pre}. We note that there appear clearly two regions, one on the left where Bn takes low values and one on the right where Bn takes high values. In figure 4.20b we consider a projection of the previous graph for $D_{pre} = 0\ ps/nm$ and we plot Bn for different values of D_{res} as a function of D_{lin}. This characteristic evolution of Bn as a function of D_{lin} As it is roughly the case for all tested values of D_{res}, Bn takes a value close to 2.5 for very low values of D_{lin}, then its value is reduced, before increasing again, passing from $Bn = 2.5$ for a value of $D_{lin,p} \simeq 0ps/nm$ and

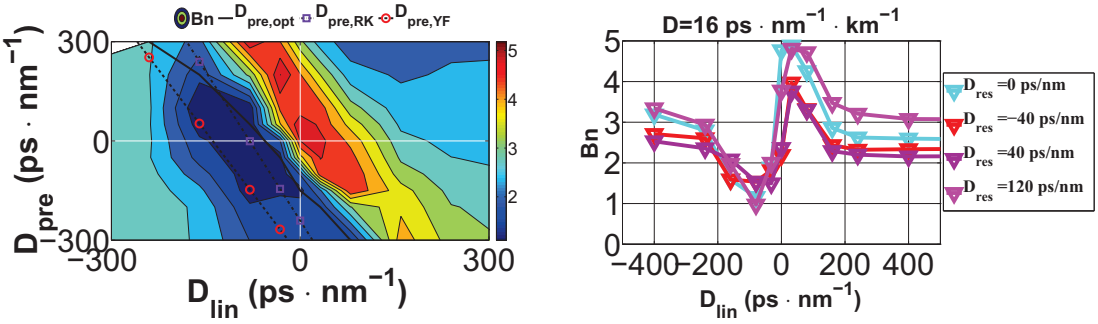

(a) Bn as a function of D_{lin} and D_{pre}.

(b) Bn as a function of D_{lin} for $D_{pre} = 0\ ps/nm$ and some specific values of D_{res}.

Figure 4.20: Bn parameter. System parameters: $D = 16\ ps \cdot nm^{-1} \cdot km^{-1}$, $P_{in} = 9\ dBm$, $N_s = 6$, $D_{res} = 0\ ps{\cdot}nm^{-1}$, D_{pre} varying from -900 to $300\ ps{\cdot}nm^{-1}$ and D_{lin} varying from -400 up to $1600\ ps \cdot nm^{-1}$.

following a symmetric behavior for positive values of D_{lin}. It can be verified that changing D_{pre}, results in a similar evolution of Bn as a function of D_{lin}, with the only difference that $D_{lin,p}$ is moved towards higher different values, once again, approximately following the laws of [43] and [67]. Qualitatively similar conclusions may be reached for all other dispersion values. In section §4.7 we try to analyze in more depth the reasons behind such peculiar constellation shapes.

4.6.2 Global phase shift

From the above sections, a question normally rising is: what does cumulative nonlinear phase (Φ_{NL}) really represent in dispersion managed transmission based on PSK modulation? In other words, does this cumulative phase really exist? Can we extract it from the received signal somehow? As shown in section §4.5, based on the fact that Φ_{NL} can provide a simple quantity used to assess the system performance, can we extract other useful information by measuring this quantity?

A preliminary answer to these questions may be given by noting that, as shown in figure 2.25c, when nonlinear effects act alone, the central samples of each state are being rotated by a quantity that is exactly equal to phase shift $-\Phi_{NL}$, given by the equation (2.141) and using the peak power P_0 for the calculation of Φ_{NL}.

On the other hand, we have also seen that the effect of chromatic dispersion results in a very small negative phase shift for the center of the state as well, calculated by the equation (2.127). However, what is the phase shift when GVD and nonlinearities act together in a dispersion-managed system?

In this section we present numerical simulation results that attempt to answer to this question. More specifically, we observe that received signal constellations exhibit an average optical phase shift θ_{rot}, generally exceeding the nonlinear cumulative phase. Furthermore, we the actual variation of θ_{rot} yields useful indications for the optimization of dispersion-managed system design.

The simulations held in this section were once more based on the generic system configuration of figure 2.39. At the transmitter, a single-channel ($\lambda = 1.55\mu m$) of a symbol rate $R = 21.5\ GBaud$ is generated with QPSK modulation. The emitted complex signal $A(t)$ is based on a 1024-long De Bruijn associate of a quaternary sequence, created from the even and odd bits of a 2047-long PRBS (like the sequence $C_{PRBS2XPrec}$ discussed in section §3.4), considering 64 samples per symbol. The initially emitted QPSK symbols are represented by four ideal complex values s_0, s_2, s_3, s_1 with corresponding phase levels $\{\pi/4, 3\pi/4, -3\pi/4, -\pi/4\}$. The link consists of N_s identical spans of a length $L_s = 100\ km$, a GVD parameter $D = 16\ ps.nm^{-}1 \cdot km^{-}1$ (no GVD slope is assumed), an attenuation coefficient $\alpha = 0.2\ dB/km$, an effective area $A_{eff} = 80\ \mu m^2$, a nonlinear index $n2 = 2.7 \cdot 10^{-20}\ m^2/W$ and a span input average power P_{in}. The variable parameters are shown in figure 2.39 and their variation range is shown in the table of figure 4.21.

Parameter ranges
D_{pre} : {-900 to 300} ps/nm (13 values)
D_{line}: {-25% to 25%} of cumulative dispersion in line fiber (11 values)
D_{res}: {-120 to 120} ps/nm by step of 20 ps/nm
P_{in}={-3 to 9} dBm (7 values)
N_{sp}=[5,10,15]

Figure 4.21: Variable parameter values.

Amplifiers are assumed to be noiseless flat-gain repeaters not taking into in first place so as to focus on GVD/nonlinearity interactions, while amplifiers

adding ASE noise are considered in a second time. As discussed in , exploiting the fact that in numerical simulations we have access to the complex field, we extract only the central sample of each time slot, before the receiver. We then divide the received extracted samples in four groups according to their initial state (s_0, s_1, s_2, s_3) and take the average complex value of each group $(\mu_0, \mu_1, \mu_2, \mu_3)$. We define the average phase shift

$$\theta_{rot} = \langle \arg(\mu_i - s_i) \rangle \, , i = 0, 1, 2, 3 \tag{4.6}$$

We note that as a result of the inherent SSFM process used in our simulations, θ_{rot} includes only the phase shift caused by the interplay of GVD and Kerr effect. In other words, with respect to the expansion of $\beta(\omega)$ (eq. (2.112)), θ_{rot} does not include any possible influence of the term β_0 (which is neglected) or β_1 (which is absorbed in eq. (2.142)). Finally, in order to perform a usual transmission quality estimation, the receiver incorporates a differential detection scheme as described in section §2.2.3.3, considering an optical filter of 2^{nd} order Gaussian shape with $3-dB$ bandwidth of 0.3 nm and balanced photo-diodes, assuming an electrical Bessel 5^{th} order electrical filter with a bandwidth of $0.7R\ GHz$. The system BER is first evaluated using a Monte-Carlo method assuming a 13 dB constant OSNR (in 0.1 nm) in front of the receiver and is then converted to an equivalent $Q^2(dB)$.

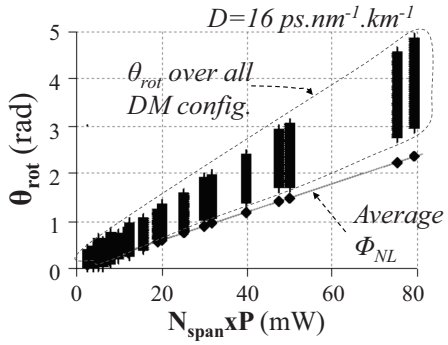

Figure 4.22: θ_{rot} as a function of the product (input power)X(number of spans) or $(P_{in} \cdot N_s)$.

In fig. 4.22, θ_{rot} is plotted for each product $P_{in} \cdot N_s$, while varying the dispersion management parameters according to fig. 4.21 (about 1900 different config-

urations). We can first observe that for the same value of the product $N \cdot P_{in}$, 1900 different values of θ_{rot} are spread vertically depending on the different DM configurations used. Furthermore, we add a straight line that corresponds to the cumulative average nonlinear phase Φ_{NL} due to SPM (given by eq. (2.141)) for each value of $N \cdot P_{in}$.

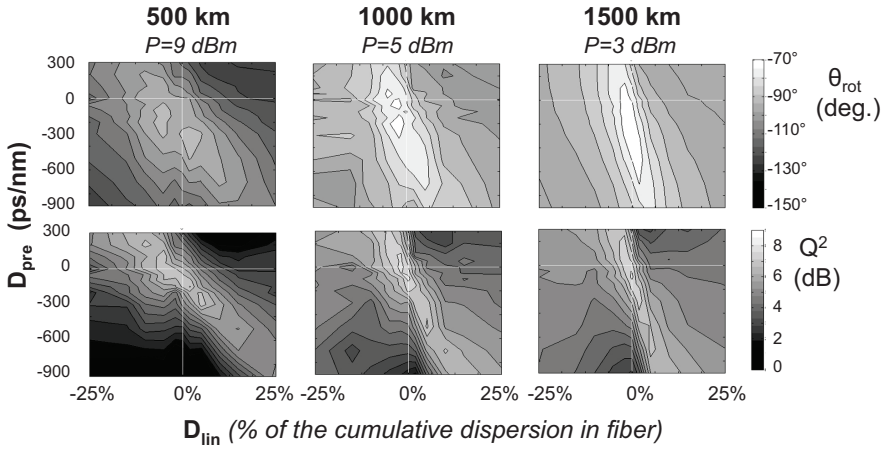

Figure 4.23: Comparison between the variations of θ_{rot} (top) and Q^2 (bottom) as a function of the dispersion management for a line fiber with $D = 16\ ps{\cdot}nm^{-1}{\cdot}km^{-1}$ and three cases of input span power and distance yielding a Φ_{NL} of about 1 *rad*.

As discussed in section §4.5, the best achievable transmission quality while optimizing DM is following a unique curve as a function of Φ_{NL} (for given fiber GVD, modulation rate and modulation format). We note from fig. 4.22 that θ_{rot} appears to strongly depend on dispersion management. In order to distinguish between configurations having the same Φ_{NL}, in fig.4.23 on the top we plot θ_{rot} as a function of D_{pre} and D_{lin}, while at the bottom we show the corresponding Q^2 obtained after differential detection. Results are presented for three different configurations of cumulative Φ_{NL} values of about 1 *rad* and couples of launch power, distance $(P_{in}(dbm), N_s \cdot L_s(km)) : (9, 500)$, $(5, 1000)$ and $(3, 1500)$. We note that while the dependency of Q^2 on the DM parameters is well-known[22],[43], a similar dependency is observed for θ_{rot} as well. Consequently, we may conclude that an optimization of the dispersion management in terms of Q^2 can also roughly induce a minimization of the difference $\theta_{rot} - \Phi_{NL}$.

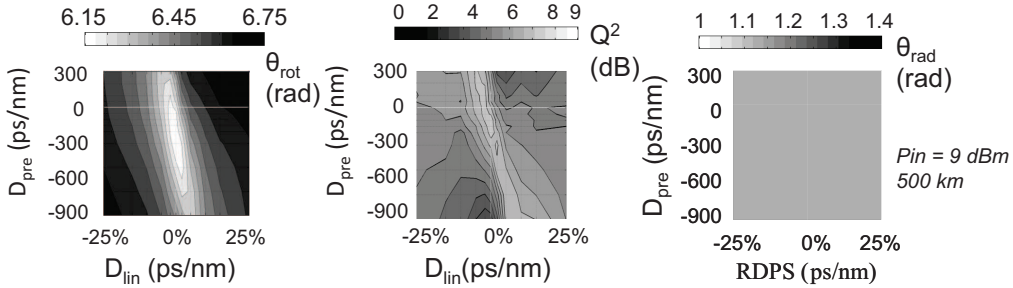

(a) θ_{rot} versus DM with noisy amplifiers.

(b) Q^2 versus DM with noisy amplifiers.

(c) Continuous wave.

Figure 4.24: Complementary investigations around θ_{rot} for $(P_{in}(dbm), N_s \cdot L_s(km)) = (3, 1500)$.

However, a series of questions rise. Is a variation of θ_{rot} observed in the same way for configurations with in-line noise? Is a variation of θ_{rot} as a function of the DM parameters observed also observed for the propagation of a CW? And finally, is θ_{rot} physically linked to the phase shift linked to a peak power or to an average power, as the notion of Φ_{NL} discussed in section §4.5? In order to address these questions and complete our analysis we perform three additional sets of simulation runs: one considering the same configuration as before but with the EDFAs adding in-line noise this time, a second where we assume the propagation of a continuous wave (CW) and a third where we assume a propagation of an RZ-QPSK signal under noiseless conditions with the same *average* power as the NRZ-QPSK tested before (but obviously with a higher peak power).

Concerning the simulation set with in-line noise, in figures 4.24a and 4.24b we reproduce the set of figure 4.23 with $P = 3\ dBm$ and $N_s \cdot L_s = 1500\ km$, while assuming noisy in-line amplifiers with realistic noise figures (NF) of 6 dB. This new scheme yields an OSNR of 23 dB at the end of the link that we complete with additional noise at the last amplifier in order to measure a BER in the same conditions of total $OSNR = 13\ dB$, as in the previous scheme without in-line noise. Commenting on figures 4.24a and 4.24b, we can see that θ_{rot} is globally shifted towards higher values and Q^2 towards lower values for all DM cases in comparison to the noiseless case, nevertheless preserving the relative differences in terms of both θ_{rot} and Q^2 between different DM configurations. Thus the

previous observation is still valid in the context of a transmission taking into consideration a realistic addition of noise by the in-line amplifiers.

Concerning the second set, we have propagated only CW signals (without in-line ASE noise) for a transmission of 500 km of fiber with 9 dBm input power. Fig. 4.24c shows the results in terms of θ_{rot} as a function of DM parameters as similarly presented in fig. 4.23. We note that θ_{rot} does not depend on the dispersion management parameters for a CW and its unique value for this set of simulations corresponds, as expected, to $\Phi_{NL} = 1.168\ rad$. This observation confirms that the difference between θ_{rot} and Φ_{NL} is actually introduced by the interplay of GVD and nonlinearities on modulated signals.

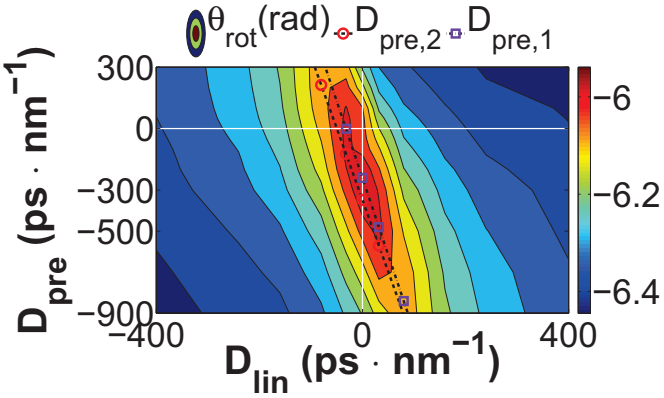

Figure 4.25: Global phase shift θ_{rot} as a function of the dispersion management for a line fiber with $D = 16\ ps \cdot nm^{-1} \cdot km^{-1}$ and $(P_{in}(dbm), N_s \cdot L_s(km)) = (3, 1500)$.

Finally, for our third test, in figure 4.25, we plot θ_{rot} as a function of the DM parameters, for the same set of parameters as before but using an RZ-QPSK modulation this time. First, we observe that the same type of dependence of θ_{rot} as a function of the DM parameters can be confirmed (as in 4.23 for NRZ-QPSK). Furthermore, by observing that the absolute values of the angle θ_{rot} are considerably higher than in the NRZ-QPSK case, we can note that, indeed, θ_{rot} appears to be linked to the peak power and not the average power of the signal.

Coming back to NRZ-QPSK signals without the addition of in-line noise, fig. 4.26a presents the transmission quality in terms of Q^2 as a function of θ_{rot} for the 1900 DM configurations of figure 4.21, previously used for fig. 4.22, but only for a 1500 km-long link and an input span power of 3 dBm. From fig. 4.26a we

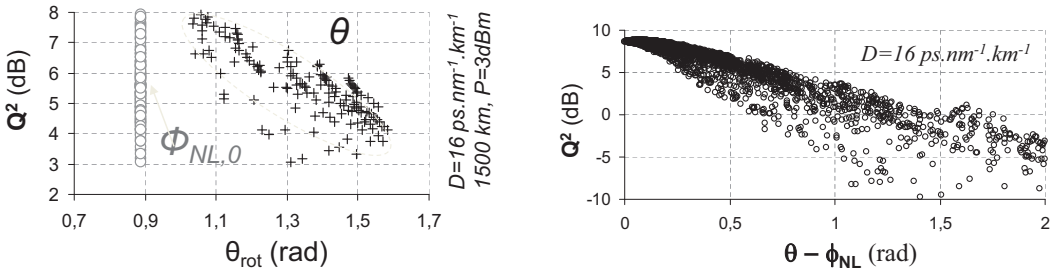

(a) Q^2 versus θ_{rot}.

(b) Q^2 versus $\theta_{rot} - \Phi_{NL}$.

Figure 4.26: Relation between Q^2 and Φ_{NL}.

note that while the transmission quality decreases from $Q^2 = 8\ dB$ to $3\ dB$, θ_{rot} correspondingly increases from about 1 to 1.6 rad, depending on the DM used. As a result, we may roughly assume that the higher the θ_{rot} of the link, the poorer the transmission quality is. On the contrary, the cumulative nonlinear phase for all these DM configurations is constant (noted $\Phi_{NL,0}$) and equal to about 0.9 rad as indicated by the round grey markers in fig. 4.26a. Thus, only the knowledge of the value of Φ_{NL} does not give any information on the optimization of the dispersion management, whereas the relative difference between θ_{rot} and Φ_{NL} may do. In effect, if dispersion management is approximately optimized, $\theta_{rot} - \Phi_{NL,0}$ is minimized. As an intuitive insight, we suggest that $\theta_{rot} - \Phi_{NL,0}$ may physically originate from a conversion by dispersion of intensity fluctuations that may be minimized following a similar procedure as in [43].

Finally, fig. 4.26b gathers the results of transmission quality as a function of $\theta_{rot} - \Phi_{NL,0}$ for all the DM configurations, all input span powers ($-3\ dBm$ to $9\ dBm$), distances (500 to 1500 km) and optimal residual dispersions. It appears that for all simulated systems in our investigation, Q^2 globally decreases while $\theta_{rot} - \Phi_{NL,0}$ increases. In conclusion, whereas, the transmission quality in terms of Q^2 is not a bi-univocal function of θ_{rot}, we may still note that best qualities are reached when the difference $\theta_{rot} - \Phi_{NL,0}$ is minimized.

Nevertheless, we should underline that θ_{rot} is obtained in the context of Split-Step Fourier simulations and its experimental estimation is still an open problem. In effect, even using a coherent detection scheme as described in [66], the receiver only estimates the phase difference between successive symbols and thus the ab-

solute value of the signal phase is not retrieved. However, even if θ_{rot} cannot be claimed to assess the absolute quality of a transmission like the BER, it remains a physical quantity that may be given by a single straight forward calculation compared to the more time consuming Monte-Carlo BER estimation. Consequently, calculating θ_{rot} and comparing it against Φ_{NL} (that can be found analytically), one may easily conclude on the efficiency of a specific dispersion management scheme.

4.7 The constellation shape based on the data sequences carried by the signal

4.7.1 Pattern-dependent nonlinear degradation

In the previous sections we have shown that different dispersion management schemes yield different constellation and PDF shapes, while it is clear that these different shapes step from the different form of interplay between chromatic dispersion and fiber nonlinearities, as dispersion management creates different conditions of interaction between different pulses. In this section we move one step forward, splitting the incoming data sequence into small-length subsequences and presenting the transmission results as a function of these subsequences. But before presenting the results we need to introduce the notion of *equivalent subsequences*.

In figure 4.27a we show an initially transmitted QPSK constellation with the correspondence of symbols to phase levels, i.e. the symbol "0" is represented by the phase level $\frac{\pi}{4}$, the symbol "2" is represented by the phase level $\frac{3\pi}{4}$ etc. In figure 4.27b we classify the received samples, with respect to the data initially carried by its m preceding and m following neighboring symbols. In this way, for each state we form 4^{2m} neighbor-pattern groups G_i, each corresponding to a distinct subsequence of $2m+1$ symbols. As our numerical simulations were based on a *PRQS* data stream, the four states are equivalent with respect to the transmission impairments[90]. This implies an equivalence between the groups G_i of each state. For example, the subsequence [031] is assumed to be *equivalent* to the subsequence [302] (G_{15} on the table of 4.27b).

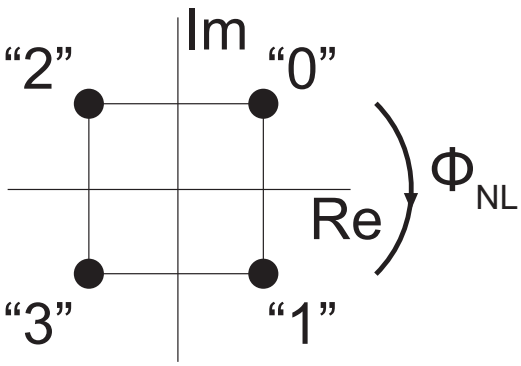

(a) Initial QPSK constellation

	0	1	2	3
G_1	000	111	222	333
G_2	001	113	220	332
...				
G_{15}	302	210	123	031
G_{16}	303	212	121	030

(b) Table of equivalent subsequences

a characteristic

Figure 4.27: Notion of equivalent subsequences demonstrated on an initial QPSK constellation.

Furthermore, we define the parameter ssf (for "subsequence spread factor") in order to quantify the pattern-dependency of transmission impairments.

$$ssf = \frac{\sqrt{\frac{1}{N_G}\sum_{i=1}^{N_G}|\mu_i - \mu|^2}}{\frac{1}{N_G}\sum_{i=1}^{N_G}\sigma_i} \tag{4.7}$$

with μ_i and $\sigma_i, i = 1, ..4^{2m}$ being the complex averages and standard deviations of the N_{sp} complex samples belonging to the group G_i, N_G being the number of groups and μ the complex average calculated over μ_i. For example, for a 4096-long sequence and $m = 1$, there are $N_G = 16$ groups of equivalent subsequences and 64 samples per group for each state.

In figure 4.28b we show a constellation example obtained for a transmission of 6 spans over a fiber with $D = 16\ ps \cdot nm^{-1} \cdot km^{-1}$, $Pin = 9\ dBm$ and DM parameters $Dpre = -300\ ps \cdot nm^{-1}$, $D_{res} = 0\ ps \cdot nm^{-1}$ and $D_{lin} = 32\ ps \cdot nm^{-1}$ (close to full dispersion compensation), while in figure 4.28c we zoom in one of the four equivalent QPSK states. In all cases, having an exact knowledge of the initially transmitted sequence, we use a different marker to signify the different subsequence groups G_i (see 4.28a). Commenting on figure 4.28c we observe that

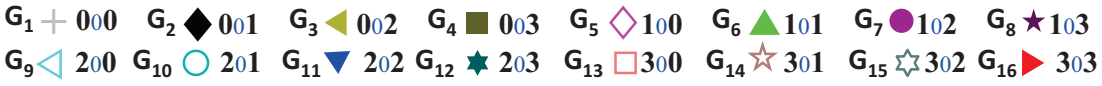

(a) Legend of markers for each subsequence

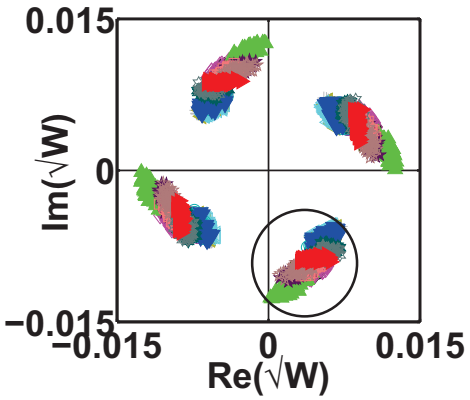

(b) NRZ-QPSK constellation

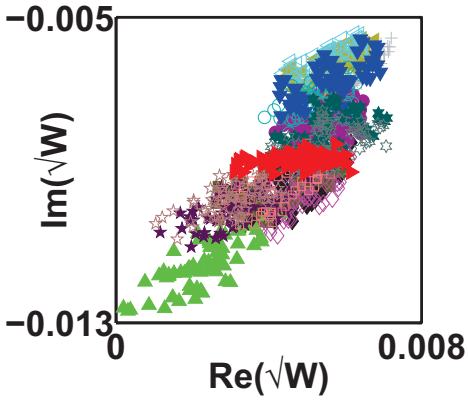

(c) Isolating an NRZ-QPSK symbol

Figure 4.28: Transmission parameters: $D = 16\ ps \cdot nm^{-1} \cdot km^{-1}$, $Pin = 9\ dBm$, $D_{pre} = -300\ ps \cdot nm^{-1}$, $D_{res} = 0\ ps \cdot nm^{-1}$, $D_{lin} = 32\ ps \cdot nm^{-1} \cdot km^{-1}$. For each group of equivalent subsequences we use the markers and colors of figure 4.28a.

samples belonging to different neighbor-pattern groups form "packets" that can be visually distinguished from one another on the complex plane. For instance, all samples belonging to the group G_6 (101) are situated at the low left corner of the constellation and they are practically not interfering with any other group of samples.

On the other hand, in figure 4.29a we show the constellation for a transmission with parameters, similar as before, with the exception of the in-line residual dispersion that this time was fixed at $D_{lin} = 1600\ ps \cdot nm^{-1}$ (no dispersion compensation). Zooming in one state (figure 4.29b), we notice that this constellation is more "Gaussian-like" and samples from different neighbor-pattern groups severely overlap. Results confirming that a "Gaussian-like" overall constellation results in the case of uncompensated links have also been reported in [26].

From the above observations, it becomes clear that pattern-dependent degradation strongly relies of the considered dispersion map.

To generalize the above observations we use the parameter ssf, given by equation (4.7). In figure 4.30a we show the full variation of ssf as a function

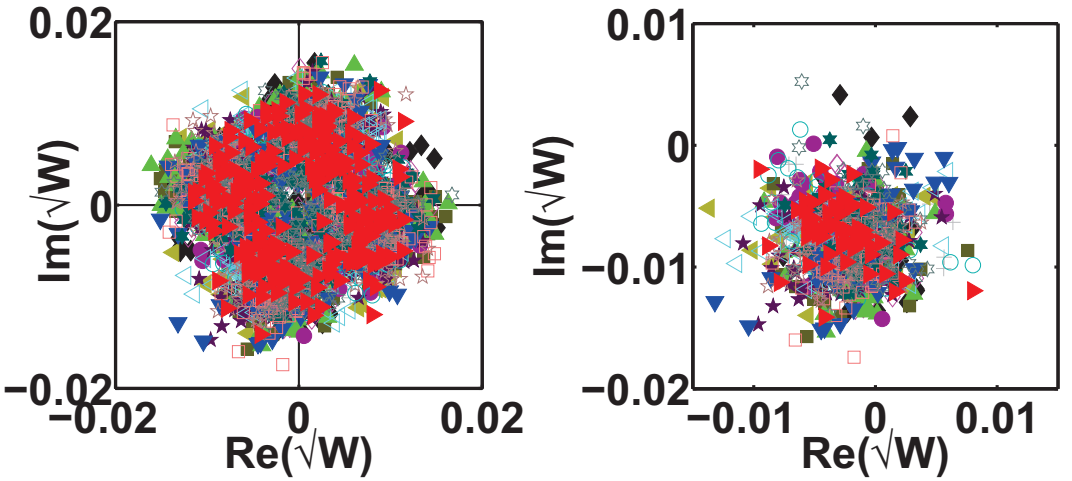

(a) QPSK constellation (b) One QPSK state

Figure 4.29: Transmission with parameters: $D = 16\ ps \cdot nm^{-1} \cdot km^{-1}$, $Pin = 9\ dBm$, $D_{pre} = -300\ ps \cdot nm^{-1}$, $D_{res} = 0\ ps \cdot nm^{-1}$, $D_{lin} = 1600\ ps \cdot nm^{-1} \cdot km^{-1}$.

of different values of D_{pre} and D_{lin} for a system with $D = 16\ ps \cdot nm^{-1} \cdot km^{-1}$, $Pin = 9\ dBm$ and $N_s = 6$, while we also plot in the same figure the laws of [67] and [43]. Commenting on figure 4.30a we first note that ssf is maximal for a range of DM parameters close to full in-line dispersion compensation. This is due to the fact that when the in-line residual dispersion is small, the memory[98] of the system is generally low and each symbol interferes with just a few of its neighbors, thus revealing a particular degradation depending on the data carried by the neighbors. On the contrary, when D_{lin} increases, each symbol interferes with a great number of neighboring symbols which results in an averaging of the degradation caused by each neighbor. The dashed line with squares corresponds to the empirical law of [67], given by the equation (4.3), that roughly fits the numerical results. Moreover, for values of D_{pre} and D_{lin} that follow the straight line law of [67] ssf maximized, confirming the above-mentioned suggestion. Qualitatively similar results are obtained for other power levels or number of spans.

In figure 4.30b we plot ssf in dB scale versus the residual dispersion per span for a system with $Pin = 9\ dBm$ and $N_s = 6$ for three different fiber chromatic dispersion parameter values (4, 8 and 16 $ps \cdot nm^{-1} \cdot km^{-1}$) and adapted values of pre-compensation (indicated on figure 4.30b). We note that the previous

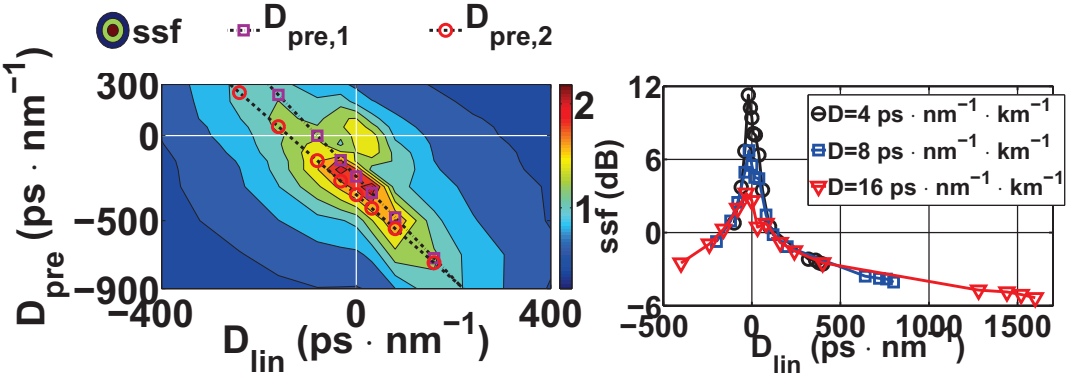

(a) ssf as a function of D_{lin} and D_{pre}, for D_{res} = 0 ps/nm

(b) ssf as a function of D_{lin} for different fiber types and adapted D_{pre}

Figure 4.30: ssf parameter as a function of D_{lin} and D_{pre}

observation stating that ssf exhibits high values for configurations with D_{lin} close to 0 $ps \cdot nm^{-1}$ (full dispersion compensation) can be generalized for all values of fiber dispersion and furthermore, ssf is higher as fiber dispersion decreases.

In configurations with a high ssf, we estimate that the benefit from algorithms mitigating pattern-dependent impairments, as the one shown in [25] will be maximal. On the contrary, this kind of algorithms may not provide an efficient gain for lines with DM configurations where dispersion is not compensated after each span. However, we should note that the above conclusions that correspond to low D_{lin} values may be altered in WDM configurations by the nonlinear inter-channel interactions that depend on the data of the channels. The exact quantification of this added deterioration in comparison to the benefit from an adapted algorithm remains to discover.

4.7.2 Most degraded subsequences

In the previous section, we have discussed the dependence of signal nonlinear degradation upon the data patterns carried by the optical signal. More precisely we have shown that the received signal constellations greatly vary as a function of the different dispersion management configurations and we have concluded that this interaction leaves a “distinct signature” in cases where the memory of the system is low and each symbol interacts with a limited number of neighboring,

in time, symbols. Based on the previous, a question is normally rising: which particular subsequences are mostly degraded by the transmission in the context of dispersion-managed QPSK systems? In other words, which are the subsequence patterns that mainly determine the bit error probability[1]?

In systems based on OOK modulation, in an effort to determine the physical mechanisms producing the errors, intra-channel nonlinear effects were classified[35] (i.e. i-XPM or i-FWM), and notions like the "ghost pulse" were introduced[1] in order to provide a visual representation of the reason behind the bit error probability degradation. For example, in the last case, it was very often found that the eye closure was caused by the energy increase of the "0" pulses and thus, subsequences with a zero between several "1"s was most likely to yield an error. In the context of QPSK modulation though, instead of energy pulses, the information is coded by phase levels and errors are produced when the phase of pulses is distorted in such a way that it is finally mistaken for the phase level of a different state.

In this section we are interested in identifying the subsequences leading to an increased symbol phase variance and consequently degrading the transmission quality in the context of QPSK transmission systems. Our numerical results indicate that these sequences severely depend on the applied DM scheme. Based on the observations we also propose a preliminary, data-sensitive phase-correction procedure that tends to reduce this phase variance overhead.

In figure 4.31a we plot the received constellation of one state after a transmission with parameters $D = 16\ ps \cdot nm^{-1} \cdot km^{-1}$, $Pin = 9\ dBm$, $D_{lin} = 80\ ps \cdot nm^{-1} \cdot km^{-1}$, $D_{res} = 0\ ps \cdot nm^{-1}$, and $D_{pre} = -500\ ps \cdot nm^{-1}$. Once more, the different markers represent the fact that each complex sample belongs to a different group according to its time-neighbors, according to figure 4.28a. The complex average of all the state samples (therefore with all groups included) is noted by μ, whereas the complex average for each group G_i is denoted by μ_i. Furthermore, we also use the phase difference

$$\Delta\varphi_i = \arg(\mu_i) - \arg(\mu) \tag{4.8}$$

[1]In the context of OOK modulation, these subsequences were often "accused of" *closing the eye diagram.*

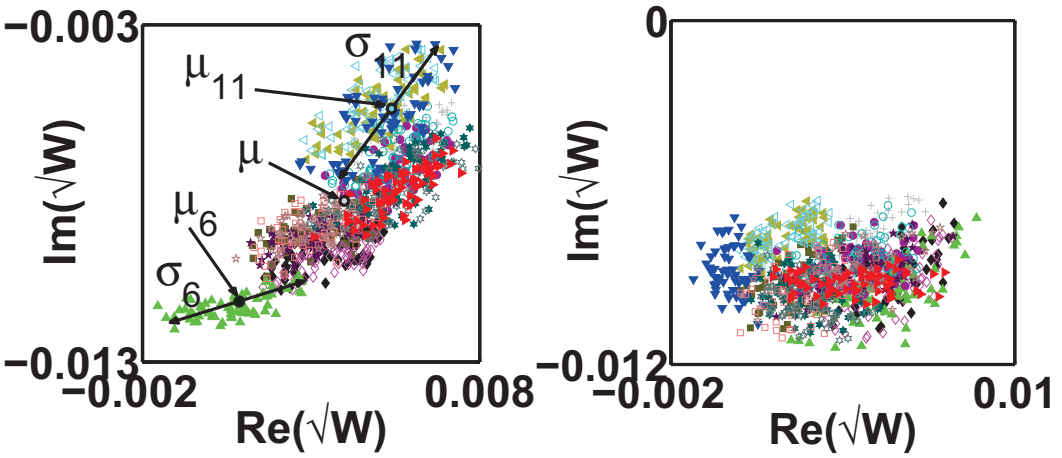

(a) $D_{pre} = -500\ ps \cdot nm^{-1}$ (b) $D_{pre} = -200\ ps \cdot nm^{-1}$

Figure 4.31: Constellations for a transmission with parameters: $D = 16\ ps{\cdot}nm^{-1}{\cdot}\ km^{-1}$, $Pin = 9\ dBm$, $N_s = 6$, $D_{lin} = 80\ ps \cdot nm^{-1} \cdot km^{-1}$, $D_{res} = 0\ ps \cdot nm^{-1}$ and variable D_{pre}. For each group i indicated by a different marker and color (see figure 4.28a), we illustrate the complex average μ_i and the angular standard deviation $\sigma_i(rad)$.

as an indicator of the fact that samples associated with a group G_i are more prone to yielding an error since the more a sample is far away from the state average, the highest the probability of it being detected erroneously. Finally, we use the phase standard deviation σ_Θ defined in section §4.1 over the samples of the group G_i, denoted σ_i.

Noting that the nonlinear phase due to Kerr effect (Φ_{NL}) increases in a clockwise manner (see figure 4.27a) we point out that in figure 4.31a the group G_6 has accumulated in average the highest Φ_{NL}, while the group G_{11} has accumulated one of the lowest Φ_{NL}. Equivalently, we may state that $\Delta\phi_6 < 0$ and $\Delta\phi_{11} > 0$. In other words, if the initially transmitted symbol "0" is surrounded by two "1"s or two "2"s (in what follows we refer to "2" and "1" as the "quadrature" neighbors of "0"), it appears to accumulate the highest or the lowest nonlinear phase respectively. On the other hand, in figure 4.31b we show an example of received constellation with the same DM parameters as before, except from the pre-compensation value which is changed to $D_{pre} = -200\ ps \cdot nm^{-}1$. It appears

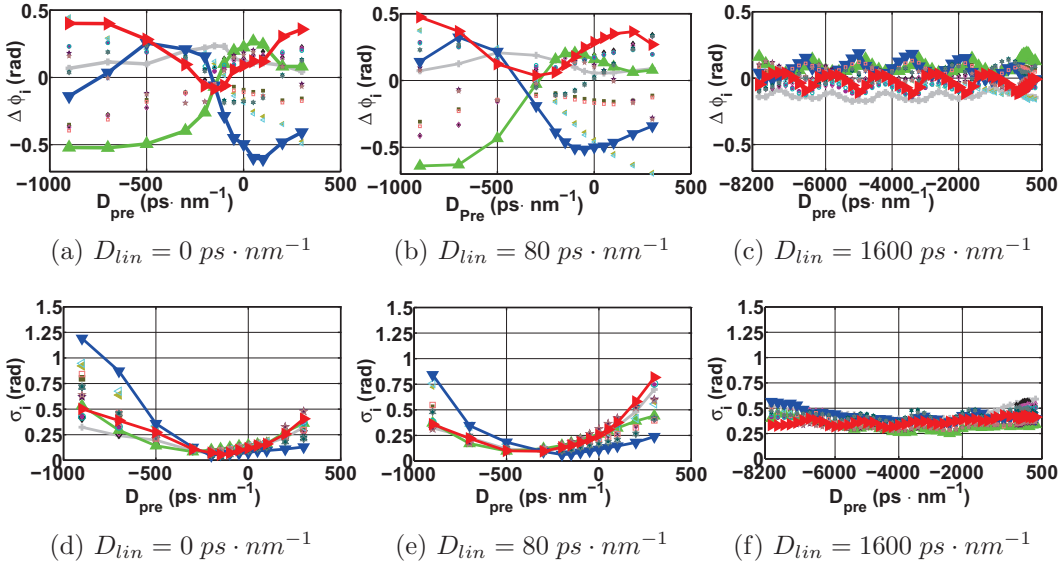

(a) $D_{lin} = 0\ ps \cdot nm^{-1}$ (b) $D_{lin} = 80\ ps \cdot nm^{-1}$ (c) $D_{lin} = 1600\ ps \cdot nm^{-1}$

(d) $D_{lin} = 0\ ps \cdot nm^{-1}$ (e) $D_{lin} = 80\ ps \cdot nm^{-1}$ (f) $D_{lin} = 1600\ ps \cdot nm^{-1}$

Figure 4.32: $\Delta\varphi_i$ and σ_i as a function of D_{pre} for some characteristic values of D_{lin}. The markers and colors used for each group of equivalent subsequences is shown in figure 4.28a.

that this change not only influences on the overall constellation shape but it has also reversed the relative position of the groups G_{11} and G_6 (i.e. $\Delta\phi_6 > 0$ and $\Delta\phi_{11} < 0$ in this case) and changed their standard deviations σ_{11} and σ_6.

Generalizing the above observations, in figure 4.32 we plot $\Delta\varphi_i$ and σ_i as a function of D_{pre} for some typical values of D_{lin} including full, partial or no in-line dispersion compensation. While the samples from all 16 groups are included in the graphs, solid lines are drawn only for the groups of symmetric neighbors, i.e. the groups G_1 (00), G_6 (11), G_{11} (22) and G_{16} (33).

Commenting on figure 4.32a and focusing, for example, on $\Delta\varphi_6$, we verify that while increasing D_{pre}, $\Delta\varphi_6$ is initially negative, then it vanishes and finally it becomes positive, with $\Delta\varphi_{11}$ roughly following the inverse evolution. Furthermore, $\Delta\varphi_{16}$ initially decreases, passes from a minimum value and then increases again, while finally $\Delta\varphi_1$ (corresponding to the group of the subsequence (000), that is the subsequence closest to a continuous wave) experiences less variation with respect to D_{pre}. In 4.32b we can also note that for a specific value of D_{pre}, referred to as $D_{pre,X}$, almost all the group averages meet. Now, if we change

D_{lin} from 0 to 80 $ps \cdot nm^{-1}$ (figure 4.32b), the $\Delta\varphi_i$ curves globally exhibit a similar behavior, except from a change in the value of $D_{pre,X}$ from about -150 to -300 ps/nm. The evolution of $D_{pre,X}$ as a function of D_{lin} may be approximated by the law of [67], a law based on the reduction of intra-channel nonlinearity for OOK systems. If we continue to increase the D_{lin} until 1600 ps/nm (no in-line DCFs), we note in figure 4.32c that all $\Delta\varphi_i$ oscillate around 0 rad as samples belonging to different groups are superposed, an observation also mentioned in [92]. Finally, we emphasize on the fact that the groups G_1 (00), G_6 (11), G_{11} (22) and G_{16} (33), i.e. the groups where the neighbors around the central symbol are the same, always yield the highest and lowest values of $\Delta\varphi_i$. From our full set of results it can be confirmed that the above observation remains valid for a range of D_{pre} and D_{lin}, about ± 200 ps/nm around the values indicated by the law of [67].

Regarding the variation of standard deviations σ_i for $D_{lin} = 0$ $ps \cdot nm^{-1}$ (see figure 4.32d) we note that they all follow roughly the same evolution as a function of D_{pre}, exhibiting a minimum value for $D_{pre} = D_{pre,X}$, nevertheless noting that when $D_{pre} < D_{pre,X}$, $\sigma_{11} > \sigma_6$ and $\sigma_{11} < \sigma_6$ for $D_{pre} > D_{pre,X}$. A similar evolution can be observed for $D_{lin} = 80$ $ps \cdot nm^{-1}$ (figure 4.32e) while for $D_{lin} = 1600$ $ps \cdot nm^{-1}$ (figure 4.32f) σ_i are globally higher than in the case with in-line DCFs, passing however, from a minimum value $D_{pre} \simeq -4500$ ps/nm, also following the law of [67].

The increase of σ_i far from $D_{pre,X}$ stems from the influence of neighbors of a higher order (or an increase in the memory of the channel[98]). In order to visualize this influence, in figure 4.33 we consider the configuration of figure 4.31a but this time we focus just on the groups G_6 (11) and G_{11} (22). Zooming in each of these groups, we use the markers of figure 4.28a to distinguish samples within the group G_i, with different pairs of second-order neighbors this time, belonging to groups denoted as $G_{i,j}$. For the example of figure 4.33, within the groups $G_6 = G_{6,j}$ and $G_{11} = G_{11,j}$ j indicates the pair of second-order neighbors and the markers initially used for the group G_6 are also used for the sub-groups $G_{11,6}$ and $G_{6,6}$. As it can be shown in figure 4.33, inside the group G_{11} the groups $G_{11,1}$ and $G_{11,11}$ appear to be the least de-phased while the groups $G_{11,6}$ and $G_{11,16}$ appear to be the most de-phased. Consequently, qualitatively similar conclusions reached

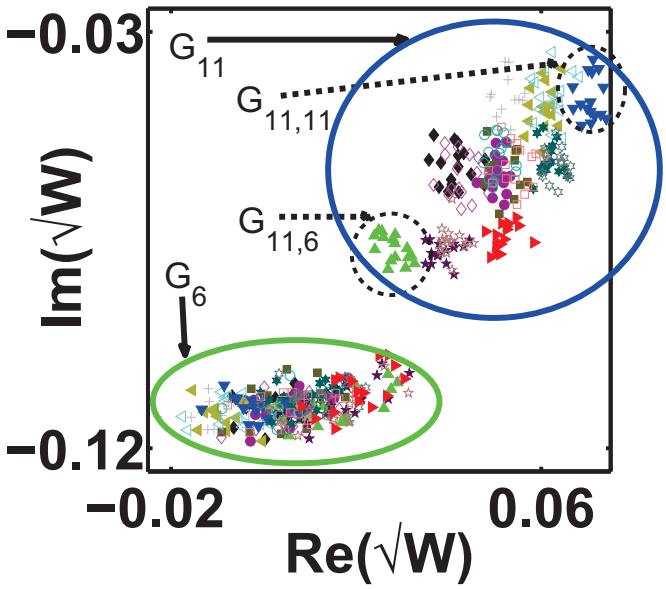

Figure 4.33: Effect of second neighbors. The markers for groups $G_{i,j}$ are the same at the markers for the groups G_i shown in figure 4.28a.

for the $\Delta\varphi_i$ of a state, remain valid for the $\Delta\varphi_{i,j}$ of the sub-group $G_{i,j}$. The above results lead to the generalized conclusion that symmetric neighbors of any order lead to increased absolute values of $\Delta\varphi_i$. We suggest that this may be the result of constructive or destructive interferences of the optical waves when the neighboring symbols have the same phase.

4.8 Conclusion

The purpose of this chapter was to numerically investigate the physical mechanisms behind signal degradation in the context of single-channel/single polarization optical QPSK transmission with variable dispersion management and coherent detection. In all cases, the received signal constellations are analyzed through the standard deviations of their phase and amplitude components, after a simplified (or idealized) coherent detection, with or without the presence of a realistic optical filter.

First, examples of degraded constellations are presented, pointing out three characteristic forms: constellations where the amplitude component is more de-

graded than the phase component, constellations where the phase component is more degraded than the amplitude component and symmetric constellations, similar to ones produced for systems impacted exclusively by white noise.

Using the statistical tools described above, we further investigated the validity of laws (or rules of thumb), developed and successfully used in the context of OOK modulation. The first such criterion used was the criterion of cumulative nonlinear phase that was found to be qualitatively valid in the context of phase modulation as well. Furthermore, some criteria for the optimization of the dispersion management were also investigated, with the analysis revealing that there are not qualitative differences between OOK and QPSK either. Furthermore, following this analysis, we have also pointed out the usefulness of global phase rotation parameter that may be used for the a posteriori optimization of the dispersion management.

Last, zooming in degraded QPSK constellations, we have attempted to reveal the nature of the pattern-dependent signal degradation for various dispersion management configurations and fiber types, i.e. the degradation with respect to the carried data. We have begun by identifying the dispersion management schemes that yield qualitatively different regimes of pattern-dependent signal degradation and we have introduced a useful parameter that can be exploited in cases where a symbol-by-symbol (or Maximum A Posteriori (MAP)) detection is performed. Furthermore, we have investigated and pointed out the data sequences that are mostly degraded in the context of dispersion-managed QPSK transmission, similarly to notions formerly introduced for OOK modulation.

Chapter 5

Conclusion

The beginning of this work coincided with radical changes in the field of optical communications, such as the revival of coherent detection, coming with the possibility to use complex modulation and/or an adapted digital signal processing at the receiver in an effort to mitigate signal distortions. The main objective of this work was to study the physical effects in a nonlinear transmission, for Quaternary Phase Shift Keying (QPSK) modulated signals, in the context of dispersion managed optical links. Similar investigations have been performed in the past for On-Off Keying (OOK) modulated, non-coherent systems and therefore, revisiting this domain gives the opportunity to elucidate the differences and clarify the motivations of using QPSK modulation.

Since high-level M-ary formats are gradually becoming omnipresent in optical communication systems, our first concern was the investigation of the data patterns that need to be used in numerical simulations, in order to achieve an unbiased description of the optical field degradation. Driven by the need to generate Pseudo-Random Quaternary Sequences (PRQSs) that could be used in numerical simulations of QPSK modulated signals, in chapter §3 we have reviewed the generation process of Pseudo-Random Sequences (PRSs) with $M = p^m$ and p a prime number. Even though we have finally used this process to generate PRQSs, the procedure described in chapter §3 may be used to generate multi-level PRSs or any order that can be used in simulations involving complex modulation, with (or without) polarization division multiplexing, such as 16-Quadrature Amplitude Modulation (QAM), 64-QAM, Polarization-Division Multiplexing (PDM)-QPSK

etc. Furthermore, we have analytically described the most important properties of PRSs and we have provided simple tools that can be used to discriminate non-PRSs, with respect to their "pseudo-random properties". The generation method and properties of PRSs is based on the theory of prime and extended Galois fields. Since this process is not described in a self-consistent way in the existing literature, our aim was to review the aforementioned generation methods and the properties of multi-level PRSs in a systematic way. Finally, we have presented numerical simulation results concerning the performance of QPSK systems, using either PRSs or commonly used non-PRSs, for typical choices of Dispersion Management (DM) schemes. Based on our simulation results we have concluded that the use of PRQSs is critical and highly recommended for a balanced estimation of the system performance, especially in cases where intra-channel nonlinearities are strong.

Having established the importance of the used data sequence, in chapter §4 we have proceeded in a numerical investigation of the intra-channel nonlinearities, in the context of optical links with QPSK-modulated signals and a variable DM. Our main motivation was to understand the underlying physics responsible for the distortion of QPSK signals, compared to the distortion of classical OOK-modulated signals. For this we have adopted a structured view, decoupling the problems of transmission and reception. Furthermore, aligned with this structured view, in the greatest part of our simulation results, the description of the signal distortion is shown by a variation on the statistics of the signal quadratures, rather than a Bit Error Rate (BER).

Concerning the choice of our research axes, our first concern was to verify that laws, such as the laws for the optimization of the dispersion management or the law of the cumulative nonlinear phase, previously developed for OOK-modulated signals, hold in the case of QPSK-modulated signals as well. The basic conclusion of this investigation was that there are no qualitative differences between QPSK and OOK modulation with respect to the aforementioned laws. Nevertheless, we observe that the degradation of the amplitude quadrature is generally not similar to the degradation of the phase quadrature, while the variation of both phase and amplitude statistics, strongly depend on the applied DM scheme. The special constellation shape resulting from this "asymmetric degradation" of the

signal quadratures has also been extensively investigated, having as a reference a signal with a symmetric degradation, i.e. an Additive White Gaussian Noise (AWGN). Finally, we have analyzed the variations on the statistics of the signal quadratures for different DM schemes, based on the observation that the nonlinear degradation of isolated symbols depends on the data being carried by its neighbors (i.e. Inter-Symbol Interference (ISI)). Grouping the received samples with respect to their neighbors and analyzing their statistics, we have also proposed a quantity representing the relative spread of these groups of samples on the complex plane, while we suggest that this quantity may be used as a rough indicator of the possible benefit that a system may have from an adapted Maximum A Posteriori (MAP) correction algorithm, as it has been recently presented by other research teams.

Nevertheless, we need to underline that in practical systems with Wavelength-Division Multiplexing (WDM) and/or PDM, the picture may be qualitatively different due to inter-channel or inter-polarization nonlinearities, as it was recently shown by the work of many research teams. Nevertheless, it would be interesting to analyze the relative contribution of these nonlinearities on the modification of the statistics of the signal quadratures. Finally, an exact quantification of the possible benefit from a MAP algorithm as a function of the dispersion management scheme, remains as well, an inspiring challenge for the future.

Appendix A

Differential encoding and decoding

In this appendix we review a way to formulate the differential encoding and decoding by using a procedure involving z transform notation, as described in [15].

At first, we describe the semi-infinite sequence $(x_n)_{n=0}^{\infty}$ through the power series

$$X(z) \triangleq \sum_{n=0}^{\infty} x_n z^{-n} \tag{A.1}$$

Following this notation, the transmitted phase sequence may be written as

$$\Phi(z) = \varphi_0 + \varphi_1 z^{-1} + \varphi_2 z^{-2} + \cdots \tag{A.2}$$

, while neglecting AWGN or any other source of signal distortion, the receiver phase sequence is given by

$$\begin{aligned} &\Phi(z) + \Theta(z) = \varphi_0 + \theta + (\varphi_1 + \theta) z^{-1} + (\varphi_2 + \theta) z^{-2} + \cdots = \\ &= \varphi_0 + \varphi_1 z^{-1} + \varphi_2 z^{-2} + \cdots + \theta \cdot (1 + z^{-1} + z^{-2} + \cdots) = \\ &= \Phi(z) + \tfrac{\theta}{1 - z^{-1}} \end{aligned} \tag{A.3}$$

It is clear that the term $\frac{\theta}{1-z^{-1}}$ corresponds to the phase ambiguity term. In order to eliminate this term we need to multiply the received sequence by $(1-z^{-1})$, which is achieved by the circuit shown in figure A.1a, called differential decoder. As explained above, in practice, the differential receiver subtracts from the phase of the current received symbol, the phase of the previously received symbol, thus removing the phase ambiguity, except from the instant $k=0$, with the received sequence being now equal to $(1-z^{-1})\,\Phi(z)+\theta$, which shows that the phase ambiguity is removed except from the instant $k=0$ that corresponds to the term θ. However, since the information sequence $\Phi(z)$ is multiplied by $(1-z^{-1})$, in order to recover exactly $\Phi(z)$ at the receiver, we need to multiply the initial sequence before the transmission by $\frac{1}{1-z^{-1}}$, something achieved by the circuit of figure A.1b, called *differential encoder*.

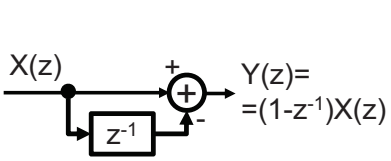

(a) Differential decoder: $Y(z) = X(z) - z^{-1}X(z) = \left(1-z^{-1}\right)\cdot X(z)$

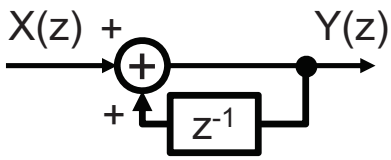

(b) Differential encoder: $X(z) + z^{-1}Y(z) = Y(z) \Leftrightarrow Y(z) = \frac{X(z)}{1-z^{-1}}$

Figure A.1: Differential decoded and differential encoder circuits.

Bibliography

[1] M. J. Ablowitz and T. Hirooka. "Resonant intra-channel four-wave mixing in strongly dispersion-managed transmission systems". In: *Proc. Optical Fiber Communication Conf. and Exhibit OFC 2001*. Vol. 3. 2001.

[2] G. Agrawal. *Nonlinear Fiber Optics*. 3rd. Academic Press, Jan. 2001.

[3] G. Agrawal. *Nonlinear Fiber Optics*. 4th. Academic Press, July 2006.

[4] Govind P. Agrawal. *Fiber-Optic Communication Systems*. 3rd. John Wiley & Sons, Inc., 2002.

[5] Govind P. Agrawal. *Lightwave Technology Telecommunication Systems*. John Wiley & Sons, Inc, 2005, p. 480.

[6] E. Agrell and M. Karlsson. "Power-Efficient Modulation Formats in Coherent Transmission Systems". In: *Journal of Lightwave Technology* 27.22 (2009), pp. 5115–5126.

[7] JD Alanen and D.E. Knuth. "Tables of finite fields". In: *The Indian Journal of Statistics, Series A* 26.4 (1964). Sequences, pp. 305–328.

[8] M. Alfiad et al. "On the Tolerance of 111-Gb/s POLMUX-RZ-DQPSK to Nonlinear Transmission Effects". In: *IEEE/OSA Journal of Lightwave Technology* 29.2 (2011), pp. 162–170.

[9] J. -C. Antona, S. Bigo, and J. -P. Faure. "Nonlinear cumulated phase as a criterion to assess performance of terrestrial WDM systems". In: *Proc. Optical Fiber Communication Conference and Exhibit OFC 2002*. 2002, pp. 365–367.

[10] J.-C. Antona et al. "Investigation of advanced dispersion management techniques for ultra-long haul transmissions". In: *Optical Communication, 2005. ECOC 2005. 31st European Conference on* (Sept. 2005), 19–20 vol.1.

[11] C. Balza, A. Fromageot, and M. Maniere. "Four-level pseudorandom sequences". In: *Electronics Letters* 3.7 (1967), pp. 313–315.

[12] P. Bayvel et al. "Coherent Electronic Compensation Techniques for Long-Haul Optical Fibre Transmission — Opportunities and Challenges". In: *Proc. 35th European Conference on Optical Communication ECOC 2009*. 2009.

[13] P.C. Becker, N.A. Olsson, and J.R. Simpson. *Erbium-Doped Fiber Amplifiers Fundamentals and Technology*. Ed. by Paul L. Kelly. Academic Press, 1999, p. 481.

[14] G. Bellotti et al. "Intensity distortion induced by cross-phase modulation and chromatic dispersion in optical-fiber transmissions with dispersion compensation". In: *IEEE Photonics Technology Letters* 10.12 (1998), pp. 1745–1747.

[15] Sergio Benedetto and Ezio Biglieri. *Principles of Digital Transmission: With Wireless Applications*. Norwell, MA, USA: Kluwer Academic Publishers, 1999.

[16] Oriol Bertran-Pardo et al. "PDM-QPSK: on the system benefits arising from temporally interleaving polarization tributaries at 100Gb/s". In: *Opt. Express* 17.22 (Oct. 2009), pp. 19902–19907.

[17] O. Bertran-Pardo et al. "Demonstration of the benefits brought by PMD in polarization-multiplexed systems". In: *Proc. 36th European Conf Optical Communication (ECOC) and Exhibition*. 2010, pp. 1–3.

[18] N. Blachman. "The Effect of Phase Error on DPSK Error Probability". In: *IEEE Transactions on Communications* 29.3 (1981), pp. 364–365.

[19] N. M. Blachman. "Gaussian noise. II. Distribution of phase change of narrow-band noise plus sinusoid". In: *IEEE Transactions on Information Theory* 34.6 (1988), pp. 1401–1405.

[20] Alberto Bononi, Paolo Serena, and Nicola Rossi. "Modeling of Signal-Noise Interactions in Nonlinear Fiber Transmission with Different Modulation Formats". In: *Proc. 35th European Conference on Optical Communication ECOC 2009*. 2009.

[21] Alberto Bononi, Paolo Serena, and Nicola Rossi. "Nonlinear signal-noise interactions in dispersion-managed links with various modulation formats". In: *Optical Fiber Technology* 16.2 (2010), pp. 73 –85.

[22] A. Bononi, P. Serena, and A. Orlandini. "A Unified Design Framework for Single-Channel Dispersion-Managed Terrestrial Systems". In: *IEEE/OSA Journal of Lightwave Technology* 26.22 (2008), pp. 3617–3631.

[23] P.A.N. Briggs and K.R. Godfrey. "Autocorrelation function of a 4-level msequence". In: *Electronics Letters* 4.11 (1968), pp. 232–233.

[24] H. Bulow, F. Buchali, and A. Klekamp. "Electronic Dispersion Compensation". In: *IEEE/OSA Journal of Lightwave Technology* 26.1 (2008), pp. 158–167.

[25] Y. Cai et al. "Experimental demonstration of coherent MAP detection for nonlinearity mitigation in long-haul transmissions". In: *Proc. Conf Optical Fiber Communication (OFC), collocated National Fiber Optic Engineers Conf. (OFC/NFOEC)*. 2010, pp. 1–3.

[26] A. Carena et al. "Statistical characterization of PM-QPSK signals after propagation in uncompensated fiber links". In: *Proc. 36th European Conf Optical Communication (ECOC) and Exhibition*. 2010, pp. 1–3.

[27] A. Cauvin, Y. Frignac, and S. Bigo. "Nonlinear impairments at various bit rates in single-channel dispersion-managed systems". In: *Electronics Letters* 39.23 (2003),

[28] Y. Chigusa et al. "Low-loss pure-silica-core fibers and their possible impact on transmission systems". In: *Journal of Lightwave Technology* 23.11 (2005), pp. 3541–3550.

[29] L. Cohen. "Comparison of single-mode fiber dispersion measurement techniques". In: *Journal of Lightwave Technology* 3.5 (1985), pp. 958–966.

[30] Stephen D. Cohen. "Explicit theorems on generator polynomials". In: *Finite Fields and Their Applications* 11.3 (2005). Ten Year Anniversary Edition!, pp. 337 –357.

[31] J. Conradi. "Bandwidth-efficient modulation formats for digital fiber transmission systems". In: *Optical Fiber Telecommunications IV B* (2002), pp. 862–901.

[32] A. Demir. "Nonlinear Phase Noise in Optical-Fiber-Communication Systems". In: *IEEE/OSA Journal of Lightwave Technology* 25.8 (2007), pp. 2002–2032.

[33] E. Desurvire, J. R. Simpson, and P. C. Becker. "High-gain erbium-doped traveling-wave fiber amplifier". In: *Opt. Lett.* 12.11 (Nov. 1987), pp. 888–890.

[34] A. Ellis, J. Zhao, and D. Cotter. "Approaching the Non-Linear Shannon Limit". In: *IEEE/OSA Journal of Lightwave Technology* PP.99 (2009), p. 1.

[35] R. -J. Essiambre, B. Mikkelsen, and G. Raybon. "Intra-channel cross-phase modulation and four-wave mixing in high-speed TDM systems". In: *Electronics Letters* 35.18 (1999), pp. 1576–1578.

[36] R.-J. Essiambre et al. "Capacity Limits of Optical Fiber Networks". In: *Lightwave Technology, Journal of* 28.4 (Feb. 2010), pp. 662 –701.

[37] J. K. Fischer and K. Petermann. "Nonlinear threshold of RZ-DBPSK and RZ-DQPSK". In: *Proc. 34th European Conference on Optical Communication ECOC 2008*. 2008, pp. 1–2.

[38] Robert A. Fisher and William K. Bischel. "Numerical studies of the interplay between self-phase modulation and dispersion for intense plane-wave laser pulses". In: *Journal of Applied Physics* 46.11 (1975), pp. 4921–4934.

[39] W.G. French et al. “Optical wave guides with very low losses”. In: *Bell System Technical Journal* 53.5 (1974), pp. 951–54.

[40] Yann Frignac. “Contribution a l’ingenierie des systemes de transmission terrestres sur fibre optique utilisant le multiplexage en longueur d’onde de canaux modules au debit de 40Gbit/s”. PhD thesis. Ecole Nationale Superieure des Telecommunications, Apr. 2003.

[41] Y. Frignac, J.-C. Antona, and S. Bigo. “Enhanced analytical engineering rule for fast optimization dispersion maps in 40 Gbit/s-based transmission”. In: *Proc. Optical Fiber Communication Conference OFC 2004*. Vol. 1. Dispersion management. 2004,

[42] Y. Frignac and P. Ramantanis. “Average Optical Phase Shift as an Indicator of the Dispersion Management Optimization in PSK-Modulated Transmission Systems”. In: *IEEE Photonics Technology Letters* 22.20 (2010), pp. 1488–1490.

[43] Y. Frignac et al. “Numerical optimization of pre- and in-line dispersion compensation in dispersion-managed systems at 40 Gbit/s”. In: *Proc. Optical Fiber Communication Conference and Exhibit OFC 2002*. Dispersion management. 2002, pp. 612–613.

[44] Christian Fuchs. *Internet and society: Social theory in the information age*. Psychology Press, 2008.

[45] A. H. Gnauck and P. J. Winzer. “Optical phase-shift-keyed transmission”. In: *IEEE/OSA Journal of Lightwave Technology* 23.1 (Jan. 2005), pp. 115–130.

[46] A.H. Gnauck et al. "High-Capacity Optical Transmission Systems". In: *Lightwave Technology, Journal of* 26.9 (May 2008), pp. 1032 –1045.

[47] Gilad Goldfarb and Guifang Li. "BER estimation of QPSK homodyne detection with carrier phase estimation using digital signal processing". In: *Opt. Express* 14.18 (Sept. 2006), pp. 8043–8053.

[48] Solomon W. Golomb. "Periodic binary sequences: solved and unsolved problems". In: *SSC'07: Proceedings of the 2007 international conference on Sequences, subsequences, and consequences*. Los Angeles, CA, USA: Springer-Verlag, 2007, pp. 1–8.

[49] Solomon W. Golomb. *Shift Register Sequences*. Laguna Hills, CA, USA: Aegean Park Press, 1981.

[50] J. P. Gordon, W. H. Louisell, and L. R. Walker. "Quantum Fluctuations and Noise in Parametric Processes. II". In: *Phys. Rev.* 129.1 (Jan. 1963), pp. 481–485.

[51] J. P. Gordon and L. F. Mollenauer. "Phase noise in photonic communications systems using linear amplifiers". In: *Opt. Lett.* 15.23 (1990), pp. 1351–1353.

[52] D. H. Green and I. S. Taylor. "Irreducible polynomials over composite Galois fields and their applications in coding techniques". In: *Proceedings of the Institution of Electrical Engineers* 121.9 (1974). Sequences, pp. 935–939.

[53] E. Grellier, J. Antona, and S. Bigo. "Are multilevel pseudorandom sequences really needed to emulate highly dispersive optical transmission

systems?" In: *Proc. 36th European Conf Optical Communication (ECOC) and Exhibition*. 2010, pp. 1–3.

[54] Edouard GRELLIER, Jean-Christophe ANTONA, and Sebastien BIGO. "Revisiting the evaluation of non-linear propagation impairments in highly dispersive systems". In: *Proc. 35th European Conference on Optical Communication ECOC 2009*. 2009.

[55] R. A. Griffin and A. C. Carter. "Optical differential quadrature phase-shift key (oDQPSK) for high capacity optical transmission". In: *Proc. Optical Fiber Communication Conference and Exhibit OFC 2002*. 2002, pp. 367–368.

[56] Simon Haykin. *Communication systems*. Ed. by Bill Zobrist. 4th. 5. John Wiley & Sons Inc, 2001.

[57] Clifford Headley and Govind P. Agrawal. *Raman Amplification in Fiber Optical Communication Systems*. Ed. by Govind P. Agrawal Clifford Headley. Elsevier Academic Press, 2005.

[58] Keang-Po Ho and Hsi-Cheng Wang. "Comparison of nonlinear phase noise and intrachannel four-wave mixing for RZ-DPSK signals in dispersive transmission systems". In: *IEEE Photonics Technology Letters* 17.7 (2005), pp. 1426–1428.

[59] Ezra Ip et al. "Compensation of dispersion and nonlinearity in WDM transmission using simplified digital backpropagation". In: *IEEE/LEOS Summer Topical Meetings, 2008 Digest of the* (July 2008), pp. 123–124.

[60] Michel C. Jeruchim, Philip Balaban, and K. Sam Shanmugan. *Simulation of Communication Systems*. KLUWER ACADEMIC PUBLISHERS, 2002.

[61] J. M. Kahn and Keang-Po Ho. "Spectral efficiency limits and modulation/detection techniques for DWDM systems". In: *IEEE Journal of Selected Topics in Quantum Electronics* 10.2 (2004), pp. 259–272.

[62] I. Kaminow. "Polarization in optical fibers". In: *IEEE Journal of Quantum Electronics* 17.1 (1981), pp. 15–22.

[63] Ivan P. Kaminow, Tingye Li, and Alan E. Willner. *Optical Fiber Telecommunications V B: Systems and Networks*. Ed. by Ivan P. Kaminow, Tingye Li, and Alan E. Willner. Elsevier Inc., 2008.

[64] K. C. Kao and G. A. Hockham. "Dielectric-fibre surface waveguides for optical frequencies". In: *Proceedings of the Institution of Electrical Engineers* 113.7 (1966), pp. 1151–1158.

[65] F. P. Kapron, D. B. Keck, and R. D. Maurer. "Radiation losses in glass optical waveguides". In: *Applied Physics Letters* 17.10 (1970), pp. 423–425.

[66] K. Kikuchi. "Coherent optical communication systems". In: *Optical Fiber Telecommunications VB: systems and networks* (2008).

[67] R.I. Killey et al. "Reduction of intrachannel nonlinear distortion in 40-Gb/s-based WDM transmission over standard fiber". In: *IEEE Photonics Technology Letters* 12.12 (2000), pp. 1624–1626.

[68] J.J. Komo and M.S. Lam. "Primitive polynomials and M-sequences over $GF(q^m)$". In: *IEEE Transactions on Information Theory* 39.2 (1993), pp. 643–647.

[69] B. Konrad and K. Petermann. "Optimum fiber dispersion in high-speed TDM systems". In: *Photonics Technology Letters, IEEE* 13.4 (Apr. 2001), pp. 299 –301.

[70] J. Lassing et al. "Computation of the exact bit-error rate of coherent M-ary PSK with Gray code bit mapping". In: *IEEE Transactions on Communications* 51.11 (2003), pp. 1758–1760.

[71] A. Lau, S. Rabbani, and J. M. Kahn. "On the Statistics of Intrachannel Four-Wave Mixing in Phase-Modulated Optical Communication Systems". In: *IEEE/OSA Journal of Lightwave Technology* 26.14 (2008), pp. 2128–2135.

[72] Mathieu Lefrancois et al. "Numerical discrimination of intrachannel cross-phase modulation and intrachannel four-wave mixing and their respective effect on 40 Gbit/s transmissions". In: *Opt. Lett.* 31.4 (2006), pp. 432–434.

[73] R. Lidl, H. Niederreiter, and PM Cohn. *Encyclopedia of Mathematics and Its Applications 20: Finite Fields*. Cambridge University Press, 1996.

[74] X. Liu, S. Chandrasekhar, and A. Leven. "Self-coherent optical transport systems". In: *Optical Fiber Telecommunications VB: systems and networks* (2008), p. 131.

[75] F.J. MacWilliams and N.J.A. Sloane. "Pseudo-random sequences and arrays". In: *Proceedings of the IEEE* 64.12 (1976), pp. 1715–1729.

[76] I. H. Malitson. "Interspecimen Comparison of the Refractive Index of Fused Silica". In: *J. Opt. Soc. Am.* 55.10 (Oct. 1965), pp. 1205–1208.

[77] P. V. Mamyshev and N. A. Mamysheva. "Pulse-overlapped dispersion-managed data transmission and intrachannel four-wave mixing". In: *Opt. Lett.* 24.21 (1999), pp. 1454–1456.

[78] D. Marcuse. *Light transmission optics*. Van Nostrand Reinhold New York, 1982.

[79] A. Mecozzi. "A Unified Theory of Intrachannel Nonlinearity in Pseudo-linear Phase-Modulated Transmission". In: *IEEE Photonics Journal* 2.5 (2010), pp. 728–735.

[80] A. Mecozzi, C.B. Clausen, and M. Shtaif. "Analysis of intrachannel nonlinear effects in highly dispersed optical pulse transmission". In: *IEEE Photonics Technology Letters* 12.4 (2000), pp. 392–394.

[81] A. Mecozzi et al. "Dispersion management in phase modulated optical transmission systems". In: *Proc. 36th European Conf Optical Communication (ECOC) and Exhibition*. 2010, pp. 1–3.

[82] P.P. Mitra and J.B. Stark. "Nonlinear limits to the information capacity of optical fibre communications". In: *Nature* 411.6841 (2001), pp. 1027–1030.

[83] T. Miya et al. "Ultimate low-loss single-mode fibre at 1.55 m". In: *Electronics Letters* 15.4 (1979), pp. 106–108.

[84] T. Okoshi and K. Kikuchi. *Coherent optical fiber communications*. Springer, 1988.

[85] Jr. Park W. J. and J. J. Komo. "Relationships between m-sequences over GF(q) and $GF(q^m)$". In: *IEEE Transactions on Information Theory* 35.1 (1989), pp. 183–186.

[86] D. Penninckx et al. "The phase-shaped binary transmission (PSBT): a new technique to transmit far beyond the chromatic dispersion limit". In: *IEEE Photonics Technology Letters* 9.2 (1997), pp. 259–261.

[87] P. Poggiolini et al. "Analytical Modeling of Non-Linear Propagation in Uncompensated Optical Transmission Links". In: *IEEE Photonics Technology Letters* 99 (2011). Early Access.

[88] O. Pretzel. *Error-correcting codes and finite fields*. Oxford University Press, USA, 1992.

[89] John Proakis. *Digital Communications*. 4. McGraw-Hill Science/Engineering/Math, Aug. 2000.

[90] P. Ramantanis, H. Badaoui, and Y. Frignac. "Quaternary sequences comparison for the modeling of optical DQPSK dispersion managed transmission systems". In: *Proc. Conference on Optical Fiber Communication - incudes post deadline papers OFC 2009*. 2009, pp. 1–3.

[91] Petros Ramantanis, Hadjira Badaoui, and Yann Frignac. "Comparaison des sequences des donnees pour l'estimation de la performance des systemes de transmission optique DQPSK". In: *Journees Nationales d'optique guidee*. Sequences. 2009.

[92] Petros Ramantanis and Yann Frignac. "Pattern-dependent nonlinear impairments on QPSK signals in dispersion-managed optical transmission

systems". In: *Proc. 36th European Conf Optical Communication (ECOC) and Exhibition*. 2010, pp. 1–3.

[93] P. Ramantanis et al. "Impact de la séquence de données sur la dégradation des signaux QPSK dans les systèmes de transmission optique". In: *Journees Nationales d'optique guidee* (2010).

[94] M. Salsi et al. "80x100-Gbit/s transmission over 9,000km using erbium-doped fibre repeaters only". In: *Proc. 36th European Conf Optical Communication (ECOC) and Exhibition*. 2010, pp. 1–3.

[95] Seb J. Savory. "Digital filters for coherent optical receivers". In: *Opt. Express* 16.2 (2008), pp. 804–817.

[96] S. J. Savory. "Coherent Detection - Why is it back?" In: *Proc. 20th Annual Meeting of the IEEE Lasers and Electro-Optics Society LEOS 2007*. 2007, pp. 212–213.

[97] E.S. Selmer. *Linear recurrence relations over finite fields*. Sequences. Published by] Department of Mathematics, University of Bergen, 1966.

[98] P. Serena, A. Orlandini, and A. Bononi. "The memory of optimized dispersion-managed periodic optical links". In: *IET Seminar Digests* 2007.1 (2007), P093–P093.

[99] I. Shake et al. "Influence of inter-bit four-wave mixing in optical TDM transmission". In: *Electronics Letters* 34.16 (1998), pp. 1600–1601.

[100] C. E. Shannon. "Communication in the Presence of Noise". In: *Proceedings of the IRE* 37.1 (1949), pp. 10–21.

[101] Y.R. Shen. "The principles of nonlinear optics". In: (1984).

[102] B. Sklar. *Digital communications*. Prentice-Hall Englewood Cliffs, NJ, 2001.

[103] V.A.J.M. Sleiffer et al. "Dispersion management in long-haul 111-Gb/s POLMUX-RZ-DQPSK transmission systems". In: Oct. 2009, pp. 569 – 570.

[104] D. Sperti, P. Serena, and A. Bononi. "Optical Solutions to Improve PDM-QPSK Resilience against Cross-channel Nonlinearities: a Comparison". In: *IEEE Photonics Technology Letters* 99 (2011). Early Access.

[105] B. Spinnler and C. Xie. "Performance Assessment of DQPSK using Pseudo-Random Quaternary Sequences". In: *ECOC* (2007).

[106] W. Stahnke. "Primitive binary polynomials". In: *Mathematics of Computation* 27.124 (1973). Sequences, pp. 977–980.

[107] M. G. Taylor. "Coherent detection method using DSP for demodulation of signal and subsequent equalization of propagation impairments". In: *IEEE Photonics Technology Letters* 16.2 (2004), pp. 674–676.

[108] S. Tsukamoto, K. Katoh, and K. Kikuchi. "Unrepeated transmission of 20-Gb/s optical quadrature phase-shift-keying signal over 200-km standard single-mode fiber based on digital processing of homodyne-detected signal for Group-velocity dispersion compensation". In: *IEEE Photonics Technology Letters* 18.9 (2006), pp. 1016–1018.

[109] S. Tsukamoto et al. "Coherent demodulation of 40-Gbit/s polarization-multiplexed QPSK signals with 16-GHz spacing after 200-km transmis-

sion". In: *Proc. Technical Digest Optical Fiber Communication Conference OFC/NFOEC*. Vol. 6. 2005, 3 pp. Vol. 5–.

[110] Andrew Viterbi and Audrey Viterbi. "Nonlinear estimation of PSK-modulated carrier phase with application to burst digital transmission". In: *IEEE Transactions on Information Theory* 29.4 (1983), pp. 543–551.

[111] Jordi Vuong et al. "Understanding Discrete Linear Mode Coupling in Few-Mode Fiber Transmission Systems". In: *Proc. 37th European Conf Optical Communication (ECOC) and Exhibition*. 2011.

[112] J. Wang and K. Petermann. "Small signal analysis for dispersive optical fiber communication systems". In: *IEEE/OSA Journal of Lightwave Technology* 10.1 (1992), pp. 96–100.

[113] Xing Wei and Xiang Liu. "Analysis of intrachannel four-wave mixing in differential phase-shift keying transmission with large dispersion". In: *Opt. Lett.* 28.23 (2003), pp. 2300–2302.

[114] L. K. Wickham et al. "Bit pattern length dependence of intrachannel nonlinearities in pseudolinear transmission". In: *IEEE Photonics Technology Letters* 16.6 (2004), pp. 1591–1593.

[115] P. Winzer and R. Essiambre. "Advanced Modulation Formats". In: *Optical Fiber Telecommunications VB: systems and networks* (2008).

[116] Dong Yang and S. Kumar. "Intra-Channel Four-Wave Mixing Impairments in Dispersion-Managed Coherent Fiber-Optic Systems Based on Binary Phase-Shift Keying". In: *IEEE/OSA Journal of Lightwave Technology* 27.14 (2009), pp. 2916–2923.

[117] A. Yariv and P. Yeh. *Optical waves in crystals*. Wiley New York, 1984.

[118] Neal Zierler. "Linear Recurring Sequences". In: *Journal of the Society for Industrial and Applied Mathematics* 7.1 (1959), pp. 31–48.

Author's publications

[42] Y. Frignac and P. Ramantanis. "Average Optical Phase Shift as an Indicator of the Dispersion Management Optimization in PSK-Modulated Transmission Systems". In: *IEEE Photonics Technology Letters* 22.20 (2010), pp. 1488–1490.

[90] P. Ramantanis, H. Badaoui, and Y. Frignac. "Quaternary sequences comparison for the modeling of optical DQPSK dispersion managed transmission systems". In: *Proc. Conference on Optical Fiber Communication - incudes post deadline papers OFC 2009*. 2009, pp. 1–3.

[91] Petros Ramantanis, Hadjira Badaoui, and Yann Frignac. "Comparaison des sequences des donnees pour l'estimation de la performance des systemes de transmission optique DQPSK". In: *Journees Nationales d'optique guidee*. Sequences. 2009.

[92] Petros Ramantanis and Yann Frignac. "Pattern-dependent nonlinear impairments on QPSK signals in dispersion-managed optical transmission systems". In: *Proc. 36th European Conf Optical Communication (ECOC) and Exhibition*. 2010, pp. 1–3.

[93] P. Ramantanis et al. "Impact de la séquence de données sur la dégradation des signaux QPSK dans les systèmes de transmission optique". In: *Journees Nationales d'optique guidee* (2010).

[111] Jordi Vuong et al. "Understanding Discrete Linear Mode Coupling in Few-Mode Fiber Transmission Systems". In: *Proc. 37th European Conf Optical Communication (ECOC) and Exhibition*. 2011.

Index

autocorrelation function, 100, 115

De Bruijn associate sequence, 119
De Bruijn sequence, 119
differential, 46
differentially coherent, 44

finite fields, 101

Galois fields, 101

Nonlinear phase, 145

precoding, 16
primitive polynomials, 104
Pseudo-random Sequences, 100

standard deviation, 29, 144
state, 13, 15